

**HYPOGENE AND SUPERGENE EVOLUTION OF THE CERRO COLORADO
PORPHYRY COPPER (-MOLYBDENUM) DEPOSIT, NORTHERN CHILE**

by

Farhad Bouzari

A thesis submitted to the Department of Geological Sciences and Geological Engineering
in conformity with the requirements for the degree of Doctor of Philosophy

Queen's University
Kingston, Ontario, Canada
August, 2003

Copyright © by Farhad Bouzari, 2003



National Library
of Canada

Bibliothèque nationale
du Canada

Acquisitions and
Bibliographic Services

Acquisitions et
services bibliographiques

395 Wellington Street
Ottawa ON K1A 0N4
Canada

395, rue Wellington
Ottawa ON K1A 0N4
Canada

Your file Votre référence

ISBN: 0-612-86215-1

Our file Notre référence

ISBN: 0-612-86215-1

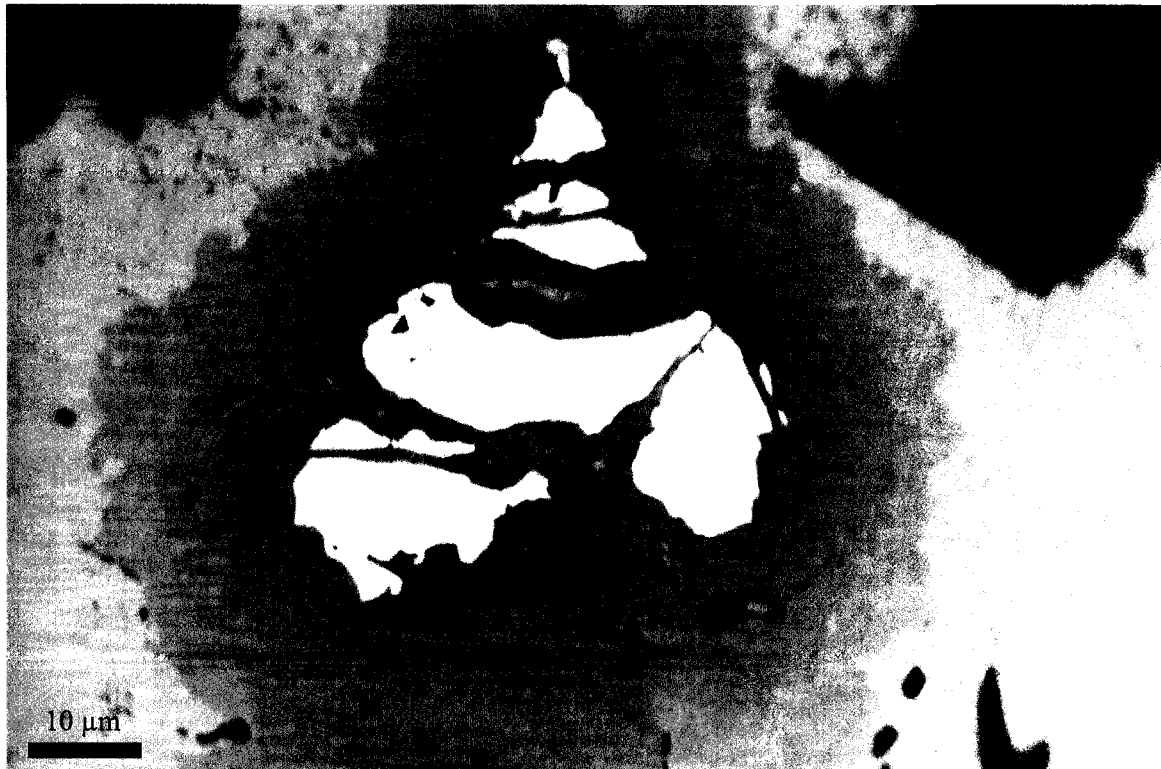
The author has granted a non-exclusive licence allowing the National Library of Canada to reproduce, loan, distribute or sell copies of this thesis in microform, paper or electronic formats.

L'auteur a accordé une licence non exclusive permettant à la Bibliothèque nationale du Canada de reproduire, prêter, distribuer ou vendre des copies de cette thèse sous la forme de microfiche/film, de reproduction sur papier ou sur format électronique.

The author retains ownership of the copyright in this thesis. Neither the thesis nor substantial extracts from it may be printed or otherwise reproduced without the author's permission.

L'auteur conserve la propriété du droit d'auteur qui protège cette thèse. Ni la thèse ni des extraits substantiels de celle-ci ne doivent être imprimés ou autrement reproduits sans son autorisation.

Canada



Frontispiece:

Photomicrograph of a polished section of ore from the Cerro Colorado deposit, showing hypogene chalcopyrite (yellow) replaced by, successively, supergene bornite (pink), digenite (dark blue) and chalcocite (pale blue).

“It’s *nature* not *nurture*, porphyry copper deposits are *born*, they are not made.”

Alan H. Clark

ABSTRACT

The 51.8 Ma Cerro Colorado porphyry Cu (-Mo) deposit, situated at 20° 2' 41" S; 69° 15' 35" W on the Pacific slope of the Central Andean Cordillera Occidental, comprises a supergene orebody with reserves of 228 Mt at 1.0 percent Cu, overlying a hypogene protore zone with Cu grades of 0.4-0.5 percent and a resource approximately double that of the supergene ore.

Initial hypogene alteration of Upper Cretaceous andesitic host-rocks generated an 8 km², pervasive, biotite-albite-magnetite blanket. The non-boiling fluids at this stage, with moderate temperatures ($\leq 380^{\circ}\text{C}$) and low salinities (≤ 8 wt percent NaCl equiv.), caused significant K-Na-Fe⁺² metasomatism but deposited no sulfides. Subsequent Main Stage alteration-mineralization, which, with decreasing depth, comprises quartz-albite, sericite-chlorite-clay, quartz-sericite-clay and andalusite-diaspore-pyrophyllite facies, was responsible for over 70 percent of the chalcopyrite in the deposit. As they rose, the hot ($\leq 544^{\circ}\text{C}$), boiling, ore-forming fluids, with salinities of ≤ 52 wt percent NaCl equiv., cooled (to $\leq 320^{\circ}\text{C}$), were diluted (to ≤ 37 wt percent NaCl equiv.), became more acid and generated quasi-contemporaneous intermediate- and advanced argillic alteration facies. Thus, the hypogene protore was the product of an unusual hybrid environment, in which a cool, barren hydrothermal system, similar in all salient aspects to those represented by non-explosive geothermal fields, abruptly evolved into one more characteristic of porphyry deposits. Whereas this transition may have been stimulated by melt incursion, such early geothermal stages and prograde histories may be inherent features of the initiation of magmatic-hydrothermal systems.

Dating of alunite-group minerals from various ore facies and elevations by laser ⁴⁰Ar/³⁹Ar incremental-heating reveals a supergene history extending over at least 20 m.y. The hypogene protore was plausibly unroofed at the onset of the Incaic orogeny at ca. 42 Ma, initiating the development of a thick chalcocite blanket, the Upper Supergene Ore, during the Oligocene. In the

Early Miocene, at ca. 21.5 Ma, major Pehuenchean uplift resulted in the formation of a lower leached zone within the preexisting chalcocite blanket, which was thickened and, at shallow levels, oxidized. Normal supergene processes were interrupted at 19.25 Ma by a thick ignimbrite which partially covered the deposit, but the imposition of lateral groundwater flow reactivated oxidation and generated incipient exotic (chrysocolla) mineralization. Significant supergene activity had terminated by ca. 14.6 Ma as a result of climatic desiccation.

The establishment of a “proto-Humboldt Current” and the onset of the Incaic orogeny in the late Eocene provided a climatic and physiographic environment favorable for supergene enrichment of Cu deposits undergoing exhumation in the rain-shadow of an uplifting terrain. Because the Upper Supergene Ore zone at Cerro Colorado formed during the Oligocene, following the Incaic Orogeny, a single Cenozoic supergene metallogenetic epoch is proposed for northern Chile, ca. 20, or even 30, m.y. in duration, but attaining its greatest efficacy in the Early Miocene.

ACKNOWLEDGMENTS

This thesis would not have been possible without the support of numerous people. First and foremost I thank my advisor, Dr. Alan Clark, for suggesting this project and for his guidance, support, intellectually and financially, and tireless editing of the manuscripts. I have learned many things about ore deposits, as well as clear and correct English writing, during the many years of working with Alan, but perhaps most importantly, he taught me how to look at both the *insides* and *outsides* of “hillsides”.

Rio Algom Exploration has partially funded this project. I would like to thank Kelly O'Connor and Tom Warren for their support. Assistance in Chile was provided by Jack McClintock of Riochilex Exploration. Angus Campbell, senior Riochilex geologist, came all the way from Antofagasta to Iquique for my first day visit at Cerro Colorado. Field works would not have been possible without the full cooperation of Compañía Minera Cerro Colorado. I thank Orlando Alvarez, chief mine geologist, Eduardo Fernández, mine geologist, and geology department staff members Wilson Araya, Eulio Huanca, Wilson Araya, Hector Luengo, Nelson Chandia, Hector Luengo and Paola Vilca. They all were happy to see me leaving the mine, with my nearly one tonne of collected rock samples, without being flattened by their big trucks!

James Macdonald and Richard Pape of BHP Billiton contributed funding for colour prints in journal publications.

Here at Queen's, I benefited greatly from the advice of Dr. Peter Roeder and Dave Kempson for microprobe analysis, and Dr. Doug Archibald for $^{40}\text{Ar}/^{39}\text{Ar}$ dating. Al Grant helped with X-ray and titration and Rob Renaud provided computer needs. Jerzy Advent and Rogers Innes prepared thin and polished sections. Discussions with Drs. Kurt Kyser, Ron Peterson, Gema Olivo, Dave Love and Herb Helmstaedt are greatly appreciated. Geology staff Dianne Hyde, Joan Charbonneau, Linda Brown, and Ellen Mulder kindly helped on my student “things” from contracts to copy cards.

Thanks to many grad students for their discussions and help. My special thanks to Tom Ullrich, Chan Quang, Amelia Rainbow, Rob Strusiewicz and Thomas Bissig.

I would like to thank the Ministry of Science Research and Technology of Iran for making it possible for me to come to Canada for post-graduate study which led to this Ph.D.

Last but not least, I would like to thank my parents, brothers and sisters in Iran, and my wife here in Kingston for their encouragement, support and sacrifices. Life would have been difficult without the joy of my daughter, Narges, and son, Ali. Thank you all.

STATEMENT OF ORIGINALITY

Although this project has benefited from discussion with many people, the major findings are based on the author's personal endeavours. In July 1996, when the fieldwork was initiated, very little was known about the geology of the Cerro Colorado porphyry copper deposit. Up to that date, there had been several drilling programs, but A. Cepeda, G.M. Ditson and D.G. Mato (unpublished report to Compañía Minera Riochilex, 1982) had documented alteration and mineralization relationships in only the shallow levels of the Main Zone. Deep drilling in the West Zone, and poor copper recovery from the Main Zone supergene ore encouraged Rio Algom Exploration to accept Alan Clark's proposal for a research on both hypogene and supergene setting of the deposit. Detailed drill core logging, field mapping and sampling by the author provided working material for further laboratory research at Queen's University. Interpretation of these data have led to major findings relevant to both hypogene and supergene processes in porphyry copper deposits worldwide which, in co-authorship with my supervisor, Dr. Alan Clark, were presented to major geological journals or meetings.

TABLE OF CONTENTS

| | |
|--|---------------|
| Frontispiece | ii |
| Citation | iii |
| Abstract | iv |
| Acknowledgments | vi |
| Statement of Originality | viii |
| Table of Contents | ix |
| List of Figures | xii |
| List of Tables | xiv |
| 1. Introduction | 1 |
| 1.1. Porphyry copper deposits: economically-critical products of processes at the bottom and top of the crust | 1 |
| Economic importance | 1 |
| Metal concentration by hypogene processes | 2 |
| Metal concentration by supergene processes | 4 |
| 1.2. Scope of investigation | 5 |
| 1.3. The scientific contributions of this study | 8 |
| 1.4. Thesis organization | 9 |
| 2. Prograde evolution of a major porphyry copper system: the Cerro Colorado protore, I Región, northern Chile | 11 |
| 2.1. Abstract | 11 |
| 2.2. Introduction | 12 |
| 2.3. Geologic Setting | 14 |
| 2.4. Host Rocks | 18 |
| Cerro Empexa Formation | 18 |
| Breccia bodies | 23 |
| Biotite-quartz-plagioclase porphyry | 25 |
| Quartz porphyry | 26 |
| Hornblende-plagioclase porphyry dikes | 26 |
| 2.5. Alteration and Mineralization | 27 |
| Early Stage alteration | 27 |
| Main Stage alteration-mineralization | 36 |
| Transitional Stage alteration-mineralization | 44 |
| Late Stage pyrite veins | 46 |
| 2.6. $^{40}\text{Ar}/^{39}\text{Ar}$ Geochronology | 48 |
| 2.7. Alteration Mass and Volume Changes | 50 |
| Calculation procedure | 52 |
| Early Stage | 54 |
| Main Stage | 58 |

| | |
|--|---------|
| 2.8. Fluid Inclusion Relationships | 60 |
| Petrography of fluid inclusions | 60 |
| Distribution and relative ages of inclusion types | 65 |
| Microthermometry | 66 |
| Entrapment pressure and depth estimates | 73 |
| Summary | 83 |
| 2.9. Evolution of the Mineralizing System | 84 |
| Early Stage | 85 |
| Main Stage | 86 |
| Transitional and Late Stages | 90 |
| 2.10. Comparison with other Porphyry Copper Systems | 92 |
| Barren potassic-sodic alteration and prograde evolution | 92 |
| Simultaneous development of intermediate to advanced argillic zones | 96 |
| Geometry of the protore body | 99 |
| 2.11. Analogies with Geothermal Systems | 100 |
| 2.12. Conclusions | 104 |
| 3. Anatomy, evolution, and metallogenic significance of the supergene orebody of the Cerro Colorado porphyry copper deposit, I Región, northern Chile | 108 |
| 3.1. Abstract | 108 |
| 3.2. Introduction | 110 |
| Central Andean supergene activity | 111 |
| The geochronologic database | 114 |
| 3.3. The Cerro Colorado Deposit | 116 |
| Hypogene relationships | 118 |
| 3.4. Post-Hypogene Tectonic and Geomorphologic Setting | 121 |
| Ignimbrite flow | 125 |
| 3.5. Supergene Alteration and Mineralization | 130 |
| Supergene profile anatomy | 130 |
| Structural relationships | 143 |
| 3.6. Supergene Alunite-Group Mineralogy | 151 |
| Sampling and analysis | 154 |
| 3.7. $^{40}\text{Ar}/^{39}\text{Ar}$ Geochronology of Alunite-Group Minerals | 160 |
| $^{40}\text{Ar}/^{39}\text{Ar}$ age spectra for alunite-group minerals | 160 |
| Age relationships | 165 |
| 3.8. Evolution of the Supergene Profile | 165 |
| 3.9. Regional Correlations and Comparisons | 176 |
| Paleocene to middle Eocene deposits | 176 |
| Upper Eocene to lower Oligocene deposits | 180 |
| Exotic mineralization | 184 |
| 3.10. Supergene Metallogeny in the Central Andes | 187 |
| 3.11. Concluding Statement | 190 |
| 3.12. Acknowledgments | 192 |

| | |
|---|---------|
| 4. Conclusions | 193 |
| 4.1. Birth of a geothermal system: barren potassic-sodic alteration | 193 |
| 4.2. Transition to the porphyry environment: prograde path | 194 |
| 4.3. Rise of the fluids: quasi-simultaneous development of intermediate- and advanced argillic alteration | 195 |
| 4.4. Protracted supergene history: complex supergene profile | 195 |
| 4.5. Climatic changes: controls on supergene metallogenesis | 196 |
| References | 197 |
| APPENDIXES | |
| Appendix 1: Drill-hole map of Cerro Colorado | 227 |
| Appendix 2: Composition of Hydrothermal Phyllosilicate Minerals at Cerro Colorado | 228 |
| Appendix 3: Analytical Techniques | 233 |
| Appendix 4: $^{40}\text{Ar}/^{39}\text{Ar}$ Analytical Data, Cerro Colorado | 235 |
| Appendix 5: Fluid Inclusion Data, Cerro Colorado | 241 |
| Vita | 251 |

LIST OF FIGURES

Chapter 1

| | |
|--|---|
| Fig. 1-1: Location of Cerro Colorado and other Cenozoic Cu deposits of the Central Andes | 6 |
|--|---|

Chapter 2

| | |
|--|-------|
| Fig. 2-1: Regional geologic map of the Cerro Colorado area | 15 |
| Fig. 2-2: Pre-mine topographic and geologic map of the Cerro Colorado area | 16 |
| Fig. 2-3: Field photographs of host-rocks | 19-20 |
| Fig. 2-4: Hand sample photographs of host-rocks | 21-22 |
| Fig. 2-5: Cross section showing host rocks and alteration zones | 24 |
| Fig. 2-6: Photographs of the Early and Main Stage alteration samples | 29-30 |
| Fig. 2-7: Photographs showing details of alteration and veining | 31-32 |
| Fig. 2-8: Cross-section of the West Zone showing details of the alteration zones | 35 |
| Fig. 2-9: Photomicrographs showing modes of occurrence of andalusite | 41-42 |
| Fig. 2-10: Photographs of the Transitional Stage alteration and mineralization samples | 43 |
| Fig. 2-11: Field photo of Late Stage pyrite veins | 47 |
| Fig. 2-12: Laser-induced $^{40}\text{Ar}/^{39}\text{Ar}$ age spectra of hydrothermal biotite and muscovite | 49 |
| Fig. 2-13: Protolith vs. altered rock of the Early and Main Stages of alteration | 53 |
| Fig. 2-14: Mass changes during the Early and Main Stage alteration | 55-56 |
| Fig. 2-15: Photomicrographs of fluid inclusion types | 62 |
| Fig. 2-16: Histogram of homogenization temperatures and salinities of fluid inclusions | 68 |
| Fig. 2-17: Diagram of salinity vs. final homogenization temperature of Main Stage fluids | 71 |
| Fig. 2-18: Pressure estimates for fluid inclusions | 75 |
| Fig. 2-19: Plot of temperature of halite dissolution vs. temperature of vapour disappearance | 79 |
| Fig. 2-20: Pressure estimates for inclusions homogenizing by salt dissolution | 80 |
| Fig. 2-21: Cross-sections comparing Palinpinon geothermal field with Cerro Colorado | 101 |

Chapter 3

| | |
|--|-----|
| Fig. 3-1: Cenozoic copper deposits and prospects in northern Chile and southern Peru | 112 |
| Fig. 3-2: Simplified regional geologic map of part of northern Chile | 117 |
| Fig. 3-3: Geologic map of Cerro Colorado area | 119 |
| Fig. 3-4: Field photo of the east wall of the Main Zone pit | 124 |
| Fig. 3-5: Field photo of ignimbrite overlying the Main Zone Leached Cap | 126 |
| Fig. 3-6: $^{40}\text{Ar}/^{39}\text{Ar}$ age spectra for biotites from the ignimbrite overlying the Main Zone | 128 |
| Fig. 3-7: Aerial view of the Cerro Colorado mine | 129 |
| Fig. 3-8: Hand-sample of supergene sulphide ore | 132 |
| Fig. 3-9: Pre-mine topography showing locations of the drill holes and cross sections | 133 |
| Fig. 3-10: E-W cross section AA' | 134 |
| Fig. 3-11: E-W cross section BB' | 135 |
| Fig. 3-12: N-S cross section CC' | 136 |
| Fig. 3-13: N-S cross section DD' | 137 |
| Fig. 3-14: N-S cross section EE' | 138 |

| | |
|--|---------|
| Fig. 3-15: N-S cross section FF' | 139 |
| Fig. 3-16: Aerial view of the Main Zone pit | 144 |
| Fig. 3-17: Field photo of Lower Leached Zone | 145 |
| Fig. 3-18: Schmidt and rose diagrams of the fractures hosting supergene mineralization | 146-147 |
| Fig. 3-19: Field photo of bench wall with chrysocolla veins | 150 |
| Fig. 3-20: Photo of hand sample with supergene alunite-group minerals | 152 |
| Fig. 3-21: Electron microscope image of supergene alunite-group minerals | 153 |
| Fig. 3-22: Ternary alkali-site diagram for supergene alunite-group minerals | 159 |
| Fig. 3-23: $^{40}\text{Ar}/^{39}\text{Ar}$ age spectra of supergene alunite-group minerals | 161 |
| Fig. 3-24: Locations of the dated alunite-group samples on cross sections | 162 |
| Fig. 3-25: Location of exotic mineralization NNE of the mine | 171 |
| Fig. 3-26: Diagram showing context of chrysocolla mineralization | 172 |
| Fig. 3-27: Diagram comparing supergene profiles of selected Andean deposits | 177-178 |

LIST OF TABLES

Chapter 2

| | |
|---|----|
| Table 2-1: Compositions of hydrothermal phyllosilicate minerals | 33 |
| Table 2-2: Whole-rock compositions and specific gravities | 51 |
| Table 2-3: Mass and volume changes | 57 |
| Table 2-4: Classification of fluid inclusion types | 61 |

Chapter 3

| | |
|--|---------|
| Table 3-1: $^{40}\text{Ar}/^{39}\text{Ar}$ ages of ignimbrite samples | 127 |
| Table 3-2: Locations, mineralogy and $^{40}\text{Ar}/^{39}\text{Ar}$ ages of supergene alunite-group samples | 156-157 |
| Table 3-3: Compositions of supergene alunite-group minerals at Cerro Colorado | 158 |
| Table 3-4: Post-hypogene events at Cerro Colorado and in N Chile and S Peru | 175 |
| Table 3-5: Supergene metallogenesis of Central Andean Paleogene porphyry Cu deposits | 179 |

INTRODUCTION

1.1. Porphyry copper deposits: economically-critical products of processes at the bottom and top of the crust

Porphyry copper-molybdenum and copper-gold deposits have been the subject of extensive field and laboratory research over the last several decades, fundamentally because of their worldwide economic importance, but also because of the unique insight they provide into metal transport and concentration in two radically contrasted contexts, viz.: the exsolution of metalliferous brines from bodies of silicic magma cooling and crystallizing in the shallow crust; and the mineralogical modification and, commonly, enrichment of the chalcopyrite-pyrite stockworks thereby generated through deep weathering under semi-arid climatic conditions. These ore-forming processes are rare-event phenomena in two major geochemical cycles, the first involving the extraction of mafic melts from asthenospheric mantle above a subduction zone and their subsequent evolution in the overlying crust, and the second the interaction of the atmosphere and hydrosphere with the mineralized end-products of such petrogenetic activity. In this thesis, the writer critically analyses the contributions of *hypogene* (i.e., ascending) and *supergene* (descending) waters to a major porphyry copper-molybdenum deposit in the Central Andes of northern Chile, a region which hosts a remarkable number of world-class magmatic-hydrothermal systems.

Economic importance

Copper has been mined since prehistoric times (Wertime, 1964), initially from supergene-enriched portions of volcanic-hosted polymetallic vein and massive sulphide deposits

in Iran, Turkey and Cyprus, and more recently from porphyry copper deposits in North and South America. The modern exploitation of porphyry systems, however, was initiated in 1904 by Utah Copper Co. when the Penrose-MacNeil group accepted Daniel C. Jackling's and Robert C. Gemmell's 1899 report on the potential profitability of large-scale mining of low-grade mineralization at Bingham, Utah (Parsons, 1933). Since then, because of their large size, enormous metal content, and amenability to low-cost extractive methods, these deposits have been the subject of intense exploration, and numerous porphyry Cu-Mo and Cu-Au deposits have been discovered and mined around the world. The majority of these deposits are located in the circum-Pacific orogenic belts of the American cordillera and eastern Asia and in the Alpine-Himalayan Tethyan belt (Sillitoe, 1997; Porter, 1998). Over 80 major porphyry deposits account for nearly two-thirds of world copper production (Gilmour et al., 1995). Moreover, porphyry deposits are becoming increasingly important relative to other Cu mineralization types, e.g., red bed, volcanic-hosted massive sulphide or orthomagmatic Cu-Ni. World copper mine production in 2001 was 13.6 Mt at an average market price of US\$ 0.82/lb (Torrible, 2002). The largest porphyry copper deposits are located in the American Cordillera (Clark, 1993), producing, from 1904 to 1991, over 15 Gt of ore containing ca. 150 Mt of Cu, and the reserves and resources of mined and unmined deposits are estimated at over 83 Gt of ore containing ca. 497 Mt of copper (Long, 1995).

Metal concentration by hypogene processes

Porphyry copper deposits are closely linked to magmatic rocks and provide a natural laboratory for the study of metal concentration by magmatic-hydrothermal processes. The association of vein, stockwork and breccia-hosted copper ore with porphyritic felsic stocks was recognized in the early years of exploration and mining at Bingham (e.g., Boutwell, 1905; Beeson, 1917) and was subsequently shown to be a salient feature of many deposits in the

southwest US (Emmons, 1927), and such deposits were soon referred to as “porphyry coppers”. Alteration and mineralization mapping at several of the earliest-mined deposits, e.g., Butte, Montana (Sales and Meyer, 1948; Meyer et al., 1968); Bagdad, Arizona (Anderson, 1950), Bingham, Utah (Hunt, 1957), San Manuel, Arizona (Creasey, 1965) and Santa Rita, New Mexico (Kerr et al., 1950), provided the basis for Meyer and Hemley’s classic 1967 synthesis of wall rock alteration facies. Lowell and Guilbert (1970) subsequently recognized concentric, “onion-skin”, alteration-mineralization zones in the San Manuel-Kalamazoo deposit, Arizona, and on the basis of comparative studies of 27 porphyry deposits suggested that such zoning is a common feature of porphyry copper deposits. Gustafson and Hunt (1975), in a detailed study at El Salvador, Chile, correlated the spatial and, critically, temporal relationships of alteration-mineralization facies with the emplacement of a succession of intrusive porphyries which, together with the volatiles, were inferred to have been derived from the roof of a deep, crystallizing pluton. Studies of the tectonically rotated, and hence comprehensively exposed, Yerington (Carten, 1986) and Ann-Mason (Dilles and Einaudi, 1992) deposits, Nevada, provided convincing evidence for such a relationship with deep intrusive units. These field relationships paralleled and stimulated the progressive refinement of the magmatic-hydrothermal model by Burnham (1967 and 1979), Burnham and Ohmoto (1980), Burnham (1981), Whitney (1989) and Fournier (1999). The main aims of such models were to clarify how metals could be concentrated from crystallizing melt and, more critically, to explain two aspects of such processes (Burnham and Ohmoto, 1980, p. 1): i.e., “(1) not all felsic porphyry stocks are hydrothermally altered and, (2) not all hydrothermally altered stocks or their wallrocks are economically mineralized”.

Burnham (1981) identified six major parameters that influence the fertility of a crystallizing melt: (1) water content, (2) temperature or heat content, (3) metal content, (4) chlorine content, (5) sulphur content, and (6) oxidation state. These criteria have been the subject of numerous experimental, theoretical and observational studies, e.g., Holland (1972), Kilinc and

Burnham (1972), Whitney (1975a and b), Norton (1982), Candela and Holland (1984 and 1986), Candela (1989a, b), Shinohara et al. (1989), Anderson et al. (1989), Cline and Bodnar (1991), Williams et al. (1991 and 1992), Webster (1992a and b), Lowenstern (1994), Williams et al. (1995), Cline (1995), Webster (1997), Xiao et al. (1998), Frank et al. (1998) and Heinrich et al. (1999), and were recently discussed in a special session at the Geological Association of Canada-Mineralogical Association of Canada annual meeting (Rowins and Williams-Jones, 2003). Overall, these studies indicate that zoned magma chambers containing mixed mafic and felsic melts with an aggregate water content of ca. 4 weight percent and crystallizing at about 1 kilobar pressure (ca. 4 km depth) represent optimal parental systems for large-scale, high-grade porphyry copper mineralization.

On a more regional scale, several studies, e.g., Sillitoe (1972), Clark et al. (1976), Gustafson (1979), Titley and Beane (1981) and Hedenquist and Lowenstern (1994), linked porphyry mineralization to the magmatic evolution of ensialic and ensimatic convergent plate margins, the loci of subduction of oceanic lithosphere. Clark (1993) examined the environments of formation and anatomies of porphyry copper deposits of widely variable size, employing the evolutionary history of the El Salvador deposit (Gustafson and Hunt, 1975) as a template for comparison. He concluded that, although physio-chemical conditions, e.g., pressure, magmatic H₂O content, etc., are critical factors in ore generation, there is no global correlation between the size of deposits and such criteria. It is therefore implicit that metallogenetic factors outweigh the ore-genetic, i.e., metallogenically fertile terrain can generate large deposits even if ore-genetic conditions are not optimal.

Metal concentration by supergene processes

The effects of atmospheric oxygen and meteoric water on the oxidation, leaching and enrichment of ore metals in the superficial subaerial environment have been appreciated for at

least a century: e.g., Emmons (1901), Kemp (1905), Graton (1913), Emmons (1913 and 1917), Anderson (1955), Anderson (1982) and Titley (1995). Indeed, such supergene processes were a prerequisite for the initiation of large-scale porphyry copper mining in Arizona and Chile. These studies recognize an overall zoning from leached to oxide to sulphide facies with increasing depth, but the anatomy of supergene profiles has rarely been as well documented as that of the associated hypogene protolith mineralization. Whereas leached capping characteristics, described in detail by Anderson (1982), are extensively used as an exploration tool, mineralogical zoning in the underlying oxide ores have only recently been studied (Chávez, 2000; Cuadra and Rojas, 2001) and few comprehensive studies of secondary sulphide ores have been carried out since the work of Sillitoe and Clark (1969).

Several studies of supergene enriched blanket have led to the recognition of the importance of interrelated phenomena such as uplift-erosion cycles, geomorphology and climatic changes as influences on ore mineralogy and the overall economic value of supergene deposits (e.g., Clark et al., 1967a and b; Sillitoe et al., 1968; Alpers and Brimhall, 1988; Clark et al., 1990a; Sillitoe and McKee, 1996; and Mote et al., 2001a). The implications of these relationships extend beyond the field of economic geology and provide evidence for the tectonic evolution of continents and of global climates (e.g., Vasconcelos et al., 1994; Gregory-Wodzicki, 2000).

1.2. Scope of investigation

The Cerro Colorado porphyry copper (-molybdenum) deposit, originally developed by Rio Algom Ltd. and now operated by BHP Billiton, has been mined since 1994. It incorporates a supergene reserve of 228 Mt at 1.0 percent Cu and is the largest operating copper mine within the Paleocene- to earliest-middle Eocene porphyry belt of northern Chile (Fig. 1-1). The deposits of

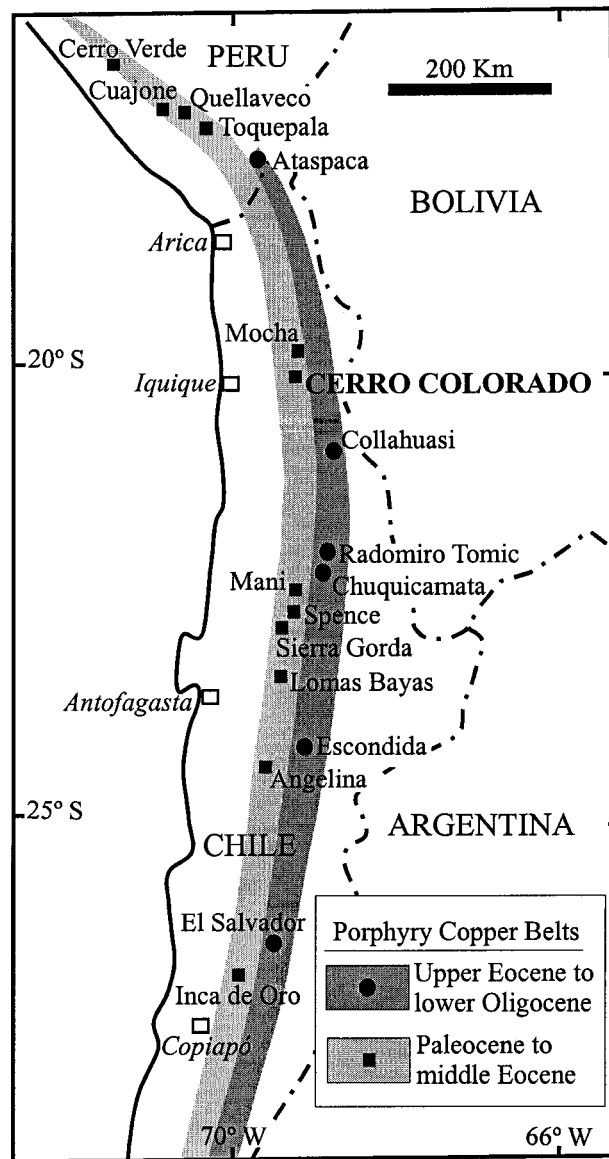


Fig. 1-1:
The location of Cerro Colorado and other Cenozoic copper deposits and prospects in northern Chile and southern Peru cited in the text.

this belt have been less studied than the generally larger upper Eocene to lower Oligocene deposits further east (Fig. 1-1). However, the large distances separating the deposits of the older Paleogene belt have stimulated the search for concealed deposits north and south of Cerro Colorado. Such a strategy came to fruition in mid-1996, when Rio Algom Ltd. discovered the buried Spence porphyry copper deposit containing a ca. 350 Mt supergene resource at 1.0 percent Cu (Sillitoe, 2000).

Clarification of the anatomy and evolution of both hypogene protore and supergene ore at Cerro Colorado could be useful in the search for similar mineralization in the same belt. Further, such studies, in conjunction with documentation of broadly coeval deposits in southern Peru (Clark et al., 1990a, b), provide a basis for interpretation of a key stage in the overall metallogenesis of the Central Andes. Thus, a proposal for research on the hypogene and supergene evolution of the Cerro Colorado was submitted to Rio Algom on March 27, 1996 and was formally accepted in June 14, 1996, leading to an initial four month field programme in July-October, 1996. Preliminary field mapping indicated that the supergene profile was exceptionally complex, incorporating several leached horizons, a feature previously unrecognized. Further, the underlying hypogene protore proved to be unusual in an Andean context, in that chalcopyrite mineralization is largely associated with intermediate argillic alteration, which had overprinted barren potassic alteration. Field and laboratory research was therefore designed to achieve the following goals:

1- to characterize the hypogene alteration and mineralization with emphasis on: (a) the spatial and temporal relationships of the ore-bearing intermediate- to advanced argillic alteration facies, and (b) the environment of formation of the extensive but sulphide-free potassic alteration.

2- to clarify the anatomy and evolution of the supergene orebody, emphasizing: (a) the duration of the supergene processes and the causes of the complexity of the profile, (b) the

metallogenetic implications of the supergene profile through comparison with those in other deposits in the Central Andes.

1.3. The scientific contributions of this study

Research at Cerro Colorado has resulted in several distinct contributions. These are:

1- documentation of the Early Stage, sulphide-free, potassic-sodic, hypogene alteration and evaluation of the reasons for its extensive development at Cerro Colorado. It is shown that such a barren or poorly mineralized “core” or “root” is a common feature in many porphyry deposits;

2- definition of a prograde thermal evolution during the transition from the Early to the Main Stages of hypogene mineralization. It is argued that such an evolution is probably a common feature in hydrothermal environments, but is widely masked by subsequent overprinting;

3- demonstration of the simultaneous development of the Main Stage intermediate- to advanced argillic alteration zones. Such a relationship is probably common in porphyry deposits, supporting the overall intimate connection between the porphyry and epithermal environments, but few previous studies have provided adequate supporting paragenetic data. Moreover, there are few published detailed descriptions of intermediate argillic, or “sericite-chlorite-clay”, alteration in porphyry deposits;

4- recognition of the close similarities between the Cerro Colorado protore system and the geothermal environment, with an analysis of the effects of such an environment on the nature and style of mineralization;

5- definition of a protracted supergene history at Cerro Colorado, involving episodes of oxidation and leaching which generated a complex leached and enriched blanket. No previous study of a supergene profile has provided such an integration of field and mineralogical relationships with $^{40}\text{Ar}/^{39}\text{Ar}$ incremental-heating age data; and

6- definition of a single Cenozoic supergene metallogenetic epoch in northern Chile, inferred to have been initiated by a “proto-Humboldt Current” at the onset of Incaic orogeny in the late Eocene.

1.4. Thesis organization

This dissertation is cast in a Manuscript Format which fulfills the requirements of the Queen’s University School of Graduate Studies and Research. Two major manuscripts were prepared for publication and form the body of this thesis. Their titles and brief outlines are listed below. At the time of submission, chapter 3 has been published in a major international journal.

Chapter 2:

Bouzari, F., and Clark, A.H., Prograde evolution of a major porphyry copper system: the Cerro Colorado protore, I Región, northern Chile. to be submitted to *Economic Geology*.

This paper describes the evolution of the hypogene protore at Cerro Colorado. Salient characteristics of the Early, Main, Transitional and Late Stages of alteration-mineralization are interpreted on the basis of field, petrographic, geochronological, fluid inclusion and mass balance studies. These relationships are compared with those in other major porphyry deposits and geothermal systems.

Chapter 3:

Bouzari, F., and Clark, A.H., 2002, Anatomy, evolution, and metallogenic significance of the supergene orebody of the Cerro Colorado porphyry copper deposit, I Región, northern Chile. *Economic Geology*, v. 97, p. 1701-1740.

This paper illustrates the anatomy of the supergene profile on the basis of newly prepared cross sections, and documents its evolution on the basis of $^{40}\text{Ar}/^{39}\text{Ar}$ dating of alunite group

minerals. The significance of these data for the overall supergene metallogeny of the central Andes is discussed.

These two chapters, forming the core of the thesis, are followed by a brief *Conclusions* section, summarizing the major outcomes of the research.

PROGRADE EVOLUTION OF A MAJOR PORPHYRY COPPER SYSTEM: THE CERRO COLORADO PROTORE, I REGIÓN, NORTHERN CHILE

2.1. Abstract

The middle Eocene hypogene protore underlying the supergene orebody of the Cerro Colorado porphyry Cu (-Mo) deposit exhibits features that are not commonly recorded in porphyry systems. Early Stage alteration of Upper Cretaceous andesite generated an extensive, 8 km², blanket of pervasive biotite (≤ 35 modal percent)-albite (≤ 40 percent)-magnetite (≤ 3 percent) alteration entirely lacking sulphide minerals. Seventy percent of the chalcopyrite stockwork mineralization was emplaced during the subsequent Main Stage in association with, at decreasing depths, quartz-albite, sericite-chlorite-clay ("SCC" of Sillitoe and Gappe, 1984), quartz-sericite-clay (QSC) and andalusite-diaspore-pyrophyllite assemblages. The subsequent Transitional Stage phyllic, i.e., quartz-sericite-pyrite \pm tourmaline, alteration was associated with the emplacement of molybdenite-rich breccia bodies. Late Stage pyrite veins cut all alteration assemblages. The occurrence of undumortieritized tourmaline veinlets cutting Main Stage andalusite-diaspore assemblages confirms that much of the advanced argillic alteration took place prior to the Transitional Stage.

Early Stage alteration was generated by non-boiling, cool ($\leq 380^{\circ}\text{C}$), low-salinity (≤ 8 wt percent NaCl equiv.) fluids which added K, Na, Mg, Fe^{+2} , Cl, F and water to the host andesite. The initial Main Stage fluids, boiling at a paleo-depth of ca. 2.5-3.0 km, were up to 160°C hotter ($T_h \leq 544^{\circ}\text{C}$) and highly saline (≤ 52 wt. percent NaCl equiv.). As these fluids rose, they cooled (to $\leq 320^{\circ}\text{C}$), were diluted (to ≤ 37 wt percent NaCl equiv.), deposited sulphides and leached considerable K, Na, Ca, Mg, Fe^{+2} and Cl from the host rocks, quasi-simultaneously generating

intermediate- to advanced argillic alteration facies. Pressure estimates require that low-density ($\leq 0.3 \text{ g/cm}^3$), and thus more acidic, fluids were responsible for the formation of the QSC and shallow advanced argillic alteration facies. Subsequent phyllic alteration was similarly generated by boiling fluids which were initially hot ($T_h \leq 486^\circ\text{C}$) and saline ($\leq 47 \text{ wt.}\%$) at depth, but cooler ($\leq 334^\circ\text{C}$), dilute ($\leq 8 \text{ wt.}\%$) and vapour-dominated at shallower levels. Terminal Stage pyrite veins were again emplaced by high-temperature (ca. $\leq 450^\circ\text{C}$), but low-salinity ($\leq 8 \text{ wt.}\%$) fluids.

Therefore, following a major prograde transition from the Early to the Main Stage, each alteration episode was generated by a pulse of high-temperature fluid which cooled and was diluted as it rose. It is argued that such changes in fluid characteristics and alteration mineralogy are likely to occur in any hydrothermal system involving rising fluids in the near-surface environment, as is well documented in numerous geothermal fields and a few porphyry-epithermal centers, e.g., Far Southeast-Lepanto, Luzon (Hedenquist et al., 1998). It is proposed that the initial stages of alteration at Cerro Colorado developed under conditions similar to those in non-explosive geothermal systems, in which rising hydrothermal fluids cool and disperse laterally in the shallow crust. Whereas the prograde transition to a mineralized porphyry environment may have been stimulated by melt incursion in the parental magma chamber, an early geothermal stage and subsequent increase in ore-fluid temperatures may be inherent concomitants of the emplacement of plutons in the cool, shallow crust. Thus, large, barren potassic zones are sparsely documented elsewhere, e.g., El Salvador, Chile, and Sierrita-Esperanza, Arizona, but evidence of an early prograde history may have been obliterated in most porphyry deposits.

2.2. Introduction

Porphyry copper deposits have traditionally been considered the epitome of magmatic-hydrothermal mineralization, generated fundamentally through the exsolution of metal-rich brines

from bodies of felsic magma cooling and crystallizing under essentially isobaric conditions in the shallow crust. Whereas the involvement of non-juvenile, meteoric waters in the later stages of hydrothermal activity has been widely recognized through stable isotope and fluid inclusion studies, and analogies repeatedly drawn with meteoric water-dominated, and almost universally barren, geothermal systems, most interpretations of porphyry mineralization have been based on the assumption of a retrograde thermal evolution paralleling the cooling trajectory of the parental magma. In more detail, the paragenetic relationships of porphyry systems have formed a rigorous basis for thermodynamic and experimental modeling of the sequential partitioning from melt to aqueous fluid of the ore-metals and the anions Cl and B in the course of the retrograde-, or second-boiling process (Candela, 1979a, b; Cline and Bodnar, 1991). This ordered history of metal concentration is exemplified by the El Salvador deposit, Chile, comprehensively documented by Gustafson and Hunt (1975), which provides a remarkably reliable guide to the life-histories of porphyry systems globally (Clark, 1993).

In the present contribution, however, we describe a large-scale porphyry deposit, the prototype for the supergene orebody of the Cerro Colorado Cu deposit, northern Chile, which departs in several key respects from the El Salvador “template”. In particular, the hydrothermal system incorporates an extensive but barren K-silicate alteration zone which developed at low temperature prior to a prograde transition to the development of mineralized hydrolytic alteration. The latter exhibits quasi-simultaneous, vertical zonation from intermediate- to advanced argillic alteration. Both features bear strong resemblance to those of numerous geothermal systems, and it is argued that Cerro Colorado represents a hybrid center with characteristics of both mineralized porphyry deposits and unmineralized geothermal fields.

2.3. Geologic Setting

The Cerro Colorado ("Red Hill") porphyry copper (-molybdenum) deposit is located in Tarapacá Province, I Región, Chile, at Latitude 20° 2' 41" S and Longitude 69° 15' 35" W, and 120 km east of Iquique (Fig. 2-1a). The open-pit mine, initiated in 1994 by Rio Algom Ltd. and now operated by BHP Billiton Base Metals, exploits a complex supergene profile with reserves of 228 Mt at 1.0 percent Cu. The preserved hypogene protore, with grades of 0.4-0.5 percent Cu and a resource approximately double that of supergene ore, lies at depths greater than 250-300 m.

Copper mineralization at Cerro Colorado has been known for many years, as is evidenced by old workings and a 200 m-long exploration adit of unknown age in an embayment of Quebrada Parca, east of Cerro Colorado summit (Fig. 2-2). Normina, a United States-Chile group, drilled four widely spaced holes south of Cerro Colorado summit during 1962-1963. Two of these, drilled on the margins of a mineralized intrusive/breccia unit located in the center of the deposit, intersected only weak and thin supergene enrichment. The other two intersected the pyritic fringe of the deposit underlying a leached cap. Exploration in 1975-76 by Sociedad del Cobre de Iquique (Nippon Mines Co.) was focused on phyllic- and supergene altered outcrops and old workings immediately southeast and south of Cerro Colorado, and a grid of 24 holes was completed. During 1982, Riochilex, a subsidiary of Rio Algom, drilled 38 holes, approximately within Nippon's grid area, and delimited the Main Zone orebody lying largely east and southeast of Cerro Colorado (A. Cepeda, G.M. Ditson and D.G. Mato, unpublished report to Compañía Minera Riochilex Ltda., Santiago, 1982). The focus of exploration and condemnation drilling subsequently moved to the west and southwest of Cerro Colorado. From 1987 to 1992, 59 holes were drilled, leading to the discovery of a potential extension of the supergene orebody (T.E. Warren, unpublished report to Rio Algom Exploration Ltd., Toronto, 1992). This was tested by 61 holes in 1994, thereby delimiting the West Zone (E.A. Campbell, unpublished report to Compañía Minera Riochilex S.A., Iquique, 1994). The Main, or East, Zone is separated from the

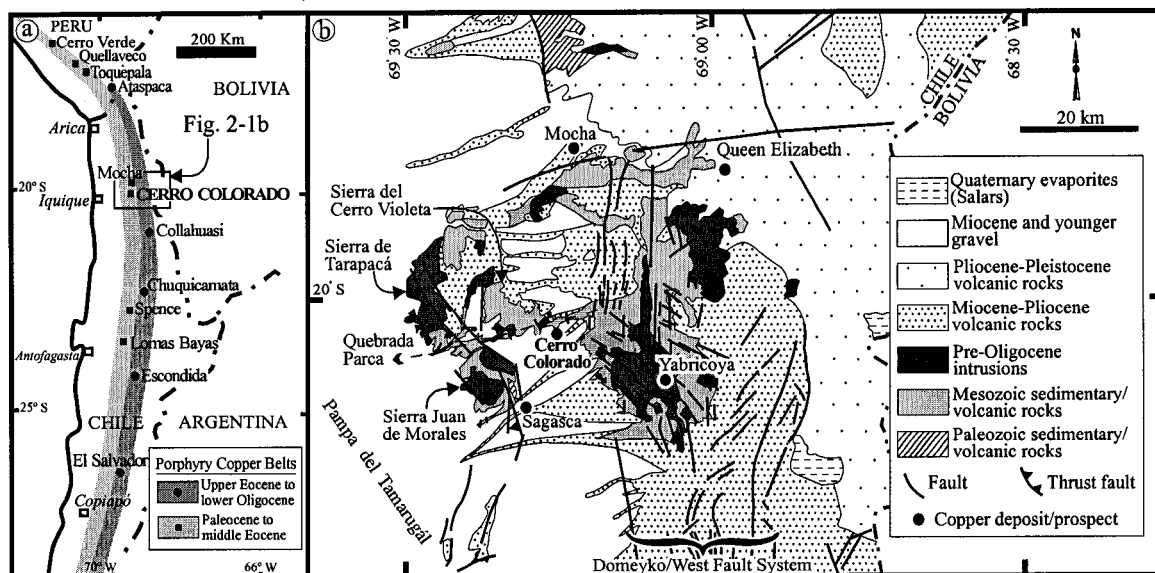


Fig. 2-1:

(a) Location of Cerro Colorado and selected other Cenozoic copper deposits and prospects in the two major porphyry belts of northern Chile and southern Peru. (b) Simplified regional geologic map of the Cerro Colorado area showing north-west-striking faults bounding the Sierra Juan de Morales, Sierra de Tarapacá and Sierra del Cerro Violeta horsts. The Paleozoic-Mesozoic basement from Sagasca to Mocha has been uplifted between these faults and the main upper Eocene-lower Oligocene Domeyko Fault System. Thick gravels, forming the Pampa del Tamarugál surface, cover the basement rocks west, north and south of this uplifted terrain (after Thomas, 1967; Galli, 1968; and Servicio Nacional de Geología y Minería, Chile, 1982).

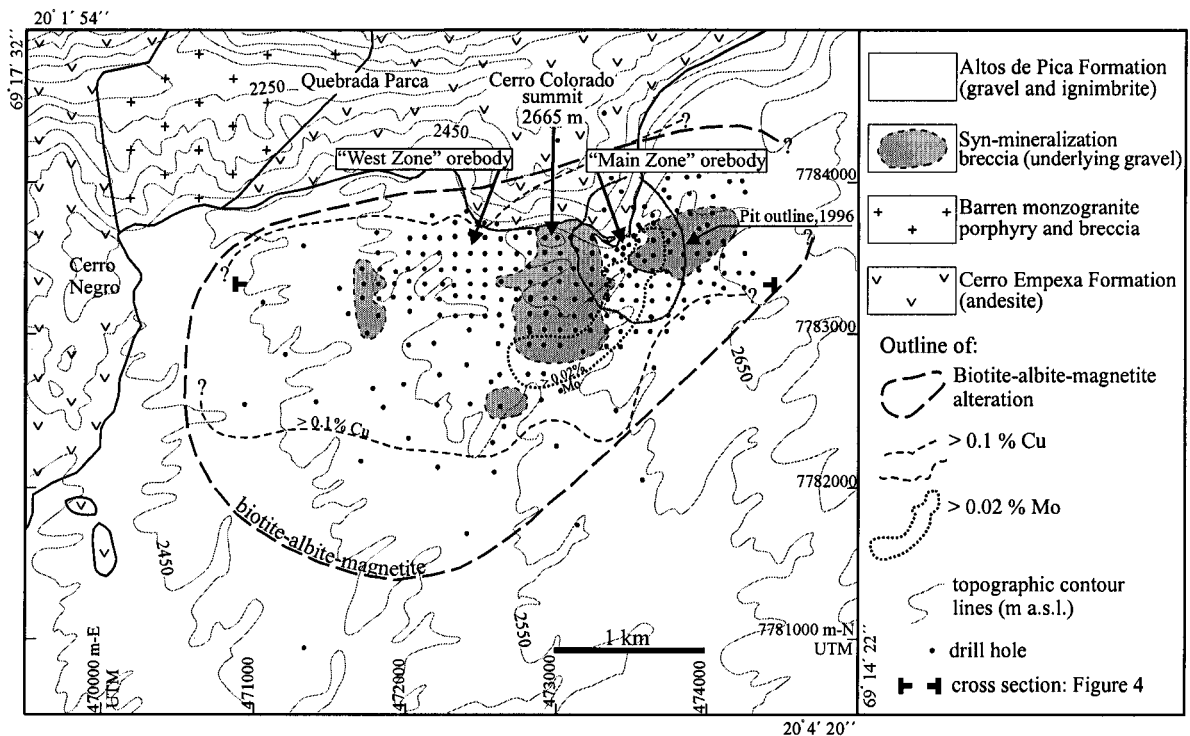


Fig. 2-2:

Pre-mine topographic and geologic map of the Cerro Colorado area showing Upper Cretaceous andesite intruded by unmineralized Upper Cretaceous (-Paleogene) monzogranitic rocks and lower Eocene mineralized breccia bodies, and partially covered by Miocene gravels and ignimbrite. Early Stage alteration of the andesite generated a large barren biotite-albite-magnetite zone, but copper deposition occurred subsequently in the areas affected by intense Main Stage intermediate -to-advanced argillic alteration, i.e., inside the 0.1% Cu grade contour. Main Stage pyrite, up to 10 percent, forms a halo outside the central copper zone. The highest concentrations of molybdenite in the Main Zone occur at the margins of breccia bodies and in contiguous andesite. Rocks exposed on Cerro Negro and along the south wall of Quebrada Parca are neither mineralized nor altered, except in the embayment north of Cerro Colorado summit. See Fig. 2-5 for cross-section (after Thomas, 1967; Galli, 1968; A. Cepeda, G.M. Ditson, and D.G. Mato, unpublished report for Compañía Minera Riochilex Ltda., Santiago, 1982; T.E. Warren, unpublished report for Rio Algom Exploration Inc., Toronto, 1992; and E.A. Campbell, unpublished report for Compañía Minera Riochilex S.A., 1994).

West Zone by a lower-grade section, but the ultimate open-pit will incorporate both (Fig. 2-2). The locations of drill-holes are shown in Appendix 1.

Cerro Colorado lies within the Paleocene to earliest-middle Eocene porphyry copper belt of the Central Andes (Fig. 2-1a). Although greatly subordinate to the upper Eocene-lower Oligocene, or “Domeyko Fault” belt, in northern Chile (Sillitoe, 1988), this becomes the dominant copper-bearing zone in southern Peru, where it is represented by an array of giant deposits from Toquepala to Cerro Verde (Fig. 2-1a, Clark et al., 1990b). The Cerro Colorado deposit crops out at a mean elevation of 2600 m a.s.l. on an upper extension of the low-relief Pampa del Tamarugál which constitutes the piedmont of the Cordillera Occidental (Figs. 2-1b, 2-2 and 2-3a). The host rocks are dominated by the Cretaceous Cerro Empexa Formation, a succession of subaerial andesite, tuff and agglomerate, which is gently folded and overlies with angular unconformity the marine to subaerial sediments and volcanic sedimentary strata of the Upper Jurassic Chacarilla Formation (Galli, 1968; Thomas, 1967). These were intruded by numerous plutonic to hypabyssal stocks during the Late Cretaceous to Early Tertiary interval (Galli, 1968; Thomas, 1967), causing restricted hydrothermal alteration and contact metamorphism.

The Paleogene and older units are overlain unconformably by the Miocene Altos de Pica Formation, which comprises two piedmont gravel units separated by an ash-flow tuff member (Figs. 2-1b and 2-2) 19.2 Ma in age (Bouzari and Clark, 2002). Northwest-trending faults (Fig. 2-1b) are the dominant structures, delimiting horsts of the pre-Andean, Upper Paleozoic basement and Mesozoic strata (Galli, 1968). Uplift related to these structures probably commenced during the late Eocene Incaic orogeny and played a significant role in the exposure and weathering history of the Paleocene to lower Eocene copper mineralization in this terrain (Bouzari and Clark, 2002). Any porphyry centers to the north and south of this uplifted block would be buried by

thick gravel (Fig. 2-1b), resulting in the large gaps between Mocha and Toquepala to the north, and Cerro Colorado and Spence to the south (Fig. 2-1a).

2.4. Host Rocks

The Cerro Colorado deposit is hosted by both volcanic units and intrusive bodies. Extensive hypogene and supergene alteration has disguised or even obliterated the original mineralogy and texture of the host rocks and hence detailed intrusive relationships cannot be determined. The main host rocks are volcanic strata of the Cerro Empexa Formation, which are intruded by several intrusive-hydrothermal breccias and dikes, delimited on the pre-mine surface (Fig. 2-2) and open pit benches (Fig. 2-3a), and in drill holes (Appendix 1).

Cerro Empexa Formation

These subarial volcanic rocks host over 70 percent of the mineralization. This Cretaceous sequence includes a succession of at least four units in the mine area (Fig. 2-3b), relatively unaltered portions of which crop out on the main south wall of Quebrada Parca and in the embayment immediately north of the deposit (Fig. 2-2). A dacitic fluidal unit, mapped by A. Cepeda, G.M. Ditson and D.G. Mato (unpublished report to Compañía Minera Riochilex Ltda., Santiago, 1982), is the lowest exposed unit in the embayment, an area now covered by mine dumps. This is overlain by ca. 100 m of coarse volcanic breccia (Fig. 2-3b) with a magmatic matrix dominated by plagioclase and hornblende; clasts are similar to the matrix but some contain a higher quartz content. A porphyritic andesite (Fig. 2-4a) overlies the breccia (Fig. 2-3b) and comprises phenocrysts of plagioclase and hornblende of variable size with rare quartz in a fine-grained matrix similar in mineral assemblage but commonly with microlitic texture. Titaniferous magnetite (ca. 1 percent), with a pinkish tint in reflected light, is disseminated in the matrix of the andesite and commonly forms microphenocrysts with lamellae of rutile. The upper contact of the

Fig. 2-3:

Field photos of host-rocks at Cerro Colorado. (a) The east wall of the Main Zone pit, looking east from the former summit of Cerro Colorado in July 1996, showing andesites of the Cerro Empexa Formation intruded by the Eastern Breccia, in turn cut by the altered hornblende-plagioclase porphyry dike. These units were later uplifted, eroded and covered by the gravels and ignimbrite of the Miocene Altos de Pica Formation. High elevations of the Cordillera Occidental can be seen at the far, eastern, distance. (b) Strata of the Cerro Empexa Formation striking ca. N40°W and dipping ca. 15° to the southwest, looking south from the floor of Quebrada Parca (ca. 2290 m a.s.l.) west of the embayment (i.e., north of the West Zone). The lower part of the sequence is composed of volcanic breccia (1) overlain by fine-grained porphyritic andesite (2) and dacitic lapilli tuff (3). These are covered by Miocene ignimbrite and gravel (4). A mine dump (pale) on the western slope of Cerro Colorado summit is visible at the top (ca. 2600 m). (c) Altered hornblende-plagioclase porphyry dike (between dashed lines) intruding the Eastern Breccia body. Abundant pyrite veins fill fractures in the dike and are coated by supergene chalcocite. Oxidation of these permeable veins to hematite caused the darker colour of the dike relative to the surrounding breccia. Main Zone, east wall of the pit (2520 m).

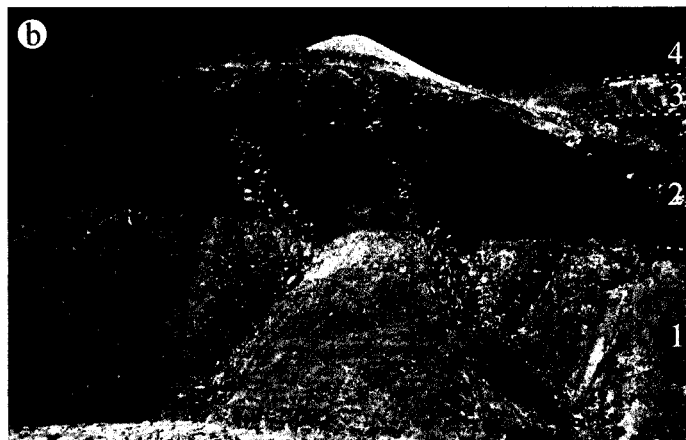
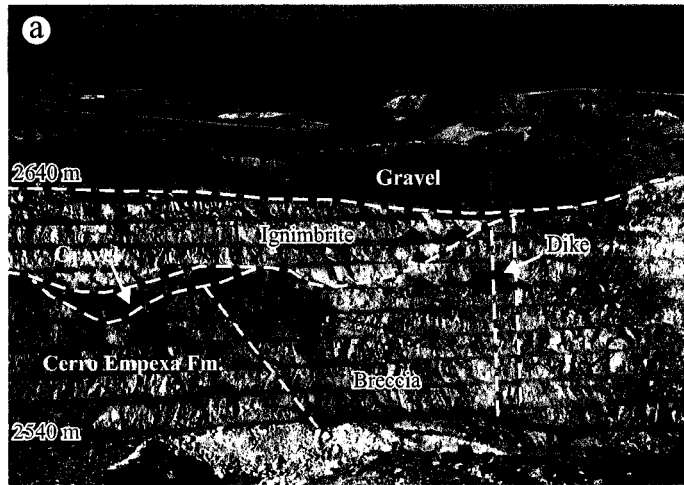
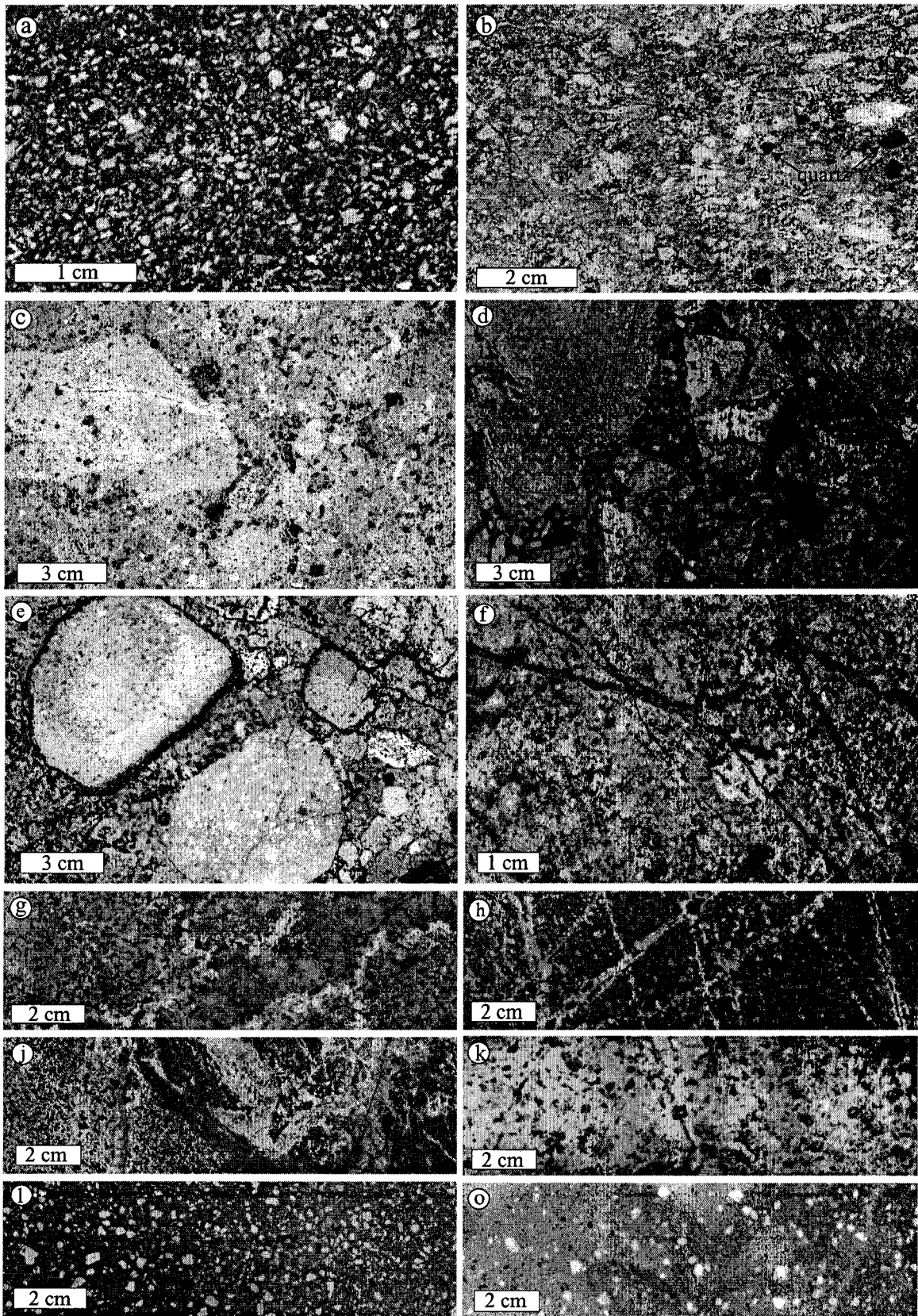


Fig. 2-4:

Photos of hand-samples of host-rocks at Cerro Colorado. (a) Characteristic unaltered, porphyritic andesite shows plagioclase and amphibole phenocrysts in a fine-grained matrix. Sample is from south wall of Quebrada Parca, immediately west of the embayment (Sample # QP 27, ca. 2400 m). (b) Lapilli tuff of the upper parts of the Cerro Empexa Formation showing lensoidal fragments with abundant quartz phenocrysts (# 225, south wall of the pit, 2580 m). (c) Eastern Breccia of the Main Zone showing variable-sized fragments in a fine-grained altered matrix. Phyllic and supergene alteration have modified the rock texture but remanent plagioclase crystals are commonly preserved in the matrix and clasts. Veins are restricted to the clasts. Dark disseminated spots are supergene hematite after pyrite (# 251, east wall of the pit, 2550 m). (d) Tourmaline-cemented Eastern Breccia with disseminations and veinlets of pyrite (# 198, east wall of the pit, 2530 m). (e) Sample from marginal part of the Eastern Breccia showing subrounded clasts in a rock-flour matrix (# 134, east wall of the pit, 2540 m). (f) Sample from lower part of the Eastern Breccia shows micro-breccia texture and contains abundant through-going quartz veins. Rock is intensely altered and is composed of quartz and sericitized plagioclase clast in a fine-grained quartz-sericite-pyrite matrix (# 26-11, 2470 m). (g) Mineralized biotite-quartz-plagioclase porphyry intrusive with abundant altered plagioclase phenocrysts. Dark disseminated mineral is chloritized biotite. A quartz vein with irregular boundaries cuts the rock and hosts chalcopyrite (# 119-17, 2300 m). (h) Barren biotite-quartz-plagioclase porphyry at the deepest levels of the Main Zone (Fig. 2-5a) with abundant fresh plagioclase and biotite phenocrysts. Alteration is restricted to thin veinlets of K-feldspar and sericite (# 83-12, 2110 m). (i) Contact of chilled margin of the barren biotite-quartz-plagioclase porphyry (left) with biotitized and albitized andesite in the deeper level of the Main Zone (# 83-41, 2196 m). (j) Quartz porphyry intrusion from lower slopes of the Cerro Colorado summit with rounded quartz eyes, sericitized matrix and sparse sulphide mineralization (# 4-10, 2408 m). (k) Hornblende-plagioclase porphyry dike rock with abundant phenocrysts of plagioclase (white) and amphibole (dark) in a very fine-grained matrix pervaded by supergene hematite (# 129, east wall of the pit, 2540 m). (l) Typical younger hornblende-plagioclase porphyry dikes with sparse phenocrysts in a very fine-grained quartz-poor matrix. These dikes do not host hypogene alteration or mineralization (# 295, south wall of the pit, 2560 m).

Note that, in all figures, samples collected from mine pit benches are assigned a single number (e.g., # 225) but those from drill cores have two numbers separated by a dashed line (e.g., # 26-11), in which the first number represents the hole number.



volcanic breccia with the overlying porphyritic andesite lies at approximately 2400 m a.s.l. on the south wall of Quebrada Parca (Fig. 2-3b). The uppermost part of the succession exposed on the valley wall is dominated by lapilli tuff (Fig. 2-3b), distinguished by irregularly shaped but commonly lensoidal fragments (Fig. 2-4b). The abundance of quartz phenocrysts reveals a transition to a dacitic composition.

All volcanic units within the deposit are affected by pervasive biotite-albite-magnetite alteration, forming a blackish rock with remanent plagioclase phenocrysts (see below). Fluidal texture is preserved in some locations but distinction between units is rarely possible. However, porphyritic andesite was identified in many drill holes, and is inferred to be the main host rock.

These volcanic strata are gently folded on a regional scale and widely dip at 5 to 35° to the west/southwest (Thomas, 1967; Galli, 1968). A. Cepeda, G.M. Ditson and D.G. Mato (unpublished report to Compañía Minera Riochilex Ltda., Santiago, 1982) mapped the lower dacitic fluidal unit in the embayment (Fig. 2-2) as striking N35°W and dipping 35° SW. Most strata exposed on both sides of Quebrada Parca, however, strike ca. N40°W and dip ca. 15° SW. Therefore, on an east-west cross section through the deposit (Fig. 2-5) the volcanic strata are shown to have an apparent westerly dip of ca. 10°, and the upper and lower contacts of the volcanic breccia unit can be approximately determined in the mineralized zone (Fig. 2-5a). On this basis, it is inferred that much of the West Zone is hosted by porphyritic andesite, whereas both volcanic breccia and porphyritic andesite host the mineralization in the Main Zone.

Breccia bodies

Several intrusive breccias cut the volcanic rocks, exhibiting abrupt contacts and upward-flaring, conical to pipe-like, forms (Figs. 2-3a, and 2-5a). Two major bodies are distinguished by A. Cepeda, G.M. Ditson and D.G. Mato (unpublished report to Compañía Minera Riochilex Ltda., Santiago, 1982). The larger, Western, breccia crops out in the western area of the Main

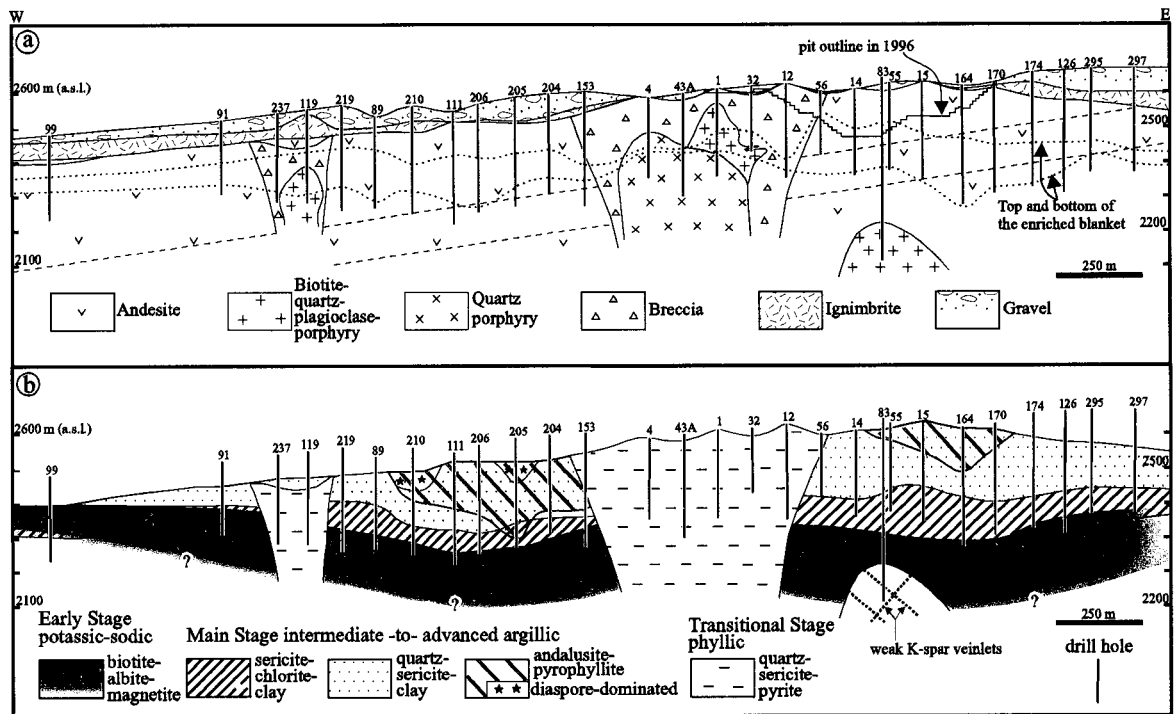


Fig. 2-5:

East-west cross section (see Fig. 2-2) through the Cerro Colorado deposit, showing (a) host rocks and (b) alteration zones. Strata of the Cerro Empexa andesite are the main host of mineralization, but are extensively altered, precluding the distinction of volcanic units (Fig. 2-3b). The approximate boundaries of the andesitic breccia unit are, however, inferred (dashed-lines) on the basis of its strike and dip (N40°W, 15° SW) on the south wall of Quebrada Parca. Early Stage barren biotite-albite-magnetite alteration was intersected in all deep drill holes but its intensity and thickness decrease towards the margins of the deposit. It is overprinted by Main Stage chalcopyrite-bearing alteration-mineralization, which generated a zoned array from deep intermediate (sericite-chlorite-clay)- to shallow advanced (andalusite-diaspore) argillic alteration. Quartz-albite veinlets (not shown) define the base of the sericite-chlorite-clay zone. Note the tabular shape of the orebody, emphasized by the sub-horizontal lower-contact of the sericite-chlorite-clay sub-facies. Transitional Stage phyllic alteration is mainly confined to the breccia bodies, which cut the Main Stage assemblages. A post-mineralization intrusion (see hole 83) hosts veinlets with minor K-feldspar alteration.

Zone, including the summit of Cerro Colorado, and the smaller Eastern Breccia is located in the eastern portion of the Main Zone (Fig. 2-2). In addition, at least two considerably smaller, unnamed, breccia bodies are located to the west and south-west of the Western Breccia (Fig. 2-2). Copper grades are slightly less in the breccia bodies than in the andesite. All breccia bodies are petrographically very similar, with variably sized clasts in an originally igneous matrix, rich in remanent plagioclase phenocrysts, which is itself brecciated and altered to fine-grained quartz, sericite, pyrite and clay minerals (Fig. 2-4c). Barren tourmaline-cemented breccia forms small irregular bodies up to a few meters wide and less commonly occurs as veins within the breccia bodies (Fig. 2-4d).

The breccias contain abundant sub-rounded clasts with well-defined boundaries in the upper levels (Fig. 2-4c), sparse rounded clasts being restricted to the contacts with the country rock (Fig. 2-4e). Veinlets are restricted to the clasts. With increasing depth, however, large clasts and fragments with sharp boundaries become less common and veinlets become throughgoing. Eventually, at the deepest exposed levels, a “micro-breccia” texture is developed (Fig. 2-4f). Much of this is, however, a by-product of pervasive phyllic alteration which has converted plagioclase into fine-grained muscovite, so that quartz grains and less-altered areas resemble clasts.

Biotite-quartz-plagioclase porphyry

Biotite-quartz-plagioclase porphyry constitutes an intrusive body emplaced in both the breccias and the volcanic rocks. It is characterized by uniformly distributed, large, subhedral plagioclase, quartz and biotite phenocrysts in a quartz-plagioclase matrix with accessory titaniferous magnetite (Fig. 2-4g). Within the breccia bodies, it is altered to quartz, sericite, pyrite, chlorite and clays (Fig. 2-4g). The copper grade varies in this unit but is generally less than that of the host breccias. A second, petrographically similar unit intrudes the altered andesite in the Main

Zone, forming a deep stock with an extension to the northeast (Figs. 2-4h, 2-4i and 2-5a). Alteration is here restricted to thin veinlets of K-feldspar with minor chlorite and sericite, and the porphyry is generally fresh and barren. No chemical analyses of these intra- and post-mineralization intrusive rocks are available, but their phenocryst mineralogy implies a dacitic composition.

Quartz porphyry

“Quartz porphyry” is a term applied by A. Cepeda, G.M. Ditson and D.G. Mato (unpublished report to Compañía Minera Riochilex Ltda., Santiago, 1982) to an intrusive unit characterized by rounded β -quartz and subhedral plagioclase phenocrysts in a matrix of microcrystalline quartz and plagioclase (Fig. 2-4j). Among the mineralized igneous rocks at Cerro Colorado, quartz porphyry contains the lowest Cu grades, and in some areas, e.g., below the summit of Cerro Colorado (Fig. 2-5a), it is essentially barren. Hence, it may represent an intrusion emplaced into the breccia bodies after major mineralizing hydrothermal activity.

Hornblende-plagioclase porphyry dikes

A 10-12 m wide, northeast-trending hornblende-plagioclase porphyry dike transects the Eastern Breccia in the Main Zone (Fig. 2-3c). It contains subhedral to euhedral plagioclase and hornblende phenocrysts in a very fine-grained matrix (Fig. 2-4k). Intense phyllic alteration and pyrite veining have destroyed the original texture, generating a mosaic of laminated bodies along the fractures. A series of northwest-trending dikes, most less than 5 m wide, also cuts the breccia bodies and andesite. These are similar to the altered hornblende-plagioclase porphyry dike, but contain sparse, commonly subhedral to anhedral, plagioclase and hornblende phenocrysts in a very fine-grained, quartz-poor matrix (Fig. 2-4l). These dikes do not record any hypogene alteration and mineralization and hence are true post-ore intrusive rocks.

2.5. Alteration and Mineralization

The Cerro Colorado deposit was the locus of multiple alteration and mineralization events. Four major stages of alteration and mineralization are defined: Early; Main; Transitional; and Late. The Main Stage, during which ca. 70 percent of the Cu was deposited, comprises, with decreasing depth, intermediate argillic, quartz-sericite-clay, and advanced argillic assemblages developed both as veins and pervasive alteration zones. Quartz-albite veins form the roots of the Main Stage alteration.

Deep drill holes in the West Zone provide access to hypogene assemblages unaffected by supergene alteration. DDH-83 in the Main Zone attained a depth of 550 m below the pre-mine surface (Fig. 2-5), intersecting the lower part of the hypogene alteration system. The distribution of the hypogene copper sulphide assemblages could not be studied in detail because of the supergene overprint, but remnants of the hypogene silicate assemblages permit reconstruction of the hypogene alteration relationships, even in the intensely leached, near-surface domain (Fig. 2-5b). Hypogene clay assemblages were studied only in very deep drill holes where supergene clays are normally absent. Erosion, however, has clearly removed several hundred meters of the hypogene assemblages (Bouzari and Clark, 2002). Vein crosscutting relationships were recorded at different scales to provide a basis for determination of the sequence of alteration and mineralization episodes. Over 840 core samples and 250 surface pit samples were collected for detailed study, which included examination of rock slabs and thin sections, feldspar staining, cathodoluminescence imaging, and X-ray diffraction and chemical analysis. These, in turn, provided a context for fluid inclusion and mass balance studies.

Early Stage alteration

The Early Stage alteration affected the andesitic rocks of the Cerro Empexa Formation prior to the emplacement of the breccia bodies (Fig. 2-5). This alteration type is characterized by

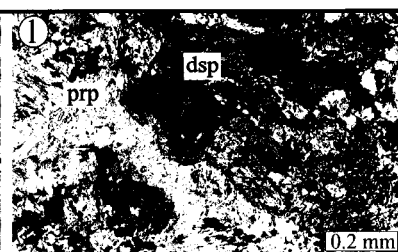
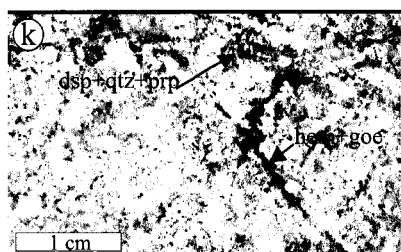
very fine-grained ($< 30 \mu\text{m}$) biotite (≤ 35 modal percent), albite (≤ 40 percent) and magnetite (> 3 percent), with accessory apatite. In hand sample, the altered rocks are black with scattered remnants of white to grayish plagioclase phenocrysts (Fig. 2-6a). Biotite-albite veinlets exist, but the greater part of the alteration is pervasive rather than fracture-controlled. Biotite intensely replaced hornblende, and invades plagioclase phenocrysts along cleavage planes (Fig. 2-6b). Cathodoluminescence image shows that calcic plagioclase phenocrysts with whitish luminescence are replaced by green-luminescent albite or oligoclase reflecting Fe^{+2} (Fig. 2-7a). Albite occurs either as sub-equant grains in the matrix or as laths, inferred to record the Na metasomatism of original plagioclase microlites (Fig. 2-7a). Hydrothermal biotite is magnesian ($\text{Mg}/\text{Mg}+\text{Fe} = 0.62$ to 0.70) and enriched in F (≤ 0.85 wt percent) and Cl (≤ 0.26 wt percent), and exhibits no systematic compositional changes with elevation or lateral position (Table 2-1, Appendix 2). It is similar in composition to secondary biotite from other porphyry systems, e.g., Santa Rita, New Mexico (Jacobs and Parry, 1979). Disseminated, fine-grained, titaniferous magnetite, pink in reflected light, is uniformly distributed in the matrix and is closely associated with biotite, including that replacing plagioclase phenocrysts along cleavage planes (Fig. 2-6b). Magmatic magnetite widely survives as isolated micro-phenocrysts, but the modal content of magnetite increases from ca. 1 percent in the unaltered andesite to over 3 percent in the Early Stage alteration. The hydrothermal magnetite plausibly formed as a result of the conversion of hornblende to biotite but also, as is shown below, reflects Fe metasomatism. The sparsity of veinlets in this facies indicates that Early Stage alteration was not accompanied by major fracturing.

The biotite-albite-magnetite alteration, mapped from drill hole intersections over an area of 8 km^2 , forms a large body, paddle-shaped in plan and elongated southwest-northeast (Fig. 2-2). The majority of drill holes were stopped in the upper 10-50 m of the alteration zone and its thickness is therefore not known in the center of the orebody, but DDH 83 intersected intensely

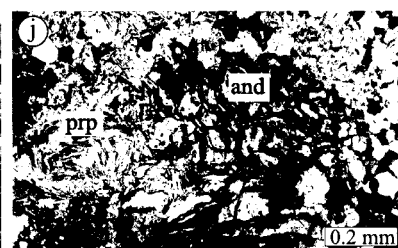
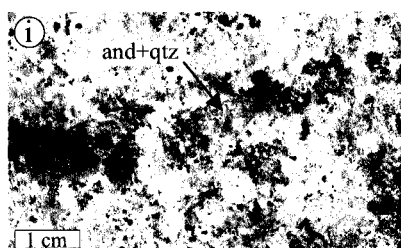
Fig. 2-6:

Representative samples of the Early and Main Stage alteration zones placed in the sequence in which they would be intersected in a vertical profile of the deposit. Photographs of cut drill core (left) are juxtaposed with corresponding photomicrographs (crossed polars). Transitions occur between the five Main Stage sub-facies. Mineral abbreviations for figures 2-6 to 2-10: ab = albite; and = andalusite; apa = apatite; bio = biotite; chl = chlorite; cp = chalcopyrite; dsp = diaspore; goe = goethite; hem = hematite; ill = illite; kao = kaolinite; mag = magnetite; mb = molybdenite; musc = muscovite; pla = plagioclase; prp = pyrope; py = pyrite; qtz = quartz; ser = sericite; sm = smectite; and tm = tourmaline.

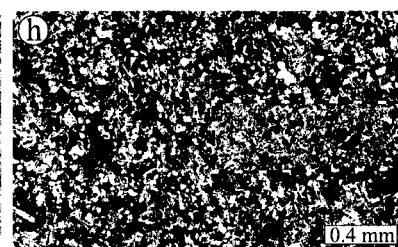
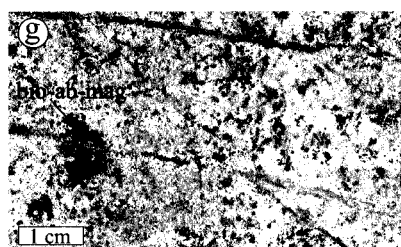
Main Stage



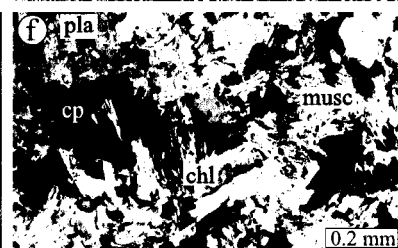
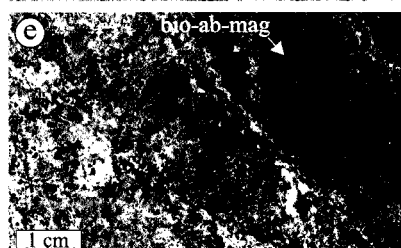
Diaspore-pyrophyllite (DP):
Diaspore with quartz and pyrophyllite occurs in the uppermost-preserved portion of the Main Stage. This assemblage is not recognizable in hand sample but locally occurs as a fine-grained sugary aggregate. Diaspore (>5 %) is associated with only traces of andalusite but abundant supergene clay.
200-30 (2442 m)



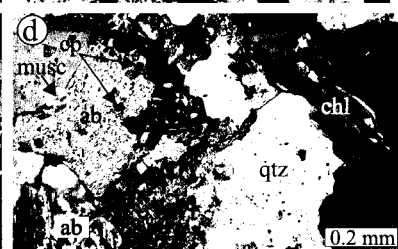
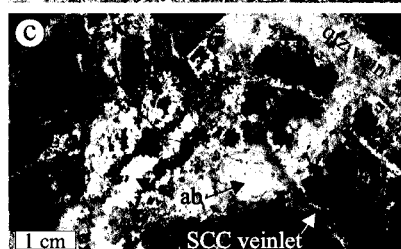
Andalusite-pyrophyllite (AP):
Abundant, disseminated andalusite and quartz with some illite, pyrophyllite and muscovite. Pale-grayish areas along a sulfide vein (now supergene hematite) contain over 80 percent andalusite. Rock is pervaded by green supergene copper silicates.
199-38 (2412 m)



Quartz-sericite-clay (QSC):
Fine-grained quartz, muscovite, illite and smectite give a whitish to pale-yellowish color to the rock. No plagioclase is preserved but the forms of the phenocrysts are visible (dashed line). The pyrite: chalcopyrite ratio is approximately 3:1. A remnant of biotite-albite-magnetite is cut by a quartz-molybdenite vein.
206-38 (2332 m)

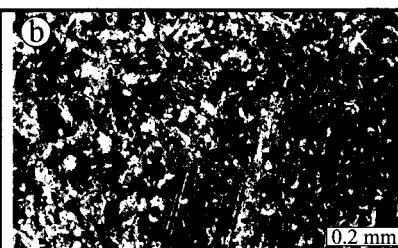


Sericite-chlorite-clay (SCC):
Pervasive SCC alteration has generated a greenish assemblage and deposited abundant sulphides. Early Stage biotite-albite-magnetite is locally preserved. Chalcopyrite is intimately intergrown with chlorite and muscovite and in this sample accounts for over 95 percent of the sulphide. Smectite and muscovite replace plagioclase.
148-10 (2325 m)



Quartz-albite (QA):
Quartz-albite vein with irregular boundary cuts the barren biotite-albite-magnetite alteration in the deepest facies of the Main Stage. No biotite is present in these veins but chlorite intergrown with sulfides and muscovite is commonly observed. Sericite-chlorite-clay veins cut the quartz-albite vein.
83-79 (2275 m)

Early Stage



Biotite-albite-magnetite (BAM):
Andesite has been intensely altered to fine-grained biotite and albite with no sulphide deposition. Magnetite is intimately associated with biotite both in the matrix and along cleavage/twin planes of plagioclase phenocryst. # 83-77 (2278 m a.s.l.)

Fig. 2-7:

Drill core photographs and photomicrographs showing details of alteration and veining: (a) A cathodoluminescence photomicrograph of Early Stage biotite-albite-magnetite alteration showing white-luminescent, more calcic plagioclase (e.g., shown by arrows) replaced by hydrothermal, green-luminescent, more sodic plagioclase. The yellow phase is apatite. (b) Quartz-albite veinlet with banded texture and straight boundaries cuts the barren Early Stage biotite-albite-magnetite alteration and is itself cut and displaced by mineralized sericite-chlorite-clay veinlets (# 83-75 at 2275 m a.s.l.). (c) Barren biotitized and albitized andesite is cut by narrow sericite-chlorite-clay veins at very deep elevations. Smectite (off-white) is the main mineral, replacing disseminated albite and phenocrysts. Chalcopyrite was deposited in these veins in close association with chlorite and muscovite (# 83-77 at 2278 m). (d) A cathodoluminescence photomicrograph of a narrow Main Stage smectite-dominated vein (see Fig. 2-7c) cutting an Early Stage Na-metasomatized plagioclase phenocryst exhibiting green cathodoluminescence. Plagioclase adjacent to the smectite veinlets luminesces orange-red, reflecting Fe^{+3} and hence the higher $f\text{O}_2$ of the Main Stage fluids. The yellow-luminescing mineral is apatite (# 83-59 at 2233 m). (e) A typical sericite-chlorite-clay (SCC) Main Stage veinlet cutting disseminations and veinlets of Early Stage biotite-albite-magnetite alteration. The green central part of the vein is dominated by chlorite and muscovite and the whitish-yellow halo is smectite-rich, with some muscovite and chlorite. Note the lack of sulphide with the biotite-albite-magnetite alteration in contrast to the abundant chalcopyrite associated with the SCC veinlet (# 83-87 at 2304 m). (f) Sericite-chlorite-clay veinlet cut by Transitional Stage quartz-molybdenite veinlet, which lacks a strong alteration halo (# 83-93 at 2319 m). (g) Photomicrograph of a thin Main Stage sericite-chlorite-clay veinlet and its envelopes, showing central muscovite-chlorite zone with chalcopyrite and pyrite (black axial zone) and a halo of smectite, largely after albite, and chlorite with disseminated chalcopyrite. Farther from the vein, disseminated biotite, albite and magnetite survive but some remanent igneous Ca-rich plagioclase phenocrysts are altered to smectite (# 83-72 at 2268 m). (h) Transitional Stage tourmaline veinlets cut andesite which was strongly advanced argillically-altered during the Main Stage, and contains over 15 percent andalusite as disseminations in the matrix with quartz (# 199-38 at 2412 m). (i) A thin Transitional Stage tourmaline veinlet (Fig. 2-7h: yellow arrow) showing unaltered tourmaline adjacent to patches of Main Stage andalusite with some pyrophyllite (See Fig. 2-6 for abbreviations).

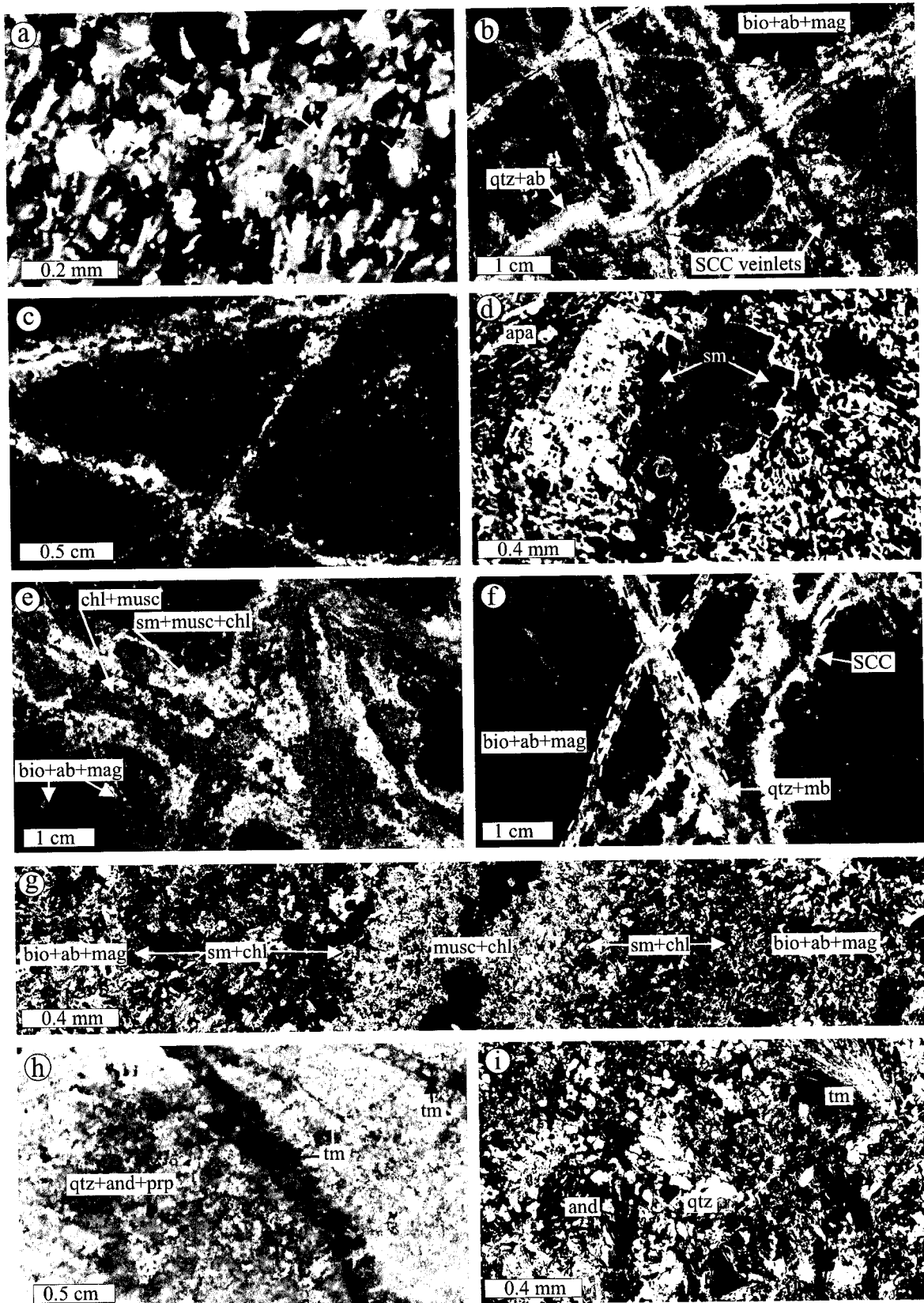


Table 2-1. Representative Compositions of Hydrothermal Phyllosilicate Minerals at Cerro Colorado¹

| Mineral | biotite | | chlorite | | muscovite | | | | | |
|--------------------------------|--------------------------|--------|------------------------|--------|------------------------|--------|--------|----------------------|-------------------|---------|
| Alteration Assemblage | biotite-albite-magnetite | | sericite-chlorite-clay | | sericite-chlorite-clay | | | quartz-sericite-caly | advanced argillic | phyllic |
| Sample number | 83-58 | 204-21 | 83-54 | 206-10 | 83-54 | 210-10 | 204-21 | 206-39 | 204-46 | 198 |
| Elevation (m a.s.l.) | 2231.3 | 2347.6 | 2221.8 | 2299.5 | 2221.8 | 2252.5 | 2347.6 | 2337.2 | 2439 | 2530 |
| SiO ₂ | 38.19 | 37.76 | 27.39 | 28.5 | 45.23 | 45.41 | 45.46 | 45.72 | 45.77 | 44.51 |
| TiO ₂ | 3.8 | 3.19 | 0.1 | — | 0.1 | 0.54 | 0.45 | 0.44 | 0.48 | 0.28 |
| Al ₂ O ₃ | 15.55 | 16.4 | 20.6 | 20.95 | 29.12 | 33.32 | 32.61 | 34.06 | 36.7 | 34.12 |
| FeO (total) | 14.67 | 13.05 | 18.41 | 9.68 | 3.96 | 2.62 | 2.46 | 2.69 | 0.46 | 0.19 |
| MnO | — | 0.13 | 0.28 | 0.42 | 0.1 | — | — | — | — | — |
| MgO | 13.87 | 15.31 | 20.72 | 26.64 | 5.61 | 1.71 | 2.59 | 1.12 | 0.33 | 0.58 |
| CaO | 0.11 | — | 0.14 | — | 0.09 | — | — | 0.1 | 0.06 | — |
| Na ₂ O | 0.13 | — | — | — | 0.13 | 0.42 | 0.37 | 0.37 | 0.54 | 0.33 |
| K ₂ O | 9.19 | 10 | — | — | 10.8 | 10.47 | 10.53 | 10.28 | 10.33 | 9.71 |
| Cl | 0.23 | 0.23 | — | — | 0.05 | — | — | 0.05 | 0.04 | — |
| F | NA | 0.85 | — | — | 0.46 | NA | 0.1 | NA | NA | NA |
| H ₂ O ¹ | 4.00 | 3.64 | 11.82 | 12.18 | 4.17 | 4.43 | 4.38 | 4.44 | 4.50 | 4.29 |
| Total % | 99.74 | 100.56 | 99.46 | 98.37 | 99.82 | 98.92 | 98.95 | 99.27 | 99.21 | 94.01 |
| Si | 5.65 | 5.55 | 5.56 | 5.61 | 6.18 | 6.15 | 6.16 | 6.16 | 6.10 | 6.23 |
| Al | 2.35 | 2.45 | 2.44 | 2.39 | 1.82 | 1.85 | 1.84 | 1.84 | 1.91 | 1.78 |
| Al | 0.36 | 0.40 | 2.48 | 2.47 | 2.87 | 3.47 | 3.38 | 3.57 | 3.86 | 3.85 |
| Ti | 0.42 | 0.35 | 0.02 | 0.00 | 0.01 | 0.06 | 0.05 | 0.05 | 0.05 | 0.03 |
| Fe | 1.82 | 1.61 | 3.12 | 1.59 | 0.45 | 0.30 | 0.28 | 0.30 | 0.05 | 0.02 |
| Mn | 0.00 | 0.02 | 0.05 | 0.07 | 0.01 | 0.00 | 0.00 | 0.00 | 0.00 | 0.00 |
| Mg | 3.06 | 3.36 | 6.27 | 7.82 | 1.14 | 0.35 | 0.52 | 0.23 | 0.07 | 0.12 |
| Ca | 0.02 | 0.00 | 0.03 | 0.00 | 0.01 | 0.00 | 0.00 | 0.01 | 0.01 | 0.00 |
| Na | 0.04 | 0.00 | 0.00 | 0.00 | 0.03 | 0.11 | 0.10 | 0.10 | 0.14 | 0.09 |
| K | 1.74 | 1.88 | 0.00 | 0.00 | 1.88 | 1.81 | 1.82 | 1.77 | 1.76 | 1.73 |
| Cl | 0.06 | 0.06 | 0.00 | 0.00 | 0.01 | 0.00 | 0.00 | 0.01 | 0.01 | 0.00 |
| F | | 0.40 | 0.00 | 0.00 | 0.20 | | 0.04 | | | |
| OH | 3.95 | 3.57 | 16.00 | 16.00 | 3.80 | 4.00 | 3.96 | 3.99 | 3.99 | 4.00 |

H₂O computed by difference. Number of ions calculated on the basis of 24 O, F and Cl for biotite and muscovite and 36 for chlorite. The low total value of sample 198 is due to the very fine-grained nature of the muscovite and possibly to contamination by clay minerals. — : undetected. NA: not analyzed.

biotite-albite-magnetite altered andesite to a depth of 450 m, where it is cut by a post-mineralization intrusion (Fig. 2-5). However, it is evident that both the intensity of biotitization and its downward extent decrease towards the margins of the deposit (Fig. 2-5b). At shallower levels, remnants of biotite-albite-magnetite alteration occur over a wide depth interval in many drill holes (Fig. 2-8) and are even observed in the leached cap of the Main Zone open pit a few meters below the pre-ignimbrite surface. It is therefore inferred that the original Early Stage alteration zone was a saucer-shaped body with horizontal dimensions of ca. 4×2 km and a thickness exceeding 0.5 km. Despite its large volume and intensity, however, Early Stage alteration was not accompanied by sulphide mineralization. Neither pyrite nor chalcopyrite occurs in direct association with disseminated or veinlet biotite or albite: where present, these sulphides are invariably in contact with biotite- and albite- destructive Main Stage minerals.

The extent, and even existence, of propylitic alteration are problematic at Cerro Colorado because only a few reverse circulation holes have been drilled outside of the biotite-albite-magnetite zone (Fig. 2-2). Andesite in these holes and along a 25-km traverse along the south wall of Quebrada Parca revealed essentially uniform saussuritization, i.e., epidote, chlorite, calcite and minor sericite development, possibly related to regional metamorphic or deuteric alteration. A wide pyritic halo which surrounds the deposit is interpreted as the outer facies of the Main Stage assemblages in which pyrite is associated with chlorite and sericite (see below), but this zone lacks the characteristics of propylitic alteration. Therefore, it is concluded that Early Stage potassic-sodic alteration was not accompanied by a propylitic zone similar to those which formed contemporaneously with mineralized potassic alteration, e.g., at Bingham, Utah (Bowman et al., 1987).

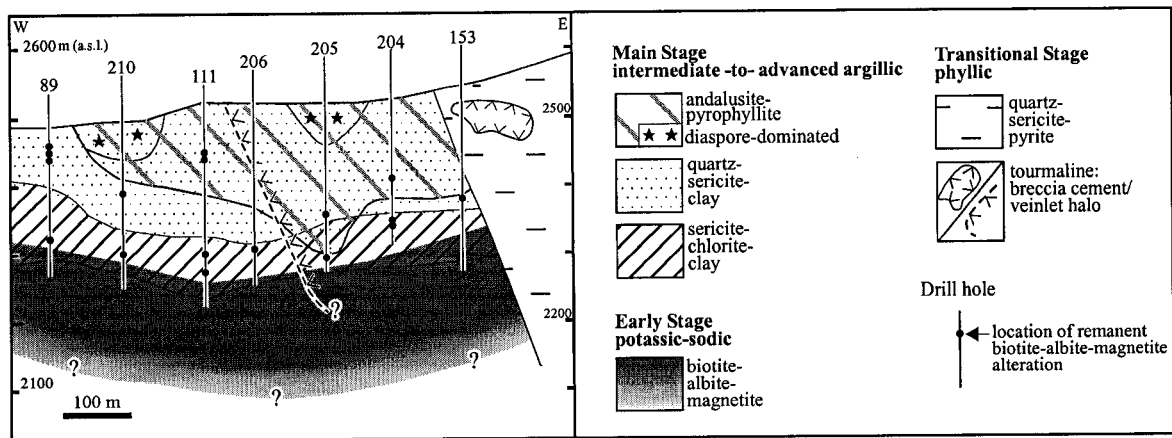


Fig. 2-8:

An enlarged east-west cross-section of part of the West Zone (Fig. 2-5) showing details of the alteration zones. Remnants of the Early Stage biotite-albite-magnetite alteration are preserved throughout the Main Stage zones. Traces of tourmaline occur in association with the phyllic alteration but small bodies of tourmaline-cemented breccia are also common. A halo of tourmaline veinlets overprints the Main Stage assemblages, including areas with intense advanced argillic, i.e., andalusite and diaspore, alteration (see Figs. 2-7h and i, and discussion in the text).

Main Stage alteration-mineralization

The Main Stage alteration overprinted the Early Stage biotite-albite-magnetite alteration prior to the emplacement of the Transitional Stage breccia bodies, and was accompanied by much of the hypogene copper mineralization. This stage generated a >400 m-thick succession of overlapping, hydrothermal assemblages with at least five recognizable sub-facies. With decreasing depth, these comprise a quartz-albite vein system (QA), and sericite-chlorite-clay (SCC), quartz-sericite-clay (QSC), andalusite-pyrophyllite (AP), and diaspore-pyrophyllite (DP) alteration-mineralization zones (Fig. 2-5b). The sericite-chlorite-clay assemblage is equivalent to the intermediate argillic alteration of Meyer and Hemley (1967) and to that documented in many Philippine porphyry deposits (Sillitoe and Gappe, 1984), for example Far Southeast (Hedenquist et al., 1998), and at several other locations, e.g., at Tanamá, Puerto Rico (Cox, 1985); Batu Hijau, Indonesia (Meldrum et al., 1994); Island Copper, British Columbia (Arancibia and Clark, 1996); Pangui area, southern Ecuador (Gendall et al., 2000); Superior District, Arizona (Manske and Paul, 2002); Bingham, Utah (Parry et al., 2002); and Cuajone, southern Peru (A.H. Clark, unpub. data). It is probable that intermediate argillic alteration is more widespread in porphyry copper deposits than its sparse documentation suggests, but has been mapped as sericitic, chloritic, argillic, or even propylitic. The andalusite-pyrophyllite and diaspore-pyrophyllite assemblages, which dominate the upper preserved section (≤ 200 m) of the Main Stage profile, unambiguously represent advanced argillic alteration, while the quartz-sericite-clay facies constitutes a transition between the intermediate and advanced argillic alteration zones.

Quartz-albite sub-facies: Quartz-albite veins cut biotite-albite-magnetite alteration at the base of the Main Stage alteration column. At shallower levels, they are less abundant and widely obliterated by sericite-chlorite-clay veinlets. They are generally less than 1.5 cm thick and composed of quartz and albite with minor, erratically distributed, chalcopyrite and pyrite (Figs. 2-

6c and d). Albite appears milky in hand sample (Fig. 2-6c) and some grains lack albite twinning (Fig. 2-6d). However, both staining and X-ray analysis confirm that albite is the only feldspar in these veins. Quartz and albite are closely intergrown but commonly form alternating bands parallel to the vein-walls (Fig. 2-7b), the veinlet boundaries ranging from irregular (Fig. 2-6c) to planar (Fig. 2-7b). These veins rarely exhibit strong alteration haloes but, in the vicinity of the zone of pervasive sericite-chlorite-clay alteration, albite in the veins and biotite and albite adjacent to the veins are altered to chlorite, sericite and clays, and are intimately associated with sulphides. Chlorite commonly occurs in these veins (Fig. 2-6d), but biotite was not observed at any depth. Towards the sericite-chlorite-clay zone, quartz-albite veins not only exhibit stronger biotite-albite- destructive alteration but are invaded by quartz-poor, sericite-chlorite-clay veinlets (Fig. 2-7b) with abundant sulphides.

Sericite-chlorite-clay sub-facies: The most strongly mineralized alteration facies, this overprints the Early Stage biotite-albite-magnetite alteration (Fig. 2-5b). At the deepest elevations, it comprises veinlets with planar boundaries, but alteration becomes more pervasive at higher levels (Fig. 2-6e). Patches of hydrothermal biotite, however, survive throughout this zone (Figs. 2-6e and 2-8). The alteration exhibits a distinctive medium-green to pale-green colour and a friable aspect in hand sample (Fig. 2-6e). Biotite is replaced by chlorite; and albite by smectite, commonly nontronite and montmorillonite, and muscovite. Chalcopyrite and pyrite are intimately intergrown with chlorite and muscovite (Fig. 2-6f). The pyrite/chalcopyrite ratio nowhere exceeds unity, and only traces of pyrite occur in some zones with over 5 percent chalcopyrite. Chalcopyrite is considerably more abundant than pyrite in patches of chlorite, but the pyrite content increases as fine-grained muscovite and quartz develop. Chlorite is more abundant at lower elevations, gradually decreasing upwards as a result of alteration to fine-grained muscovite. Quartz is a minor constituent at deeper levels, but becomes more abundant as veins and

disseminations in association with fine-grained muscovite in the upper levels of this zone, where illite also increases in proportion. At the deepest levels, where only narrow veins cut the biotite-albite-magnetite alteration, smectite is the dominant mineral replacing albite (Fig. 2-7c). Small amounts of chlorite and muscovite also commonly occur in these veins, and are clearly associated with chalcopyrite (Fig. 2-7c). The phenocrysts exhibit green cathodoluminescence response and are inferred to have experienced Early Stage Na-metasomatism under reducing conditions (see above), whereas the albite adjacent to the smectite veinlets luminesces orange-red (Fig. 2-7d), probably reflecting the higher Fe^{+3} , thus higher $f\text{O}_2$ of the Main Stage fluids. As alteration progresses, the smectite envelopes propagate outward and abundant chlorite and sericite form in the centres of the veins (Figs. 2-7e and g). Smectite is usually difficult to identify in association with pervasive alteration in the matrix, but X-ray analyses of clay separates confirm that it occurs both in the remanent plagioclase phenocrysts and in the sericitic matrix.

The muscovite is strongly depleted in F and Cl relative to the precursor biotite, and halogens were not detected in chlorite (Table 2-1). Chlorite in the upper levels exhibits very weak green pleochorism and is considerably depleted in FeO and enriched in MgO relative to that at lower elevations. Muscovite is enriched in FeO (> 2.0 wt. percent) and MgO (up to 5.6 wt. percent) at the expense of Al_2O_3 (Table 2-1). The highest concentrations of FeO and MgO in muscovite commonly occur at the lower elevations of this zone. All titaniferous magnetite grains have been largely oxidized to hematite and rutile. This, in addition to the rutile formed through replacement of hornblende by biotite in the Early Stage and in the alteration of biotite to chlorite, has resulted in the generation of over 1 percent rutile within the deposit. Thus, this mineral may have exploration and economic importance, as suggested previously for porphyry deposits (Williams and Cesbron, 1977; Force et al., 1980; Czamanske et al., 1981).

Quartz-sericite-clay sub-facies: Sericite-chlorite-clay alteration is gradually supplanted by quartz-sericite-clay assemblages at the higher elevations of the Main Stage domain (Fig. 2-5b). These impart a white to yellowish-gray colour (Fig. 2-6g) and, where unaffected by supergene argillic alteration, increased hardness to the rock. The base of this zone is delimited at the level where chlorite becomes unstable and is reduced to less than 5 percent of the alteration assemblage. Quartz concomitantly becomes the dominant phase (≤ 35 modal percent), occurring as very fine-grained, equigranular aggregates intergrown with muscovite and illite (Fig. 2-6h). Illite (>25 modal percent) is the dominant clay phase, followed by smectite. Plagioclase phenocrysts have been totally altered to muscovite and clay, but their outlines are preserved locally (Fig. 2-6h). The MgO and FeO contents of the muscovite are lower than in the underlying sericite-chlorite-clay zone (Table 2-1). Pervasive alteration and quartz flooding have destroyed most original textural relationships, but patches of biotite-albite-magnetite alteration, commonly a few mm in diameter, are widely observed (Fig. 2-6g). Both chalcopyrite and pyrite are intergrown with quartz and sericite, but are generally completely or partially replaced by chalcocite or hematite. However, where the supergene overprint is weak, the pyrite/chalcopyrite (+chalcocite) ratio exceeds 3:1. This alteration is distinguished from Transitional Stage phyllic (i.e., quartz-sericite-pyrite) alteration by its significantly lower proportion of pyrite and the absence of disseminated tourmaline and molybdenite (see below).

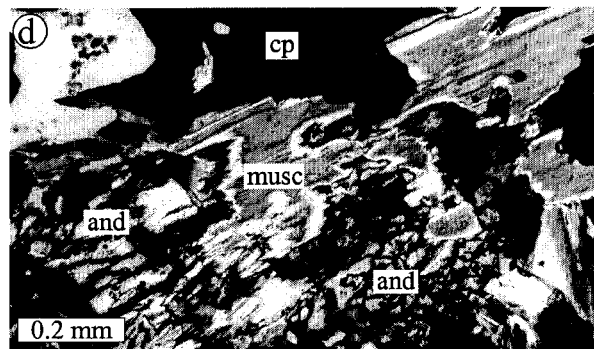
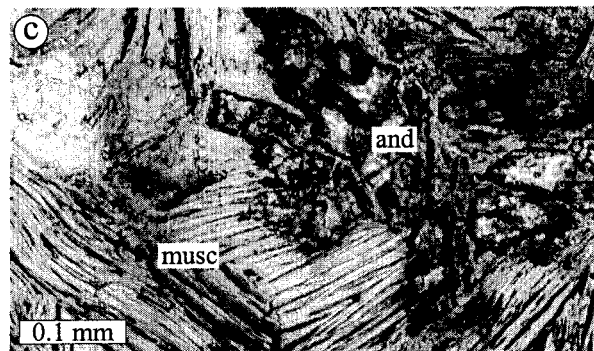
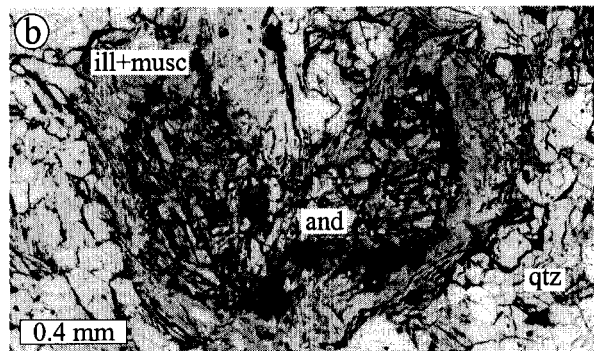
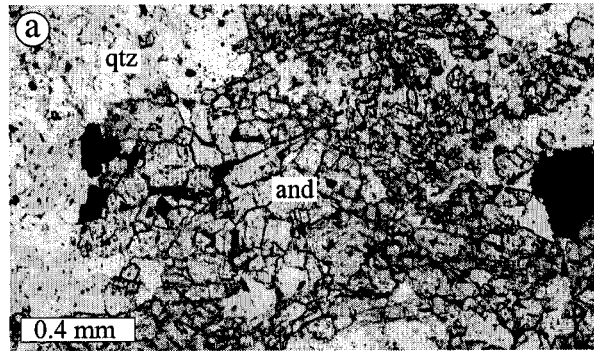
Advanced argillic sub-facies: At Cerro Colorado, the advanced argillic alteration is extensively masked by intense supergene alteration, and clay minerals, e.g., dickite and kaolinite, which form in both hypogene and supergene environments, cannot be used to characterize the hypogene relationships. Andalusite, diaspore and pyrophyllite, however, are widely preserved in the upper parts of the Main Stage (Fig. 2-5b). These represent the deeper and/or higher-temperature equivalent of the advanced argillic environment (Meyer and Hemley, 1967), and it is

inferred that the upper part of the advanced argillic alteration zone was destroyed during the prolonged Eocene-Miocene erosion of the deposit (Bouzari and Clark, 2002). Fine-grained andalusite and diaspore resemble quartz in hand sample (Figs. 2-6i and k), but are readily identified in transmitted light (Figs. 2-6j and l). Pyrophyllite, however, resembles muscovite in both hand sample and thin-section, and its distinction was only possible by X-ray analysis. No electron microprobe analyses of illite or pyrophyllite were carried out, but muscovite occurring with andalusite has only traces of MgO and FeO and the highest Al₂O₃ content determined for Main Stage mica (Table 2-1).

The advanced argillic alteration is distinctly zoned: andalusite, illite and pyrophyllite are most widely developed in the lower parts (Figs. 2-5b, 2-6i, 2-6j and 2-8), whereas diaspore, pyrophyllite and illite predominate at higher elevations (Figs. 2-5b, 2-6k, 2-6l and 2-8). Within the lower section, the modal percentage of andalusite increases upward from less than 1 percent to over 20 percent, but this mineral was observed as deep as 300 m below the current surface, within the sericite-chlorite-clay alteration sub-facies. At the shallowest levels, andalusite occurs as large, commonly elongated, crystals intergrown with and surrounded by quartz (Fig. 2-9a), but at greater depth it forms smaller crystals in contact with, and locally surrounded by, fine-grained muscovite and illite (Fig. 2-9b). Although the latter relationships could be interpreted as evidence for replacement of andalusite by muscovite, both kaolinite and alunite, presumably supergene, have commonly replaced the cores of aggregates of sericite (Fig. 2-10). Moreover, at deeper levels and in areas where both large muscovite crystals and remnants of plagioclase are present, andalusite unambiguously replaces muscovite (Figs. 2-9c and d). Neither andalusite nor diaspore has been observed in contact with plagioclase, which is everywhere altered to sericite, and it is therefore inferred that andalusite formed through the alteration of muscovite/illite at shallower levels. At the highest levels, illite is preferentially altered to diaspore and there is no conclusive

Fig. 2-9:

Photomicrographs showing modes of occurrence of andalusite in a vertical profile through the Main Stage advanced argillic alteration sub-facies: (a) Andalusite-rich alteration showing abundant andalusite intergrown with quartz and sulphides in the shallowest preserved level of the alteration zone (plan-polarized transmitted light; # 204-46 at 2439 m a.s.l.). (b) In the middle portion of the profile, andalusite is largely restricted to areas of illite and fine-grained muscovite and is in part surrounded by the latter minerals. This is inferred to record replacement of the muscovite by andalusite (plane-polarized transmitted light; # 204-36 at 2403 m). (c and d) Occurrences of andalusite in the deepest parts of the advanced argillic sub-facies, where coarse muscovite of the sericite-chlorite-clay alteration sub-facies is widespread. Andalusite clearly replaces muscovite (c: plan-polarized transmitted light; # 205-26 at 2340 m; d: crossed-nicols transmitted light; # 199-10 at 2278 m).



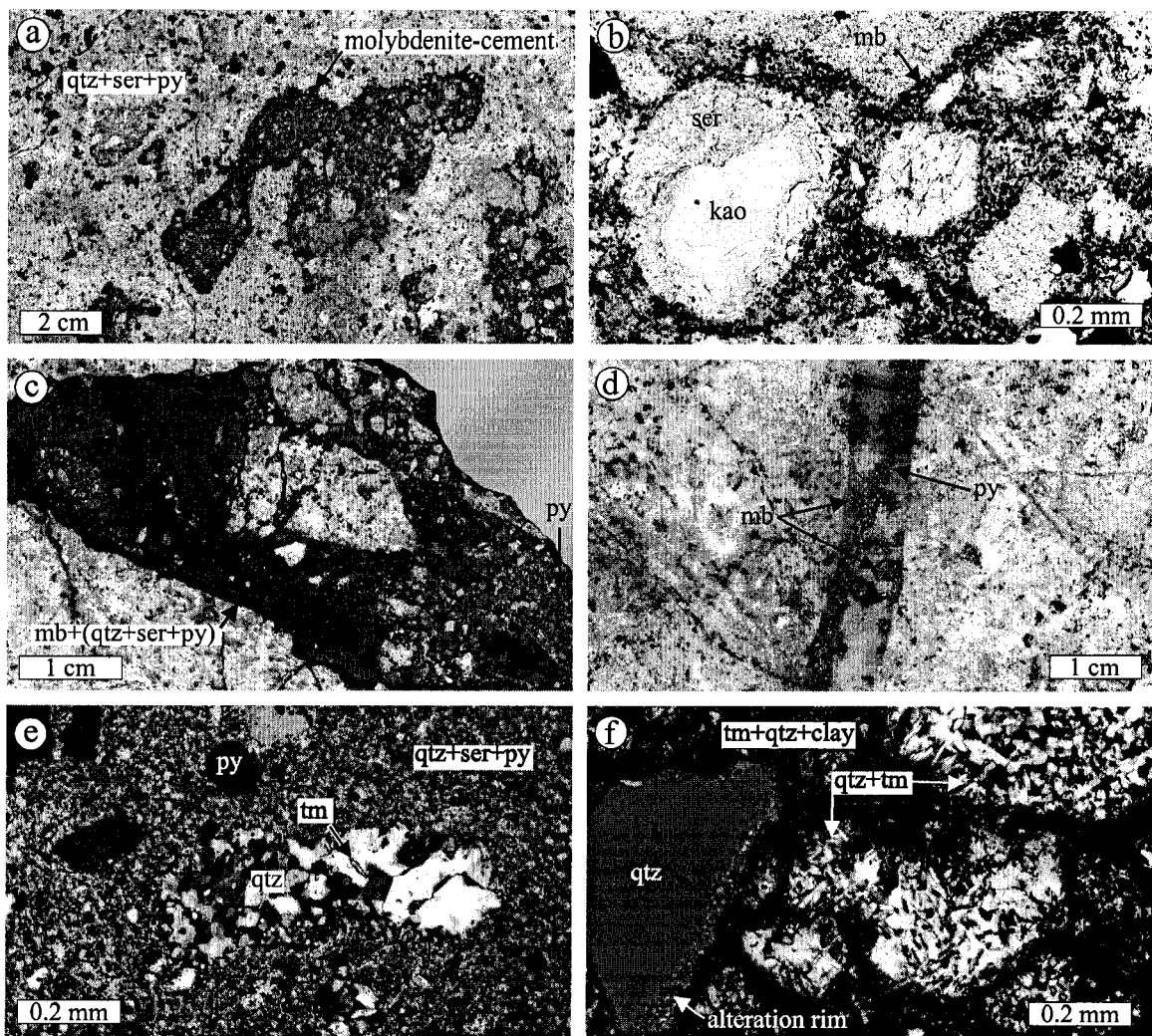


Fig. 2-10:

Mineralogic and textural characteristics of the Transitional Stage alteration and mineralization: (a) A typical phyllically-altered breccia sample with abundant sericite and quartz (white background) and disseminated pyrite (coated by supergene chalcocite). Chalcopyrite (< 2 percent) is replaced by supergene chalcocite. Dark amoeboid bodies are areas in which fine-grained-molybdenite occurs in the matrix of the breccia (# 102 at 2530 m a.s.l.). (b) Photomicrograph of the molybdenite-rich areas of figure 2-10a showing disseminated fine-grained opaque phases in the matrix dominated by molybdenite, with minor pyrite and traces of chalcopyrite and rutile. Note development of kaolinite, probably supergene, inside the sericite body (c) Very fine-grained molybdenite occurs as a thin vein at the deeper levels of the phyllic alteration. Molybdenite is accompanied by very fine-grained quartz, sericite and pyrite in these veins. Pyrite also occurs as larger clasts in the vein (# 329 at 2450 m). (d) Quartz-molybdenite veinlet cutting Main Stage quartz-sericite-clay alteration and, in turn, cut by a Late Stage pyrite vein (# 211-12 at 2299 m). (e) Photomicrograph of the phyllic alteration showing the multigrain quartz bodies interpreted as sites of volatile-rich domains in the upper portion of the breccia. Note occurrence of a few large tourmaline crystals inside these bodies. Matrix is fine-grained sericite and quartz in addition to pyrite (# 323 at 2450 m). (f) Photomicrograph of tourmaline-cemented breccia showing both multigrain quartz bodies with abundant coarse tourmaline, and quartz clast with alteration rim of quartz and sericite. Dark matrix is very fine-grained tourmaline, quartz, sericite and clays (# 201 at 2655 m). See Fig. 2-6 for abbreviations.

evidence of replacement of andalusite by diaspore. Pyrophyllite is more abundant in the upper portions of the advanced argillic zone, where it coexists with both andalusite and diaspore. This relationship differs from that observed at El Salvador, Chile, where andalusite replaces hydrothermal K-feldspar at depth but is itself replaced by muscovite at shallow levels during the “transitional-late stage” alteration (Gustafson and Hunt, 1975; Watanabe and Hedenquist, 2001).

At Cerro Colorado, the gradual transition from alkali-rich minerals at depth (e.g., the muscovite of the sericite-chlorite-clay sub-facies) to alkali-free minerals at the shallow levels (e.g., andalusite of the advanced argillic sub-facies), together with the progressive upward change in the composition of muscovite, is interpreted as evidence for the contemporaneity of all Main Stage sub-facies. Moreover, the scarcity of advanced argillic alteration assemblages in the subsequent Transitional Stage, and the cross-cutting relationships exhibited by the latter with the advanced argillic assemblages (see below), strongly imply that the greater part of the andalusite-diaspore assemblages formed during the Main Stage. Except for the advanced argillic sub-facies, the Main Stage alteration exhibits a strikingly tabular geometry, overprinting the Early Stage zone which itself may have had a quasi-tabular configuration. The lower limit of the sericite-chlorite-clay sub-facies was intersected in several drill holes both in the Main and West Zones, defining approximately a horizontal plane paralleling its upper interface with the quartz-sericite-clay sub-facies. This unusual configuration does not appear to reflect stratigraphic relationships because the Cerro Empexa host-rocks dip ca. 15° to the west (Fig. 2-5). Alteration and mineralization were not strictly stratabound.

Transitional Stage alteration-mineralization

Transitional Stage alteration and mineralization were broadly coeval with the emplacement of the hydrothermal breccia bodies (Figs. 2-5a and b) and are characterized by the quartz-sericite (muscovite)-pyrite assemblage (Fig. 2-10a), corresponding to the phyllic or

sericitic alteration of Meyer and Hemley (1967). The mica is similar in composition to that of the preceding Main Stage advanced argillic assemblages, exhibiting only traces of MgO and FeO (Table 2-1). Chalcopyrite was deposited during this stage, but in lesser quantities than in the Main Stage. Pyrite averages 7 to 10 volume percent and the pyrite/chalcopyrite ratio ranges from 5:1 to 10:1. Much of the molybdenite in the deposit was deposited during this stage as a breccia cement, as veinlets cutting the breccias and as stockworks in the andesite (Fig. 2-10). Assay data, available only for the Main Zone orebody, reveal that the highest Mo concentrations (0.02-0.03 percent) are located at the margins of breccia bodies and in contiguous andesite (Fig. 2-2). Molybdenite commonly occurs in quartz veins, lacking alteration haloes and cutting the Main Stage assemblages in the andesite (Figs. 2-7f and 2-10d). Within the breccia bodies, however, it occurs as black, amoeboid, commonly ghost-like breccia cements (Figs. 2-10a and b). In these areas, very fine-grained ($< 10\ \mu\text{m}$) molybdenite is the dominant opaque phase, associated with quartz, sericite, pyrite and minor chalcopyrite (widely replaced by supergene chalcocite) and rutile. In the deeper parts of the breccia bodies, fine-grained molybdenite occurs in veins in association with sericite, quartz and pyrite (Fig. 2-10c). Tourmaline is locally abundant, but occurs in trace amounts in most parts of the breccia matrix. However, molybdenite and tourmaline do not occur in association.

The quartz of the phyllic alteration exhibits three distinct modes of occurrence: disseminated, clast overgrowth, and multigrain aggregates. Very fine-grained disseminated quartz formed throughout the alteration zone in close association with sericite (Fig. 2-10e), but is more abundant in the upper levels of the alteration zone. Quartz clasts in the breccias show evidence of dissolution and reprecipitation to form alteration rims which incorporate sericite (Fig. 2-10f). Quartz clasts range from a few mm to over 20 cm in diameter. Multigrain aggregates have sub-rounded -to- rounded boundaries and include abundant interlocking grains larger than the disseminated quartz (Fig. 2-10e), but the aggregates rarely exceed 1 mm in size. Tourmaline is

generally very fine-grained where associated with disseminated quartz, but larger tourmaline crystals have grown in the multigrain quartz aggregates (Fig. 2-10e and f). The latter are abundant at the shallow-levels of the breccia bodies and plausibly represent sites at which hydrothermal volatile phases were concentrated and channeled.

The Transitional Stage alteration clearly postdated all facies of the Main Stage. Thus, andalusite- and diaspore-rich areas of the earlier advanced argillic alteration occur in sharp contact with the phyllic alteration of the breccia bodies (Fig. 2-8). However, andalusite and/or diaspore occur very rarely in the upper levels of the breccia bodies, where tourmaline also has been partially altered to dumortierite. Overprinting of the Main Stage assemblages by pyrite and other minerals of the phyllic alteration has occurred, but its extent could not be mapped because of the similarities of the assemblages and, particularly, the supergene leaching. Tourmaline veinlets, however, occur in a halo extending as far as 300 m from the breccia bodies (Fig. 2-8). These veins cut all Main Stage alteration assemblages, including those of the advanced argillic sub-facies. Thus, unaltered tourmaline veinlets were observed cutting a rock matrix strongly altered to andalusite and diaspore (Figs. 2-7h and i). Dumortierite was nowhere observed with the Main Stage advanced argillic alteration. Tourmaline is unstable at the low pH and moderate temperatures attending advanced argillic alteration (Arancibia and Clark, 1996; and O.N. Arancibia, unpub. data).

Late Stage pyrite veins

The Late Stage is characterized by pyrite and quartz-pyrite veins ranging from a few mm to tens of cm in width. These cut all previous alteration assemblages in the andesite and breccia bodies (Figs. 2-10d and 2-11). Thicker and more abundant veins, however, are commonly observed in the breccia bodies.

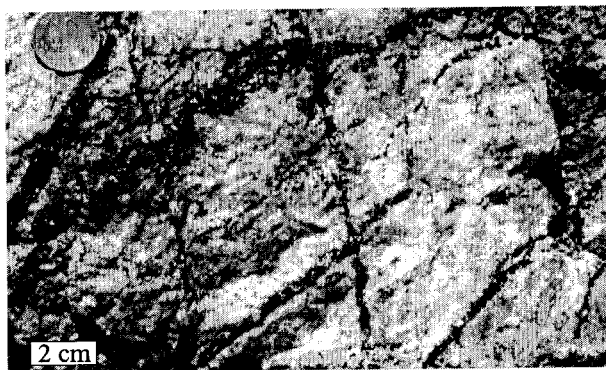


Fig. 2-11:
Stockwork of Late Stage pyrite veins cutting the breccia unit. The widths of the veins locally exceed 30 cm. The larger veins commonly occur in the breccia bodies, promoting in strong leaching and supergene alteration. Main Zone pit, south wall.

2.6. $^{40}\text{Ar}/^{39}\text{Ar}$ Geochronology

Hydrothermal micas were selected for $^{40}\text{Ar}/^{39}\text{Ar}$ geochronology in order to establish the age relationships of the hydrothermal system. These comprise: a biotite sample (# 83-60 at 2237 m a.s.l.) from intense Early Stage biotite-albite-magnetite alteration; coarse-grained muscovite (# 206-14 at 2258 m) from pervasive Main Stage sericite-chlorite-clay alteration; and one sample composed of fine-grained mixture of muscovite and chlorite (# 83-53 at 2216 m) from a thin Main Stage sericite-chlorite-clay veinlet cutting biotite-albite-magnetite alteration. Analytical techniques are documented in Appendix 3 and the analytical data are recorded in Appendix 4 and figure 2-12.

Both biotite and coarse-grained muscovite yielded excellent (i.e., > 99 percent of the ^{39}Ar released) plateaux, with ages of 50.18 ± 1.95 (2σ errors) and 51.8 ± 0.6 Ma, respectively (Figs. 2-12a and b). Therefore, the ages of the Early and Main Stage alteration stages cannot be resolved within analytical error. The slightly younger apparent age of the Early Stage biotite could, however, record resetting of the Ar systematics during Main Stage metasomatism, given the relatively low temperature of Ar-retention of biotite (ca. 310°C: Harrison et al., 1985). The mixture of fine-grained muscovite and chlorite yielded higher ages in the lower-temperature steps, probably as a result of recoil effects caused by chlorite. This sample, however, yielded a plateau age of 51.8 ± 0.5 Ma (74.3 percent of the ^{39}Ar released), identical to that of the coarse-grained muscovite (Fig. 2-12c). These data are in permissive agreements with $^{40}\text{Ar}/^{39}\text{Ar}$ furnace-heating dates for biotite (one sample) and muscovite (two samples) (A.H. Clark, unpub. report for Rio Algom Exploration Inc. Toronto, 1995).

Cerro Colorado is therefore essentially coeval with the Cuajone deposit (52.4 Ma; Clark, 2003) and with the terminal stages in the evolution of the Toquepala (52 Ma; Clark, 2003) deposit, representing the youngest mineralization in the Paleocene-middle Eocene belt. Despite the possibility of resetting of the biotite date, and the uncertainty in the biotite age, a large hiatus

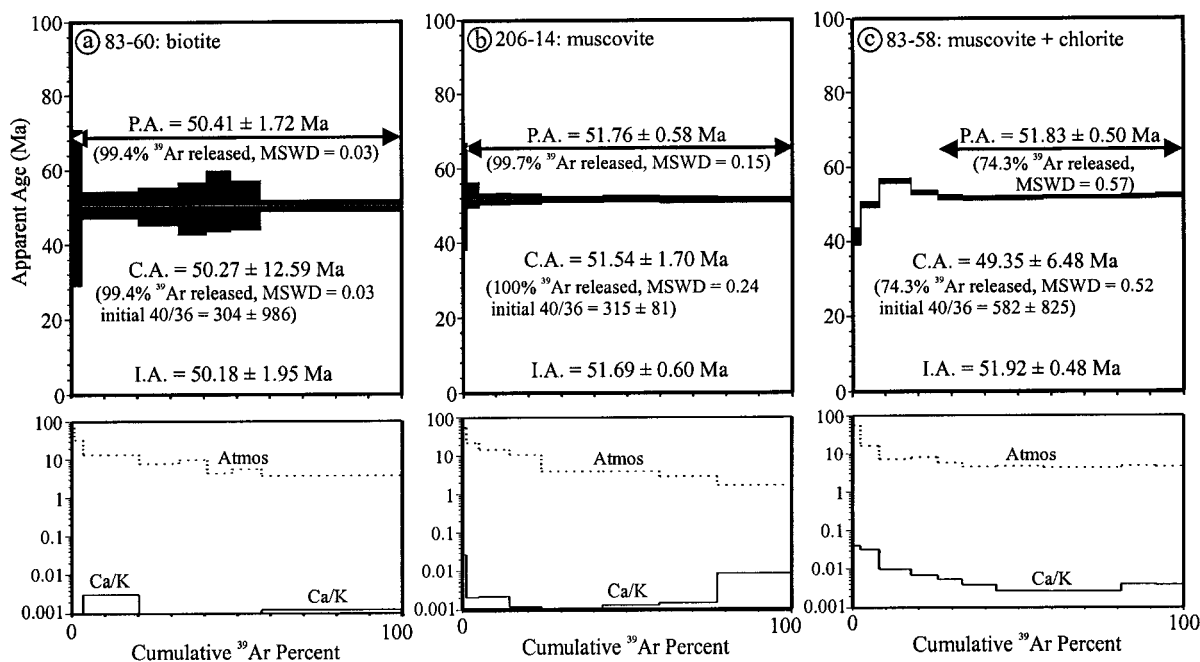


Fig. 2-12:

Laser-induced $^{40}\text{Ar}/^{39}\text{Ar}$ age spectra, with atmospheric argon content and Ca:K ratio for each heating step, for Early Stage biotite and Main Stage muscovite from Cerro Colorado. See text for discussion. Summary of analytical data are given in Appendix 4. P.A. = plateau age; C.A. = correlation age; I.A. = integrated age.

between the Early and Main Stage alteration events is considered unlikely. The Early Stage alteration is spatially related to the Main Stage alteration, which is focused in its core (Figs. 2-2 and 2-5), and the Early and Main stages of alterations are interpreted to represent events in the evolution of a single, coherent, hydrothermal system.

2.7. Alteration Mass and Volume Changes

Samples representing the host andesite and Early and Main Stages of alteration were selected for bulk chemical analysis as a basis for estimation of the nature and extent of metasomatism which occurred during the establishment and development of the Cerro Colorado hydrothermal system. The analyzed samples included unaltered porphyritic and brecciated andesite (n = 5), biotite-albite-magnetite - altered andesite (5) and sericite-chlorite-clay - altered andesite (5). An attempt was made to avoid samples exhibiting veining and overprinting of various alteration assemblages, but those of biotite-albite-magnetite alteration included hair-like Main Stage veinlets containing traces of chalcopyrite. Moreover, the “unaltered” andesite, from the south wall of Quebrada Parca ca. 1 km north of the deposit (Fig. 2-2), exhibits minor saussuritization. All alteration samples were taken from drill-core in the lower parts of the deposit, unaffected by supergene alteration.

Samples were crushed by a ceramic pulverizer to avoid contamination by Ta and W etc., and rock grain densities were measured on using a *Micrometric* 1303 helium-air pycnometer with a measurement accuracy of $\pm 0.01\text{g cm}^{-3}$. Major elements and Sc, V and Zr were analyzed by lithium metaborate/tetraborate fusion ICP at Activation Laboratories Ltd., Ontario. S, Cl, Cu, and Ga were analyzed by XRF, and all other trace elements by ICP mass spectrometry at the Memorial University of Newfoundland. FeO was determined by colorimetric titration at Queen's University. Analytical methods, detection limits and results are recorded in Table 2-2.

Table 2-2. Whole-Rock Compositions and Specific Gravities of Protolith and Alteration Assemblages, Cerro Colorado ¹

| | Sample no. | Method | Detection limit | Unaltered andesite | | | | | Biotite-albite-magnetite altered andesite | | | | | Sericite-chlorite-clay altered andesite | | | | |
|---------------------------------|------------|--------|-----------------|--------------------|--------|---------|---------|---------|---|---------|---------|---------|---------|---|---------|---------|--------|--------|
| | | | | QP1 | QP4 | QP13 | QP21 | QP27 | 83-64 | 83-66 | 83-89 | 152-10 | 151-12a | 151-12b | 83-87 | 199-10 | 207-13 | 211-15 |
| Wt% | | | | | | | | | | | | | | | | | | |
| SiO ₂ | ICP | 0.01 | 59.85 | 60.29 | 56.45 | 54.83 | 51.23 | 56.70 | 55.75 | 55.25 | 50.61 | 50.66 | 53.93 | 54.29 | 63.46 | 56.98 | 67.91 | |
| TiO ₂ | ICP | 0.001 | 0.878 | 0.778 | 0.871 | 0.964 | 0.894 | 0.975 | 0.944 | 1.033 | 1.034 | 1.133 | 1.183 | 1.059 | 1.034 | 0.939 | 0.844 | |
| Al ₂ O ₃ | ICP | 0.01 | 16.97 | 15.98 | 17.15 | 16.46 | 18.72 | 20.17 | 19.88 | 19.64 | 20.11 | 21.37 | 23.73 | 20.74 | 20.26 | 17.54 | 16.21 | |
| FeO | Titration | 0.1 | 3.28 | 2.52 | 3.85 | 4.28 | 4.25 | 3.08 | 3.91 | 3.60 | 5.15 | 3.96 | 1.02 | 2.23 | 1.23 | 5.53 | 2.14 | |
| Fe ₂ O ₃ | ICP | 0.01 | 3.65 | 2.56 | 3.77 | 4.65 | 3.44 | 0.85 | 2.12 | 1.92 | 2.68 | 1.00 | 1.04 | 3.05 | 1.18 | 2.31 | 0.22 | |
| MnO | ICP | 0.001 | 0.130 | 0.121 | 0.195 | 0.103 | 0.512 | 0.023 | 0.020 | 0.021 | 0.031 | 0.026 | 0.025 | 0.013 | 0.004 | 0.192 | 0.018 | |
| MgO | ICP | 0.01 | 3.31 | 3.23 | 3.32 | 3.04 | 4.02 | 4.64 | 4.37 | 4.74 | 6.25 | 7.29 | 6.49 | 4.67 | 3.53 | 4.54 | 4.22 | |
| CaO | ICP | 0.01 | 6.05 | 4.80 | 4.55 | 4.73 | 4.30 | 3.34 | 4.33 | 2.08 | 2.15 | 2.09 | 0.28 | 0.48 | 0.22 | 0.26 | 0.26 | |
| Na ₂ O | ICP | 0.01 | 2.96 | 2.81 | 3.51 | 4.98 | 3.86 | 3.93 | 3.11 | 5.53 | 4.43 | 4.53 | 0.22 | 3.23 | 0.21 | 0.10 | 0.42 | |
| K ₂ O | ICP | 0.01 | 1.27 | 3.49 | 2.66 | 3.17 | 3.03 | 2.94 | 2.93 | 3.70 | 4.11 | 4.02 | 5.33 | 3.88 | 4.09 | 4.75 | 3.36 | |
| P ₂ O ₅ | ICP | 0.01 | 0.17 | 0.17 | 0.19 | 0.20 | 0.23 | 0.18 | 0.20 | 0.20 | 0.19 | 0.20 | 0.19 | 0.26 | 0.15 | 0.12 | 0.10 | |
| LOI | ICP | 0.01 | 1.36 | 3.29 | 2.88 | 2.39 | 4.56 | 3.41 | 2.82 | 2.67 | 2.30 | 2.83 | 5.39 | 4.91 | 4.10 | 5.49 | 4.02 | |
| Total | | | 99.88 | 100.04 | 99.40 | 99.80 | 99.05 | 100.24 | 100.38 | 100.38 | 99.05 | 99.11 | 98.83 | 98.81 | 99.47 | 98.75 | 99.72 | |
| H ₂ O = LOI - (S+Cl) | | | 1.27 | 3.22 | 2.80 | 3.34 | 4.48 | 3.27 | 2.66 | 2.52 | 2.15 | 2.65 | 4.77 | 1.48 | 3.15 | 2.50 | 3.09 | |
| ppm | | | | | | | | | | | | | | | | | | |
| Li | ICP-MS | 0.434 | 27.749 | 32.986 | 26.075 | 21.758 | 29.783 | 21.082 | 22.159 | 30.058 | 34.408 | 32.993 | 44.400 | 28.751 | 7.619 | 34.737 | 19.482 | |
| S | XRF | 25 | 222 | 195 | 191 | 106 | 221 | 196 | 146 | 125 | 155 | 270 | 2387 | 13675 | 3752 | 11912 | 3675 | |
| Cl | XRF | | 284 | 179 | 214 | 232 | 179 | 765 | 977 | 987 | 881 | 923 | 163 | 136 | 108 | 70 | 108 | |
| Sc | ICP | 1 | 18 | 18 | 14 | 16 | 12 | 23 | 21 | 30 | 18 | 22 | 16 | 17 | 21 | 22 | 15 | |
| V | ICP | 5 | 103 | 127 | 135 | 172 | 148 | 194 | 182 | 192 | 161 | 226 | 121 | 140 | 100 | 200 | 119 | |
| Cu | XRF | 5 | 29 | 48 | 33 | 16 | 34 | 365 | 256 | 238 | 358 | 387 | 2454 | 8768 | 3229 | 1506 | 2827 | |
| Ga | XRF | 4 | 20 | 18 | 19 | 18 | 20 | 20 | 20 | 17 | 22 | 24 | 19 | 14 | 18 | 19 | 14 | |
| Rb | ICP-MS | 0.046 | 59.310 | 110.808 | 92.460 | 122.139 | 74.304 | 124.439 | 116.671 | 128.109 | 148.638 | 156.681 | 233.682 | 109.863 | 119.600 | 284.959 | 92.891 | |
| Sr | ICP-MS | 0.71 | 376.12 | 230.32 | 335.13 | 396.77 | 317.41 | 325.74 | 329.47 | 363.23 | 151.12 | 173.09 | 7.30 | 66.96 | 68.12 | 5.66 | 32.43 | |
| Y | ICP-MS | 0.007 | 18.472 | 27.159 | 19.107 | 17.003 | 16.195 | 12.377 | 11.980 | 11.720 | 10.710 | 10.510 | 12.846 | 16.221 | 7.930 | 13.150 | 9.637 | |
| Zr | ICP | 4 | 123 | 203 | 140 | 112 | 124 | 107 | 103 | 97 | 152 | 183 | 192 | 100 | 133 | 123 | 124 | |
| Nb | ICP-MS | 0.013 | 9.166 | 11.495 | 10.017 | 7.302 | 8.712 | 4.680 | 5.276 | 4.892 | 10.732 | 10.488 | 3.159 | 2.027 | 3.509 | 5.947 | 2.974 | |
| Mo | ICP-MS | 0.132 | 1.071 | 3.382 | 1.778 | 1.326 | 1.373 | 1.248 | 1.675 | 2.644 | 1.697 | 2.321 | 74.322 | 205.080 | 78.998 | 25.126 | 35.089 | |
| Cs | ICP-MS | 0.013 | 2.662 | 4.153 | 2.363 | 1.121 | 1.119 | 5.349 | 5.128 | 3.751 | 3.361 | 3.290 | 6.557 | 3.139 | 1.515 | 6.240 | 1.211 | |
| Ba | ICP-MS | 0.15 | 381.09 | 687.81 | 665.16 | 451.51 | 1145.44 | 334.19 | 287.85 | 423.83 | 310.15 | 305.91 | 247.61 | 512.43 | 301.19 | 135.95 | 287.07 | |
| La | ICP-MS | 0.013 | 19.030 | 27.563 | 21.323 | 10.803 | 25.094 | 23.173 | 11.439 | 19.391 | 11.131 | 19.174 | 35.588 | 9.219 | 16.963 | 27.651 | 20.046 | |
| Ce | ICP-MS | 0.011 | 38.584 | 54.706 | 31.867 | 25.673 | 48.505 | 41.166 | 23.792 | 38.971 | 22.141 | 41.563 | 74.660 | 18.686 | 35.045 | 55.486 | 40.078 | |
| Pr | ICP-MS | 0.004 | 5.071 | 7.199 | 4.902 | 3.967 | 6.173 | 4.846 | 3.135 | 5.083 | 2.804 | 5.234 | 9.537 | 2.529 | 4.622 | 7.030 | 5.112 | |
| Nd | ICP-MS | 0.092 | 18.518 | 26.452 | 22.034 | 16.753 | 23.212 | 16.955 | 12.814 | 20.088 | 10.770 | 19.124 | 34.472 | 9.459 | 18.097 | 26.165 | 18.142 | |
| Sm | ICP-MS | 0.044 | 4.046 | 6.038 | 4.901 | 4.263 | 5.257 | 3.353 | 2.842 | 4.393 | 2.237 | 3.918 | 6.597 | 2.425 | 3.994 | 5.145 | 3.863 | |
| Eu | ICP-MS | 0.022 | 1.148 | 1.203 | 1.350 | 1.209 | 1.841 | 0.985 | 0.894 | 1.169 | 0.701 | 0.990 | 1.558 | 0.858 | 1.041 | 1.293 | 0.986 | |
| Gd | ICP-MS | 0.019 | 3.915 | 5.494 | 4.314 | 4.468 | 4.578 | 2.898 | 2.675 | 3.431 | 1.986 | 3.162 | 4.922 | 2.851 | 3.296 | 4.273 | 3.252 | |
| Tb | ICP-MS | 0.004 | 0.571 | 0.862 | 0.596 | 0.620 | 0.652 | 0.415 | 0.413 | 0.473 | 0.291 | 0.404 | 0.625 | 0.451 | 0.384 | 0.591 | 0.418 | |
| Dy | ICP-MS | 0.029 | 3.219 | 5.046 | 3.579 | 3.315 | 3.457 | 2.435 | 2.383 | 2.377 | 1.818 | 2.328 | 3.099 | 2.776 | 1.893 | 2.926 | 2.058 | |
| Ho | ICP-MS | 0.010 | 0.659 | 0.972 | 0.657 | 0.628 | 0.569 | 0.436 | 0.462 | 0.429 | 0.379 | 0.412 | 0.506 | 0.560 | 0.309 | 0.497 | 0.352 | |
| Er | ICP-MS | 0.060 | 1.969 | 2.789 | 1.575 | 1.587 | 1.155 | 1.335 | 1.132 | 1.118 | 1.017 | 1.111 | 1.237 | 1.584 | 0.745 | 1.338 | 0.820 | |
| Tm | ICP-MS | 0.012 | 0.292 | 0.371 | 0.254 | 0.216 | 0.138 | 0.174 | 0.186 | 0.148 | 0.154 | 0.142 | 0.154 | 0.192 | 0.082 | 0.163 | 0.099 | |
| Yb | ICP-MS | 0.073 | 1.612 | 2.291 | 1.608 | 1.399 | 0.769 | 1.073 | 1.000 | 0.853 | 0.812 | 0.812 | 0.835 | 1.104 | 0.421 | 0.941 | 0.469 | |
| Lu | ICP-MS | 0.009 | 0.282 | 0.325 | 0.196 | 0.184 | 0.093 | 0.132 | 0.134 | 0.132 | 0.126 | 0.128 | 0.108 | 0.150 | 0.034 | 0.135 | 0.067 | |
| Hf | ICP-MS | 0.069 | 0.537 | 3.282 | 1.155 | 2.421 | 1.181 | 0.517 | 0.190 | 0.533 | 0.179 | 0.218 | 0.479 | 0.073 | 0.486 | 0.181 | 0.436 | |
| Ta | ICP-MS | 0.014 | 0.607 | 0.758 | 0.586 | 0.438 | 0.539 | 0.280 | 0.302 | 0.279 | 0.583 | 0.633 | 0.182 | 0.125 | 0.224 | 0.354 | 0.189 | |
| Tl | ICP-MS | 0.018 | 0.120 | 0.682 | 0.518 | 0.552 | 0.678 | 0.525 | 0.548 | 0.555 | 0.802 | 0.792 | 0.673 | 0.403 | 0.424 | 1.360 | 0.504 | |
| Pb | ICP-MS | 0.125 | 11.867 | 21.007 | 20.542 | 2.639 | 46.657 | 11.687 | 9.649 | 5.868 | 9.221 | 8.716 | 4.253 | 6.414 | 1.686 | 5.929 | 5.250 | |
| Bi | ICP-MS | 0.012 | 0.036 | 0.110 | 0.045 | 0.038 | 0.197 | 0.082 | 0.035 | 0.658 | 0.367 | 1.644 | 0.205 | 0.491 | 0.268 | 0.777 | 0.122 | |
| Th | ICP-MS | 0.022 | 5.520 | 11.935 | 7.121 | 2.790 | 3.041 | 2.119 | 2.409 | 2.230 | 3.977 | 5.611 | 7.617 | 0.654 | 2.372 | 3.985 | 3.596 | |
| U | ICP-MS | 0.012 | 1.113 | 2.550 | 1.363 | 0.654 | 1.015 | 0.502 | 0.364 | 0.445 | 0.761 | 0.268 | 0.639 | 5.367 | 0.739 | 0.813 | 0.419 | |
| ρ (g cm ⁻³) | | | 2.84 | 2.70 | 2.74 | 2.77 | 2.73 | 2.46 | 2.42 | 2.44 | 2.48 | 2.61 | 2.84 | 2.72 | 2.61 | 2.90 | 2.65 | |

LOI = loss on ignition; H₂O by difference and may contain other volatiles (e.g., CO₂); ICP = inductively coupled plasma emission spectroscopy; ICP-MS = inductively coupled plasma emission mass spectroscopy; XRF = X-ray fluorescence (on pressed pellet).

Calculation procedure

The bootstrap statistical procedure of Ague and van Haren (1996) was used to calculate mass and volume gains and losses, as well as their confidence intervals. This method is based on a statistical procedure of Aitchison (1986, 1989) which takes full account of the special properties of compositional data, including closure, by using ratios of constituents on a multivariate basis, and on Efron's (1979) nonparametric bootstrap method, which provides confidence intervals using a calibrated percentile interval approach (Ague and van Haren, 1996). Mass (τ) and volume (ε) change calculations were carried out using the following equations (Ague and van Haren, 1996; Ague, 1994, Brimhall and Dietrich, 1987):

$$\tau^j = \left[\left(\frac{C_i^\circ}{C_i'} \right) \left(\frac{C_j'}{C_j^\circ} \right) - 1 \right] \quad \varepsilon = \left[\left(\frac{C_i^\circ}{C_i'} \right) \left(\frac{\rho^\circ}{\rho'} \right) - 1 \right]$$

, where: C_i° and C_i' are the concentrations of a reference immobile species i in the parent and altered rock, respectively; C_j° and C_j' are the concentrations of a mobile constituent j in the parent and altered rocks, respectively; and ρ° and ρ' are the bulk densities of the parent and altered rocks, respectively. Therefore, computation of the change in the mass of a mobile element does not require knowledge of rock density, but this is needed for calculation of volume changes.

Water contents were approximated by subtraction of S and Cl from loss-on-ignition values (Table 2-2). Calculations were performed on oxide weight percent data (using the FORTRAN 77 computer code of Ague and van Haren (1996); provided by J.J. Ague) on the Queen's University workstation. 10,000 bootstrap samples were generated to determine the distribution and 10,000 more were generated for each of these samples for the calibration. A 95 percent confidence interval was determined for each variable. Reference species were selected from a group of immobile and/or less-mobile species by examination of the concentration ratio of a constituent between protolith and altered rock (Fig. 2-13). Thus, Sm, Eu, Tm, Ta, and Pb were

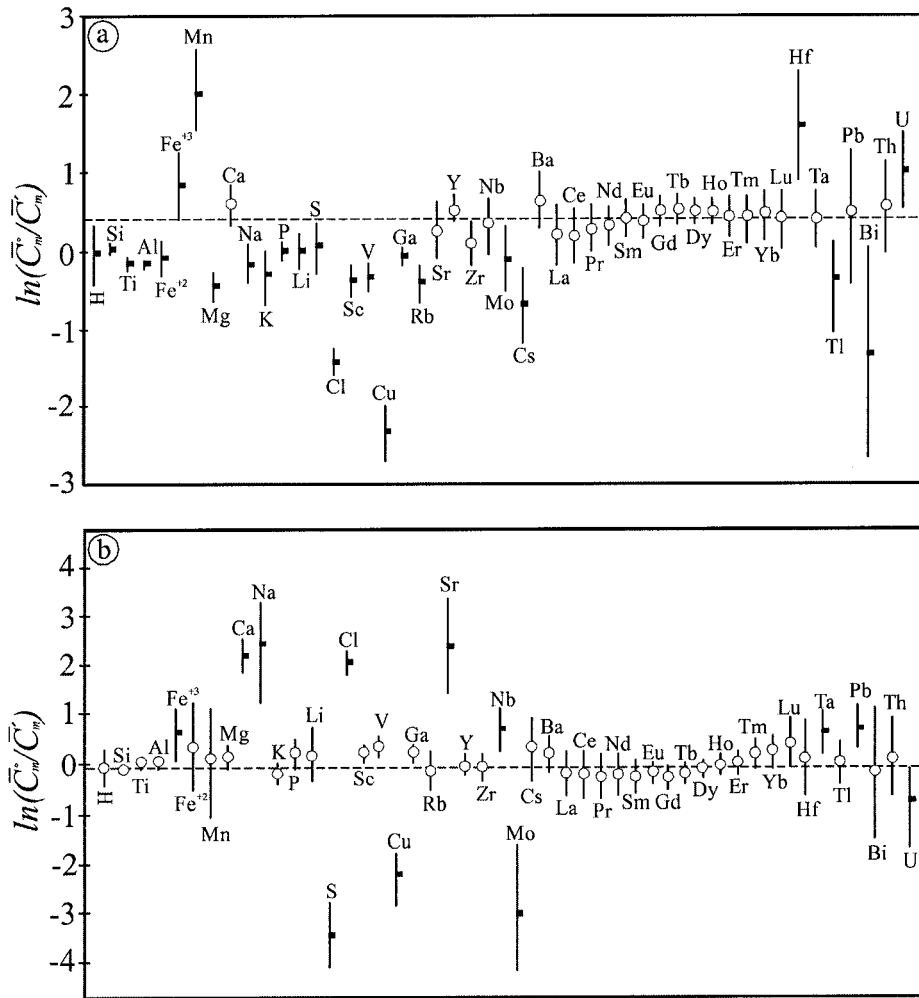


Fig. 2-13: Natural logarithms of the ratios of oxide concentrations in protolith and altered rock ($r_m = \bar{C}_m / \bar{C}'_m$) at the 95 percent confidence interval, shown by vertical bar, for: (a) the unaltered andesite versus biotite-albite-magnetite alteration; and (b) biotite-albite-magnetite alteration versus sericite-chlorite-clay alteration. Note that all REE, La to Lu, maintain similar ratios during both Early and Main Stage alteration. These and other species with similar ratios, shown by open circles, are assumed to have experienced minor, or perhaps negligible, mass transfer during alteration because metasomatism is unlikely to have produced such similar ratios for such a broad range of elements. The best estimate of the reference ratio (mr) is shown by the dashed line ($\ln mr$). Elements whose ratio (r_m) was closest to this line were selected as reference species for mass and volume calculations (see option "B" of Ague and van Haren, 1996). Because mr is greater than 1 ($mr = 1.50$; $\ln mr = 0.40$), a significant overall mass gain occurred during Early Stage alteration (a), whereas the mass change during the subsequent Main Stage alteration (b) was minimal ($mr = 0.92$; $\ln mr = 0.08$).

selected as reference species for comparison of unaltered andesite and biotite-albite-magnetite alteration, and Y, Zr, Dy and Ho for comparison of biotite-albite-magnetite and sericite-chlorite-clay alteration facies. Mass change percentages for all constituents are shown in figures 2-14a and b, and calculated mass (grams/1 kg of rock) and volume gains or losses are shown in Table 2-3. The gains or losses of many constituents could not be defined unambiguously because their 95 percent confidence intervals overlapped the line for zero mass change. A conservative approach is taken by considering only those phases for which gain or loss could be established at this confidence level (Fig. 2-14c, Table 2-3).

Early Stage

Comparison of the biotitized and albitized andesite with unaltered andesite shows that, at the 95 percent confidence level, 20 elements were added but only 2 lost during Early Stage alteration (Fig. 2-14a and c). Several major elements, viz., Al, Mg, Na, K and Fe^{+2} , as well as water, were added, in addition to the trace elements, Ti, Cl, P, V, Rb, Li, Sc, Ga, Cs, Tl and Bi. The REE remained relatively immobile and Mn and Hf were lost. Apparent addition of small amounts of copper (0.6 g CuO /kg of rock; Table 2-3), as well as Mo and S, are on petrographic grounds ascribed to thin Main Stage veinlets. These did not, however, contribute significantly to the overall mass changes because all elements added during the Early Stage alteration were lost during the ensuing Main Stage (see Figs. 2-14b and c). Addition of Al, K, Mg and, possibly, some Fe^{+2} is inferred to be related to the formation of biotite after hornblende and plagioclase (Fig. 2-6b), and the higher content of magnetite in the Early Stage assemblages relative to the unaltered andesite is inferred to reflect iron metasomatism. Addition of Fe^{+2} , which was apparently associated with loss of Fe^{+3} (Table 2-3), implies a relatively reduced environment during this stage. Na was added, presumably through the conversion of calcic plagioclase to oligoclase and albite, but a mass loss of Ca could not be established at the 95 percent confidence

Fig. 2-14: Mass changes during the Early Stage biotite-albite-magnetite alteration of andesite (a), and Main Stage sericite-chlorite-clay alteration of the biotitized and albitized rock (b). Best estimates of absolute mass gain or loss are shown in (c) for constituents that were added or lost during the Early or Main Stages of alteration at a 95 percent level (see also Table 2-2). Note the differing abscissa scales in (a) and (b), and the use of ppm for trace constituents in (c). See text for discussion.

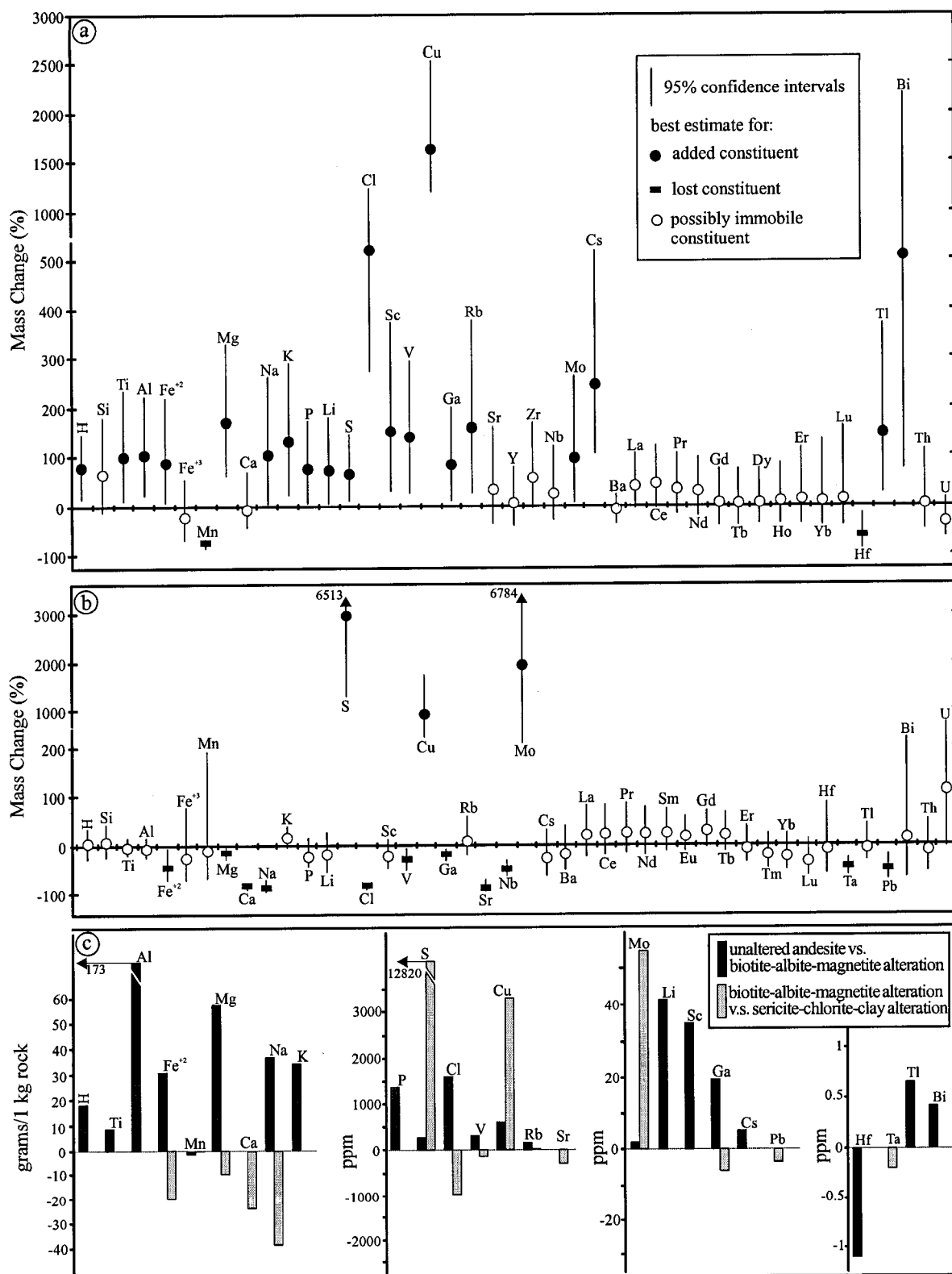


Table 2-3. Mass and Volume Changes¹

| Unaltered andesite vs. Early Stage Alteration (g kg ⁻¹) | | | Early Stage vs. Main Stage Alteration (g kg ⁻¹) | | |
|---|-----------|-------------------------|---|-----------|-------------------------|
| SiO ₂ | 346.71652 | [1019.65425, -35.08760] | SiO ₂ | 23.05702 | [222.66112, -131.92511] |
| * Al ₂ O ₃ | 173.02630 | [381.33819, 34.87973] | * SO ₃ | 12.84067 | [28.11459, 5.83762] |
| * MgO | 57.22875 | [111.02815, 20.79920] | K ₂ O | 5.10619 | [12.65167, -1.48091] |
| * Na ₂ O | 36.36476 | [93.32746, 0.05229] | * CuO | 3.33124 | [6.94209, 1.79068] |
| * K ₂ O | 33.73134 | [74.87050, 5.69764] | LOI | 0.29547 | [10.15424, -7.36686] |
| * FeO | 30.22181 | [78.48670, 0.75457] | * MoO ₃ | 0.05489 | [0.18963, 0.01079] |
| * LOI | 18.49537 | [36.53796, 2.46251] | Rb ₂ O | 0.01116 | [0.08118, -0.03090] |
| * TiO ₂ | 8.59493 | [20.77746, 0.87773] | Ce ₂ O ₃ | 0.00718 | [0.03079, -0.00860] |
| * Cl ₂ O | 1.62239 | [3.31982, 0.72174] | Nd ₂ O ₃ | 0.00495 | [0.01990, -0.00522] |
| * P ₂ O ₅ | 1.37513 | [3.28080, 0.00172] | La ₂ O ₃ | 0.00317 | [0.01538, -0.00491] |
| * CuO | 0.63360 | [0.95795, 0.45383] | Pr ₂ O ₃ | 0.00106 | [0.00397, -0.00091] |
| * V ₂ O ₅ | 0.33466 | [0.70885, 0.06288] | Sm ₂ O ₃ | 0.00082 | [0.00279, -0.00055] |
| * SO ₃ | 0.27569 | [0.65910, 0.04189] | Gd ₂ O ₃ | 0.00078 | [0.00227, -0.00020] |
| * Rb ₂ O | 0.15207 | [0.36864, 0.02672] | UO ₂ | 0.00055 | [0.00257, -0.00003] |
| SrO | 0.11995 | [0.62129, -0.14185] | EuO | 0.00014 | [0.00057, -0.00015] |
| ZrO ₂ | 0.09945 | [0.31181, -0.01381] | Tb ₂ O ₃ | 0.00008 | [0.00030, -0.00007] |
| * Li ₂ O | 0.04168 | [0.10628, 0.00234] | Bi ₂ O ₃ | 0.00003 | [0.00088, -0.00019] |
| * Sc ₂ O ₃ | 0.03493 | [0.08855, 0.00732] | Zero Line | | |
| * GaO | 0.01936 | [0.04677, 0.00198] | Tm ₂ O ₃ | -0.00004 | [0.00004, -0.00009] |
| Ce ₂ O ₃ | 0.01906 | [0.05375, -0.00342] | HfO ₂ | -0.00004 | [0.00029, -0.00021] |
| La ₂ O ₃ | 0.00887 | [0.02414, -0.00093] | Lu ₂ O ₃ | -0.00006 | [0.00001, -0.00010] |
| Nd ₂ O ₃ | 0.00856 | [0.03464, -0.00774] | Tl ₂ O | -0.00006 | [0.00027, -0.00021] |
| * Cs ₂ O | 0.00524 | [0.01349, 0.00220] | Er ₂ O ₃ | -0.00011 | [0.00050, -0.00049] |
| Nb ₂ O ₅ | 0.00303 | [0.01618, -0.00396] | * Ta ₂ O ₅ | -0.00024 | [-0.00014, -0.00031] |
| * MoO ₃ | 0.00226 | [0.00644, 0.00015] | Yb ₂ O ₃ | -0.00027 | [0.00021, -0.00055] |
| Pr ₂ O ₃ | 0.00183 | [0.00653, -0.00115] | ThO ₂ | -0.00043 | [0.00164, -0.00192] |
| * Tl ₂ O | 0.00066 | [0.00169, 0.00011] | Cs ₂ O | -0.00134 | [0.00137, -0.00278] |
| * Bi ₂ O ₃ | 0.00041 | [0.00164, 0.00006] | * Nb ₂ O ₅ | -0.00514 | [-0.00317, -0.00643] |
| Er ₂ O ₃ | 0.00021 | [0.00236, -0.00075] | * PbO | -0.00516 | [-0.00213, -0.00708] |
| Gd ₂ O ₃ | 0.00021 | [0.00389, -0.00210] | * GaO | -0.00580 | [-0.00230, -0.00881] |
| Dy ₂ O ₃ | 0.00016 | [0.00317, -0.00158] | Sc ₂ O ₃ | -0.00836 | [0.00334, -0.01673] |
| Y ₂ O ₃ | 0.00010 | [0.01900, -0.00972] | Li ₂ O | -0.01226 | [0.01439, -0.03307] |
| Yb ₂ O ₃ | 0.00009 | [0.00221, -0.00071] | MnO | -0.03614 | [0.45890, -0.16817] |
| Ho ₂ O ₃ | 0.00003 | [0.00068, -0.00030] | BaO | -0.07995 | [0.13297, -0.19640] |
| Lu ₂ O ₃ | 0.00003 | [0.00036, -0.00010] | * V ₂ O ₅ | -0.11587 | [-0.01990, -0.18099] |
| Tb ₂ O ₃ | 0.00002 | [0.00054, -0.00030] | * SrO | -0.27437 | [-0.21990, -0.29198] |
| Zero Line | | | P ₂ O ₅ | -0.47294 | [0.29305, -0.90526] |
| ThO ₂ | -0.00015 | [0.00674, -0.00288] | TiO ₂ | -0.68790 | [1.55460, -2.41224] |
| UO ₂ | -0.00053 | [0.00021, -0.00088] | * Cl ₂ O | -0.98171 | [-0.93337, -1.01718] |
| * HfO ₂ | -0.00111 | [-0.00029, -0.00147] | Fe ₂ O ₃ | -4.85506 | [12.23418, -11.67923] |
| BaO | -0.06973 | [0.15508, -0.25499] | * MgO | -9.96543 | [-3.64097, -15.68549] |
| * MnO | -1.35437 | [-1.17645, -1.46808] | Al ₂ O ₃ | -17.21014 | [30.18744, -51.91327] |
| CaO | -3.47757 | [36.22077, -24.00936] | * FeO | -19.86585 | [-2.62085, -28.97472] |
| Fe ₂ O ₃ | -9.21238 | [21.43832, -23.90099] | * CaO | -24.09094 | [-22.13562, -25.18752] |
| | | | * Na ₂ O | -39.11432 | [-30.17925, -41.26262] |
| Rock Mass (%) | 69.503 | [183.180, -1.079] | Rock Mass (%) | -7.308 | [20.376, -28.419] |
| Volume Strain (%) | 88.230 | [213.461, 10.136] | Volume Strain (%) | -16.131 | [12.050, -36.884] |

g kg⁻¹ = mass changes in grams per kilogram of rock ordered from the greatest gain (top) to the greatest loss; Braketted numbers are end points of 95 confidence intervals; " * " denotes constituents that are either added or lost at 95 confidence.

level (Fig. 2-14a). Some Ca was plausibly sequestered by the introduced P to form apatite (Fig. 2-7a), absent in unaltered andesite. Several introduced trace elements were probably accommodated in the biotite structure, through the substitution of Rb and Cs for K and the occupation of octahedral sites by Ti, Li and V.

Overall rock mass increased by 69.5 percent (Table 2-3), but grain density decreased by 10 percent, from, on average, 2.76 to 2.48 g cm⁻³. On this basis, the volume is inferred to have increased by 88 percent. The large uncertainty in these values (Table 2-3) should, however, be emphasized, because they include constituents whose gain or loss cannot be confirmed at 95 percent confidence. If only those constituents which were unambiguously added or removed are considered (Fig. 2-14c, Table 2-3), the total mass and volume changes would be 36 and 51 percent, respectively. Much of this mass change is related to addition of Al, Mg, Na, K, Fe⁺² and water (Fig. 2-14c, Table 2-3), whereas the contribution of the lost phases, Mn and Hf, is insignificant (- 0.13 percent). Thus, approximately 2.7 billion tonnes of materials, including 136 billion litres of water, were added during Early Stage alteration to form the current mapped biotite-albite-magnetite alteration with dimensions of 4×2×0.5 km. Moreover, a 51 percent increase in volume, assuming no lateral expansion, would correspond to a ca. 170 m vertical expansion during the Early Stage, i.e., the unaltered parent andesite body had dimensions of ca. 4×2×0.33 km. The upward expansion would be less if some lateral expansion occurred.

Main Stage

Comparison of Main Stage sericite-chlorite-clay alteration samples with those affected by Early Stage biotite-albite-magnetite alteration shows that, at 95 percent confidence, 11 constituents were lost and 3 added during the main Cu mineralization event (Fig. 2-14b and c). Thus, Na, Ca, Fe⁺², Mg, Cl, Sr, V, Ga, Pb, Nb and Ta were removed and S, Cu and Mo were introduced. The strong depletions in Na, Ca, Fe⁺² and Mg are interpreted to reflect the

replacement of biotite and plagioclase by muscovite, during which process numerous trace elements, particularly Cl, Sr, V and Ga, were also lost, but sulphides deposited (e.g., Fig. 2-6e). Indeed, S and Cu account for much of the material added during Main Stage pervasive alteration (Fig. 2-14c, Table 2-3), but the amount of material that was added (1.6 percent) was insignificant relative to that at the Early Stage (36.2 percent). Conversely, more material was removed during the Main Stage (9.4 percent) relative to the Early Stage (0.13 percent). Rock mass decreased overall by 7.8 percent and grain density increased by 10 percent, from, on average, 2.48 to 2.74 g cm⁻³ during the Main Stage. Thus, volume decreased by 16 percent (Table 2-3). Discounting constituents for which gains or losses are uncertain would not significantly affect the overall mass and volume change estimates. However, uncertainty regarding the volume change is introduced if porosity changed significantly during alteration. Although neither the Early and Main Stage assemblages exhibit void spaces at megascopic or microscopic scales, the existence of very small voids cannot be ruled out, especially for the Main Stage assemblages, which were associated with over 9 percent material loss. Therefore, the 16 percent estimate is considered as a maximum value for volume strain during the Main Stage.

In summary, these data strongly suggest that major metasomatic exchange occurred during both the Early and Main Stages of alteration. Significant amounts of materials were added to the andesitic host-rocks during the Early Stage, whereas the Main Stage alteration was mainly characterized by loss of components of silicate minerals. Water was the dominant added volatile phase during the Early Stage but there was no net addition or loss of water during the Main Stage. Biotite formed extensively at the Early Stage and was subsequently replaced by chlorite and muscovite during the Main Stage alteration. Therefore, on mass balance and petrographic grounds, the Early Stage alteration was characterized by strong hydration and the Main Stage by strong hydrolysis, during which sulphides were deposited. Moreover, Early Stage alteration may be characterized as the result of K-Na-Fe metasomatism.

2.8. Fluid Inclusion Relationships

Fluid inclusion microthermometry was undertaken to constrain the pressures, temperatures and compositional history of the hydrothermal fluids responsible for the various facies of alteration and mineralization. Petrographic study of fluid inclusions was carried out on 46 double-polished samples, and 28 samples containing fluid inclusion unambiguously related to a specific alteration facies (Roedder, 1984; Shepherd et al., 1985) were selected for microthermometric measurements. Samples were collected from the Main Zone open pit and from diamond drill core to a depth of 449 m below the pre-mining land surface from both Main and West Zones.

Two main goals of this study were: (i) to identify the reason for the lack of sulphides in the Early Stage biotite-albite-magnetite alteration zone; and (ii) to establish vertical gradients in fluid temperature, salinity and physical state in the quasi-contemporaneously zoned Main Stage event.

Petrography of fluid inclusions

Fluid inclusions are abundant in quartz associated with the Main Stage intermediate argillic and quartz-sericite-clay alteration facies, Transitional Stage phyllic alteration and Terminal Stage pyrite veins. No quartz could be unambiguously related to the Main Stage advanced argillic alteration, and the only microthermometric data for this type of alteration derive from a single andalusite grain. Quartz is also uncommon in the Early Stage biotite-albite-magnetite alteration and microthermometric measurement was only possible for small inclusions in disseminated albite using a high magnification (100X) lens.

Fluid inclusions were classified into four types according to the number, the nature, and the estimated volumetric proportions of the phases present at room temperature (Table 2-4, Fig. 2-15), thus:

Table 2-4. Classification of Fluid Inclusion Types, Cerro Colorado

| |
|---|
| Type 1: saline; L + V + H + two O (hem, cp) ± T |
| Type 1a: final homogenization by V disappearance |
| Type 1b: final homogenization by H dissolution |
| Type 2: multi-salt; L + V + H + two or more salts |
| + two O (hem, cp) ± T |
| Type 2a: final homogenization by V disappearance |
| Type 2b: final homogenization by salt dissolution |
| Type 3: liquid rich; L + V |
| Type 4: vapour rich; V + L + 1 or 2 O |

Abbreviations: L = liquid, V = vapor, H = halite, O = opaque daughter mineral (hem = hematite, cp = chalcopyrite), T = translucent

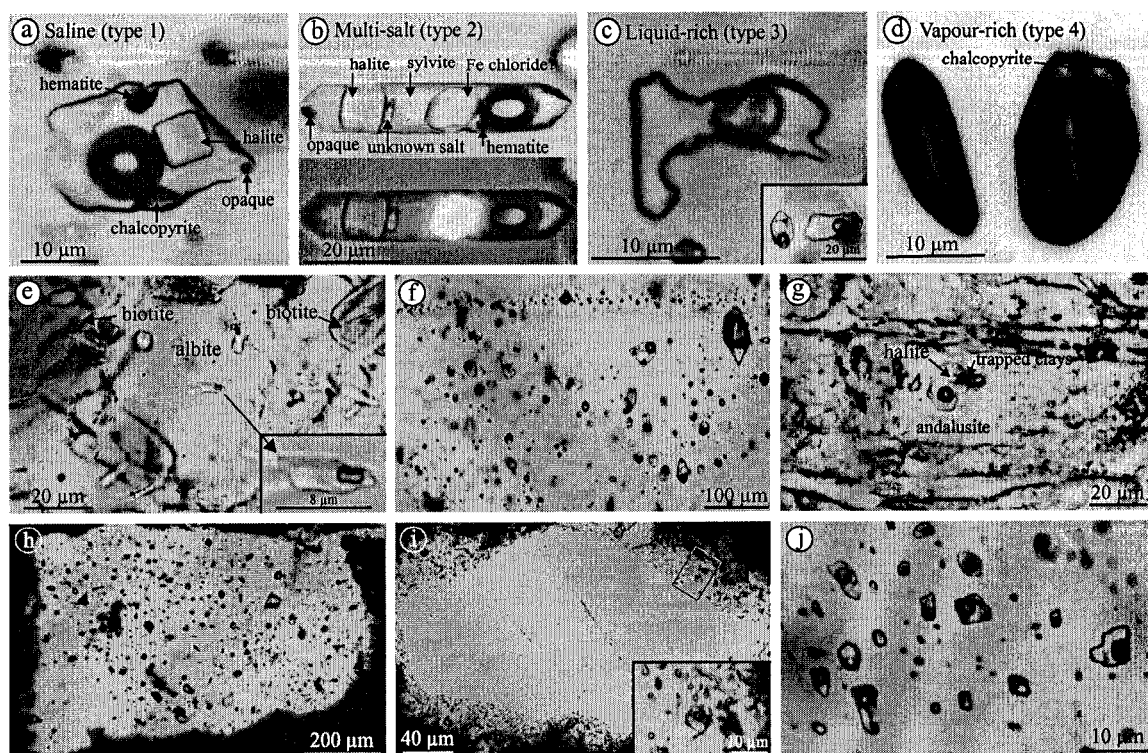


Fig. 2-15:

Photomicrographs showing various types of fluid inclusions and their mode of occurrence in each alteration assemblage. (a) Saline fluid inclusion (type 1) containing daughter crystals of halite, chalcopyrite and hematite. An uncommon third unidentified opaque phase in this inclusion is a trapped mineral (magnetite?). (b) Multi-salt inclusion (type 2) containing at least four, and possibly five, different salts. Lower photomicrograph taken under cross-polarized light to show the strong birefringence of the hydrous Fe chloride. Sylvite is slightly out of focus but its rounded shape is visible in cross-polarized light. The small crystalline body between the halite and sylvite is possibly an aggregate of two salts, one with high relief and birefringence and the other, much smaller, with darker color. (c) Liquid-rich inclusion (type 3). The inset shows a liquid-rich inclusion associated with a saline inclusion from the sericite-chlorite-clay alteration zone. (d) Vapour-rich inclusions (type 4) with gas filling the entire volume of inclusion (more common) or with a vapour slightly smaller than the inclusion and showing its daughter chalcopyrite crystal. (e) Small primary-looking liquid-rich inclusion hosted in albite which is in equilibrium with biotite of the Early Stage biotite-albite-magnetite alteration. No vapour-rich inclusions exist and small black dots in the albite are magnetite or hematite. (f) Photomicrograph showing mode of occurrence of the fluid inclusions associated with the Main Stage intermediate argillic alteration. All fluid inclusion types are randomly distributed, with no evidence of age relationships. However, a small trail at the top shows salt-bearing inclusions coexisting with vapour-rich inclusions, which may have been produced by immiscibility (see text). (g) An exceptionally large saline inclusion hosted in andalusite representing fluids responsible for the advanced argillic alteration. Halite is obscured by trapped dark clays. (h) Quartz clast in Transitional Stage breccia body, hosting abundant inclusions similar to those of the Main Stage alteration. The background is very fine-grained sericite, clays and quartz, appearing dark because of thickness of the section. (i) A quartz clast of the breccia body, affected by shallow-level phyllic alteration, showing an alteration rim of quartz and clays which has also trapped liquid-rich inclusions. (j) Dominantly liquid-rich inclusions associated with the quartz of the Terminal Stage pyrite vein.

Saline inclusions (Type 1): These contain liquid, vapour and a cubic crystal of salt (Fig. 2-15a), identified as halite on the basis of its shape, isotropism and refractive index. Qualitative electron microprobe analysis of several decrepitated saline inclusions confirmed the presence of Na and Cl, with some K and Ca. The presence of Ca is supported by the low first-melting temperature of these inclusions (see below). Salt and vapour each occupies approximately 20 percent of the total volume of the inclusion. Two opaque phases are commonly seen and in many inclusions they are reliably identified as daughter crystals of hematite (red, platy) and chalcopyrite (triangular, brassy-yellow in reflected light). It was not always possible to identify opaque phases, especially at room temperature, because of their location in a dark corner or their anhedral shape, but in many inclusions identification was possible during or after homogenization, when they changed position. Saline inclusions are further subdivided according to the sequence of phase disappearance during final homogenization. Thus, *type 1a* inclusions homogenize by vapour bubble disappearance, and *type 1b* by halite dissolution.

Multi-salt inclusions (Type 2): These inclusions, less abundant than the simpler type 1 saline inclusions, contain two or more salt crystals in addition to liquid, vapour and, commonly, two opaque phases (Fig. 2-15b). Inclusions with two salts are the most common, but examples with five or more species are observed. Halite is ubiquitously present in multi-salt inclusions and was invariably the last salt to melt during heating. If only two salts are present, the second is commonly sylvite, with a slightly smaller size than the halite, or a much smaller unidentified granular mineral with high relief and birefringence. Sylvite is identified by its rounded corners and faster dissolution rate than halite (Roedder, 1992), and consistently melted at low temperature before halite. A very high-birefringence salt with rhombic shape (Fig. 2-15b) observed in many multi-salt inclusions is similar to the hydrous Fe chloride phase in polyphase inclusions of the Chorolque Sn deposit, Bolivia (Grant et al., 1977). Qualitative electron microprobe analysis of

several decrepitated multi-salt inclusions has revealed the presence of Na, K, Ca, Fe and Mg. The Fe-K α peak was significantly higher in inclusions which contained the apparent hydrous Fe chloride. Multi-salt inclusions are again subdivided into two groups: *type 2a* inclusions homogenize by vapour bubble disappearance, and *type 2b* by halite dissolution.

Liquid-rich inclusions (Type 3): These contain abundant liquid (> 80 percent) and a vapour bubble, but lack salt or opaque daughter phases (Fig. 2-15c). Some liquid-rich inclusions are associated with saline and multi-salt inclusions but in these samples they are the least abundant inclusion types. Elsewhere, e.g., in late pyrite veins, they are the dominant high-density phase (see below).

Vapour-rich inclusions (Type 4): Representing the most abundant inclusion type throughout the deposit, these contain a vapour phase that typically fills the entire observable volume of the inclusion (Fig. 2-15d). However, a smaller number of inclusions of this type (< 20 percent) contain slightly less vapour (Fig. 2-15d). Chalcopyrite, and possibly another opaque phase, commonly occur in vapour-rich inclusions, but the darkness of the inclusions prevented clear observation in most cases. Microthermometric measurements were obtained only from few inclusions that had narrow extremities, allowing more accurate observation of final vapour expansion.

The presence of CO₂ was confirmed in saline and multi-salt inclusions by their very low first-melting temperature and, in a few inclusions, by a rim of liquid CO₂ which homogenized to vapour at ca. 31°C. During cooling, this phase formed CO₂ crystals which melted at -56°C. In the majority of inclusions, however, estimation of the proportion of CO₂ was prevented by the difficulty of observing the clathrate melting point, probably because the low proportion of CO₂

caused ice to melt after clathrate (Diamond, 2001). Sluggish crystallization and melting of hydrohalite, which consumes H_2O , may also have hindered clathrate formation/observation.

Magnetite was identified in a few inclusions by its movement towards a magnetic needle, and an acicular translucent mineral with high birefringence was interpreted as accidentally trapped rutile. At room temperature, saline and multi-salt inclusions exhibiting final homogenization by vapour disappearance appeared indistinguishable from those which homogenized by salt dissolution.

Distribution and relative ages of inclusion types

Vapour-rich inclusions were observed with all sulphide-bearing alteration assemblages at all levels, but are absent in the Early Stage biotite-albite-magnetite alteration (see below). However, zones dominated by vapour-rich inclusions, such as those in the upper parts of the Far Southeast porphyry, Philippines (Hedenquist et al., 1998), were not observed at Cerro Colorado. This may be plausibly explained by the deeper erosion of the latter. Multi-salt inclusions are commonly seen at the roots of the Main Stage sericite-chlorite-clay alteration zone (i.e., in quartz-albite veins) but their proportion decreases upward through the sericite-chlorite-clay facies and they are not observed in association with quartz-sericite-clay alteration. Further, the number of salts in the multi-salt inclusions decreases from deeper to shallow levels. Thus, four- and three-salt bearing inclusions are commonly seen in deep quartz-albite veins in which type 2 inclusions constitute over 30 percent of all salt-bearing inclusions. Inclusions associated with the sericite-chlorite-clay alteration have fewer multi-salt bearing inclusions (ca. 15 percent of the total of salt-bearing inclusions), and inclusions with four salts are absent.

Liquid-rich inclusions occur in association with all alteration types and at all levels. However, their abundance in Main Stage assemblages increases upward from the deeper parts of the sericite-chlorite-clay zone to the shallower quartz-sericite-clay alterations facies. Liquid-rich

inclusions also dominate the shallower parts of the phyllic alteration (i.e., in fine-grained disseminated quartz) and the quartz associated with the late pyrite veins. From these observations it may be concluded that, in the Main and Transitional Stages, the density of the trapped fluids decreases from the deeper to the shallower levels of the hydrothermal system. The most obvious cause would be mixing of saline magmatic fluids with meteoric water (e.g., Beane and Titley, 1981; Nash, 1976). However, gravitational settling of dense fluids generated by boiling may have also contributed to the overall distribution of the fluid inclusion types, and some portion of the low-salinity fluid may have been formed through condensation of vapour-rich fluids which traveled upward and absorbed cold meteoric water (Watanabe and Hedenquist, 2001).

Inclusions were randomly distributed within the mineral grains and are assumed to be primary or pseudo-secondary. But, there is no clear evidence of inclusions trapped along growth zones or of cross-cutting relationships between trails of different inclusion types (Fig. 2-15f). Therefore, the relative ages of different inclusion types could not be established. However, vapour-rich inclusions are commonly intimately associated with saline and multi-salt inclusions occurring randomly or in trails (Fig. 2-15f). This may indicate that at least some of these inclusions formed simultaneously through boiling. Nonetheless, the saline and multi-salt inclusions that homogenize by salt dissolution (types 1b and 2b) could not be in equilibrium with the spatially associated vapour phase (Bodnar, 1994). Therefore, these types of inclusions are inferred to have formed at a different time than inclusions that formed during boiling, i.e., those that homogenize by vapour disappearance and coexist with vapour (see below).

Microthermometry

Heating and freezing experiments were conducted on a *Linkam* THMS600 stage. Temperature measurements were restricted to an upper limit of 600°C. At temperatures above ca. 500°C the majority of all inclusions were homogenized and some decrepitated. This was

confirmed by examining several parts of each sample under a constant high temperature. Very high temperature (e.g., $>600^{\circ}\text{C}$) inclusions were therefore probably rare or absent. Microthermometric measurements were conducted on samples representing each alteration assemblage and including: biotite-albite-magnetite alteration (3 samples); quartz-albite veins (7 samples); sericite-chlorite-clay veins (6 samples); quartz-sericite-clay alteration (3 samples); a quartz vein in mineralized biotite-quartz-plagioclase porphyry (2 samples); phyllic alteration (4 samples); late pyrite veins (2 samples); and andalusite alteration (1 sample). Salinities were calculated using the equations of Bodnar and Vityk (1994) and are shown graphically in Figure 2-16, along with homogenization temperatures. Measurements are included in Appendix 5. The reported salinity is expressed as wt. percent NaCl equivalent and is considered a minimum value because it does not take into account the presence of other cations present in the inclusions. Because few measurements were made on vapour-rich inclusions, the numbers of this type of inclusion shown on the frequency diagrams are not representative of its abundance.

Biotite-albite-magnetite alteration: Fluid inclusions associated with this alteration facies are hosted in fine-grained disseminated albite which coexists with biotite. They are liquid-rich and occur as a few isolated bodies (Fig. 2-15e). Inclusion size is in the range of <2 to $10\text{ }\mu\text{m}$ and a 100X lens allowed heating measurements on inclusions as small as $2\text{ }\mu\text{m}$. However, most of the freezing and heating data are from inclusions $5\text{--}6\text{ }\mu\text{m}$ in diameter. Homogenization temperatures and salinities range from 186 to 311°C and 0.2 to 7.9 wt. percent NaCl equiv., respectively (Figs. 2-16a and b). Most inclusions homogenized at $220\text{--}260^{\circ}\text{C}$ and had salinities of $3\text{--}5$ wt. percent NaCl equiv. No vapour-rich or other types of inclusions were observed in association with these inclusions. Thus, their homogenization temperatures are considered minima and require correction for confining pressure. Because of the very small size of the inclusions, no accurate first-melting temperatures could be obtained.

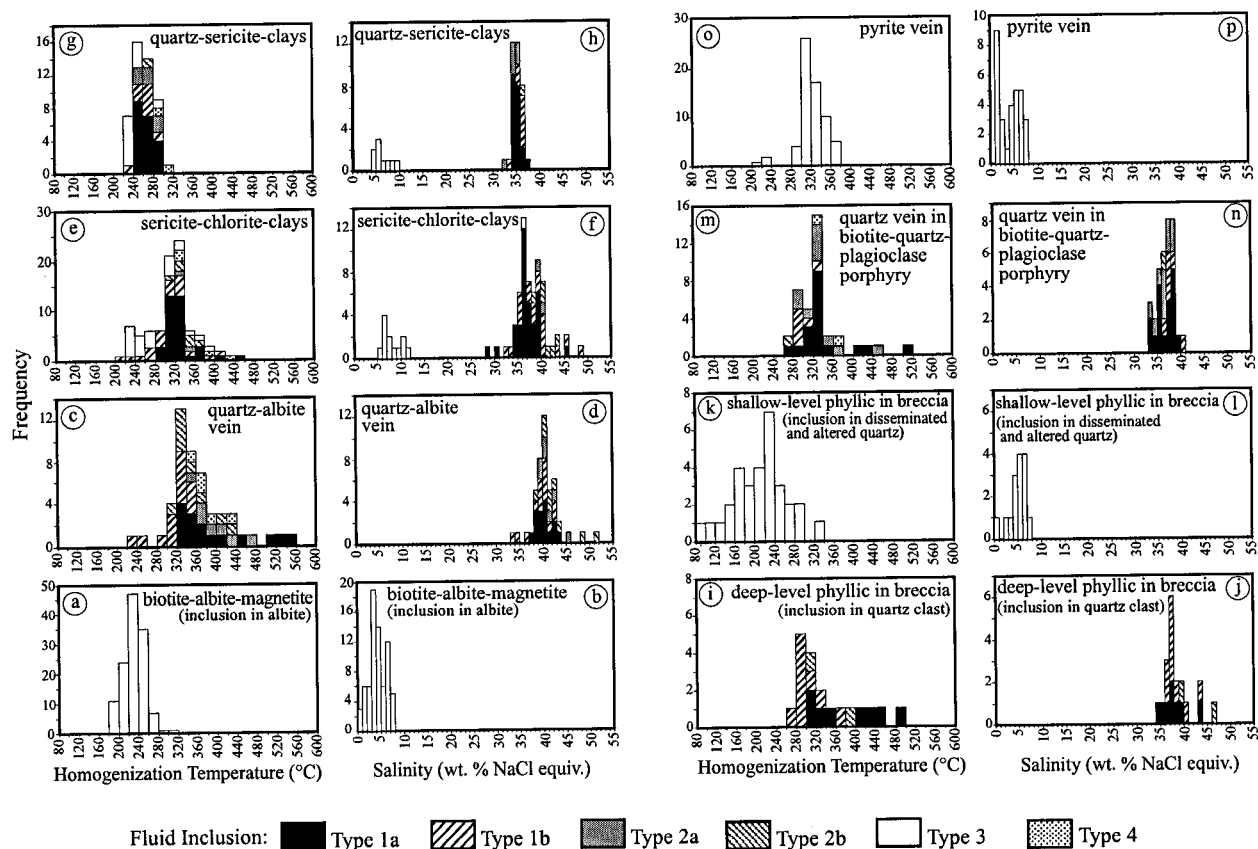


Fig. 2-16:

Histograms of homogenization temperature and salinity of fluid inclusion assemblages characteristic of various alteration facies. The Early Stage fluids related to the biotite-albite-magnetite alteration (a and b) are of moderate temperature but low salinity. The Main Stage intermediate argillic alteration (c through h) is characterized by high-temperature, high-salinity fluids at depth (quartz-albite veins, c and d). As these moved upward, successively generating sericite-chlorite-clay (e and f) and quartz-sericite-clay (g and h) alteration, both temperature and salinity decreased, possibly through mixing with low-salinity meteoric fluids. Fluid inclusions occurring in the deeper-level Transitional phyllic alteration of the breccia bodies have high temperature and salinity (i and j) but those at the shallower-level have variable temperatures but low salinity (k and l). Fluid inclusions associated with phyllic alteration of intrusive bodies cutting the breccias have high temperature and salinities (m and n). Terminal Stage pyrite veins are associated with higher-temperature fluids (o), similar to those of the deeper-level phyllic inclusions, but with low salinities (p), similar to those of shallower-level phyllic alteration. See text for discussion.

Quartz-albite veins: Quartz-albite veins cut the biotite-albite-magnetite alteration (Fig. 2-6c) and represent the roots of the Main Stage alteration/mineralization column. Albite is typically altered to smectite but quartz contains numerous large ($>20\ \mu\text{m}$), apparently, primary inclusions (Fig. 2-15f). Vapour-rich inclusions are abundant (ca. >70 percent), and saline and multi-salt inclusions occur in approximately equal numbers. Liquid-rich inclusions are not common. First-melting temperatures were as low as -50 to -56°C , indicating the possible existence of CO_2 and/or CaCl_2 . The $\text{NaCl}/(\text{NaCl}+\text{KCl})$ ratio of the multi-salt inclusions varies from 0.61 to 0.70, as determined from the dissolution temperatures of halite and sylvite (Roedder, 1984). These inclusions record a wide range of both homogenization temperature, from 235 to 544°C , and salinity, from 34 to 52 wt. percent NaCl equiv. (Figs. 2-16b and c). Saline and multi-salt inclusions recording final homogenization by vapour disappearance (types 1a and 2a), as well as vapour-rich inclusions, homogenized above 320°C . Inclusions homogenizing by salt dissolution (types 1b and 2b) are absent in the very high temperature range ($>440^\circ\text{C}$), but increase in proportion as homogenization temperature decreases. Inclusions with the lowest homogenization temperatures ($<320^\circ\text{C}$) invariably homogenized by salt dissolution and no vapour-rich inclusion homogenized within this range. The salinities of the majority of inclusions are between 37.5 and 43.9 wt. percent NaCl equiv. However, high-temperature multi-salt inclusions have up to 51.4 wt. percent NaCl equiv., and low-temperature type 1b saline inclusions have salinities as low as 33.7 wt. percent NaCl equiv.

Sericite-chlorite-clay alteration: Coarse-grained quartz is not common in association with the early stages of the sericite-chlorite-clay alteration, but wider veins contain quartz with abundant large inclusions ($> 20\ \mu\text{m}$). Vapour-rich inclusions are the dominant type, followed by saline inclusions, liquid-rich inclusions, and multi-salt inclusions. First-melting temperatures are similar to those of inclusions in quartz-albite veins. The $\text{NaCl}/(\text{NaCl}+\text{KCl})$ ratio of the multi-salt

inclusions ranges from 0.52 to 0.62. Homogenization temperature varies from 216 to 444°C and salinity from 28.6 to 48.2 wt. percent NaCl equiv. for salt-bearing inclusions, and from 5.1 to 11.7 wt. percent NaCl equiv. for liquid-rich inclusions (Figs. 2-16e and f). Higher-temperature inclusions (>350°C) have larger salinity variations while lower temperature inclusions are more consistent (Fig. 2-17). The observed gap between low-salinity, liquid-rich, and other inclusions is inferred to be real (see Ahmad and Rose, 1980). Thus, inclusions associated with this type of alteration have a narrower range of homogenization temperature, are up to 100°C cooler, and are slightly less saline than those of the deeper-level quartz-albite veins. However, the most abundant inclusions in both alteration types have a homogenization temperatures of around 330°C. Liquid-rich inclusions have variable homogenization temperatures, but most are < 280°C. Inclusions homogenizing by salt dissolution are less abundant, and they are the only saline inclusions with homogenization temperatures less than 280°C.

Quartz-sericite-clay alteration: Inclusions related to this alteration facies were studied in disseminated fine-grained quartz intergrown with sericite and clays (Fig. 2-6h). Inclusions are smaller (less than 20 µm, but usually 10-15 µm) than those at greater depth. Most inclusions contain only one opaque phase. This was identified as chalcopyrite in less than one-third of the observed inclusions, but generally had a rounded shape and/or was too small to identify. A few measured multi-salt inclusions had NaCl/(NaCl+KCl) ratios similar to those in the sericite-chlorite-clay alteration. Final homogenization temperatures ranged from 221 to 320°C, and the salinity from 32.1 to 37 wt. percent NaCl equiv. for salt-bearing inclusions, and 4.2 to 10 wt. percent NaCl equiv. for the liquid-rich (Figs. 2-16g and h). Liquid-rich inclusions yielded the lowest homogenization temperatures, 221-260°C. Therefore, the fluid inclusions overall are up to 124°C cooler and slightly less saline than those related to the sericite-chlorite-clay alteration.

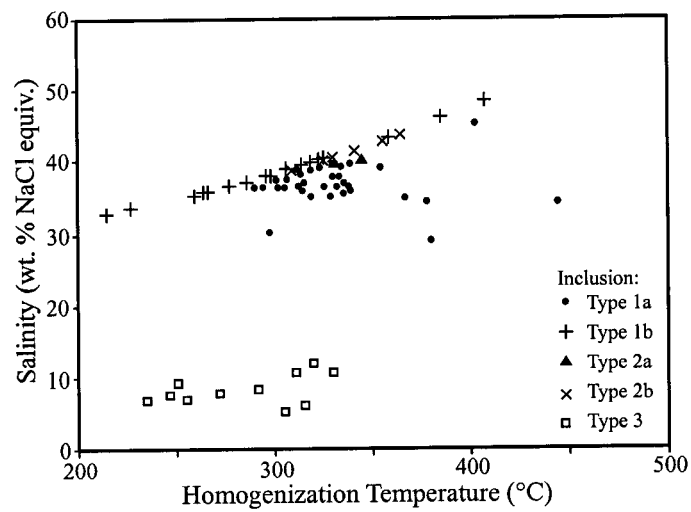


Fig. 2-17:
Salinity vs. final homogenization temperature diagram for fluid inclusions associated with the Main Stage sericite-chlorite-clay alteration. Types 1b and 2b inclusions, homogenizing by salt dissolution, define the halite saturation curve, but the actual total salinity extends beyond this line due to the presence of other cations. Types 1a and 2a inclusions have a greater salinity variation at higher than at lower temperatures. Note that very low-temperature, high-salinity inclusions are dominantly of type 1b and that there is a major hiatus in salinity from 12 to 28 wt. percent NaCl equiv.

The most abundant are also ca. 80°C cooler. Over two-thirds of the saline and multi-salt inclusions that homogenized by vapour disappearance exhibited vapour and salt homogenization at very similar temperatures.

Advanced argillic alteration: The andalusite which replaced clay minerals (illite) in the advanced argillic alteration facies typically contains extremely small inclusions unsuitable for microthermometry. However, one measurement was possible on an exceptionally large inclusion which contained vapour, a cubic salt and trapped clays (Fig. 2-15g). This inclusion exhibited final homogenization by salt dissolution (type 2) at 270°C (the vapour homogenized at 232°C), and a salinity of 36 wt. percent NaCl equiv. Thus, its temperature and salinity fall within the ranges observed for the quartz-sericite-clay alteration.

Phyllic alteration: Phyllic alteration is developed in the breccia bodies and is associated with two distinct types of fluid inclusion assemblage. Inclusions in quartz clasts (Fig. 2-15h) are very similar to those associated with quartz veins of the biotite-quartz-plagioclase porphyry intrusion (see below), with abundant vapour-rich, saline and multi-salt types. At deeper levels, where micro-breccia textures dominate (see above), these constitute the major inclusion type associated with phyllic alteration. They exhibit final homogenization between 280 to 486°C, and salinities of 34.9 to 46.9 wt. percent NaCl equiv. (Figs. 2-16i and j), although saline inclusions in a few clasts did not homogenize at 600°C. In contrast, fluid inclusions in fine-grained quartz aggregates (Fig. 2-10e) in quartz-clay alteration rims of the clasts (Figs. 2-10f and 14i), and in disseminated quartz, are dominantly liquid- and vapour-rich. Liquid-rich inclusions had a wide range of homogenization temperature, from as low as 90°C to 334°C, and their salinity ranged from between 0.1 and 7.6 wt. percent NaCl equiv. (Figs. 2-16k and l). Therefore, fluids related to

the phyllic alteration may be subdivided into two populations: deeper-level fluids are saline and high-temperature, whereas those at shallower levels are dilute and significantly cooler.

Quartz vein in biotite-quartz-plagioclase porphyry: The biotite-quartz-plagioclase porphyry is an intrusive unit associated with Transitional Stage breccia emplacement (see above). It contains abundant quartz veins, some with irregular boundaries (Fig. 2-4g). Homogenization temperatures and salinities vary from 245 to 510°C and 33 to 40 wt. percent NaCl equiv., respectively (Figs. 2-16m and n). Therefore, except for one high-temperature inclusion (510°C), their homogenization temperature and salinity are similar to those of the inclusions associated with sericite-chlorite-clay and deep-level phyllic alterations.

Late pyrite veins: Euhedral quartz crystals commonly enveloping and intergrown with pyrite contain liquid-rich inclusions (Fig. 2-15j). Vapour-rich inclusions occur as trails that cut the quartz crystals and they apparently do not coexist with the randomly distributed liquid-rich inclusions. The latter inclusions have homogenization temperatures of from 218 to 377°C and salinities of 1.2 to 7.9 wt. percent NaCl equiv. (Figs. 2-16o and p). These inclusions, therefore, have homogenization temperatures higher than the fluids related to the shallower-level phyllic alteration (i.e., fine-grained quartz aggregates), but similar to those of the deeper phyllic alteration. The salinity of the late pyrite vein fluids is, however, very similar to that of the shallower-level phyllic alteration.

Entrapment pressure and depth estimates

The entrapment pressure of fluids showing evidence of formation in an immiscible or boiling system, i.e., coeval liquid/saline-rich and vapour-rich inclusions with identical homogenization temperatures, can be estimated on the basis of microthermometric observations

on bodies in which vapour is the last phase to homogenize (Roedder and Bodnar, 1980). Further, the hydrostatic depth can be estimated assuming that the boiling liquid is open to the surface and vapour is contained in pockets and not suspended in the liquid (Haas, 1971). Petrographic and microthermometric data strongly suggest that in the Main and Transitional Stages the majority of the saline, multi-salt saline (types 1a and 2a) and liquid-rich inclusions formed by immiscibility. Their trapping pressures may therefore be estimated using the experimental data of Urusova (1975), Haas (1976) and Bodnar et al. (1985), as is shown graphically in figure 2-18. For non-boiling assemblages, e.g., those in late pyrite veins, the estimated pressure should be considered a minimum value. Arguments for accurate depth estimates are considerably weaker because of fluctuation between hydrostatic and lithostatic environments and variation of the density of the fluid load, as discussed below.

Quartz-albite veins contain inclusions with the highest homogenization temperatures, $\leq 544^{\circ}\text{C}$, and salinities, ≤ 52 wt. percent NaCl equiv., corresponding to entrapment pressures of up to approximately 590 bars. At these temperatures, rocks behave in a plastic manner, with pore pressures exceeding the hydrostatic load and approaching the lithostatic pressure (Fournier, 1999). Thus, entrapment depth was equal to, and possibly greater than the equivalent lithostatic load (ca. 2300 m), but considerably less than the equivalent hydrostatic load (ca. 6000 m). The majority of inclusions in these veins, and almost all of those associated with the sericite-chlorite-clay alteration, located only ca. 100 m higher, have homogenization temperatures of less than 440°C , and most are less than 400°C . Evidence of ductile behavior was observed in some quartz-albite veins with irregular or curved boundaries (Fig. 2-6c). Most of the quartz-albite veins, however, and all veins related to the sericite-chlorite-clay alteration, have abrupt and planar boundaries implying formation in a brittle environment. Therefore, the lower-temperature (\leq ca. 400°C) inclusions in these veins could have been formed in a brittle environment under hydrostatic conditions. Boiling fluids with temperatures of ca. 400°C and a salinity of 40 wt.

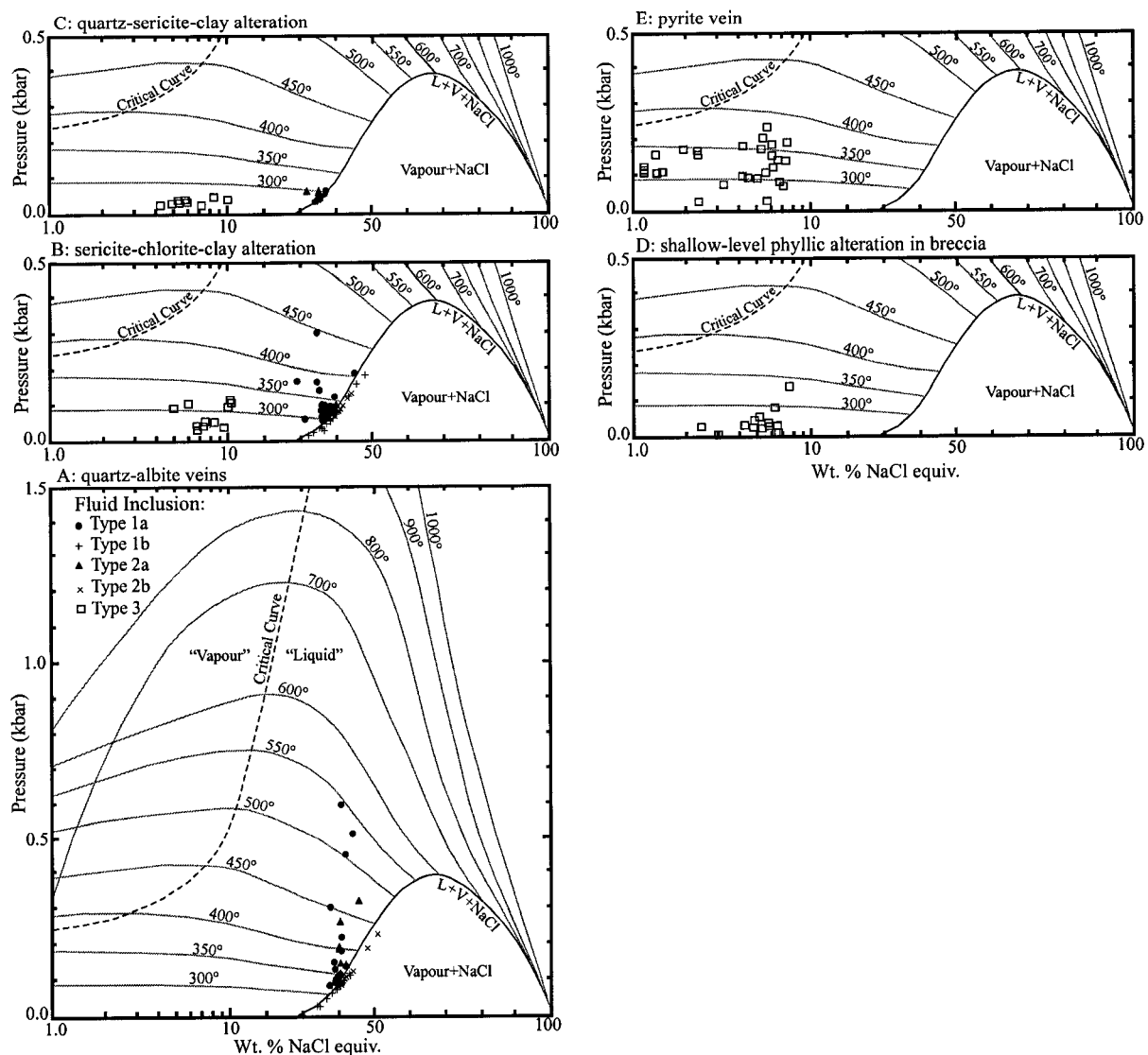


Fig. 2-18:

Pressure estimates for fluid inclusions that exhibited final homogenization by vapour disappearance (types 1a and 1b). Types 1b and 2b inclusions are treated differently for trapping pressure estimation (see Fig. 2-20 and text), but they are shown here to provide a minimum pressure estimate. See text for discussion. The phase diagram is after Sourirajan and Kennedy (1962), Urusova (1975) and Bodnar et al., (1985).

percent NaCl equiv. correspond to a hydrostatic pressure of approximately 200 bars and a depth of 2000 m below the paleowater table. This is considered a minimum depth because of uncertainty regarding the mean density of the fluid load (see below). Therefore, the transition from ductile to brittle conditions and the initiation of extensive sericite-chlorite-clay alteration occurred at some greater depth, probably between 2.5 and 3 km.

Fluid inclusions in disseminated quartz associated with the higher-level quartz-sericite-clay alteration were considerably cooler on trapping, with a maximum temperature of ca. 300°C, and slightly less saline, with 37 wt. percent NaCl equiv. These data correspond to a hydrostatic pressure of only 60 bars and a depth of only 500 m below the paleowater table, assuming fluid entrapment in a boiling system (see above). The quartz-sericite-clay samples were taken from approximately 200 m below the present-day surface. Thus, if the inclusions were trapped at 500 m below the paleosurface, only 300 m of erosion can have occurred since the hypogene mineralization event, in gross disagreement with the evidence for deep erosion provided by the thick supergene leached and oxidized zones (Bouzari and Clark, 2002). Moreover, the quartz-sericite-clay samples are located only 100 m above the sericite-chlorite-clay alteration, which formed at an approximate depth of 2.5 km. Two km of erosion during the Main Stage hypogene event appears extremely unlikely. The most reasonable explanation for this dichotomy is the existence in the hydrostatic head of an average density considerably less than unity, such as would be caused by suspended vapour, or, more probably, different densities at different depths. The boiling of an exsolved magmatic fluid with a salinity of ca. 8 wt. percent NaCl equiv. at a depth of 3 km would generate a hypersaline liquid (ca. 50 wt. percent NaCl equiv.) and a vapour (ca. 0.7 wt. percent NaCl equiv.), the latter accounting for over 90 wt. percent of the total exsolved water (Shinohara and Hedenquist, 1997). This vapour phase would constitute over 99 volume percent of the boiled fluid. Vapour-rich inclusions are the dominant observed phase in Main and Transitional Stage fluid inclusions (see above) and constitute approximately 70 to 80

percent of the total volume of the observed inclusions. Therefore, a large portion of the vapour must have escaped to shallow levels which are now eroded. Areas dominated by vapour-rich inclusions are documented from the shallow parts of very young deposits which have suffered minimal erosion, such as the Far Southeast-Lepanto porphyry and epithermal deposit, Philippines (Hedenquist et al., 1998). At these shallow levels, the vapour (superheated steam) condenses and absorbs cold meteoric water (Hedenquist et al., 1998). This will in turn cause lowering of the pressure at the top of the liquid column, thereby triggering further boiling (Semat, 1966).

The upper parts of a boiling fluid column in a fractured rock under hydrostatic conditions are thus dominated by a mixture of low-salinity steam, condensed steam, vapourized ground water and groundwater. The existence of this low-density fluid at the top of a column of boiling liquid will cause the depth of inclusion trapping to be significantly underestimated (Roedder and Bodnar, 1980: p. 268). If the quartz-sericite-clay alteration developed under 60 bars pressure and at a depth comparable to that at which the immediately underlying sericite-chlorite-clay formed, the overall density of the hydrostatic column must have been around one-third of that prevailing during sericite-chlorite-clay alteration, regardless of trapping depth and the density of the sericite-chlorite-clay alteration fluids. Thus, assuming trapping at 2.5 km depth, the transition from high- to low-density fluid would have occurred at least 1.5 km below the paleosurface, depending on the exact density of each fluid.

The above argument also applies to the trapping depth of fluids related to the sericite-chlorite-clay alteration and quartz-albite veins. Thus, depending on the extent of vapour accumulation at shallow levels during the early stages of hydrostatic boiling (ca. 400°C at 200 bars), the assumed 2000 m depth would be considered a minimum value and trapping plausibly occurred at around 2.5-3 km. Continued boiling, upward migration of vapour and accumulation of the low-density fluids, and cooling of the liquid phase by the host rock and invading meteoric

water, are inferred to have been responsible for the formation of lower-temperature and lower-pressure inclusions (as low as 300°C and 60 bars: Fig. 2-18) in these veins.

Inclusions that homogenize by halite dissolution (types 1b and 2b) must have been trapped in the liquid-stable, vapour-absent field (Bodnar, 1994; Cline and Bodnar, 1994). These inclusions typically have lower homogenization temperatures than other saline inclusions (types 1a and 2a). They are the only salt-bearing inclusions herein with homogenization temperatures below 320°C (quartz-albite veins: Fig. 2-16c) or 280°C (sericite-chlorite-clay: Fig. 2-16e). No vapour-rich inclusions had homogenization temperatures below these ranges. Thus, these fluids were relatively cool and not boiling at the time of trapping. The differences between halite dissolution and vapour disappearance temperatures (ΔT) show a systematic decrease from the deep quartz-albite veins ($\Delta T \leq 120^\circ\text{C}$) to the shallower quartz-sericite-clay alteration ($\Delta T \leq 64^\circ\text{C}$), as shown on figure 2-19. Bodnar (1994) has experimentally modeled the H_2O -NaCl system and determined halite liquidus and isochores for a 40 wt. percent NaCl solution. Therefore, knowing vapour homogenization and halite dissolution temperatures, trapping pressures may be estimated for inclusion types 1b and 2b of the quartz-albite veins and sericite-chlorite-clay alteration with salinity of 40 ± 1 wt. percent NaCl equiv. (Fig. 2-20). Over 60 percent of these inclusions define a pressure of < 0.6 kbar ($\Delta T \leq 30^\circ\text{C}$), but pressures of up to 1.8 kbar ($\Delta T = 86^\circ\text{C}$) and 2.3 kbar ($\Delta T = 109^\circ\text{C}$) are obtained for sericite-chlorite-clay alteration and quartz-albite veins, respectively (Fig. 2-20). Inclusions exhibiting final homogenization through halite dissolution are commonly interpreted as recording entrapment at high pressure under lithostatic conditions (Cline and Bodnar, 1994). Clusters of inclusions with trapping pressures of < 0.6 kbar correspond to the maximum pressure obtained from boiling assemblages (0.59 kbar). Thus, these inclusions may have been produced by cooling and possibly slight pressure fluctuation of the boiling assemblage fluids (path 1 in Fig. 2-20), as proposed for San Rafael,

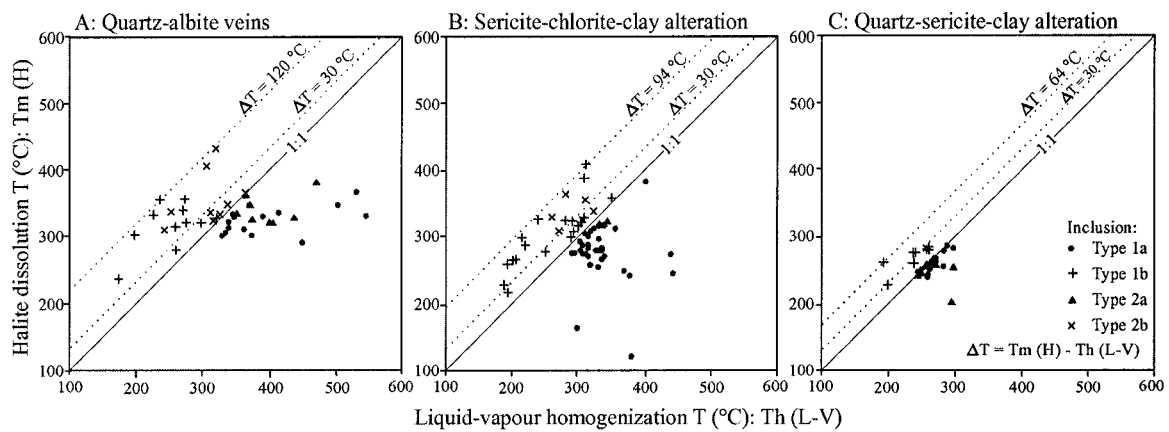


Fig. 2-19:

Plot of temperature of halite dissolution against temperature of vapour disappearance for fluid inclusions associated with the Main Stage alteration assemblages. The differences between halite dissolution ($T_m(H)$) and vapour disappearance ($T_h(L-V)$) temperatures of the types 1b and 2b inclusions (ΔT) decrease from deep quartz-albite veins to shallower-level quartz-sericite-clay alteration. In the latter alteration, ΔT is very small or negligible in the majority of inclusions. This may be related to greater pressure at depth or to convergence of the temperatures of the fluid and rock at shallower levels (see text for discussion).

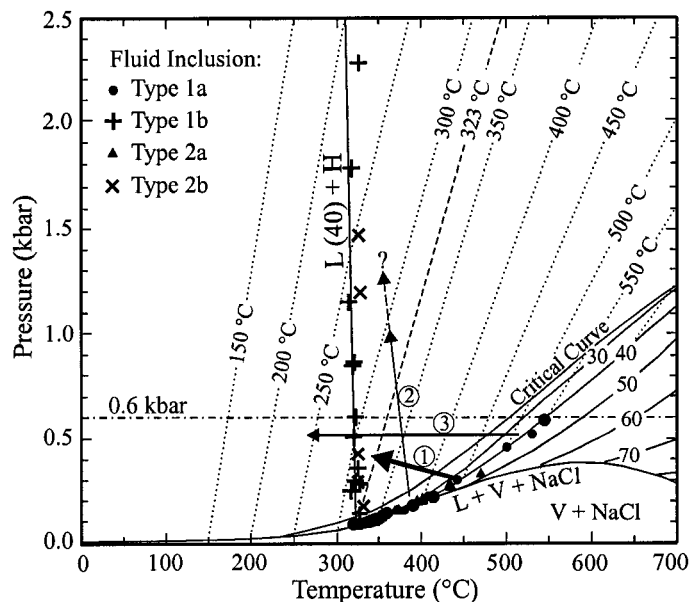


Fig. 2-20:

Pressure estimates for inclusions homogenizing by salt dissolution (types 1b and 2b) and with salinities of 40 ± 1 wt. percent NaCl equiv. Types 1a and 2a inclusions with similar salinity are shown for comparison. The dashed line labeled 323°C and those parallel to it are lines of constant liquid-vapour homogenization temperature (iso-Th) for inclusions with 40 percent salinity (Bodnar, 1994). Inclusions trapped to the right of iso-Th 323°C have their final homogenization by vapour disappearance, and those trapped to the left, by salt dissolution. The horizontal line labeled 0.6 kbar is the maximum pressure obtained from the boiling types 1a and 2a inclusions. Most types 1b and 2b inclusions yield pressures of < 0.6 kbar, and they may therefore have formed by cooling and a slight increase of the pressure of boiling fluids (path 1). In contrast, inclusions with very high pressure (> 1 kbar) could not have been formed only by cooling and the pressure must have significantly exceeded the hydrostatic load (path 2) to form them. However, quenching of hot fluids may have caused trapping in the halite-stable field (path 3), thus giving erroneously high-pressure values if the iso-Th lines are used. See text for discussion. Phase diagram is after Bodnar et al. (1985) and Bodnar (1994).

Peru, by Kontak and Clark (2002). Assuming an entrapment depth of 2.5 to 3 km, higher-pressure inclusions may have formed by fluid and tectonic overpressuring when mineral deposition sealed the vein channels and a lithostatic environment prevailed (path 2 in Fig. 2-20), as proposed for Questa, New Mexico (Cline and Bodnar, 1994). However, significantly higher-pressure inclusions (≥ 1.5 kbar) are difficult to interpret unless they were trapped at much greater depths. Roedder (1984), in discussing pressure estimates obtained for inclusions with final homogenization by halite dissolution, noted that such high pressures are in gross disagreement with measured pressures required to decrepitate inclusions in quartz (850 bars). Bodnar et al. (1989) set this limit for synthetic inclusions with diameters of about 5 and 10 μm at 1-3 kbar. The majority of the measured inclusions at Cerro Colorado have dimensions of 20 - 30 μm , and therefore the maximum pressures they could sustain probably approach the lower limit proposed by Bodnar et al. (1989).

Alternatively, however, these inclusions could have been produced by rapid, quasi-isobaric cooling of the boiling fluids which brought them to the halite-saturated field (path 3 in Fig. 2-20). Thus, halite crystals were present at the trapping temperature (barring metastability), but were not trapped in the inclusions (Roedder, 1984: page 453). On cooling after trapping, halite would form immediately and the inclusion would follow its isochore until vapour formed when it intersected the liquid-vapour curve. Under these conditions, application of Bodnar's (1994) phase diagram (Fig. 2-20) would result in significant error in estimating the trapping pressure. Thus, the maximum ΔT shown in Figure 2-19 may simply represent the extent of the cooling of the fluids rather than overpressuring. During the early stages of fluid flow along fractures, very hot fluids interact with cold country rock and their temperature must decrease significantly and rapidly. As the fluid flow continues, rock and fluid temperatures converge. This is shown by the very wide range of homogenization temperature of the quartz-albite veins and

more restricted and lower temperatures of the ensuing sericite-chlorite-clay and quartz-sericite-clay alteration facies (Figs. 2-16c, e, and g).

Pressure and depth estimates for fluid inclusions in clasts of the breccia pipes and quartz veins in the biotite-quartz-plagioclase porphyry intrusive unit associated with the breccia body (i.e., deeper-phyllitic alteration) are similar to those for sericite-chlorite-clay alteration. This implies that no major erosion occurred between the Main Stage and the emplacement and alteration of the Transitional Stage intrusive units. However, inclusions associated with the shallow-level phyllic alteration, e.g., in quartz aggregates and disseminations, display a significantly lower homogenization temperature, and record pressures (Fig. 2-18) corresponding to depths of up to 1550 m. As discussed above, the existence of a low-density hydrostatic load would increase this depth. Vapour-rich inclusions coexist with these low-salinity inclusions, but their homogenization temperatures could not be measured because most inclusions were gas-filled. Hence, there is no strong evidence that all shallower-level phyllic fluids were boiling at the time of trapping, and some of the very low-temperature ($<150^{\circ}\text{C}$), low-salinity (< 1 wt. percent NaCl equiv.) inclusions may represent heated groundwater which did not boil.

Fluid inclusions associated with the Late Stage pyrite veins have homogenization temperatures of up to 377°C and a salinity of around 5 wt. percent NaCl equiv. There is no compelling evidence of boiling at the time of trapping of the liquid-rich inclusions (see above), implying a minimum pressure and depth of 230 bars and 900 m, respectively.

It should be emphasized that the above estimates do not take into account the occurrence of CO_2 and salts other than halite, which would, respectively, increase (Hedenquist et al., 1985) and decrease (Roedder, 1984) the estimated entrapment pressures.

Summary

The Early Stage alteration was generated by non-boiling, low-salinity (ca. 8 wt. percent NaCl equiv.) fluids, with lower homogenization temperatures (186-311°C) than those responsible for the succeeding Main Stage alteration. Assuming entrapment at depths similar to those of inclusions associated with the Main Stage, i.e., ca. 3 km, a “pressure correction” of 65 to 70°C would be applicable to the homogenization temperature of the Early Stage inclusions (Potter, 1977), indicating trapping temperatures of 251-381°C. Thus, the Early Stage fluids would have been of lower salinity, and up to 163°C cooler than the later Main Stage fluids, indicating an overall prograde thermal evolution in the earlier stages of evolution of the hydrothermal system.

The Main Stage alteration was attended by fluid immiscibility at high temperatures, >500°C, and depths of ca. 2.5-3 km, presumably recording the influx of new hot fluids into the shallow crust and their subsequent boiling. However, release of pressure, such as would be caused by movement along major structures or erosion, may have also contributed to the boiling. As the fluids moved upward and cooled, they reached the brittle environment, caused the extensive fracturing and alteration related to the Main Stage mineralization at < 400°C and depths of 2.5-3 km, and deposited over two-thirds of the hypogene copper budget. The quartz-albite veins at the roots of the Main Stage alteration zone are considered to have been emplaced in a transitional zone between very high-temperature ductile and brittle environments. The fluids thereafter moved upward, mixed with ground water, cooled by up to 244°C, and were diluted by up to 14 wt. percent NaCl equiv., producing the zoned Main Stage pattern of alteration and mineralization from deep quartz-albite veins to, ultimately, shallow advanced argillic alteration. The fluids also evolved from deeper high-density to shallower-level low-density, the latter preferentially generating quartz-sericite-clay and advanced argillic alteration. Retrograde collapse

of the hydrothermal system caused further inward migration of the low-density, low-salinity fluids and replacement of the sericite-chlorite-clay alteration by quartz-sericite-clay assemblages.

Transitional Stage phyllic alteration related to breccia bodies was initiated by high-temperature and high-salinity fluids (up to 486°C and 44 wt. percent NaCl equiv.), evidence of which is preserved at deeper levels. However, shallower-level phyllic alteration was caused by cooler (< 334°C) and markedly less saline (< 8 wt. percent NaCl equiv.) fluids. Overall, the upward evolution of the fluids responsible for the phyllic alteration was therefore strikingly similar to that of fluids which generated the deeper and shallower-level Main Stage alteration facies.

Late Stage pyrite veins formed by non-boiling fluids with homogenization temperatures of up to 377°C, similar to those of fluids which generated deeper-level phyllic alteration. However, they have very low salinity (1.2 to 7.9 wt. percent NaCl equiv.), comparable to that of the fluids which generated the shallower-level phyllic alteration. Therefore, the latest stage of the mineralization, even at shallow levels, was associated with high temperature fluids. It is not, however, known if the low salinity of these fluids was caused by a lack of boiling or by dilution.

2.9. Evolution of the Mineralizing System

At Cerro Colorado, all silicate alteration and sulphide assemblages with mineralogical and textural features similar to those of porphyry deposits worldwide (e.g., Titley and Beane, 1981) occur within a coherent area surrounding a cluster of phreato-magmatic breccia bodies (Fig. 2-2). This, in addition to the geochronologic data (Fig. 2-12), strongly suggests that the deposit records the evolution of a single porphyry-type hydrothermal system. Although the Transitional Stage breccia bodies may reflect the location of the main centers of orthomagmatic activity at depth, the present exposure interval provides no information regarding any igneous bodies directly related to the Early and Main Stages of alteration, and no stable isotope data are

available to shed light on the source of alteration fluids. However, the field, mineralogical, chemical, geochronologic and fluid inclusion relationships documented herein provide a strong basis for reconstruction of the mineralizing system.

Early Stage

The Early Stage was the product of moderate-temperature (ca. $\leq 380^{\circ}\text{C}$), low-salinity (≤ 8 wt percent NaCl equiv.), non-boiling fluids which generated a large volume of sulphide-free potassic-sodic alteration, 4×2 km in area, with little or no stockwork development. The extensive metasomatic exchange (Fig. 2-14), particularly the introduction of considerable K, Na, and Fe^{+2} , and the F-rich nature of the newly-formed biotite, rule out a metamorphic origin. If magmatogene fluids were involved, they must have cooled significantly before generating the pervasive alteration. This may reflect their origin in a relatively deeply emplaced magma chamber. It is plausible that single-phase, low-salinity (6-8 percent), high-temperature ($> 500^{\circ}\text{C}$) brines exsolved during the crystallization and retrograde boiling of silicic magma at depth of 6-7 km depths (Burnham, 1979; Burnham and Ohmoto, 1980; Fournier, 1999), rose towards surface and extensively cooled because of a low fluid flux. During the early stages of development of a shallow intrusive complex, rising magmas encounter relatively cold country rock. Only a thin shell of plastic rock surrounds the still molten portion of the crystallizing magma (Fournier, 1999), and therefore the exsolved fluids do not accumulate before ascent. A lack of syn-alteration intrusive dikes or major structural breaks that could focus the hydrothermal fluids would promote dispersion of fluids over a large area, resulting in lower fluid:rock ratios and greater heat loss. In such an environment, the fluids would probably not intersect the solvus (e.g., H_2O -NaCl), and boiling and, hence, extensive stockwork development would be precluded. It is therefore, envisaged that fluids would have been discharged laterally into lithostatically pressured wall rock (Hodgson, 1995) at depth of ca. 3 km, equilibrating with the Cerro Empexa andesite and causing

extensive mass exchange and pervasive alteration. The existence of fluid inclusions with salinities of less than 2 wt percent NaCl equiv. may indicate incorporation of connate or, more probably, meteoric water at this stage.

Early Stage alteration is sulphide-barren and thus the fluids did not achieve saturation in either chalcopyrite or pyrite. However, mass balance relationships indicate that considerable Cl was added during alteration, so that Cu would have been readily transported. Moreover, cooling through ca. 350°C would have been accompanied by a major decrease in chalcopyrite solubility: thus, Xiao et al. (1998) demonstrated experimentally that the bulk of dissolved Cu would precipitate between 350 and 250°C. Therefore, temperature may not have been the critical factor in the non-precipitation of chalcopyrite or pyrite, which may have resulted from an inherently low reduced sulphur content of the fluids, despite the relatively reduced conditions revealed by the Fe⁺² metasomatism. The possibility cannot, however, be ruled out that major amounts of Cu and Fe sulphides were deposited at higher temperatures at greater depths, i.e., the Early Stage fluids were “spent”, a relationship which would integrate the unusually low temperatures with the lack of sulphides. A further possibility is that the lack of sulphides may be related to a gradual increase in fluid:rock ratio resulting in protracted heating of the alteration zone, i.e., the Early Stage may have been inherently prograde.

Main Stage

Main Stage alteration and mineralization assemblages cut and replace Early Stage alteration. Except for the quartz-albite veins, the mineral assemblages of the Main Stage were radically out of equilibrium with those of the Early Stage. Therefore, Main Stage alteration, during which much of the protore copper was deposited, was generated by fluids with significantly different characteristics than those which formed the preceding Early Stage zone. Irregular quartz-albite veins at the base of Main Stage record the most primitive Main Stage

fluids, with temperatures as high as 544°C and salinities up to 52 wt percent NaCl equiv. The larger differences between salt dissolution and vapour disappearance temperatures in the types 1b and 2b inclusions of these veins (Fig. 2-19a) relative to those of the shallower, lower-temperature, pervasive, quartz-sericite-clay alteration (Fig. 2-19c), indicate that Main Stage fluids cooled rapidly on encountering fractured, cool, biotitized and albitized host rock. The high-temperature fluids of the Main Stage may have been generated as a result of incursion of hotter, i.e. mafic, melt into the underlying magma chamber and/or magma emplacement at shallow depth (e.g., < 4.5 km). This would have resulted in an increase in strain rate in the overlying rocks causing brittle behavior to occur at greater depth (Fournier, 1999), and permitting the rapid discharge of large quantities of accumulated magmatic fluids to shallower levels, where they boiled. Decompression at the brittle-plastic transition, at ca. $\geq 400^{\circ}\text{C}$, would have caused quartz and albite supersaturation in the fluids (Fournier, 1999), generating the banded quartz-albite veins and local massive silicification at the base of the Main Zone.

As fluids moved through the stockwork in the brittle zone, they equilibrated with the host rocks and fluid and rock temperatures converged (Fig. 2-19). Thus, the fluids cooled from $\geq 544^{\circ}\text{C}$ to $< 320^{\circ}\text{C}$ (Figs. 2-16c, e and g), and salinity decreased from ≥ 52 to < 37 wt percent NaCl equiv. (Figs. 2-16d, f, and h). At shallower levels, corresponding to the transition from the quartz-albite to the quartz-sericite-clay facies, progressively greater proportions of very low-salinity fluids, e.g. < 10 wt percent NaCl equiv., were involved (Figs. 2-16d, f, and h). This plausibly occurred as a result of mixing with non-magmatic fluids and/or density segregation which led to the development of a stack of fluid volumes, ranging from high-density at depth to low-density and vapour-dominated at shallower levels. pH decreased upwards through condensation of the abundant vapour-rich fluids. These processes resulted in the quasi-simultaneous development of an array of alteration zones from intermediate- to advanced argillic

sub-facies (Fig. 2-5), i.e., the Main Stage alteration pattern was the product of variations in fluid pH and temperature.

Mass exchange relationships between Early Stage and Main Stage sericite-chlorite-clay sub-facies indicate that the major effects of these fluids were the leaching of Na, Ca and Mg, through hydrolysis of feldspar and biotite, and the deposition of sulphides (Figs. 2-14b and c). Higher acidity at shallower levels caused stronger hydrolysis, and the loss of K through muscovite breakdown. A gradual change is apparent from chlorite-muscovite stability in the intermediate argillic alteration horizon, through muscovite-illite (i.e., alkali-deficient muscovite) stability in the quartz-sericite-clay alteration, to pyrophyllite (i.e., alkali-free phyllosilicate) stability in the advanced argillic alteration sub-facies (Fig. 2-8). Similar compositional trends are shown by individual phyllosilicates: the Fe content of chlorite and the Fe and Mg contents of muscovite decrease upwards (Table 2-1). The formation of abundant andalusite and diaspore after muscovite and illite at shallow levels (Fig. 2-5) implies extreme acidity associated with low-density vapour accumulation in the uppermost preserved portion of the Main Stage system.

Several other factors, in addition to temperature and pH, may also have contributed to the distribution and zoning of the Main Stage mineral assemblages. Most notably, the fluid:rock ratio and its possible effect on clay mineral distribution need to be emphasized. Clay minerals were generated throughout but their original distribution is not fully established because of overprinting at shallow levels, where the abundant smectite is assumed to be of supergene origin. Illite and smectite are, however, the main clay minerals in Main Stage assemblages with minimal supergene overprint. The proportion of hypogene smectite group clays increases with depth, and in the deepest drill core intersections illite is absent and smectite, commonly nontronitic, replaces albite in Main Stage veinlets (Fig. 2-7e). The replacement of both disseminated albite and relict plagioclase phenocrysts by smectite preceded the development of chlorite or muscovite (Fig. 2-7c), and fluid inclusion microthermometry shows that these veins formed at temperatures as high

as 444°C (Fig. 2-16e). This is in disagreement with the generally accepted upper thermal stability limit of smectite (Velde, 1992), inferred from studies of diagenesis (Perry and Hower, 1970) and geothermal systems (Yau et al., 1988), as well as from laboratory synthesis (Aja et al., 1991a, b). These studies indicate that smectite forms at very low temperature ($< 25^{\circ}\text{C}$) and that there is a transition from smectite to mixed layer illite/smectite at ca. $100\text{-}120^{\circ}\text{C}$. The proportion of smectite decreases with increasing temperature and it does not generally survive above $200\text{-}220^{\circ}\text{C}$. Smectite, however, is widely reported in association with submarine massive sulphide deposits as an alteration product of basalt, e.g., on the Galapagos Ridge (Embley et al., 1988), or as a direct precipitate from hydrothermal solutions at temperatures exceeding 300°C (Alt and Jiang, 1991). Seyfried and Bischoff (1981) and Seyfried and Mottl (1982) showed that basalt was completely replaced by smectite during experimental reaction with both seawater and a 0.45 m NaCl solution at 300°C . In a transmission electron microscopic study of intermediate argillic alteration assemblages at Butte, Montana (Sales and Meyer, 1948; Meyer and Hemley, 1967), Page and Wenk (1979) demonstrate that the first product of plagioclase alteration is smectite. In the main stage veins of this deposit, which formed at ca. 300°C (Meyer et al., 1968), smectite envelops a central sericitic zone and gradually diminishes outward to fresh rock (Sales and Meyer, 1948; Page and Wenk, 1979) a relationship very similar to that in the Main Stage veins at Cerro Colorado (e.g., Fig. 2-7e). At Bingham, Utah, Parry et al. (2002) document the formation of smectite/illite in association with both phyllic and intermediate argillic alteration, and emphasize that the proportion of smectite increases with depth. They estimate a formation temperature of $200\text{-}220^{\circ}\text{C}$ on the basis of smectite content and ordering of illite/smectite of clay assemblages (see above references). However, they acknowledge that these temperature estimates for the associated phyllic assemblages are “at the lower end of the fluid inclusion measurements at other porphyry copper deposits” (Parry et al., 2002, page 236). Therefore, there is convincing

evidence from various hydrothermal environments that smectite can form at temperatures significantly higher than its generally accepted upper stability limit.

Essene and Peacor (1995) argue that most clays are not distinct minerals or phases, but are metastable and out of equilibrium with their formation environment, exhibiting assemblages incompatible with Schreinemaker's phase rule. Therefore, the successive conversion of smectite to illite/smectite and then to illite depends not only on temperature but also on alteration duration and fluid:rock ratio. Thus, illite/smectite formed in pelitic sedimentary rocks at 130-150°C with reaction times of $<10^6$ yr, and at 90-100°C for reaction times of $>10^7$ yr (Perry and Hower, 1970; Hower and Altaner, 1983). It is concluded, therefore, that Main Stage smectite at Cerro Colorado, at least in the deepest part of the zone, formed under metastable conditions. However, abundant smectite at the shallowest levels, as at Bingham (Parry et al., 2002: their Table 3; samples 7, 8, 14, 15 and 16) may have been generated under more stable conditions by low temperature fluids in a supergene or hypogene environment.

Transitional and Late Stages

Phyllic alteration at Cerro Colorado is centered in the breccia bodies and forms an inverted conical halo in the surrounding andesite, but intrusive porphyries that cut the breccia bodies are also extensively affected. Therefore, phyllic alteration was closely associated with the breccia and porphyry emplacement during the Transitional Stage. The temporal relationships of these events are not clear but, on the basis of cross-cutting relationships (Fig. 2-5), intrusion of the porphyries plausibly occurred after the main breccia emplacement, becoming progressively more felsic and less mineralized. Thus, the quartz porphyry which cuts biotite-quartz-plagioclase porphyry is weakly mineralized and in some areas copper grades fall below 0.1 percent. The fluids that caused phyllic alteration in the breccias were boiling, hot ($\leq 486^\circ\text{C}$) and saline (≤ 47 wt percent NaCl equiv.: Figs. 2-16i and j), but at shallower levels became progressively cooler (\leq

334°C) and less saline (≤ 8 wt percent NaCl equiv.), defining trends similar to those of the Main Stage. Fluids related to the phyllic alteration in the porphyries were also very hot ($\leq 510^\circ\text{C}$), boiling and saline (≤ 40 wt percent NaCl equiv.: Figs. 2-16m and n).

Fluids trapped in the intrusive porphyries and in lower parts of the breccia bodies were therefore as hot as the deep Main Stage fluids, and there was no retrograde relationship between Main and Transitional Stages. Dilute fluids, however, were significantly more abundant at the shallow levels of the Transitional than of the Main Stage, some with temperatures as low as 90°C . This is interpreted as evidence for a greater influx of meteoric water and/or vapour condensation as a result of the permeability of the breccia bodies.

Towards the terminal stages of hydrothermal activity, massive pyrite veins were deposited from non-boiling, low-salinity (≤ 8 wt percent NaCl equiv.: Fig. 2-16p) fluids with homogenization temperatures of less than 377°C . Trapping temperatures, assuming a depth of 2.5-3.0 km, would have been around 450°C . Thus, these fluids were as hot as those in the deeper parts of the previously altered breccia bodies (Figs. 2-16i and j). The final magmatic activity at Cerro Colorado is recorded by hornblende-plagioclase porphyry dikes emplaced both during the final stages of phyllic alteration and after all significant alteration-mineralization. These dikes contain minor quartz but abundant hornblende. The more mafic characteristics of these dikes may provide evidence of the incursion of mafic melt deep in the felsic pluton which may have contributed much of the heat, and perhaps the metals, since the onset of the Main Stage. Progressive rise of the more felsic melts of the upper portion of the pluton as breccia bodies and porphyry plugs caused the mixed, yet denser, melts in the deeper levels of the pluton to ascend to the shallower, vacated volumes of the magma chamber (Rowland, 1998), permitting their emplacement as dikes before the final consolidation of the pluton.

2.10. Comparison with other Porphyry Copper Systems

Four apparently anomalous, and plausibly in part interrelated, aspects of the development of the hypogene protore at Cerro Colorado, viz. the barren nature of the extensive Early potassic alteration zone, the prograde transition from the Early to the Main Stage of mineralization, the quasi-simultaneous development of deep intermediate-argillic and shallow advanced-argillic alteration facies during the Main Stage, and the horizontally extended, blanket-like form of the Early and Main Stage alteration zones, prompt a search for similar relationships in other porphyry copper deposits.

Barren potassic-sodic alteration and prograde evolution

In numerous well documented examples of porphyry deposits, hypogene Cu-Mo (e.g., El Salvador, Chile: Gustafson and Hunt, 1975); or Cu-Au (e.g., Bingham, Utah: Bowman et al., 1987; Bajo de la Alumbrera, Argentina: Ulrich et al., 2001) mineralization is closely associated with potassic alteration. In these major centers, high-temperature K-silicate alteration-mineralization was overprinted by cooler, less strongly mineralized, or even barren, phyllic and argillic alteration systems, and an overall retrograde fluid evolution clearly exhibited. Thus, the association of sulphide-free, moderate-temperature Early Stage alteration and subsequent higher-temperature ore-forming Main Stage alteration at Cerro Colorado do not conform to accepted genetic models for porphyry systems (Clark, 1993). However, scattered observations, largely from the uneconomic zones of several major porphyry Cu deposits, reveal similarities with the relationships at Cerro Colorado and highlight features that may be a fundamental aspect of these deposits.

The classic study of the El Salvador deposit by Gustafson and Hunt (1975) demonstrated that as much as 75 percent of the hypogene copper mineralization accompanied early stage K-silicate alteration. At depth, however, the copper grade falls below 0.1 percent in andesites

intensely altered to K feldspar-biotite-quartz-albite assemblages (Gustafson and Quiroga, 1995). “Early Biotite” veinlets in this zone, with or without sulphides, quartz, albite, anhydrite and actinolite, are interpreted by Gustafson and Quiroga (1995) as the deep equivalents of the strongly mineralized “A” quartz veins which dominate the hypogene protore. Overall, sulphides and hydrothermal K-feldspar diminish in abundance with depth, whereas albite, magnetite and actinolite increase. No microthermometric data are reported for the sparse primary fluid inclusions in the barren potassically-altered zone. Liquid-rich, with small bubbles and no solid phase, these are described as similar to inclusions in the late, moderately-mineralized D veins and in late overgrowths on B vein quartz, which have low salinity and homogenization temperatures below 350°C (Gustafson and Hunt, 1975). Nonetheless, Gustafson and Quiroga (1995, p. 12) suggest that they “most probably formed at a higher temperature and have moderate salinity”. At the same time, the occurrence of pyrrhotite in addition to chalcopyrite and specularite deep in the hydrothermal system was tentatively interpreted as evidence for a prograde evolution for the potassic alteration, the “specularite veinlets presumably represent[ing] an outer, more oxidized and lower temperature, i.e., earlier, stage than the pyrrhotite-chalcopyrite” (Gustafson and Quiroga, 1995, p. 15).

Thus, at depth El Salvador is similar in several respects to the Early Stage at Cerro Colorado: both are characterized by a lack or paucity of sulphides, potassic-sodic alteration assemblages, low-salinity, non-boiling fluid inclusions, and an overall prograde evolution towards the ore-forming stage. The differences between these deposits are, however, more fundamental. The potassic (-sodic) alteration at El Salvador is intensely mineralized in its upper levels, whereas no major mineralogical changes or sulphides were observed at any depth in the potassic-sodic alteration at Cerro Colorado. It is possible that Early Stage alteration at Cerro Colorado was mineralized at very shallow, or deeper, levels, but all sulphides are unambiguously assigned to the Main Stage biotite-albite destructive alteration or to later stages. Gustafson and

Quiroga (1995) attributed the weak chalcopyrite precipitation at depth at El Salvador to the lack of boiling and resulting minimal hydrofracturing. This may have been a factor in the Early Stage at Cerro Colorado, but cannot explain the absence of both chalcopyrite and pyrite throughout this stage.

The Yerington (Carten, 1986) and Ann-Mason (Dilles and Einaudi, 1992) deposits of the Yerington mining district of western Nevada are characterized by dominant potassic alteration, i.e., biotite + K-feldspar, in the ore zone and barren sodic-calcic alteration, comprising oligoclase + actinolite + titanite, below and outside of the potassic core. On the basis of phase equilibria and fluid inclusion studies at Ann-Mason, Dilles and Einaudi (1992) constrained the temperature and salinity of the sodic-calcic fluids to the ranges 250 to >400°C and 31-41 wt. percent NaCl equiv., whereas the ore-forming fluids were hotter (<400 to 700°C) and largely more saline (32-62 wt percent NaCl equiv.). The potassic alteration was inferred to have been generated by magmatic fluid saturation and hydrofracturing related to the intrusion of the Luhr Hill granite, but the sodic-calcic alteration was ascribed to the prograde incursion of sedimentary brines into the fractured batholith, a process which leached Cu and Fe (Dilles and Einaudi, 1992; Dilles et al., 2000). Thus, although these deposits differ from Cerro Colorado in their association of ore with high temperature potassic alteration, a common feature is the occurrence of a sulphide-barren zone with a prograde history beneath the ore zone.

At the Sierrita-Esperanza porphyry copper deposit, Arizona, Titley et al. (1986) and Titley (1993) emphasize that the ca. 1.5 km² orebody lies within a zone of over 30 km², ca. 7×5 km, of potassic alteration, clearly bearing similarities with that at Cerro Colorado. Preece and Beane (1982) demonstrated that the largely barren early stage quartz+biotite+K-feldspar+albite alteration was initiated by fluids with homogenization temperatures of 300-370°C and salinities of 37-41 wt percent NaCl equiv., which were supplanted by boiling fluids with salinities of 10-15 wt percent NaCl equiv. and homogenization temperatures of 400-430°C. The fluids then cooled

to below 300°C and the bulk of the sulphides were deposited in a central zone in association with “propylitic” chlorite-epidote-sericite-clay assemblages. Titley (1993, 1995b) argues that such large, quasi-pervasive, potassic alteration zones are a typical feature of porphyry copper deposits of the southwest US, but are rarely documented, perhaps owing to their potential value in mineral exploration. He (1995b) envisages the widespread scavenging of Cu and S from the early potassic zone during subsequent hydrolytic alteration. He further notes (1993, p. 458) that “early, high-temperature alteration ... may have developed during prograding thermal effects, as well as successive overprinting alteration stages ...”, to be, in turn, “overprinted in a collapsing thermal environment ...”. Finally, it is proposed (1995b, p. 382) that “prograding is suggested from the apparent outward growth of propylitic effects during early stages of wall-rock heating”.

No comparable large-scale zones of potassic alteration have been documented from porphyry systems of the central Andes, and in several cases, e.g., the Toquepala and Quellaveco deposits, southern Peru (A.H. Clark, unpubl. studies), such alteration effects are absent. Only Titley (1993, 1995) has suggested that such alteration systems may be widespread features of porphyry copper deposits, and that they may have developed during wall-rock heating. None of Arizonan zones of biotitization has been described in detail, and therefore comparison with that at Cerro Colorado remains difficult. However, it is widely accepted that the majority of porphyry copper deposits were emplaced at a considerable distance above the parental magma chamber, so that the initial incursion of magma-derived fluids must in many cases have involved their thermal equilibration with cool country-rocks. On the basis of field observations and electrical resistivity and seismic data, Norton and Knapp (1977) suggested that permeabilities are large enough ($>10^{-14}$ cm²) in the upper crust at depths of 10-20 km to permit convective heat transfer. Moreover, Norton and Knight (1977) inferred that the heat flux at the top of an intruding pluton and in the surrounding rocks initially increases, and then remains at a constant maximum, before decreasing gradually. The average temperature of a volume of magmatically-driven fluid interacting with a

body of rock is, therefore, likely to increase before both host rock and fluids reach a maximum. The temperature of the fluids invading a body of rock+fluid may also increase because of the incursion of hotter melt into the magma chamber. Further, the periodic emplacement of intrusive stocks or plugs and injection of new hot fluids would reset the temperature of the earlier fluids as well as that of the host rocks. A change in the rate of emplacement of the pluton, e.g., rapid upward migration, and in the flow path of the fluids to the potential mineralized zone would also influence the overall temperature of the fluids at the site of mineralization. It is thus apparent that the almost universally accepted retrograde fluid evolution for porphyry Cu deposits is probably an over-simplification and, as emphasized by Gustafson and Quiroga (1995), ore formation is rather a dynamic and evolving process involving both prograde and retrograde stages.

Simultaneous development of intermediate to advanced argillic zones

Landmark studies on porphyry copper deposits, e.g., Gustafson and Hunt (1975) and Bowman et al. (1978), have generally assigned specific alteration/mineralization assemblages to specific evolutionary stages on the basis of field and petrographic studies (Clark, 1993). Sulphide assemblages vary with alteration stage. Thus, at El Salvador, Chile (Gustafson and Hunt, 1975), early A veins with potassic alteration contain chalcopyrite and bornite, whereas pyrite is the dominant sulphide in late D veins with sericitic alteration. These studies have also identified a zoned pattern of sulphide assemblages from inner bornite-chalcopyrite, through chalcopyrite-pyrite to outer pyrite \pm sphalerite \pm galena. Such zoning is commonly ascribed to variations in metal solubilities in a single fluid due to changes in temperature, pH and salinity (Hemley and Hunt, 1992). However, the capability of such a single fluid to generate a zoned pattern of alteration has been less widely evaluated.

Sillitoe and Gappe (1984) compared the vertical alteration zoning of 48 porphyry copper centers in the Philippines, identifying a consistent downward sequence from advanced argillic

through intermediate argillic to K-silicate alteration. Advanced argillic alteration caps in several porphyry deposits around the world, moreover, host high-sulphidation style mineralization (Sillitoe, 1983). In many such settings, however, the relative ages of the different alteration facies are uncertain. The best documented example of such relationships comprises the Far Southeast porphyry and contiguous Lepanto epithermal deposits, Luzon (Hedenquist et al., 1998), in which K-silicate alteration (biotite-magnetite \pm K-feldspar) is overprinted by intermediate advanced argillic alteration (chlorite-sericite), which in turn grades upward and outward to the advanced argillic assemblages, pyrophyllite-diaspore \pm kandite and, at the shallowest level, quartz-alunite. On the basis of the K-Ar ages of hydrothermal biotite and alunite, it was demonstrated that the quartz-alunite alteration which hosts the Lepanto high-sulphidation Cu-Au deposit formed at essentially the same time, ca. 1.4 Ma, as the underlying K-silicate alteration. Hedenquist et al. (1998) therefore proposed that a rising ca. 550 °C magmatic fluid unmixed to form hypersaline liquid and vapour which generated K-silicate and advanced argillic alteration, respectively. However, the bulk of the porphyry and epithermal Cu and Au mineralization occurred during a slightly later stage, 100,000 yr in duration, and from cooler (ca. 350°C) fluids which developed sericite (-chlorite) and pyrophyllite alteration zones (Hedenquist et al., 1998). Unlike that at Far Southeast, the Early Stage alteration at Cerro Colorado was probably not associated with contemporaneous advanced argillic alteration because vapour phase separation did not occur. However, the earlier stages in both deposits were overprinted by the main ore deposition event, which generated a zoned pattern of alteration from deep sericite-chlorite/quartz-sericite to shallow pyrophyllite zones. Thus, the vertical alteration zoning of main stage mineralization at Far Southeast-Lepanto is strikingly similar to that of the Main Stage at Cerro Colorado.

In the Ohio Creek-Lookout Rocks Cu-Mo-Au prospect, Thames district, New Zealand, Brathwaite et al. (2001) show that the upper part of a K-feldspar-magnetite \pm biotite alteration zone is overprinted by intermediate argillic and phyllic alteration zones, which are in turn capped by

pyrophyllite-diaspore-dickite-kaolinite and quartz-alunite-dickite advanced argillic alteration zones. The advanced argillic alteration extends laterally to the nearby Lookout Rock area, forming a barren high-sulphidation shoulder to the underlying Ohio Creek porphyry deposit. On the basis of fluid inclusion, stable isotope and K-Ar studies, Brathwaite et al. (2001) concluded that these alteration zones formed as overlapping episodes during the evolution of a single hydrothermal system at 10.7-11.6 Ma. As at Far Southeast, K-silicate alteration at Ohio Creek deposit is weakly mineralized and the bulk of the copper mineralization is associated with intermediate argillic and/or sericitic alteration (Brathwaite et al., 2001).

At Ann-Mason, Yerington District, Nevada, Dilles and Einaudi (1992) and Dilles et al. (2000) describe a complex array of alteration zones which postdated the deep, main stage, potassic and sodic-calcic alteration stage. With decreasing depth, these are defined by albite-chlorite-tourmaline-sericite-pyrite, quartz-sericite-pyrite, and quartz-pyrophyllite assemblages. These differ in detail from those at Cerro Colorado, but the overall upward trend from chlorite/sericite-dominated to advanced argillic alteration is similar. Furthermore, Dilles et al. (2000, p. 64) proposed that following intrusion of the Luhr Hill granite, aqueous fluid saturation led to “upward movement of magmatic hydrothermal fluids to form deep K-silicate alteration with Cu-Fe sulphide mineralization and shallow sericitic and advanced argillic alteration in the subvolcanic environment”.

On a smaller scale, Main Stage veins at Cerro Colorado exhibit zoned alteration envelopes from inner chlorite/sericite to marginal smectite/kaolinite (Figs. 2-7e and g). Similar relationships are apparent at, e.g., Butte, Montana, where main stage veins are surrounded successively by zones of sericite, kaolinite, and montmorillonite-nontronite, which forms a greenish band against the fresh quartz monzonite host rock (see Fig. 1 of Sales and Meyer, 1948). The greater abundance of chlorite at Cerro Colorado is plausibly due to the more mafic host rocks. The zonal pattern of alteration along these veins is ascribed (Sales and Meyer, 1948) to a

single fluid and provides convincing evidence that larger-scale zoned intermediate- to advanced argillic alteration could be generated by a single rising fluid.

Therefore, it is apparent that a zoned pattern of alteration from intermediate- to advanced argillic is a fundamental theme among porphyries with different settings and histories, supporting overall intimate relationships between porphyry and epithermal environments.

Geometry of the protore body

Porphyry copper deposits commonly display steep, crudely cylindrical forms similar to the overall shape of the syn-mineralization porphyry stocks or dikes (Sillitoe and Gappe, 1984; Titley, 1993). The horizontal, tabular, or manto, form of the alteration-mineralization system at Cerro Colorado is therefore unusual: to our knowledge, the three-dimensional form of the extensive biotite alteration zones around Sierra-Esperanza and other Arizonan deposits (Titley, 1993, 1995a) has not been established. It should be emphasized that the original shape of the Cerro Colorado alteration zone is not fully known because of the erosion of its upper parts, while biotite-albite-magnetite alteration may extend below the deepest exploratory drill-holes (Fig. 2-5). However, even considering these possibilities, it is unlikely that the vertical extent of the deposit exceeded its horizontal diameter, i.e., 4 km. Mineralized Main Stage assemblages form a smaller body within the Early Stage potassic-sodic zone (Fig. 2-2), with the advanced argillic facies having an inverted-conical form. However, as discussed above, the lower boundary of the Main Stage stockwork system, intersected in many drill-holes, is strikingly horizontal (Fig. 2-5). Host-rock stratigraphy, although it may have had some influence, was not responsible for this geometry because the alteration zones are transgressive to the volcanic strata. On the other hand, the subsequent Transitional Stage alteration-mineralization, which was associated with emplacement of breccia bodies and intrusive porphyries, assumed the crudely cylindrical form characteristic of porphyry systems (Fig. 2-8). Overall, the extent of the alteration zones decreases from the Early

to the Transitional Stages, and the Early and Main Stages of alterations are inferred to have developed under conditions which permitted extensive lateral fluid movement and, by implication, which retarded the rise of fluids towards surface.

2.11. Analogies with Geothermal Systems

Active geothermal fields are commonly cited as modern-day analogues of epithermal-type ore deposits (e.g., Lindgren, 1933; Weissberg et al., 1979; and White, 1981). Paradoxically, however, such links are rarely (e.g., Rae et al., 2003) proposed in detail for porphyry copper deposits despite the widely accepted spatial relationship between epithermal and porphyry activity. A review of major geothermal fields around the world reveals striking similarities between these systems and the Cerro Colorado hydrothermal center, particularly in terms of alteration patterns and fluid evolution.

Reyes (1990) documents the distribution of secondary minerals in Philippine geothermal fields and, on the basis of drill hole studies of thirteen major systems, e.g., Tongonan and Palinpinon, identified four major facies (Fig. 2-21a), viz.: biotite (270-340°C), illite (230-320°C), transitional (180-230°C) and smectite (ambient to 180°C), with decreasing depth. The transitional facies is characterized by interlayered illite-smectite but, where permeabilities are low, this assemblage persists to higher temperature (Reyes, 1990). Fluid upflow and outflow usually conform to a T-shaped pattern with the alteration facies boundaries commonly sub-horizontal and paralleling the measured isotherms. Advanced argillic (“acid”) alteration occurs along narrow, commonly structurally controlled zones (Fig. 2-21a) and includes assemblages of pyrophyllite ± illite ± diaspore ± andalusite (230-320°C), dickite ± pyrophyllite (200-250°C), dickite ± kaolinite (120-200°C), and kaolinite (ambient to 120°C). Rae et al. (2003) inferred that, at Palinpinon, hydrothermal biotite ($^{40}\text{Ar}/^{39}\text{Ar} = 0.6\text{-}0.7$ Ma) and alunite ($\text{K}/\text{Ar} = 0.8\text{-}0.9$ Ma) formed essentially contemporaneously with the underlying pluton ($^{40}\text{Ar}/^{39}\text{Ar} = 0.3\text{-}0.7$ Ma), although no analytical

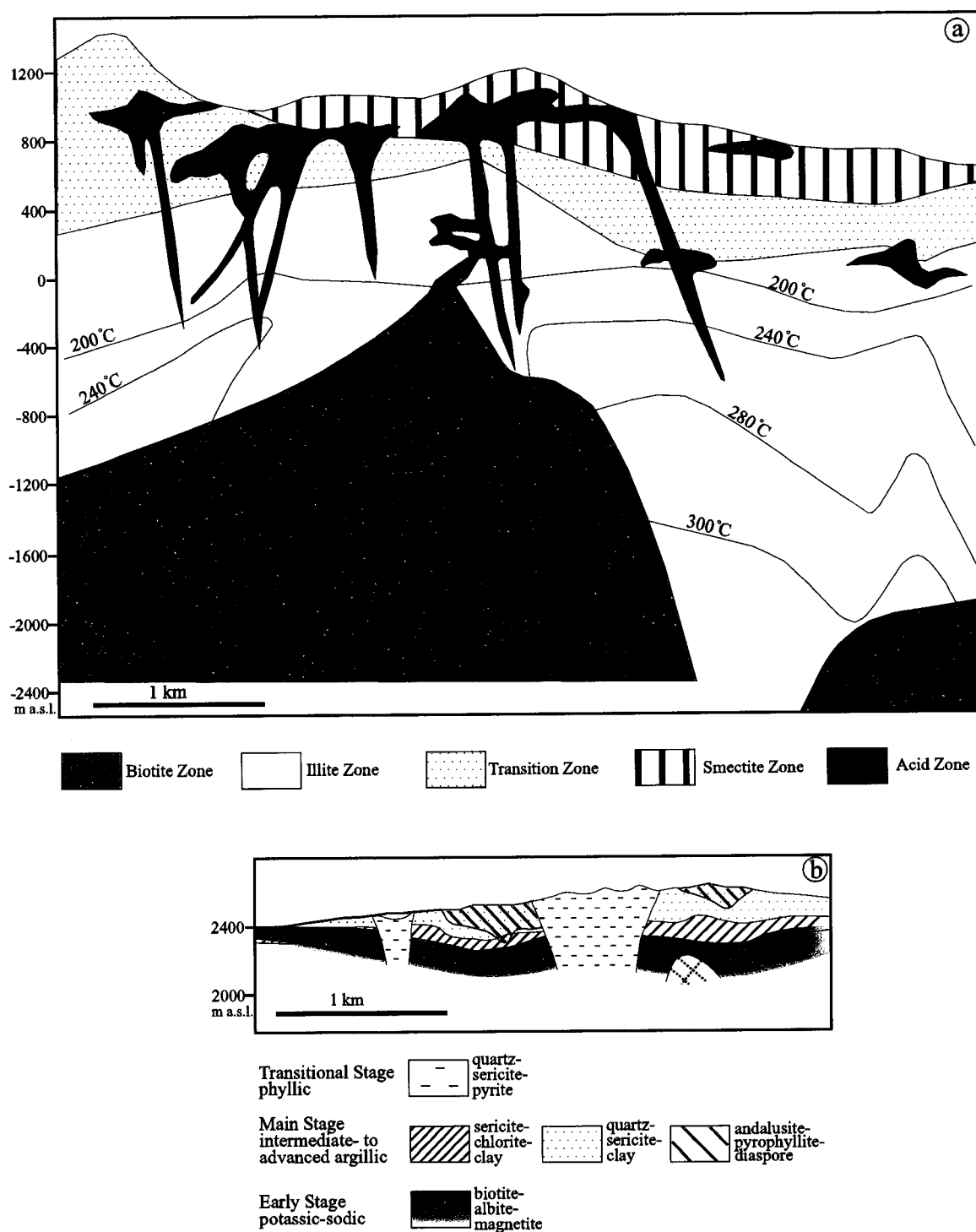


Fig. 2-21: Cross-section of the hydrothermal alteration facies of part of the Palinpinon geothermal field, Philippines (a), after Reyes (1990), showing their similarities to those at Cerro Colorado (b). In both systems a vertical zonation from biotite through illite (sericite)-chlorite to advanced argillic (acid) alteration is apparent. Only the central portion of the over 20 km wide Palinpinon geothermal field is shown, highlighting the much stronger focus of hydrothermal activity characteristic of mineralized systems.

errors are given for the dates. In the major Broadlands-Ohaaki geothermal system, New Zealand, Hedenquist (1990), and Simmons and Browne (2000) document low-sulphidation epithermal gold and silver mineralization associated with a zoned pattern of alteration comprising albite/adularia, illite, illite/smectite, and smectite facies with decreasing depth. The temperature falls from over 250°C in the feldspar zone to below 150°C in the smectite zone.

Similar alteration patterns are recorded in the Salton Sea geothermal field, California, which is hosted by Pliocene and Quaternary shale and sandstone (McKibben and Hardie, 1997), the main source of the heat being tholeiitic basalts intruded along the axis of the Salton Trough. Two distinct geothermal fluid types exist: deep hypersaline (15-28 wt percent total dissolved salt), and shallow, less saline (0-15 wt percent total dissolved salt) brines, the interface between the two transgressing the sedimentary layering (Williams and McKibben, 1989). These fluids have generated a zoned pattern of alteration with decreasing depth from 1547 to 256m, of biotite ($\geq 310^{\circ}\text{C}$), chlorite (220-310°C) and illite/smectite (115-220°C) (Yau et al., 1988). The Fe content of chlorite decreases upward. Albite and K-feldspar are common in the biotite zone and in lower parts of the chlorite zone. Similar thermal and alteration zoning is documented in geothermal fields around the world, e.g., Pantelleria, Italy (Fulignati et al., 1997); and Reykjanes, Iceland (Tomasson and Kristmannsdottir, 1972).

Geothermal fields commonly exhibit a multi-stage and prograde thermal history. Further, thermal activity often shifts from one locality to another. For example, at Palinpinon, Reyes (1991) demonstrated, from mineral geothermometers and direct measurement of fluid temperature, that the southeastern sector is becoming hotter whereas the western is cooling due to incursion of cooler fluids. Moore et al. (2000) document a thermally prograde multi-stage evolution at the Tiwi geothermal system, Philippine, on the basis of vein cross-cutting, fluid inclusion and $^{40}\text{Ar}/^{39}\text{Ar}$ studies. The earliest alteration stage was characterized by deposition of chalcedony and clays at temperatures of less than 180°C. The ensuing main stage of alteration, at

ca. 314-200 ka, was initiated by the deposition of sericite and evolved from quartz \pm adularia \pm epidote \pm pyrite \pm base metal sulphides deposition, through sericite, wairakite \pm epidote and calcite to actinolite alteration at temperatures of up to 333°C. Subsequently, the system cooled to below 235°C, but is now once more prograde, with temperatures of 275°C and renewed deposition of sericite. Similar evolutionary increases in temperature are documented in several other geothermal fields (e.g., Valles Caldera, New Mexico: Lambert and Epstein, 1980).

The striking similarities between hydrothermal features in such geothermal fields and Cerro Colorado and other ore deposits (see above) provide a firm basis for interpretation of the patterns of alteration and mineralization in the latter (Fig. 2-21). Thus, the zoned pattern of alteration from intermediate- to advanced argillic facies is shown to be a common pattern in both geothermal systems and porphyry deposits in which fluids ascend to shallow levels, boil and segregate into high- and low-density phases, cool, mix with other fluids and become dilute. The fluids inherently rise but at shallow levels they adopt a major outflow component, generating mushroom-shaped patterns of thermal gradients and alteration facies. Advanced argillic alteration assemblages widely occur along zones with greater permeability, forming pockets or inverted cones, as at Cerro Colorado (Fig. 2-5) or in the Palinpinon geothermal field (Fig. 2-21), but elsewhere develop blanket-shaped bodies, e.g., at Lepanto, Philippines (Hedenquist et al., 1998). The biotite-albite-magnetite alteration at Cerro Colorado formed prior to the Main Stage assemblages but similar potassic zones in geothermal fields, e.g., the Salton Sea, may have formed at the same time as the overlying intermediate argillic alteration. The pervasive biotite alteration at temperatures of ca. 300-350°C documented in numerous geothermal fields suggests that Early Stage alteration at Cerro Colorado may have occurred under similar conditions.

Despite the similarities with respect to alteration patterns and fluid characteristics between geothermal fields and porphyry copper and epithermal deposits, mineralization at active geothermal fields (e.g., Palinpinon and Broadlands-Ohaaki fields) rarely attains economic

concentrations of base or precious metals. This is commonly attributed to poor permeability and insufficient fluid flux (Rae et al., 2003; Simmons and Brown, 2000). However, the pervasive alteration in these fields suggests that such factors were not determinants. Direct analogies are apparent with the Early Stage alteration at Cerro Colorado. Furthermore, despite the prograde thermal histories and drilling to depth of greater than 2.5 km, fluid temperatures greater than 350-400°C have rarely been encountered in geothermal fields. In contrast, such high temperature (>450°C) fluids, as well as hydrothermal breccia pipes representing enormous mechanical energy release, are characteristics of porphyry deposits, or the roots of epithermal systems. The lack of these features in explored active geothermal fields may reflect the rarity of these phenomena, but may also be due to an avoidance of systems with high gas content and explosivity in the search for geothermal power sources. Overall, the existence of high temperature fluids capable of dissolving and transporting large quantities of metals to shallow levels, and of a mechanical energy release sufficient to create fractures for rapid cooling of the metal-bearing fluids, may be the two most important ore-forming factors, apart from the metal budget of the exsolved fluids.

2.12. Conclusions

The Cerro Colorado porphyry copper deposit exhibits alteration assemblages typical of porphyry systems, in particular an evolution from alkali-exchange to hydrolytic facies. However, both the styles of alteration and its association with sulphide assemblages are apparently anomalous, and the retrograde thermal path almost universally documented for porphyry centers is not evident.

The generation of a large, blanket-like, sulphide-free, potassic-sodic alteration system by non-boiling, moderate-temperature, low-salinity fluids is for the first time documented in detail in a major porphyry copper deposit. The lack of sulphide mineralization plausibly reflects a minimal sulphur content in the Early Stage fluids, which may have resulted from an inherently low sulphur

content in the crystallizing melt, weak partitioning of sulphur from melt to the exsolved fluids, loss of sulphur at greater depths through deep sulphide mineralization, or a combination of these. The moderate-to-low temperature and low salinity of the early fluids contrast with those which generated the strongly mineralized potassic zones of many porphyry deposits (e.g., Bingham, Utah: Bowman et al., 1987), despite the similarities in alteration mineralogy and metasomatic exchange relationships. However, both in fluid temperature and salinity and alteration zone geometry, striking analogies are apparent with many productive or potentially productive geothermal fields. These extensively documented, non-explosive systems commonly lack even sub-economic mineralization despite the existence of pervasive alteration. In its initial stages, therefore, Cerro Colorado plausibly developed under conditions similar to those at geothermal fields, albeit with a much stronger focus (Fig. 2-21). The existence of extensive volumes of barren or low-grade potassic-sodic alteration in the deep (e.g., El Salvador, Chile: Gustafson and Quiroga, 1995) or peripheral (e.g., Sierrita-Esperanza, Arizona: Titley et al., 1986) sectors of mineralized porphyry systems suggests that such zones may represent the dominance of a geothermal-style of alteration prior to the main, more localized, porphyry mineralization.

The transition to the Main Stage mineralized porphyry environment at Cerro Colorado involved a marked increase in the temperature of the fluids, accompanied by fluid boiling, stockwork development and moderate-to-intense hydrolytic alteration. These fluids cooled and became increasingly acidic as they rose and condensed, generating a quasi-simultaneous vertical zonation from intermediate- to advanced argillic alteration. Such a zoning would be expected to occur in any hydrothermal system associated with shallow rising fluids, and has been well documented in numerous geothermal fields and a small number of mineralized porphyry -cum-epithermal centers, most clearly at Far Southeast-Lepanto, Luzon (Hedenquist et al., 1998)

This study highlights the importance of defining paragenetic relationships in detail in the elucidation of ore-fluid evolution. Thus, the occurrence of veinlets of undumortieritized

tourmaline cutting andalusite-diaspore assemblages confirms that the advanced argillic alteration took place before the Transitional Stage. It was therefore contemporaneous with Main Stage alteration, rather than being the product of late, “retrograde”, shallow-level processes (cf. Island Copper, British Columbia: Arancibia and Clark, 1996). Instead, the Main Stage alteration zoning records the retrograde path of a rising single fluid through heat loss to the host rocks and condensation into meteoric water.

The subsequent Transitional and Late Stage alterations were associated with fluids with temperatures as high as those of the Main Stage. Thus, although the chemistry of the fluids changed towards more sericite- and pyrite-stable conditions, no major retrograde relationship is observed between the various stages, i.e., following a major prograde transition from Early to Main stage, each alteration episode was generated by a pulse of high temperature fluid which cooled and diluted as it rose. Therefore, the crystallizing melt or melts released high-temperature fluids during the entire Main-to-Late stages of alteration-mineralization, although both the volume and chemistry of the exsolved fluids changed.

The Cerro Colorado center incorporates a substantial tonnage of protore with Cu grades of 0.4-0.5 percent, comparable to those reported for most of the Paleocene-middle Eocene porphyry deposits of the central Andes and probably exceeding the hypogene grades of the majority of deposits in Arizona and, particularly, British Columbia (Clark, 1993). Sillitoe (1986) has argued that even the enormous deposits associated with the Domeyko Fault in northern Chile commonly possessed primary grades not exceeding 0.6 percent. However, it is proposed that Cerro Colorado represents an unusual hybrid environment, in which a cool, unmineralized hydrothermal system similar in all salient aspects to those in many non-explosive geothermal fields evolved into one more characteristic of porphyry deposits in general. Whereas this transition, recording an increase in ore-fluid temperature, may have been stimulated by melt

incursion or perturbation in the parental magma chamber, it is suggested that such prograde relationships are probably an inherent feature of the initiation of magmatic-hydrothermal systems.

ANATOMY, EVOLUTION, AND METALLOGENIC SIGNIFICANCE OF THE SUPERGENE OREBODY OF THE CERRO COLORADO PORPHYRY COPPER DEPOSIT, I REGIÓN, NORTHERN CHILE

3.1. Abstract

The 51.8 Ma Cerro Colorado porphyry Cu (-Mo) deposit is situated at 20° 2' 41" S; 69° 15' 35" W at an altitude of 2600 m a.s.l. on the Pacific slope of the central Andean Cordillera Occidental. Supergene processes at Cerro Colorado generated a complex weathering profile which attains a present depth of 450 m and incorporates the ca. 228 Mt at 1.0 percent Cu orebody. The extant supergene profile comprises four facies: (1) Leached Cap, underlying the Choja Pediplain, a regionally extensive mid-Tertiary erosion surface; (2) Upper Supergene Ore; (3) Lower Leached Zone; and (4) Lower Supergene Ore. Both the Leached Cap and Lower Leached Zone are mainly hematitic, implying chalcocite-rich precursors. The Upper Supergene Ore is dominated by brochantite and atacamite with relics of chalcocite, but includes a superimposed zone of abundant chrysocolla veins. Chalcocite, commonly accompanied by supergene kaolinite and smectite, is the main ore mineral of the Lower Supergene Ore, which overlies the 0.4-0.5 percent Cu hypogene protore.

Dating of supergene alunite-group mineral separates from different ore facies and elevations by laser $^{40}\text{Ar}/^{39}\text{Ar}$ incremental-heating reveals a supergene history extending over at least 20 m.y. Fifteen multi-step age spectra for alunite, natroalunite and jarosite yielded acceptable plateau dates, ranging from the earliest-Oligocene, 35.26 ± 0.68 Ma, to the Middle Miocene, 14.59 ± 2.46 Ma; 5 samples of alunite-natroalunite mixtures, however, produced staircase spectra with no direct age significance. Following hypogene mineralization in the middle Eocene, the deposit was probably unroofed at ca. 42 Ma, at the initiation of the Incaic

orogeny in northern Chile. An age of 35.26 ± 0.68 (2σ) Ma for alunite associated with hematite in a clast in gravel overlying the Leached Cap demonstrates that both formation and oxidation of a *Stage I* chalcocite blanket had occurred by the earliest-Oligocene. During *Stage II* ($> 35.26 \pm 0.68$ Ma to $< 22.42 \pm 1.6$ Ma), continued uplift and pedimentation caused leaching and thickening of the blanket, forming the surviving hematitic Leached Cap and chalcocite-dominated Upper Supergene Ore. *Stage III* ($> 21.49 \pm 0.49$ Ma to 19.25 ± 0.43 Ma) was initiated by the major Pehuenchean (Aymará) tectonic event, when rapid regional uplift and a drastic fall in the water table effected a renewal of intense leaching to form the Lower Leached Zone. At this time the chalcocite blanket was thickened below the Lower Leached Zone, generating the Lower Supergene Ore, and oxidized above it to form the Cu-oxide -dominated Upper Supergene Ore. At 19.25 ± 0.43 Ma, an ignimbrite flow, up to 95 m thick, covered much of the deposit, temporarily interrupting supergene activity, but imposing lateral groundwater flow through the lower 20 m of the ignimbrite and underlying supergene profile during *Stage IV*. Oxidation was then reactivated, generating chrysocolla veins along NW-trending fractures, which are inferred to be genetically linked to exotic mineralization in gravels below the ignimbrite 1.5 km north of the deposit. Further uplift and climatic desiccation in the Middle Miocene, during *Stage V* ($< 14.59 \pm 2.46$ Ma), terminated significant supergene processes and preserved the existing supergene orebody from lateral metal dispersion.

Evidence from Cerro Colorado and elsewhere in northern Chile (e.g., Spence and Angelina) confirms that Paleocene to middle Eocene porphyry and allied Cu deposits experienced intense enrichment both in the late Eocene to early Oligocene and the late Oligocene to Early Miocene. We argue that the establishment of a “proto-Humboldt Current” and the onset of the Incaic orogeny in the late Eocene provided a climatic and physiographic environment favorable for supergene enrichment of Cu deposits undergoing exhumation in the rain-shadow of an uplifting terrain. Some of the earliest, upper Eocene, deposits emplaced along the Domeyko Fault

System (e.g., El Salvador) may similarly have been upgraded during the Incaic orogeny, but the main enrichment in the upper Eocene to lower Oligocene Cu deposits occurred during the late Oligocene to Early Miocene, coinciding with formation of the Lower Leached Zone at Cerro Colorado. The pyrite-rich hypogene assemblages of the giant deposits of the younger belt, e.g., Chuquicamata and Escondida, resulted in stronger and more rapid enrichment than in the relatively pyrite-poor older deposits, including Cerro Colorado, despite the more protracted supergene histories experienced by the latter. The low enrichment rate of the Paleocene to middle Eocene deposits may also be attributed to the lateral copper loss during the Oligocene pedimentation. Because the Upper Supergene Ore at Cerro Colorado formed during the Oligocene tectonic quiescence following the Incaic Orogeny, we propose the occurrence of a single Cenozoic supergene metallogenic epoch in northern Chile, ca. 20 or even 30 m.y. in duration, but attaining its greatest efficacy in the Early Miocene.

3.2. Introduction

The fundamental geochemical and mineralogical processes involved in the supergene oxidation, leaching and enrichment of base and precious metal ore deposits have been understood for at least a century (S.F. Emmons, 1901; Kemp, 1905). Early recognition of the economic implications of the weathering of Cu-Fe sulphide minerals in dry cordilleran environments led to the establishment of Graton's "Secondary Enrichment Investigation" in 1913, and is exemplified by W.H. Emmons' classic 1913 and 1917 U.S.G.S. bulletins. Ensuing field and laboratory research on the intrinsic and extrinsic factors that influence the development of supergene profiles in porphyry copper and allied deposits has, moreover, been widely reviewed and synthesized (e.g., Anderson, 1955; Anderson, 1982; Titley, 1995a; Chávez, 2000; Brimhall, 2000). Nonetheless, despite recent advances in the understanding of the nature and origin of such ores,

few major supergene systems have been documented as fully as their associated hypogene protolith mineralization (cf. Gustafson and Hunt, 1975; Swayne and Trask, 1960). Indeed, the description of the supergene profile of the Radomiro Tomic deposit (Fig. 3-1) by Cuadra and Rojas (2001) represents one of the few modern comprehensive accounts of such a system. The present investigation of the genesis of the entirely supergene orebody of the Cerro Colorado porphyry copper deposit, I Región, northern Chile (Fig. 3-1), is based on detailed field and core-logging analysis of its internal mineralogical and geochemical zonation, coupled with a laser-induced $^{40}\text{Ar}/^{39}\text{Ar}$ incremental-heating geochronologic study of a suite of alunite-group mineral separates. This integrated study provides evidence for the protracted evolution of the supergene profile over at least 20 m.y., from the late Eocene to the Middle Miocene.

Central Andean supergene activity

Although the majority of major Cenozoic porphyry copper deposits in the central Andean orogen of central and northern Chile, and contiguous northwest Argentina and southern Peru (Fig. 3-1), exhibit hypogene Cu grades of at least 0.5 percent, the critical role of supergene upgrading and/or mineralogical transformation has been universally recognized. The development of oxidation and sulphide-enrichment zones in numerous Paleogene deposits has been placed in the physiographic context of mid-Tertiary, largely upper Oligocene to Lower Miocene, erosional pediments. These planar landforms dominate the Pacific piedmont in southern Peru and northern Chile, and were generated rapidly under semi-arid climatic conditions during the initial stages of the “Quechuan” (sensu lato) orogenic uplift (Steinmann, 1929) which resulted in the present-day Cordillera Occidental. Integrated geomorphologic and geochronologic research in several transects has led to the conclusion that episodes of monoclinal tilting and pedimentation were separated by generally longer periods of relative tectonic quiescence, and hence landform stability. Intense supergene activity has therefore been assigned to similarly brief intervals (e.g.,

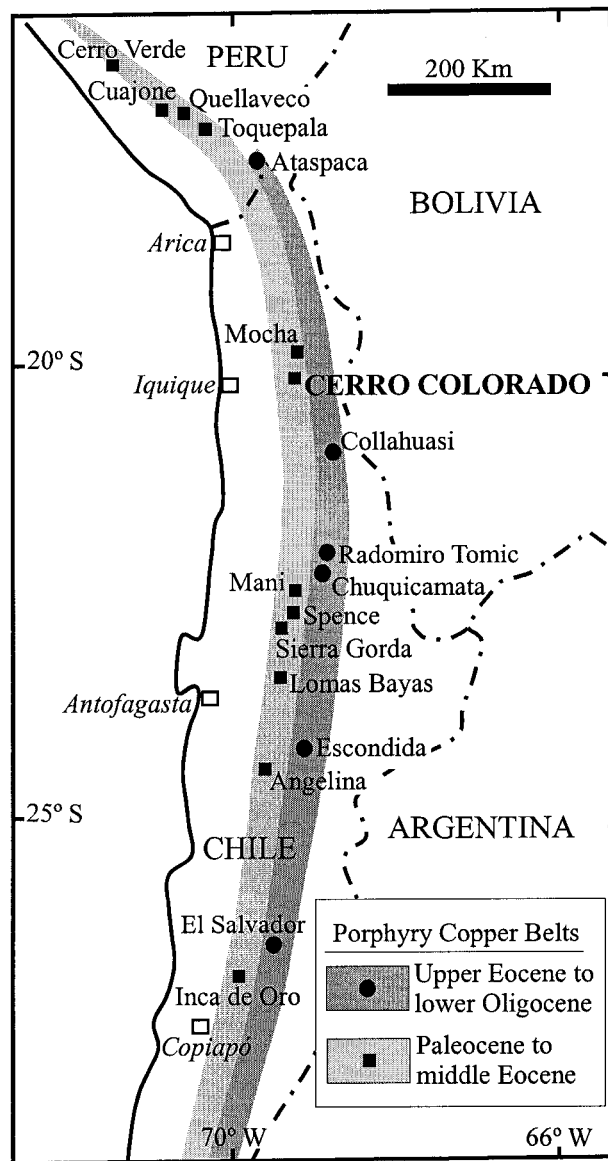


Fig. 3-1:
The location of Cerro Colorado and other Cenozoic copper deposits and prospects in northern Chile and southern Peru cited in the text. The easterly upper Eocene to lower Oligocene deposits define the trajectory of the Domeyko Fault System (see Fig. 3-2).

Clark et al., 1967a and b, 1990a; Sillitoe et al., 1968; Mortimer, 1973; Mortimer et al., 1977; Alpers and Brimhall, 1988), representing, therefore, distinct metallogenic episodes. Consensus has also been reached that, although supergene processes persisted into the Pliocene in the more pluvial environments of central Chile and western Argentina and Bolivia (e.g., Atkinson et al., 1996; Darke et al., 1997), the onset of hyper-arid conditions on the western slopes of the cordillera between latitudes 16 and 28° S in the later-Middle Miocene (Mortimer, 1973; Alpers and Brimhall, 1988) terminated economically significant oxidation and enrichment at 9-10 Ma (Marsh et al., 1997). This extreme desiccation has been ascribed (e.g., Gregory-Wodzicki, 2000) to the persistence of the south Pacific subtropical anticyclone, the extension of the Antarctic ice-cap and hence invigoration of the cool Humboldt Current, and the rain-shadow effect of renewed Andean uplift.

The ca. 15-25 Ma supergene event has thus been widely considered to constitute a clearly-defined metallogenic episode commensurate in economic impact with the hypogene emplacement of the parental porphyry deposits. Nonetheless, there is uncertainty regarding its duration and, particularly, its possible mid-Cenozoic antecedents. Thus, whereas Sillitoe et al. (1968) identified a considerably older, ca. 55 Ma, enrichment episode, inferred to be recorded by shallow chalcocite blankets in several deposits of the Copiapó mining district (ca. 28° S; Fig. 3-1), the postulated controlling Cumbre (“summit”) Surface (Mortimer, 1973) probably represents a cluster of Eocene caldera floors (Arévalo et al., 1994) rather than a continuous regional pediplain. It is therefore unclear whether the two distinct sulphide enrichment horizons exhibited by deposits such as the vertically extensive Dulcinea de Llampos Cu-Au vein (Sillitoe et al., 1968; Sillitoe, 1969) record differing stages in a single major tectonic and supergene event, or formed in response to uplift episodes more widely separated in time, as is recorded by Titley (1978) in a radically different climatic environment. Similar uncertainties are widespread in the region: thus, the overall age relationships of the unusually thick (ca. 450 m) and apparently multi-stage

enrichment profile of the Toquepala porphyry deposit, southern Peru (Anderson, 1982; Clark et al., 1990a), are poorly constrained.

The geochronologic database

Radiometric dating of supergene K-rich minerals has long been recognized as having the potential to define the age and hence duration of supergene activity. Although the first such study in the central Andes was McBride's (1972) K-Ar analysis of supergene cryptomelane (2.7 ± 0.8 (2σ) Ma) in the 6.55 ± 0.14 Ma Farallón Negro epithermal Au-Ag vein system, northwest Argentina (Sasso and Clark, 1998), Gustafson and Hunt's (1975) investigation of alunites from the El Salvador porphyry deposit (Fig. 3-1) initiated a more widely exploitable approach to the dating of the supergene alteration of porphyry and allied copper deposits in the region. (NB. all errors in K-Ar and $^{40}\text{Ar}/^{39}\text{Ar}$ dates are hereinafter given at 2σ). Two alunite K-Ar dates, 36.1 ± 1.8 and 36.0 ± 5.0 Ma, for the leached zone of this ca. 41 Ma deposit led those authors to conclude that "the main period of supergene oxidation and enrichment probably followed no more than 5 million years after the hypogene event", whereas 5 jarosite K-Ar dates in the range 10-21 Ma were rejected as invalid, because two were younger "than the 10-13 m.y. gravels capping the erosion surface [i.e., the Atacama Pediplain: Clark et al., 1967a; Sillitoe et al., 1968; Mortimer, 1973] that truncates the enrichment blanket" (Gustafson and Hunt, 1975, p. 880). However, the concept that supergene processes at El Salvador began at the Eocene-Oligocene boundary, in the later stages of the Incaic Orogeny, and may have persisted to the Middle Miocene, was generally discounted because of the perceived lack of correlation with the erosion surfaces in the wider Atacama Province (e.g., Clark et al., 1990a).

Subsequently, in a study of chemical mass balance relationships in a major enrichment system, Alpers and Brimhall (1988 and 1989) determined several K-Ar dates for supergene alunite from the Escondida deposit (Fig. 3-1), which were interpreted as evidence for relatively

protracted, but essentially single-cycle, enrichment in response to water table depression in the Early to Middle Miocene (from 18.0 ± 1.4 Ma to 14.7 ± 1.2 Ma). This timing is in broad agreement with Mortimer et al.'s (1977) temporal constraints on supergene enrichment and exotic, chrysocolla-rich, mineralization in the wider Chuquicamata district (Fig. 3-1). Sillitoe and McKee (1996), in a K-Ar study of supergene alunites from numerous northern Chilean porphyry Cu deposits, similarly confirmed the importance of the Early Miocene (15.2-21.1 Ma, overall) supergene episode for the upper Eocene to lower Oligocene centers associated with the Incaic Domeyko Fault System. However, they also recorded markedly older dates, in the range 30.3-34.3 Ma, for two centers in the Paleocene to Eocene belt, viz., the Angelina prospect (Fig. 3-1) and Cerro Colorado, the subject of the present study.

In the most comprehensive $^{40}\text{Ar}/^{39}\text{Ar}$ study of a single supergene system to date, Mote et al. (2001a) provide incremental-heating age data for alunites from the rhyolitic cap over the main El Salvador orebody and for cryptomelane and birnessite from the associated Damiana and Quebrada Turquesa exotic deposits. They were unable to reproduce Gustafson and Hunt's (1975) ca. 36 Ma ages for alunite, obtaining considerably younger plateau ages of 12.89 ± 0.06 Ma to 19.44 ± 0.60 Ma. Nonetheless, a date of 35.35 ± 1.6 Ma, inferred from an age spectrum for a single sample of birnessite from Damiana, was accepted as evidence that supergene activity, both in situ and exotic, had begun by that time, albeit peaking much later in the Early to Middle Miocene. In support of this conclusion, Gustafson et al. (2001) provide $^{40}\text{Ar}/^{39}\text{Ar}$ ages of 35.85 ± 3.18 and 43.9 ± 2.6 Ma for coarse and fine fractions, respectively, of a jarosite sample from quartz-alunite -altered rhyolite high on Cerro Indio Muerto. They consider the possibility of disturbance to account for the younger date, but suggest (p. 342) that these ages are "not incompatible with the idea of oxidation and copper leaching at the end of the hypogene 41 to 42 Ma event". Supergene processes may therefore have been initiated while hypogene activity persisted.

In the present study, the mineralogical zonation and $^{40}\text{Ar}/^{39}\text{Ar}$ age relationships are defined for the supergene profile of a porphyry copper deposit of the older, ca. 51-58 Ma belt of the central Andes, in which the incipient development of exotic chrysocolla mineralization is also documented.

3.3. The Cerro Colorado Deposit

Cerro Colorado constitutes a link in a chain of major lower- to earliest-middle Eocene porphyry copper deposits (Sillitoe, 1988; Clark et al., 1990b), which parallels (Fig. 3-1) the plate boundary of southern Peru and northern Chile from Lat. $16^{\circ} 30'$ (Cerro Verde) to $22^{\circ} 30'$ S (Spence), and was associated with a coherent subaerial volcano-plutonic arc initiated in the Late Cretaceous. The northernmost demonstrably economic porphyry copper deposit in Chile, it is centered at Latitude $20^{\circ} 2' 41''$ S and Longitude $69^{\circ} 15' 35''$ W, in I Región, 120 km east of Iquique (Fig. 3-1). The deposit crops out at a mean elevation of 2600 m a.s.l. on an upper extension of the low-relief Pampa del Tamarugál. This slopes westwards at ca. 2.5° towards the axis of the *Valle Longitudinal* (Longitudinal Valley, Fig. 3-2), or Central Basin, a Neogene physiographic feature separating the *Cordillera de la Costa* (Coastal Cordillera) from the Precordilleran foothills of the *Cordillera Occidental* (e.g., Mortimer and Sarič, 1975; Muñoz and Charrier, 1996).

The open-pit mine, initiated in 1994 by Rio Algom Ltd. and now operated by BHP Billiton Base Metals, exploits a complex supergene profile incorporating approximately equal proportions of oxide and sulphide minerals. SX-EW recovery of Cu attained 98,660 t in 1999 and 117,400 t, at US \$0.43/lb, in 2000, and expanded by 10 percent in 2001 (BHP Billiton plc.). Reserves are 228 Mt at 1.0 percent Cu, whereas the preserved hypogene protore averages 0.4-0.5 percent Cu. Supergene processes, therefore, may be tentatively inferred to have approximately doubled the Cu grade.

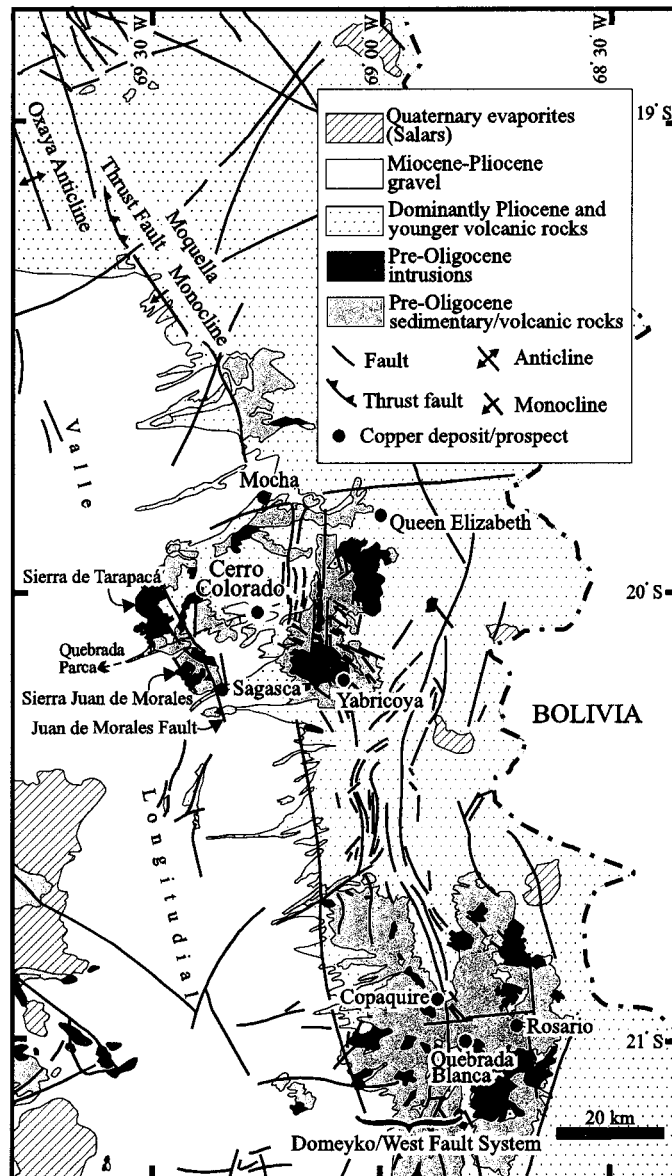


Fig. 3-2:

Simplified regional geologic map of part of northern Chile showing major structural features which postdated the early-middle Eocene hypogene mineralization at Cerro Colorado. NW-striking faults diverge from the main upper Eocene to lower Oligocene Precordilleran or Domeyko/West Fault System in the Yabricoya area. Similarly trending faults extend to the west and southwest of Cerro Colorado, bounding the horsts of the Sierra Juan de Morales and Sierra de Tarapacá. These structures experienced reverse movement during the contraction related to the Early Miocene uplift of the Altiplano, when W-verging thrust faults developed in the Moquella area. Continued uplift incised numerous WSW-trending valleys, e.g., Quebrada Parca, shown by dashed line, which expose the volcanic rocks underlying the pampa gravel (After Thomas, 1967; Galli, 1968; Servicio Nacional de Geología y Minería, Chile, 1982; Muñoz and Charrier, 1996; and Carrasco et al., 1999).

Hypogene relationships

Hydrothermal activity at Cerro Colorado was associated with a cluster of largely quartz-phyric, probably dacitic porphyry stocks and hydrothermal breccia bodies intruding andesite. The hypogene evolution of the deposit is summarized herein to provide a context for interpretation of the supergene assemblages and history.

Host-rocks: The principal host for mineralization is a succession of porphyritic to aphanitic andesites of the Upper Cretaceous to, possibly, Paleocene Cerro Empexa Formation (Galli, 1968), a gently dipping sequence of subaerial volcanic and volcano-sedimentary rocks which underlies extensive areas of the northern Chilean piedmont. Upper Cretaceous and Paleogene porphyritic hypabyssal stocks intrude the andesites in the broader Cerro Colorado district (Fig. 3-3). In the immediate mine area, several of the stocks were emplaced into two major breccia complexes, the Eastern and Western Breccia bodies. The intensely altered breccias comprise clasts of various porphyries in a fine-grained matrix of quartz, sericite, pyrite and clay. Barren tourmaline-cemented breccia forms small bodies within the large breccia complexes. The breccia bodies are in general less mineralized than adjacent andesite. Biotite-quartz-plagioclase porphyry stocks intruded both the breccias and andesite, preceding the emplacement of quartz porphyry stocks. The latter contain the lowest Cu grades and in some areas, as on the now-excavated summit of Cerro Colorado, are essentially barren. Plagioclase porphyry dikes, with no hypogene copper mineralization, cut the breccias and represent the youngest local intrusive units.

Alteration and mineralization: Hydrothermal activity in the earliest-middle Eocene (51.8 ± 0.5 Ma, $^{40}\text{Ar}/^{39}\text{Ar}$ laser-induced incremental-heating hydrothermal biotite and sericite dates: A.H. Clark, E. Farrar, D.A. Archibald, and A. Ortega, unpublished report for Rio Algom

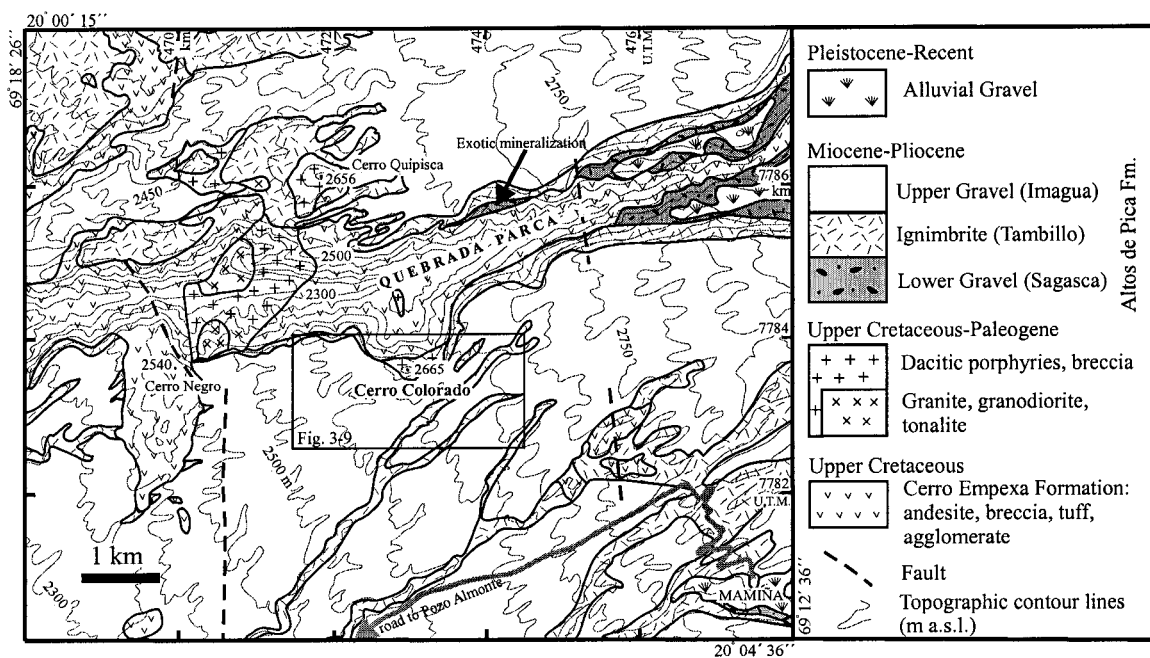


Fig. 3-3:
Geologic map of Cerro Colorado area. Upper Cretaceous to Paleogene rocks occur as inliers surrounded by the Miocene to Pliocene ignimbrite and gravels which define the sub-planar topography of the WSW-dipping Pampa del Tamarugál. An embayment on the south wall of Quebrada Parca exposed the north part of the deposit. Exotic mineralization, inferred to have been derived from Cerro Colorado, occurs in andesitic bedrock and overlying gravels below the ignimbrite flow on the north wall of the canyon. Contour intervals are 50 m. The inset delimits the area of Figure 3-9. (After Thomas, 1967; Galli, 1968).

Exploration Inc, Toronto, 1995; this study, see Chapter 2) generated an E-W elongated mineralized zone. *Early Stage* alteration comprises fine-grained biotite-albite assemblages, originally affecting a large volume of the host andesite but now well preserved only in deep drill holes. Despite its intensity, this alteration was barren: no chalcopyrite or even pyrite can be unambiguously assigned to the *Early Stage*. In contrast, the succeeding *Main Stage* was responsible for much of the chalcopyrite mineralization. The associated alteration is largely characterized by pale-green assemblages of sericite, chlorite and clay minerals, which overprint the upper section of the *Early Stage* alteration zone. Chlorite replaces biotite, sericite replaces plagioclase and biotite, and clay minerals replace albite. Smectite formed early, but, as alteration progressed, illite and kaolinite group clay minerals became dominant. This type of alteration grades upwards into quartz-sericite-clay assemblages, which in turn are overlain by a zone with varying proportions of quartz, muscovite, pyrophyllite, illite, kaolinite, diaspore and andalusite. The *Main Stage* sericite-chlorite-clay, quartz-sericitic-clay, and advanced-argillic alteration assemblages are interpreted as constituting contemporaneous facies in a strongly zoned pattern, the pH of the hydrothermal fluids having decreased dramatically towards the land-surface. True phyllic, i.e., quartz-sericite-pyrite, alteration was mainly associated with later *Transitional Stage* breccia emplacement, when only moderate copper but much of the molybdenum were deposited (F. Bouzari and A.H. Clark, unpublished report for Rio Algom Exploration Inc., Toronto, 1996). *Late Stage* veins are poor in chalcopyrite but contributed pyrite for the ensuing supergene processes.

Relict hypogene assemblages in the lower part of the supergene profile suggest that it developed largely within the sericite-chlorite-clay, quartz-sericite-clay and phyllic alteration facies, and in the surrounding sulphide-poor, biotite-albite alteration.

3.4. Post-Hypogene Tectonic and Geomorphologic Setting

Hypogene mineralization at Cerro Colorado occurred prior to the mid-Cenozoic Incaic (Steinmann, 1929) tectonic event. This, and the succeeding late-Cenozoic Quechuan episode, generated the present-day Andean Cordillera. Both orogenic episodes, responses to major changes in the rate and direction of convergence between the South America and Pacific lithospheric plates (Pardo-Casas and Molnar, 1987), are shown herein to have influenced the supergene evolution of the deposit.

Although Paleogene arc magmatism was interrupted in much of southern Peru at 52 Ma immediately following emplacement of the Cuajone deposit, probably as a result of an episode of flat subduction (Clark et al., 1990b; Clark, 1993; Sandeman et al., 1995), it persisted through the Eocene (e.g., Huete et al., 1977) in northern Chile. After ca. 45 Ma, hypabyssal intrusive and volcanic activity was focused along a narrow N-S belt (ca. 68° 50' W) in the vicinity of the Domeyko, or Precordilleran, Fault System. This major structure, initiated in the late Eocene in the Incaic orogeny, is the locus of an array of supergiant porphyry copper deposits (Fig. 3-1) and records a protracted and complex displacement history extending into the Miocene (Mpodozis et al., 1993, 1999; Tomlinson and Blanco, 1997). Faulting was underway by 42 Ma, when arc magmatism and porphyry Cu mineralization were active at the northern extremity of the fault system, at Ataspaca, southernmost Peru (Clark et al., 1990b: Fig. 3-1), and as far south as El Salvador (Gustafson et al., 2001). Mpodozis et al. (1999) demonstrate that at ca. 23°S, a thick succession of tuffaceous conglomerate accumulated at 39-42 Ma in the Salar de Atacama Basin east of the Domeyko Fault, which was then experiencing sinistral-transpressive displacement. Moreover, on a regional scale, Horton et al. (2001) identify a westerly, i.e., Chilean, source for the thick succession of clastic sediments making up the Potoco Formation on the present Bolivian altiplano, much of which accumulated in the late Eocene to early Oligocene. Thus, although

demonstrably Incaic structures have not been confirmed from the immediate Cerro Colorado mine area, it is probable that the deposit experienced uplift and exhumation at this time.

At ca. 20° S, two major strands of the Domeyko Fault System strike northwards (Fig. 3-2), enclosing the ca. 37 Ma (McBride, 1977) Queen Elizabeth porphyry Cu prospect, exposed in Quebrada Mina Cucho 33 km northeast of Cerro Colorado. In addition, major NW-trending faults diverge from the main Domeyko Fault in the Yabricoya district (Thomas, 1967), extending towards, and to the southwest of, the Cerro Colorado mine area (Fig. 3-2), where they partially delimit horsts of Upper Paleozoic basement and Lower Mesozoic strata (Galli, 1968). These uplifted blocks include the Sierra Juan de Morales, which separates the upper *pampa* surrounding Cerro Colorado from the main Pampa del Tamarugál to the west (Fig. 3-2), and is a link in a discontinuous chain of broadly NNW-elongated Precordilleran ranges, the *Mittelkordillere* of Gerth (1955). The bounding structures were presumably generated during the Incaic orogeny, but Galli (1968) inferred that both the NW- and N-trending structures delimiting the Sierra Juan de Morales were also active in the Neogene. Moreover, he interpreted minor folds and fractures associated with the Juan de Morales Fault as evidence that the latest displacement was reverse and ENE-vergent, while small inliers of skarned Jurassic limestone on the ridge between the Quebradas Juan de Morales and Sagasca were considered to be *klippen* related to thrusting. Longitudinal, Neogene thrust faults are well documented elsewhere in northernmost Chile. About 80 km north of Cerro Colorado, at ca. 19° 15' S (Fig. 3-2), Muñoz and Sepulveda (1992) and Muñoz and Charrier (1996) document a major west-vergent, thick-skinned thrust system, including the NW-trending Moquella Fault, active since the late Oligocene, which contributed to the uplift of the western border of the altiplano between ca 17 and 4.8 Ma. The Cerro Colorado area, therefore, may have been shortened, and further uplifted, between these two sets of NW-striking reverse faults in the Early Miocene.

The deposit lies on the southern margin of the ca. 300 m deep, WSW-trending Quebrada Parca canyon (Figs. 3-2 and 3-3) which incises the subdued landscape of the Pampa del Tamarugál and its eastern extensions, a fossil landform in the prevailing hyperarid climate. Fifteen kilometers to the east, the *pampa* terminates against the western boundary of the Cordillera Occidental, a topographic step probably recording uplift on a southern extension of the Moqueella thrust system (Fig. 3-2). On a more regional scale, the *pampa* forms part of the monoclinical structure which dominates the Pacific piedmont of northernmost Chile and contiguous southern Peru (Mortimer and Sarič, 1975; Tosdal et al., 1984; Isacks, 1988; García et al., 1999). In the immediate vicinity of the mine, the monotonous surface of the *pampa* is interrupted by several low bedrock hills, formerly including Cerro Colorado itself, features of importance in the interpretation of the supergene history.

As in much of northernmost Chile, the subdued topography in the mine area is strongly influenced by an extensive rhyodacitic ignimbrite flow. However, this flow in turn overlies a regionally-extensive planar erosion surface, termed the Choja Pediplain by Galli (1967). A late Oligocene age was inferred by that author and Mortimer and Sarič (1975); this is confirmed by the better established landform history of southern Peru (Tosdal et al., 1984) where directly correlative uplift and intense planar erosion had terminated by 24.02 ± 0.89 Ma (C. Quang, A.H. Clark and J.K.W. Lee, unpublished report to Rio Tinto Mining and Exploration Ltd., Lima, 2001). The pediplain, in its final configuration, eroded the early leached cap and sulphide enrichment blanket of the Cerro Colorado deposit, and lenses of reddish gravels, with clasts of supergene hematite- and alunite-rich assemblages, locally separating the ignimbrite from the underlying deposit (Fig. 3-4).

Prior to mining, the supergene profile at Cerro Colorado was exposed on the steep slopes of a 1 km-wide, crudely hemispherical embayment in the south wall of Quebrada Parca (Fig. 3-3). The canyon itself hosts an ephemeral stream which dries up towards the coast.

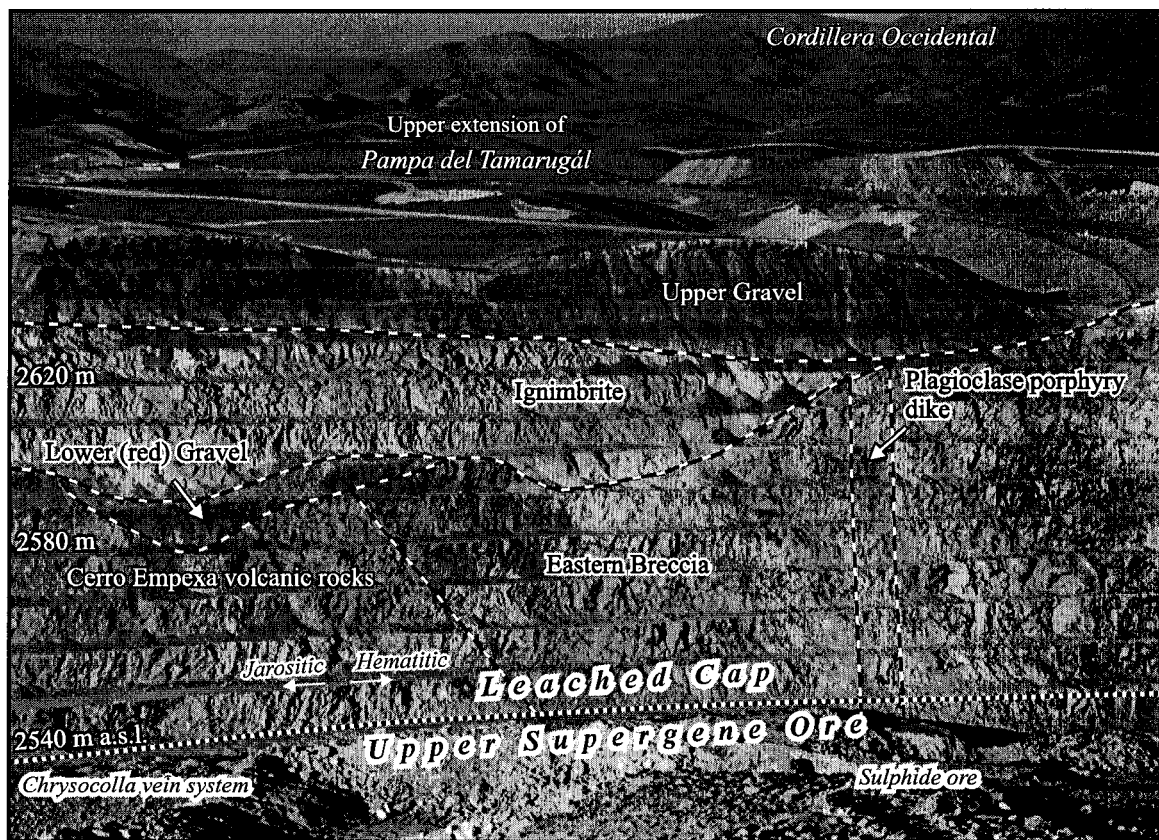


Fig. 3-4:

The east wall of the Main Zone pit at Cerro Colorado, looking east from the former summit of Cerro Colorado on July 4, 1996, showing ignimbrite flow covering much of the Leached Cap and, in turn, covered by gravel. A more restricted red gravel unit, with clasts of early-formed Leached Cap, accumulated in a small valley prior to the eruption of the ash-flow. The western slopes of the Cordillera Occidental rise to elevations of over 4500 m a.s.l., ca. 1500 m above the upper, eastern extension of the Pampa del Tamarugál, 18 km east of the mine. Major units of the host-rocks of the hypogene mineralization are shown. The Leached Cap is hematitic in the originally sulphide-rich (hypogene) breccia body above the supergene sulphide ore, whereas jarosite is more common in andesite with less pervasive sericite-chlorite-clay alteration above the oxide ore. The oxide ore contains abundant chrysocolla but the main series of thick chrysocolla veins lies 20 m below this elevation (see Fig. 3-19).

Ignimbrite flow

The ash-flow tuff body overlying the deposit attains a maximum preserved thickness of 95 m. Its lower part incorporates angular fragments of Cerro Empexa Formation andesite and underlies whitish tuff with a clastic or sandy texture (Fig. 3-5). This is in turn overlain by brown tuff with abundant melanocratic clasts with the dreikanter form and highly polished surfaces characteristic of desertic ventifacts. The core of the ignimbrite is a black vitrophyre, and all facies of the flow are interpreted as constituting a single thick cooling-unit.

Four samples from the ignimbrite were selected for laser-induced $^{40}\text{Ar}/^{39}\text{Ar}$ incremental-heating dating. Their locations are documented in Table 3-1 and the age spectra are illustrated in Figure 3-6. The $^{40}\text{Ar}/^{39}\text{Ar}$ techniques used in this work are summarized in Appendix 3 and analytical details are provided in Appendix 4. Separates of unaltered phenocrystic biotite from two samples taken from the brown horizon of the ignimbrite yielded acceptable, concordant $^{40}\text{Ar}/^{39}\text{Ar}$ plateaus (Fig. 3-6a and b) of 19.25 ± 0.43 Ma (west wall of Main Zone pit) and 19.12 ± 0.61 Ma (500 m northeast of the Main Zone). As is normal for biotite in Cenozoic ignimbrites in this region, the lower-temperature heating increments release considerable atmospheric argon, and hence give high errors, but all steps in each sample yielded similar apparent ages. In contrast, two biotites from the basal white ignimbrite gave very disturbed age spectra (Fig. 3-6c and d), all steps exhibiting unacceptable errors. The spectra would, however, be in permissive agreement with the diffusional loss of Ar from a ca. 20 Ma mica at approximately 10-15 Ma. Field observations indicate that the ignimbrite locally filled a small valley (Figs. 3-5 and 3-7), and the phenocrystic biotite in this zone is strongly altered to clay minerals and calcite. This process was probably responsible for the Ar loss, as is supported by the high and variable Ca/K ratios, and may be attributed to lateral groundwater flow through the lower parts of the ignimbrite (see below).

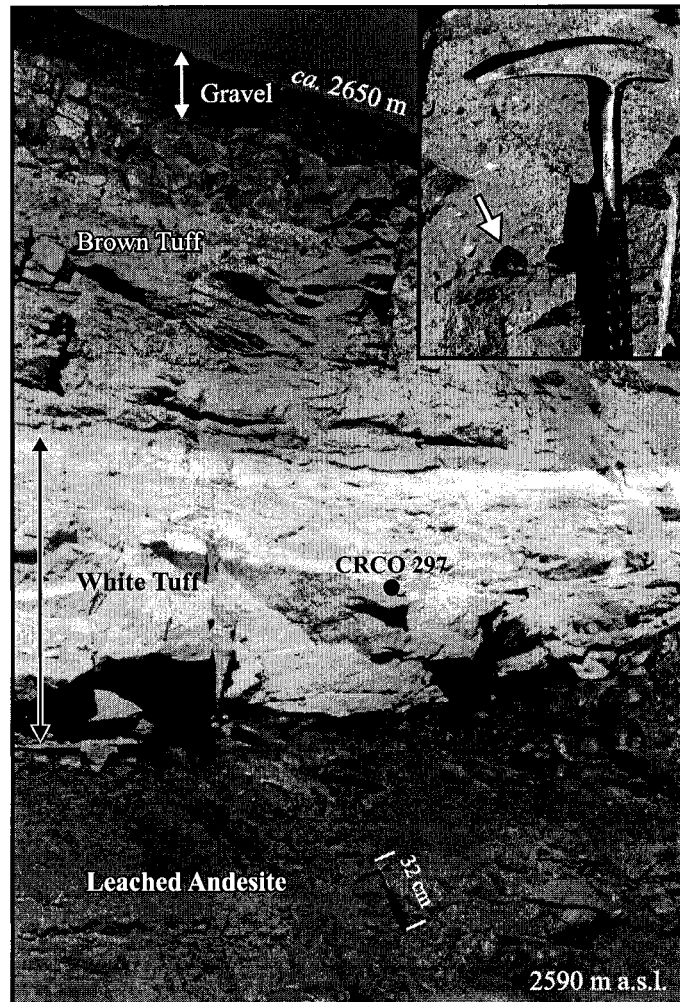


Fig. 3-5:
Highly foreshortened view of 40 m thick ignimbrite overlying the Main Zone Leached Cap and covered by gravel: east wall of pit, looking east. The lower part of the ignimbrite consists of white tuff, which has filled a small valley (see also Fig. 3-7) and is overlain by brown tuff. Location of one dated, but altered, sample (CRCO 297) is shown. The inset is a closer view of the brown ignimbrite containing a blackish andesitic clast (arrow) with dreikanter form and desert varnish.

Table 3-1. $^{40}\text{Ar}/^{39}\text{Ar}$ ages of ignimbrite samples from Cerro Colorado

| Sample no. | U.T.M. coordinates | Elevation m a.s.l. | Location | Appearance | Age $\pm 2\sigma$ (Ma) |
|-------------|----------------------|--------------------|---|--|------------------------|
| CRCO 339 | 473370E, 7783120N | 2600 | Main Zone, west wall of the pit, upper part of the ignimbrite unit | brown ignimbrite with reddish-brown biotite | 19.25 ± 0.43 |
| CRCO 313-21 | 474200E, 7784000N | 2640 | East of the Main Zone; upper part of a 70 m-thick ignimbrite unit | brown ignimbrite with reddish-brown biotite | 19.12 ± 0.61 |
| CRCO 297 | 473710E, 7783740N | 2590 | Main Zone, east wall of the pit; lower part of the ignimbrite unit | white ignimbrite with yellowish-pale brown biotite | $(1.31 \pm 7.04)^1$ |
| CRCO 313-28 | 474200E, 7784000N | 2580 | East of the Main Zone; lower part of the 70 m-thick ignimbrite unit | white ignimbrite with yellowish-pale brown biotite | (7.14 ± 3.75) |

¹ Dates in brackets represent integrated ages for samples for which plateaus were not attained.

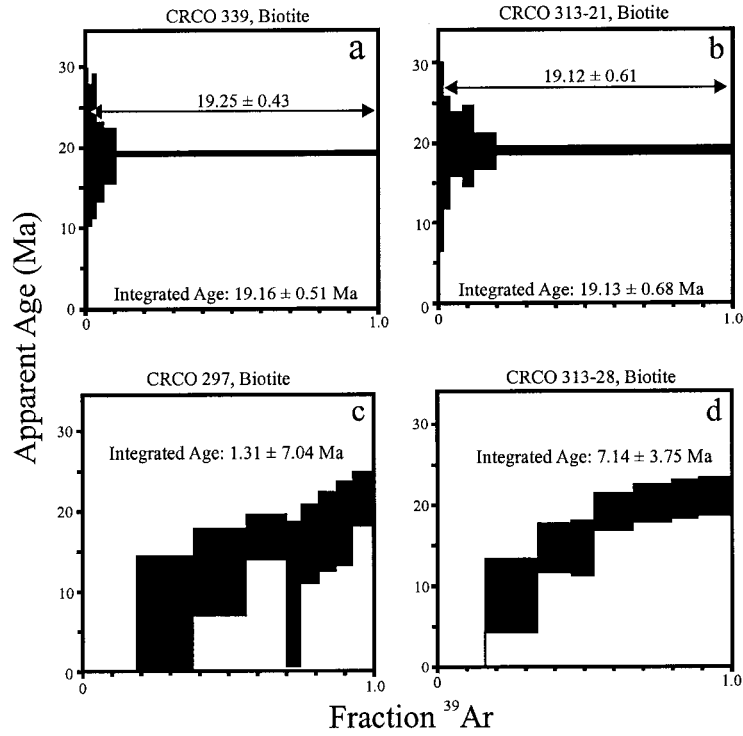


Fig. 3-6:

$^{40}\text{Ar}/^{39}\text{Ar}$ step-heating age spectra for magmatic biotites from the ignimbrite overlying the Main Zone. Biotites in the brown tuff (a and b) yielded acceptable plateau ages (see text), but those in the underlying white tuff (c and d) gave staircase dates with large errors (see Table 3-1 for locations of samples).

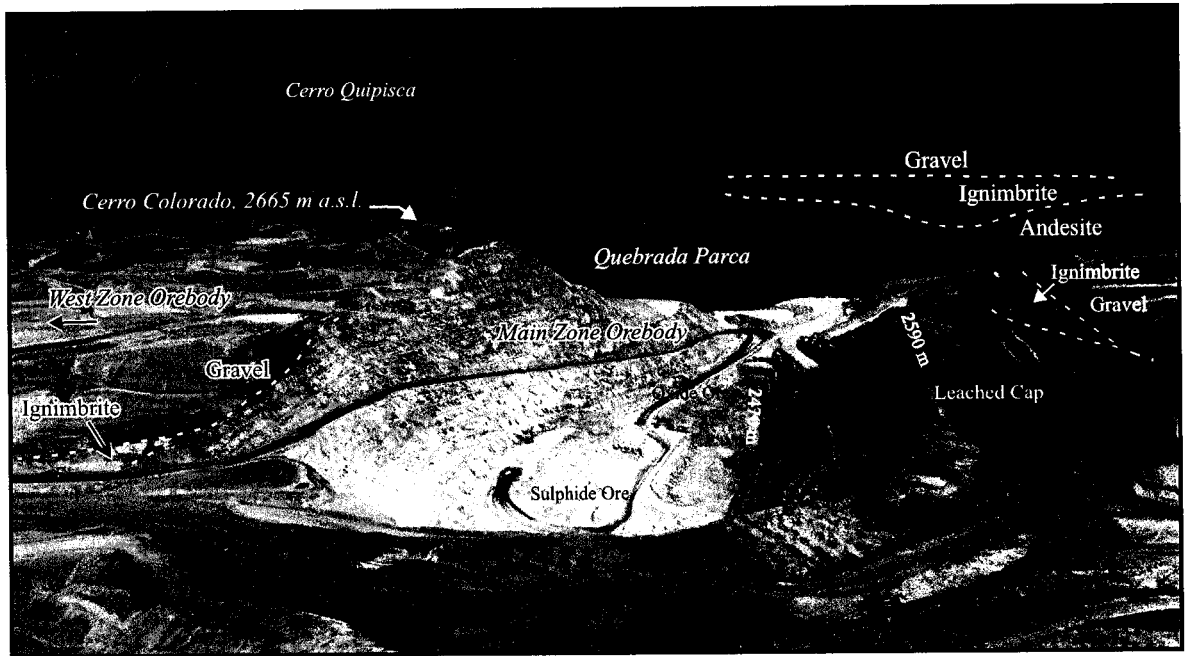


Fig. 3-7:

Oblique aerial view of the Cerro Colorado mine, August, 1995, looking north, showing the Main Zone orebody in the second year of production and the location of the then undeveloped West Zone orebody on the left margin. The supergene blanket was covered by ignimbrite and gravels except on Cerro Colorado and on the steep slopes of an embayment (center, middleground) on the south wall of Quebrada Parca. Variations in the thickness of the ignimbrite on the far (north) side of Quebrada Parca reveal the existence of a shallow N-S Early Miocene valley. The extent of the valley can be seen to the south, on the east wall of the Main Zone (see also Fig. 3-5). Cerros Colorado and Quipisca probably represent remnants of an old landscape, predating the Choja Pediplain of Galli (1967) which here underlies the ignimbrite. In the Main Zone, the Leached Cap extends down to the ca. 2500 m elevation, and is underlain by sulphide and oxide-rich facies of the Upper and Lower Supergene Ores, respectively (see text). Mine pit is approximately 690 m wide.

The Early Miocene (ca. 19.25 Ma) age for the unaltered ash-flow at Cerro Colorado is similar, but probably slightly younger than that of the ignimbrite which overlies the Eocene Mocha porphyry (Fig. 3-2) prospect 24 km north of Cerro Colorado (20.07 ± 0.61 Ma: F. Bouzari and A.H. Clark, unpublished report for Rio Algom Exploration Inc., Toronto, 2000), whereas Vergara et al. (1986) record younger conventional K-Ar biotite ages of 17.3-18.6 Ma for ignimbrites in the Sagasca area, 18 km south of the mine (Fig. 3-2). The Neogene felsic ash-flows in this region have traditionally been assigned to the Tambillo Member (Fig. 3-3) of the Altos de Pica Formation (e.g., Galli, 1968; Mortimer et al., 1974), a southerly correlative of the Oxaya Formation of the piedmont in the Arica area (García et al., 1999), where major eruptions persisted from ca. 25 to 19 Ma. It is therefore apparent that the Cerro Colorado deposit was blanketed by one of the youngest major Neogene ignimbrites in this Andean segment, a relationship of significance for its supergene history.

3.5. Supergene Alteration and Mineralization

Supergene profile anatomy

The almost horizontal, EW-trending Cerro Colorado orebody has a ca. 2.8 km strike length, is 1.0 km wide (N-S) and 100-180 m thick, and lies below a 50-200 m-thick leached zone. The supergene mineralization was first explored to the east of the summit of Cerro Colorado (A. Cepeda, G.M. Ditson, and D.G. Mato, unpublished report to Compañía Minera Riochilex Ltda., Santiago, 1982), but a major extension was subsequently discovered (E.A. Campbell, unpublished report to Compañía Minera Riochilex S.A., Iquique, 1994) to the west of the hill (Fig. 3-7). The Main, or East, Zone is separated from the West Zone by a lower-grade section, but the ultimate open-pit will incorporate both. Mineralogical variations are herein defined by petrographic and X-ray powder diffraction study and electron microprobe analysis. The supergene sulphide ores

are dominated by chalcocite *sensu stricto* and the oxide ores by brochantite, followed in decreasing proportions by atacamite, chrysocolla and malachite (Fig. 3-8). Chrysocolla is more abundant in the upper sections of the oxide ore, whereas brochantite and atacamite are more common in the lower parts.

Two E-W and four N-S cross sections (Fig. 3-9) showing copper grade distributions, supergene facies and host-rocks (Figs. 3-10, 3-11, 3-12, 3-13, 3-14 and 3-15) were constructed during this study on the basis of logging of drill core and RC (reverse circulation) chips integrated with assay data for total and soluble copper. Grade data were available for all drill holes for 2 m intervals and were manually grouped and colour coded, in general following the ore zoning method at Climax, Colorado (Ranta et al., 1984). Detailed core logging and mapping has shown correlations between grades and ore types, and, in many places ore types exhibit abrupt mutual boundaries. Therefore, contouring would impute false continuity to the grade zones. Grade intervals were correlated manually with those in adjacent holes, as with the ore types. There were no exposures of the West Zone when the fieldwork was carried out. Sparse records indicate that the current elevation of the water table is ca. 2290 m a.s.l., i.e., close to the floor of Quebrada Parca.

Four major supergene facies are herein defined and delimited in both the Main and West Zones. With increasing depth these are:

1. Leached Cap
2. Upper Supergene Ore (mainly oxidic, but with abundant remanent supergene sulphides in some areas)
3. Lower Leached Zone
4. Lower Supergene Ore (mainly sulfidic, but locally dominated by oxides)

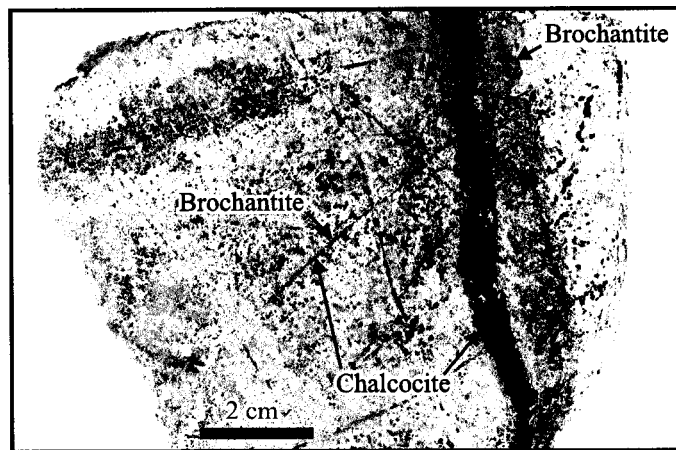


Fig. 3-8:
Hand-sample of supergene ore from lower part of the Upper Sulphide Ore of the Main Zone, level 2450 m, showing disseminations and veins of chalcocite (black) partly oxidized to brochantite (green). The whitish areas are dominated by supergene kaolinite, smectite and quartz.

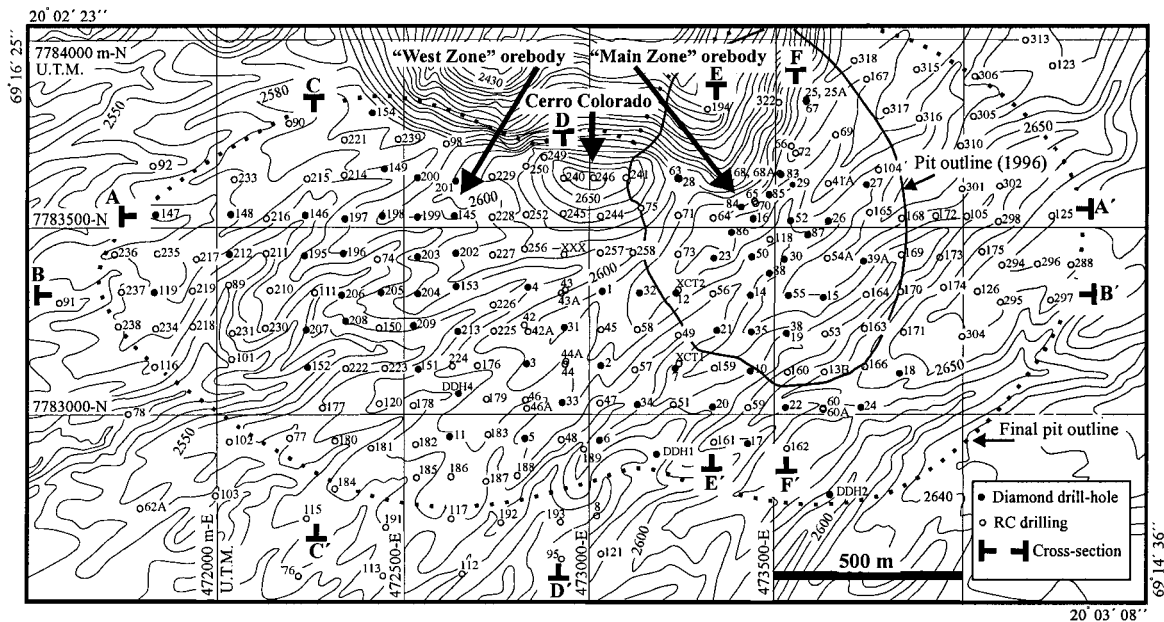


Fig. 3-9:
Pre-mine topography of the Cerro Colorado area showing locations of the drill holes and cross sections in Figs. 3-10 through 3-15. Approximate surface projection of the supergene orebody is shown by the final pit outline. Contour interval is 10 m. Note the embayment which incises the northern parts of the Main and West Zone orebodies (after A. Cepeda, G.M. Ditson, and D.G. Mato, unpublished report for Compañía Minera Riochilex Ltda., Santiago, 1982; T.E. Warren, unpublished report for Rio Algom Exploration Inc., Toronto, 1992; and E.A. Campbell, unpublished report for Compañía Minera Riochilex S.A., 1994).

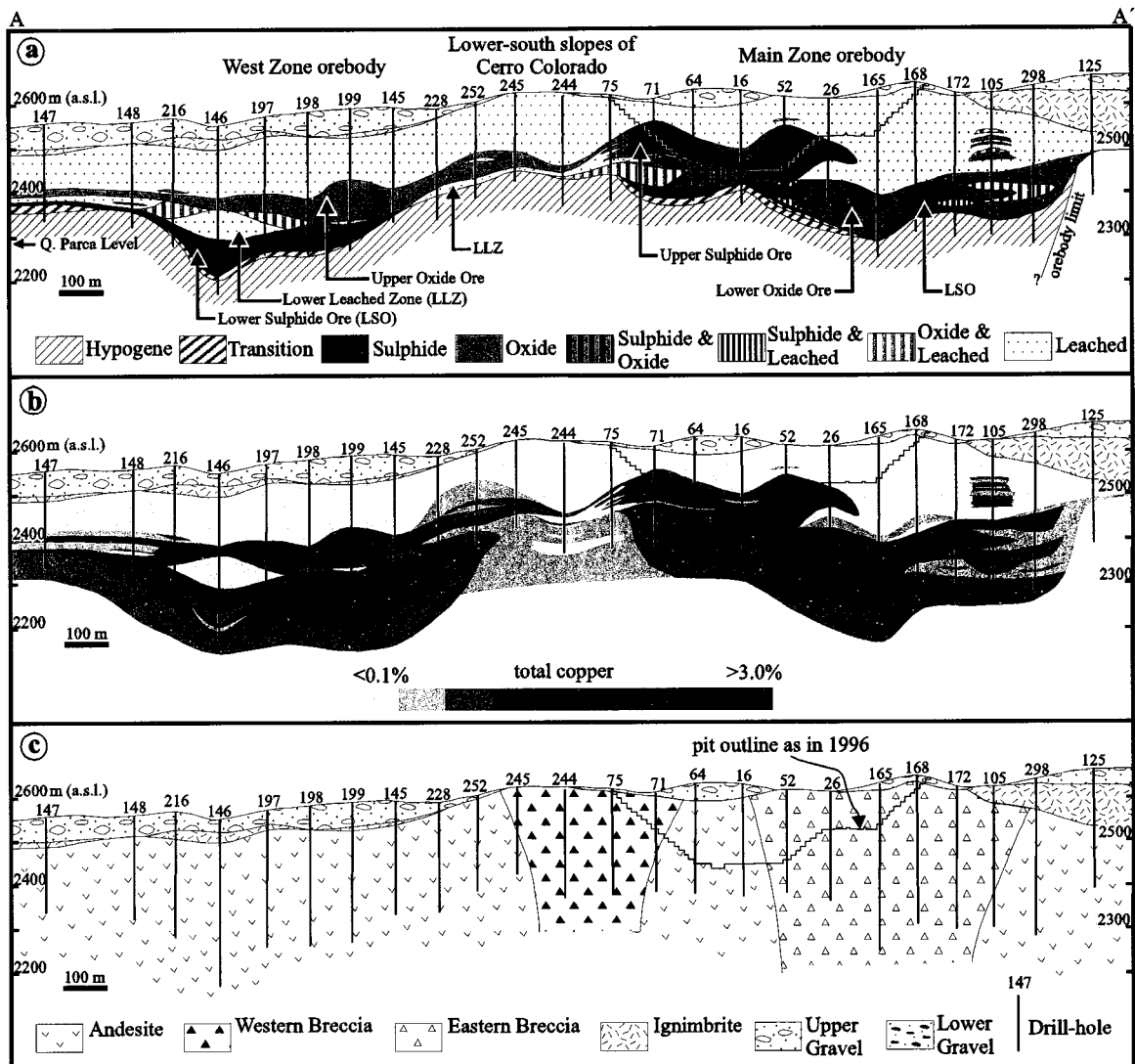


Fig. 3-10:

E-W cross section AA' (Fig. 3-9) showing supergene ore facies (a), grade distribution (b) and host-rock geology (c), with drill hole framework. The variation in the elevation of the pre-ignimbrite surface suggests the existence of a paleo-hill over the Main Zone orebody where the Upper Sulphide Ore is preserved at higher elevations. Development of the Lower Leached Zone has thickened the Lower Sulphide Ore at lower elevations (e.g., hole 146 in the West Zone) which was, in turn, locally oxidized to form the Lower Oxide Ore (hole 165 in the Main Zone). Similar ornaments used for Figures 3-10 to 3-15.

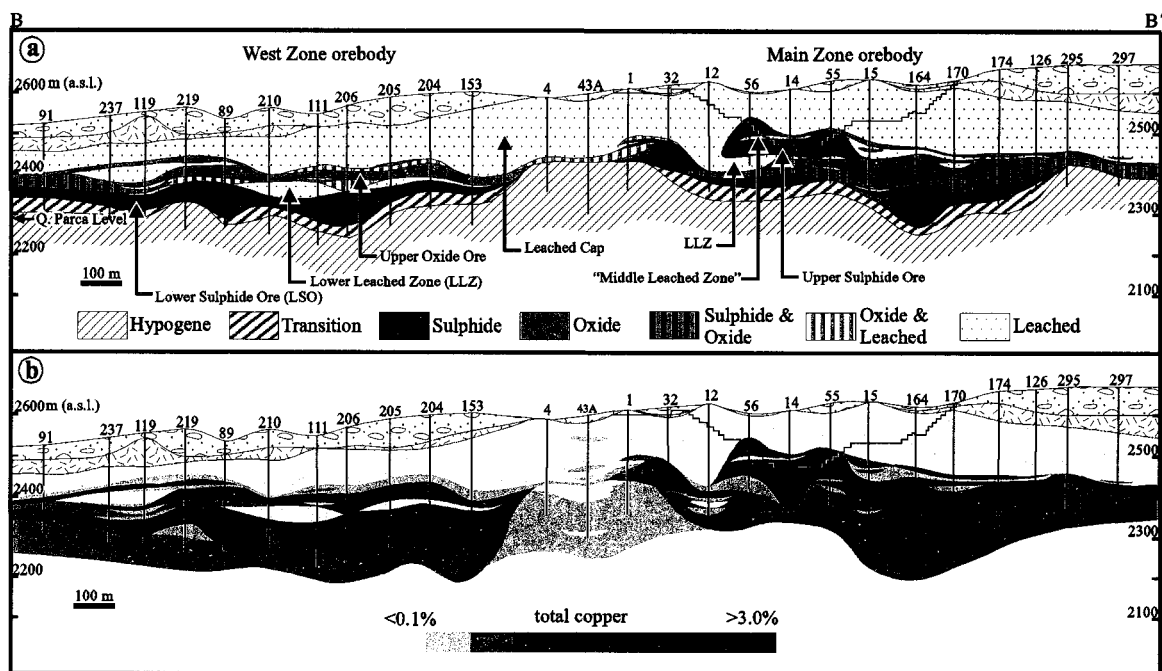


Fig. 3-11:

E-W cross section BB' showing supergene ore facies (a) and grade distribution (b). The sub-planar geometry of the supergene blanket below the gentle westward dip of the Choja Pediplain (pre-ignimbrite surface) probably resulted in the more extensive erosion of the blanket in the western part of the West Zone. The Lower Leached Zone is less continuous in the Main Zone and grades laterally to the oxide ore. Note development of a Middle Leached Zone at an elevation of 2490 m (hole 56); this thickens to the south (cf. Fig. 3-14). Similar horizons are observed in the oxide ore of the West Zone, but their continuity throughout the blanket was not established.

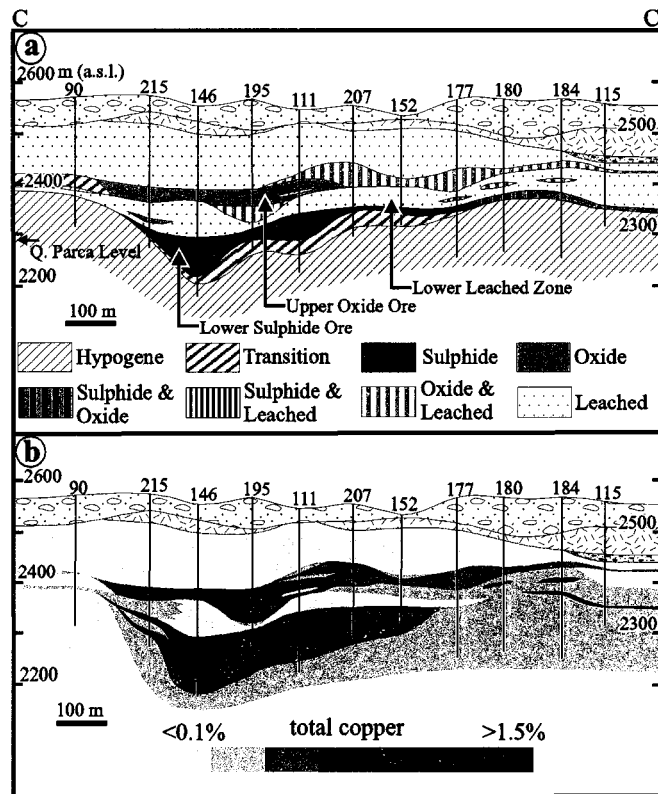


Fig. 3-12:
N-S cross section CC' through West Zone showing ore facies (a) and grade distribution (b). The Lower Leached Zone is more continuous here than in the Main Zone and divides the ore blanket into Upper Oxide and Lower Sulphide Ores.

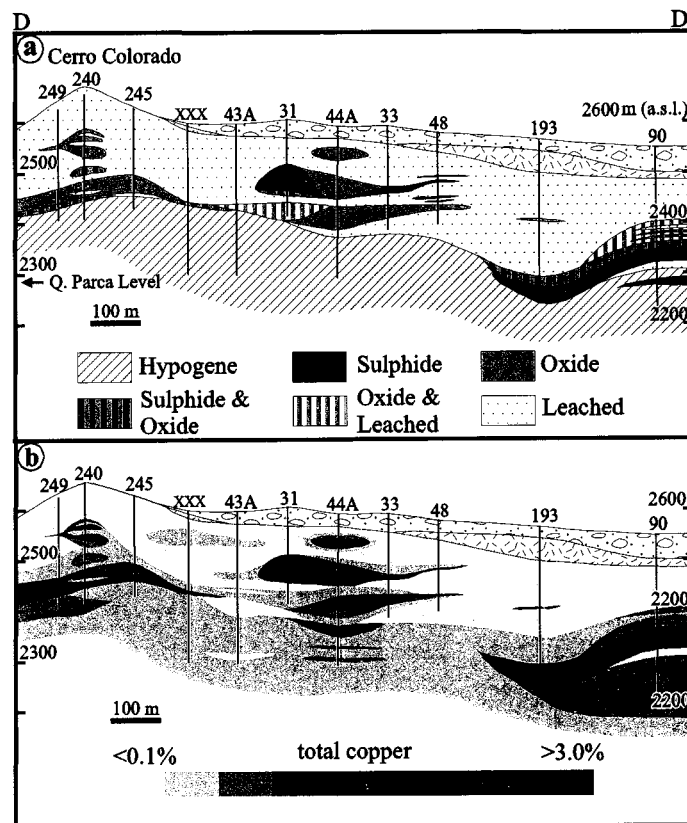


Fig. 3-13:
N-S cross section DD' through Cerro Colorado showing ore facies (a) and grade distribution (b). Low-grade hypogene mineralization resulted in the development of a weak and discontinuous supergene profile in the area between the Main and West Zones.

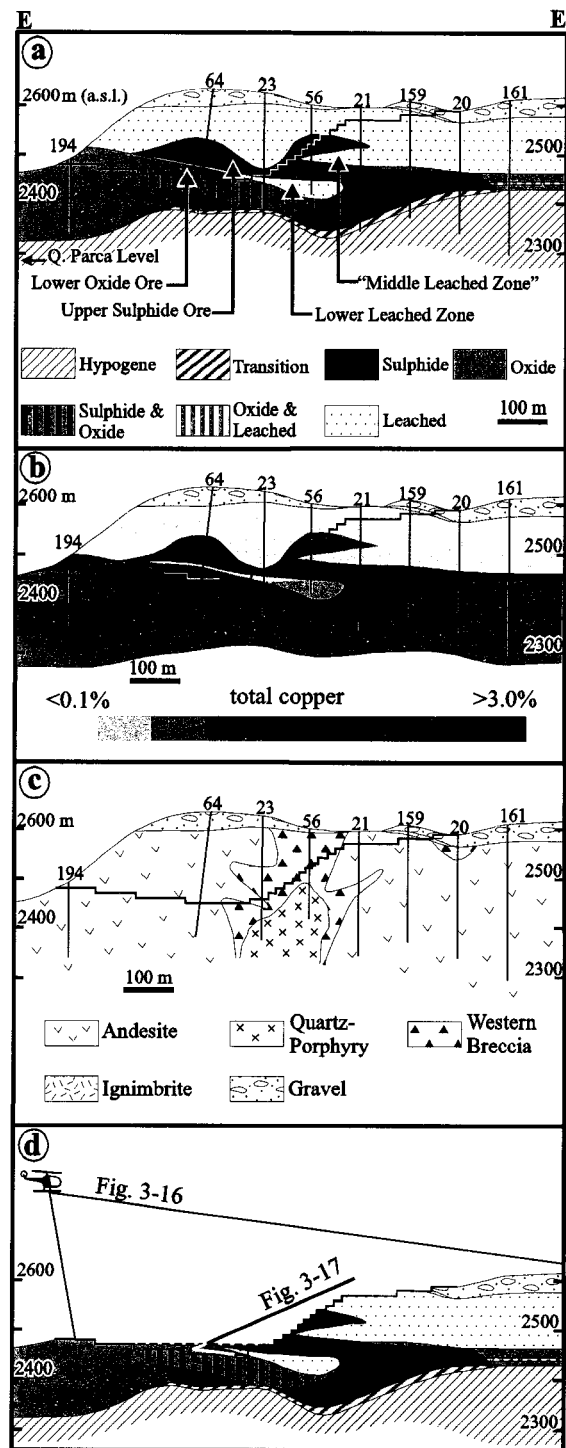


Fig. 3-14:

N-S cross section EE' through western part of the Main Zone, showing ore facies (a), grade distribution (b) host-rock geology (c) and locations of Figures 3-16 and 3-17 (d). The elevation of the Lower Leached Zone falls to the south and its thickness increases in the pyrite-rich Western breccia-intrusive unit, resulting in the thickening of the sulphide ore, but it vanishes further to the south in the andesite. The Upper Sulphide Ore is separated from the Lower Oxide Ore by a thin Lower Leached Zone north of hole 23. Pit outline as in 1996 but the location of the bottom of the pit in 1995 is shown by dashed line in d. The position of the south wall in 1995 was very similar to that shown for 1996.

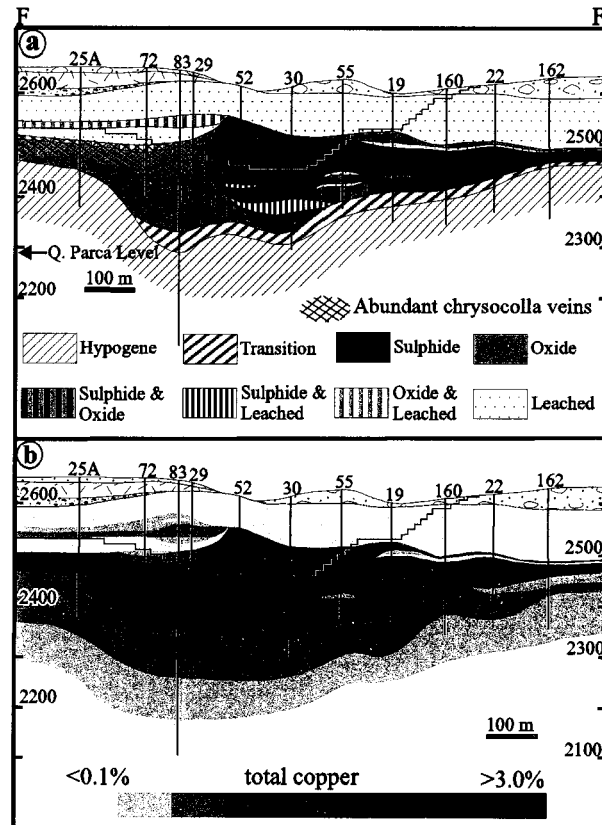


Fig. 3-15:
N-S cross section FF' through central part of Main Zone showing ore facies (a) and grade distribution (b). Much of the northern sector of the blanket is oxidized, probably because of development of a paleo-valley. Note the concentration of chrysocolla in the upper part of the oxide ore, the lower parts of which are dominated by brochantite and atacamite.

In addition to these major zones, a less important, and impersistent, Middle Leached Zone occurs within the Upper Sulphide Ore in the Main Zone. For simplicity, the oxide-dominated facies of the *Upper Supergene Ore* is referred to herein as the Upper Oxide Ore and its sulphide-rich facies as the Upper Sulphide Ore. Similarly, the *Lower Supergene Ore* comprises the Lower Sulphide Ore and the Lower Oxide Ore. The supergene zones are described from top to bottom.

Leached Cap: The Leached Cap is defined as an iron oxide-rich zone, generally with less than 0.1 percent Cu but in some areas attaining 0.3 percent, and overlying the Upper Supergene Ore. The thickness of the Leached Cap increases from west to east across the West Zone, decreases eastwards over the Main Zone, where the Upper Sulphide Ore is best developed, and finally increases across the eastern section of the Main Zone (Figs. 3-10a and 3-11a). For the same E-W sections, the present elevation of the pre-ignimbrite surface increases from west to east, reaching a maximum over the Main Zone and then falling eastwards. These relationships suggest the existence of a paleo-hill, with a summit over the Main Zone, which in the latest-Oligocene stood above the Choja Pediplain. It is inferred that the water table lay at higher elevations beneath the hill during supergene activity, resulting in the formation of a chalcocite blanket (Main Zone) at higher elevations than in the surrounding areas (West Zone). Subsequent erosion has brought the Main Zone orebody closer to the surface. The original height of the hill cannot be determined but it may have risen 200-300 m above the current surface elevation of the Main Zone (ca. 2600 m a.s.l.) when the early supergene processes were underway.

Supergene Cu-bearing assemblages are preserved at the highest elevations of the Leached Cap as supergene sulphide or oxide ore. Figure 3-13a shows that oxide ore is preserved at elevations above 2550 m (see holes 44A and 240). In the same cross section, remnants of an old supergene sulphide ore horizon, now almost entirely leached and hence not shown as a distinct

ore facies in the cross section, can be traced on the grade distribution cross section where remanent sulphide minerals raise the leached grade from less than 0.1 percent to 0.1-0.3 percent Cu (Fig. 3-13b: holes 43A and “XXX”). The Leached Cap in most areas of the mine is hematitic, except at the northeastern extremity of the deposit and north of Cerro Colorado, where jarosite is dominant. The hematite exhibits a wide variety of colours in hand specimen, including red, reddish-brown, and even black. From these observations it can be concluded that the present Leached Cap records the site of an older supergene sulphide horizon. Thus, pyrite which accompanied chalcocite was converted to hematite during the oxidation, and, under these markedly acidic conditions, copper was leached from chalcocite (Anderson, 1982; Titley, 1995a).

Upper Supergene Ore: The Leached Cap is underlain by the Upper Supergene Ore. This is represented by the Upper Oxide Ore, with a mean elevation of ca. 2420 m at its top (Figs. 3-10a, 3-11a and 3-12a) except in the Main Zone, where the thick Upper Sulphide Ore extends above 2440 m (Figs. 3-10a and 3-11a), with abundant supergene clays. The lower boundary of the Upper Supergene Ore is defined in most sections by the Lower Leached Zone. However, a further leached zone is developed within the Upper Sulphide Ore of the Main Zone at an elevation of ca. 2490 m (Figs. 3-11a and 3-14a: hole 56). This thin Middle Leached Zone is older than the Lower Leached Zone, which is well represented at lower elevations (2420 m in the Main Zone), but is presumably younger than the Leached Cap. Figure 3-14a shows that the Middle Leached Zone and the Leached Cap are better developed to the south, where they merge to eliminate much of the upper part of the Upper Sulphide Ore. If this process had continued, at least half of the thickness of the Upper Sulphide Ore would have been leached, lowering its upper surface to elevations of less than 2440 m (i.e., closer to the mean elevation of the Upper Oxide Ore in the West Zone).

Lower Leached Zone: The Lower Leached Zone, which is dominated by hematite and hence again had a chalcocite-rich protolith, is well developed in the West Zone and the western sector of the Main Zone (Figs. 3-10a, 3-11a and 3-12a). In contrast, it is poorly developed in the southeast part of the Main Zone, where the leached facies grades laterally to oxide and mixed sulphide-oxide ores (e.g., Fig. 3-11a: holes 14, 55, 15 and 164) or mixed sulphide-leached ores (Fig. 3-15a: hole 30). The thickness of the Lower Leached Zone varies from ca. 2 m (Fig. 3-10a: hole 71; Fig. 3-14a: hole 64) to more than 65 m (Figs. 3-10a and 3-12a: hole 146).

Lower Supergene Ore: The Lower Leached Zone is underlain by the Lower Supergene Ore, which comprises the Lower Sulphide Ore in the West Zone (Fig. 3-12a) and the Lower Sulphide and Oxide Ores in the Main Zone (Fig. 3-10a). In the latter area, the oxide ore either replaced the upper parts of the sulphide ore (see the upward transition from sulphide ore, through mixed sulphide-oxide, to oxide ore in Figure 3-11a, holes 14, 15, 164 and 174) or obliterated it (Fig. 3-10a: holes 26 and 165). It is evident that the Lower Sulphide Ore formed, or at least was thickened, as a result of the development of the Lower Leached Zone (Fig. 3-10a: hole 146). It is also clear that the Lower Oxide Ore is younger than the contiguous Lower Sulphide Ore, strongly implying that the Lower Oxide Ore also in part developed after the Lower Leached Zone. This interpretation would be valid only if a Lower Leached Zone is well developed and especially if the Lower Oxide Ore has replaced much of the Lower Sulphide Ore (e.g., Fig. 3-10a: hole 26). However, in areas where the Lower Leached Zone is poorly developed (e.g., Fig. 3-11a: holes 55 and 15), the Lower Oxide Ore probably formed contemporaneously with development of the Lower Leached Zone elsewhere.

Variations in the thickness and inclination of the above ore zones result in complex facies and grade relationships in the eastern part of the orebody. For example, the Lower Leached Zone, very thin in the northern part of the Main Zone, dips gently (10-12°) to the south as its thickness

increases in the pyrite-rich Western Breccia (Figs. 3-14a and c). In this section, the Lower Leached Zone is overlain by the Upper Sulphide Ore and underlain by the Lower Oxide Ore, which itself grades laterally into the Lower Sulphide Ore. These complex relationships explain the abrupt lateral juxtaposition of supergene sulphide and oxide ores on the 2470 m level of the Main Zone pit (Figs. 3-7, 3-14d and 3-16). As the pit was deepened, the contact was seen to be displaced to the south until, finally, a thick Lower Leached Zone was intersected on the south wall of the pit below the Upper Sulphide Ore (Fig. 3-17).

Variations in the mineralogy and grade of the hypogene assemblages are also inferred to have had a significant effect on the distribution of the ore. The very thin and low-grade supergene mineralization beneath, and south of, the summit of Cerro Colorado, separating the Main and West Zones, directly reflects the occurrence of poorly-mineralized intrusive bodies within the Western Breccia (Figs. 3-10a, b and c). In addition, the northern part of the Main Zone is dominated by oxide ore (Fig. 3-14a: hole 194; Fig. 3-15a: hole 25A). This also may reflect peripheral, less pervasive sericite-chlorite-clay alteration, with abundant surviving hydrothermal biotite that buffered the acidic supergene waters, resulting in weak enrichment and *in situ* oxidation of the ore (cf. Anderson, 1982). However, as discussed below, this oxidation may also reflect the incision of a valley, a precursor of the present embayment, causing drastic local changes in the water table. If this is the case, this oxidation was probably among the youngest supergene events at Cerro Colorado.

Structural relationships

Fracture analysis was carried out in the Main Zone pit to determine the structural environment of the evolving supergene profile; 443 measurements from different supergene zones are summarized in Figure 3-18. For each measurement, fracture orientation and continuity,

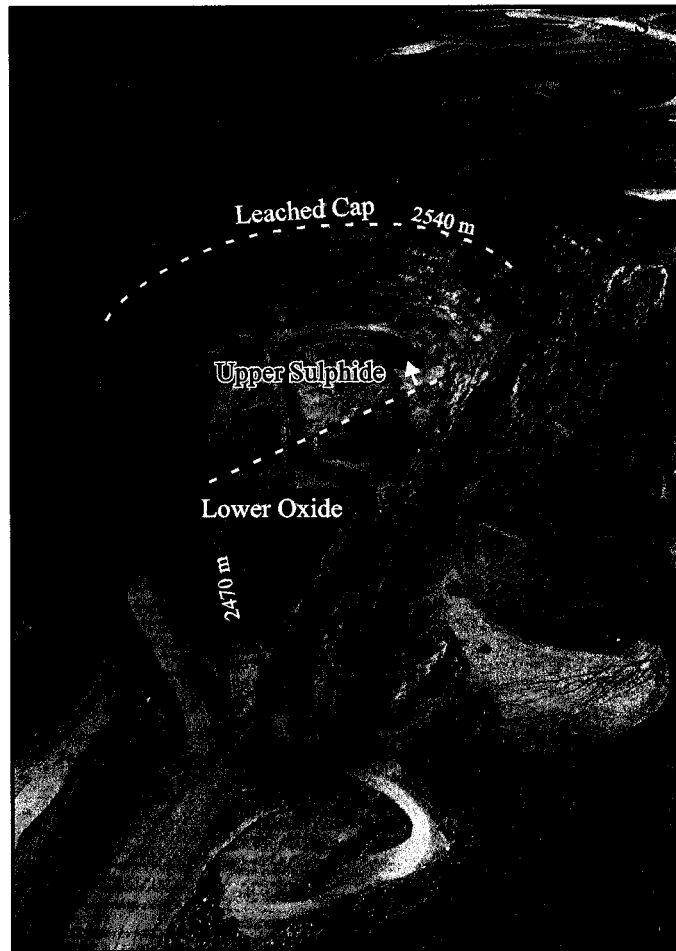


Fig. 3-16:

Oblique aerial view of the Main Zone pit (August, 1995), looking SSE, showing the abrupt transition from the Upper Sulphide (pale bluish-gray) to the Lower Oxide Ores (green) on the 2470 m level. These zones are separated by a thin Lower Leached Zone, not visible here, that dips 10-12° to the south as it thickens (see Fig. 3-14d). As the pit was deepened, the contact migrated to the south and a thicker Lower Leached Zone was intersected 10 m below this elevation at location shown by yellow arrow (see Figs. 3-14d and 3-17). N-S length of the pit at level 2470 m (i.e., bottom of the pit) is approximately 540 m.

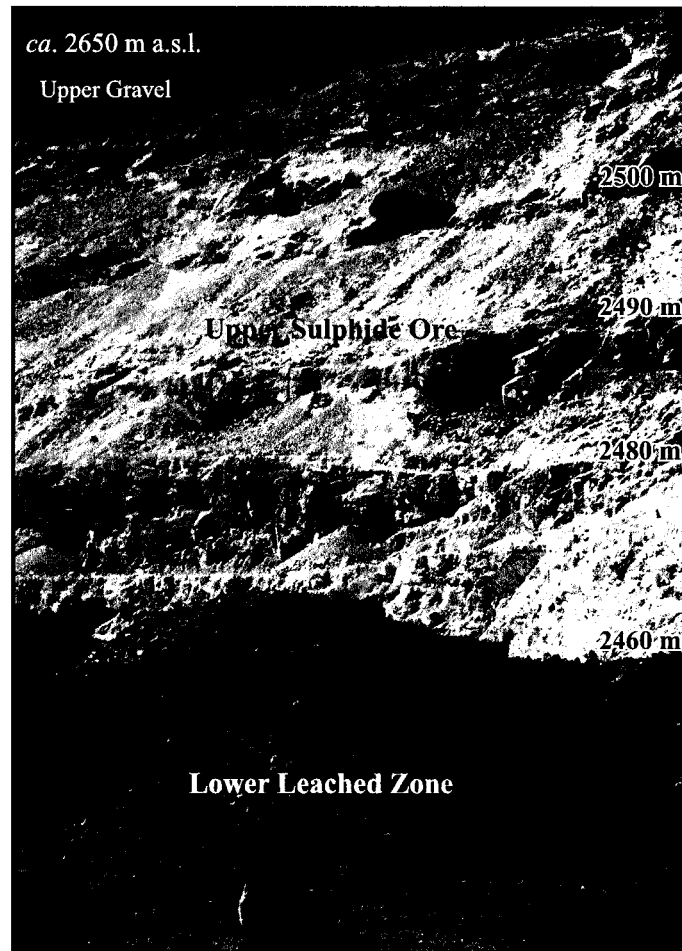
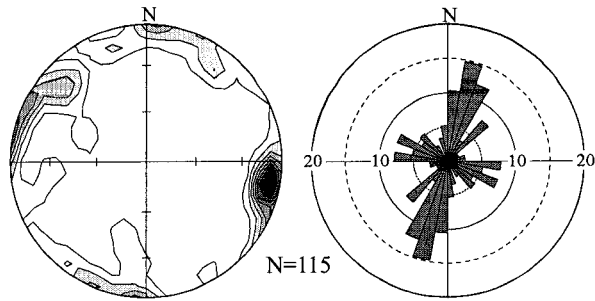


Fig. 3-17:

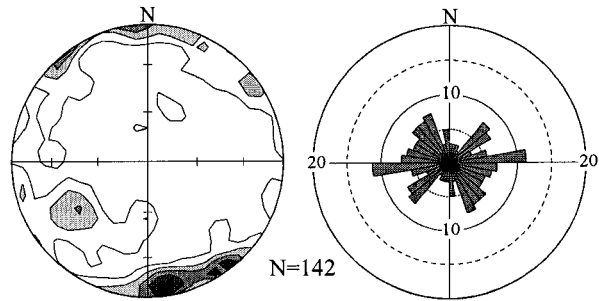
Lower Leached Zone (dark brown, loose rock and bench wall), hematitic but with some goethite and traces of copper oxides, well developed below the Upper Sulphide Ore (white) with a sharp contact at 2460 m. The bleached appearance, due to supergene clays, is characteristic of the sulphide-enriched zone, where Cu recovery is lower than for the oxide ore. Main Zone, looking SSE, on the 2460 m level, October, 1996 (see Fig. 3-14d and yellow arrow in Fig. 3-16 for location).

Fig. 3-18:

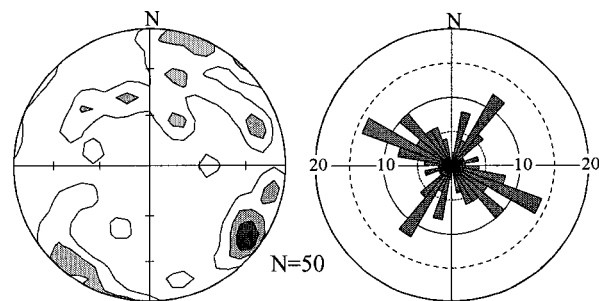
Equal-area Schmidt and rose diagrams of the fractures hosting Main Zone supergene mineralization. Orthogonal fractures trending northwest and northeast host both brochantite-dominated oxidic and chalcocite veins (a and b). Development of syn-mineralization fractures in the breccia body exhibit ca. 40° clockwise rotation relative to those hosting ore in andesite (c and d). Thick chrysocolla veins (e) are restricted to the NW-trending fractures, whereas the NE-trending fractures contain only thin veinlets of iron oxides.



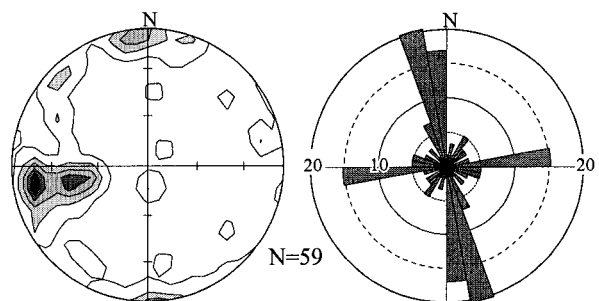
a: supergene oxide (brochantite) in andesite



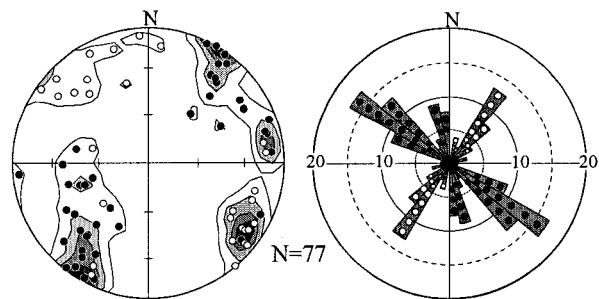
b: supergene sulfide in breccia body



c: jarositic zone in andesite



d: jarositic zone in breccia body



e: chrysocolla veins (•) and barren fractures (◊) in andesite

intensity and type of supergene mineralization were recorded. This analysis shows that supergene sulphide and brochantite-dominated veins exhibit broadly northwest and northeast strikes with dips averaging 75° to the northeast and northwest, respectively (Figs. 3-18a and b). No measurements were recorded from the deep hypogene protore because of lack of exposure, but observations on the jarositic cap confirmed that both NW- and NE-trending fracture systems had similarly localized hypogene mineralization (Figs. 3-18c and d). There is no major difference in the intensity of the remanent hypogene mineralization hosted by the NW- and NE-trending fractures, but there are marked differences in the trends of fractures in the andesite and the breccia complexes, including their associated porphyry intrusions. Thus, fractures in the andesite trend ca. N 70° W and ca. N 30° E (Figs. 3-18a and c), whereas those in the breccia bodies trend ca. N 40° W and ca. N 80° E (Figs. 3-18b and d). Because the andesites host much of the Main Stage sericite-chlorite-clay hypogene alteration, and the breccias were emplaced during the succeeding Transitional Stage, this implies a clockwise, ca. 40°, rotation of fracture development during the hypogene evolution of the deposit. Many of the measured fractures in the breccia bodies contain abundant residual pyrite, indicating that they probably formed during the Late Stage mineralization. Two major dikes that cut both breccia and andesite trend N 37° W and N 85° E, respectively, orientations very similar to those of the pyrite veins.

Fracture orientations are documented from few porphyry Cu deposits, but such broadly orthogonal systems are probably widespread (Tosdal and Richards, 2001), as at Sierrita, Arizona (Titley, 1993), Panguna, Bougainville (Clark, 1990), and Highland Valley, British Columbia (Osatenko and Jones, 1976). They presumably record near-surface subhorizontal extension, at Cerro Colorado possibly controlled by pre-existing NW-SE fault patterns. It is therefore evident that, predictably, the veins that constitute the chalcocite- and brochantite-rich stockworks which dominate the supergene ore inherited their orientations from the chalcopyrite-bearing hypogene fractures, and that both NW- and NE-trending structures are comparably mineralized.

Significantly different relationships are, however, exhibited by the chrysocolla veins, which achieve their richest development on the 2520 to 2280 m levels in the northeast quadrant of the Main Zone pit (Figs. 3-4 and 3-15a). Here, in an originally pyrite-dominated andesite domain, numerous essentially monomineralic chrysocolla veins attain widths of 2 cm (Fig. 3-19). Moreover, these veins cut all brochantite as well as chalcocite veins and incorporate no relics of these minerals. As for the earlier supergene veins, the chrysocolla-rich stockwork comprises NW- and NE-striking fractures (Fig. 3-18e). However, the NW-trending structures are strongly dilated and mineralized whereas those trending northeast are “tight” and either weakly mineralized or barren, hosting only supergene iron-oxide minerals (Fig. 3-19). NW-trending fractures in the lower, altered, part of the ignimbrite flow (white tuff) also contain small amounts of chrysocolla.

It is therefore apparent that the chrysocolla veins represent a distinct, terminal phase in the supergene history of the deposit, postdating its blanketing by the ignimbrite flow at 19.25 Ma, and record fracture dilation conditions differing from those that prevailed during early supergene oxidation and sulphide enrichment. Extension related to relaxation after a contraction episode may explain late-stage preferential dilation of the NW-trending fractures. Thus, NE-verging reverse movement along the NW-trending structures in the Cerro Colorado area (Galli, 1968), probably contemporaneous with the Early Miocene SW-verging thrusting on the Moquella fault system (Muñoz and Charrier, 1996), may have resulted from SW-NE compression, and hence contributed to the uplift of the mine area (Fig. 3-2; see above). The subsequent release of stress may have resulted in opening of the NW-trending fractures and deposition of chrysocolla. An alternative model ascribes local extension along pre-existing, NW-trending zones of weakness to Early Miocene, sinistral - transcurrent displacement along the Domeyko Fault System (Carrasco et al., 1999). Under these conditions, the NE-trending fractures would have remained tight.

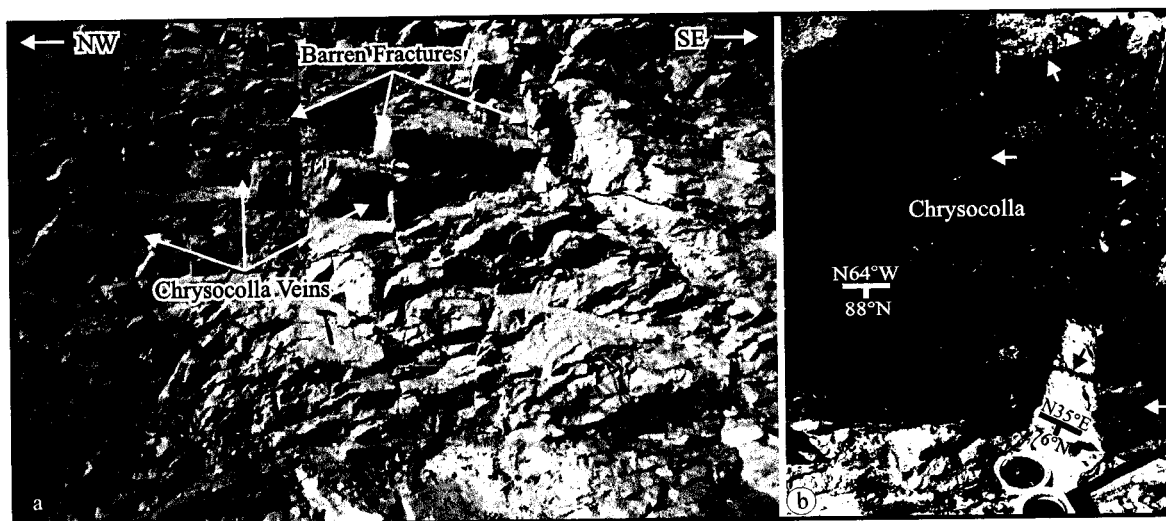


Fig. 3-19:

(a) Bench wall in the chrysocolla-rich area of the Main Zone, level 2520 m, showing NW-trending chrysocolla veins (blue), sub-parallel to the face and dipping away from the viewer. These are cut by barren NE-trending fractures (there is a rock hammer for the scale in the middle of the photograph). (b) Closer view showing sub-vertical chrysocolla vein on the face cut by barren fractures (white arrows). The host-rock is strongly leached andesite (yellow arrow). A thick chrysocolla vein is indicated by a black arrow. The rock exposure has been wetted so that the chrysocolla veins appear bluer than in 19a.

3.6. Supergene Alunite-Group Mineralogy

The alunite group comprises more than 15 minerals (Jambor, 1999), of which the most common at Cerro Colorado and in other supergene profiles, generated under markedly acidic conditions where pyrite undergoes oxidation (Hemley et al., 1969), are alunite proper, $\text{KAl}_3(\text{SO}_4)_2(\text{OH})_6$, and jarosite, $\text{KFe}_3(\text{SO}_4)_2(\text{OH})_6$. The extent of Fe-for-Al substitution is limited in these minerals, but K^+ , Na^+ , and $(\text{H}_3\text{O})^+$ solid solution may be extensive. Natroalunite, $(\text{Na},\text{K})\text{Al}_3(\text{SO}_4)_2(\text{OH})_6$, and natrojarosite, $(\text{Na},\text{K})\text{Fe}_3(\text{SO}_4)_2(\text{OH})_6$, are defined as containing moles $\text{Na} > \text{moles K}$ in the alkali site (Okada et al., 1982).

Supergene alunite-group minerals occur over a vertical interval of at least 360 m at Cerro Colorado, from the top of the eroded Leached Cap (2665 m elevation) down to 2300 m a.s.l. Alunite occurs as cm-thick, megascopically-monomineralic veinlets (Fig. 3-20). Such veinlets are thicker (up to 10 cm) and more abundant in the Eastern and Western Breccias, which had undergone intense hypogene quartz-sericite-pyrite alteration, than in andesite. Alunite veinlets are conspicuous in the Leached Cap and in the upper part of the supergene ore zones, but those in the lower parts of the supergene blanket, and especially in the sericite-chlorite-clay -altered andesite, are considerably thinner. In the present study, alunite-group minerals were sampled from a representative array of sites in the supergene profiles of the West and Main Zones as a basis for a detailed $^{40}\text{Ar}/^{39}\text{Ar}$ dating program.

In hand specimen, the supergene alunite exhibits a massive, very fine-grained and porcelaneous appearance similar to that described by Sillitoe and McKee (1996). Some coarser-grained samples have a sugary texture, which at high magnification reveals rhombohedral forms such as are characteristic of supergene alunite (Fig. 3-21a). A wide variety of colours is observed, including whitish-gray, pale-olive, pale to dark-yellow and reddish-brown. X-ray powder diffraction study shows that dark-yellow samples are mixtures of jarosite and alunite, whitish samples are natroalunite, and greenish-yellow to pale-olive samples are alunite,

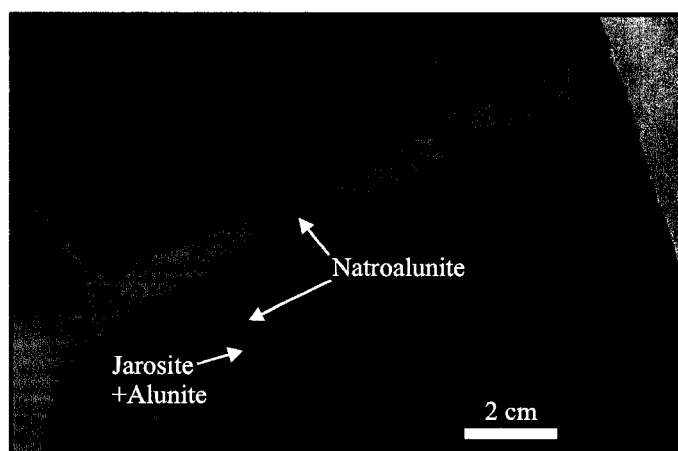


Fig. 3-20:
Characteristic occurrence of fine-grained, porcelaneous, supergene alunite-group minerals, showing mixed, dark-yellowish alunite-jarosite veinlets (see Fig. 3-21b) cut by natroalunite veins. Sample CRCO 331 from 2620 m level, Cerro Colorado summit, Western Breccia.

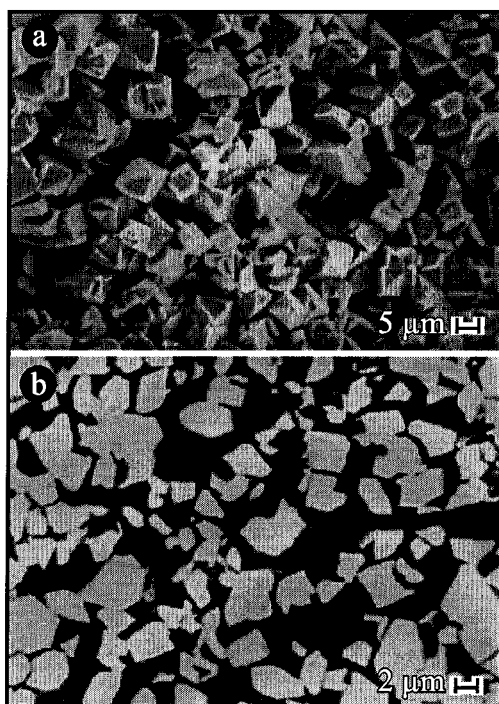


Fig. 3-21:

- (a) Scanning electron microscope image of supergene porcelaneous natroalunite showing typical rhombohedral forms (sample CRCO 328).
- (b) Back-scattered electron image of a cut surface of sample CRCO 331A showing earlier fragmented jarosite (pale) cemented by alunite (dark matrix).

natroalunite or, in most cases, a mixture of these in which either may dominate.

None of the veinlets shows textural evidence of replacement by a later alunite species generation, but in some samples it is clear that different species were deposited at different times. For example, sample CRCO 331, from the (former) summit of Cerro Colorado, exhibits two loci of alunite-group minerals: disseminations and veinlets of dark-yellowish porcelaneous material, representing a very fine-grained mixture of jarosite and alunite (CRCO 331A); and white to yellowish-gray natroalunite veins (331B), cutting the former (Fig. 3-20).

Alunite may also develop as a component of hypogene advanced argillic alteration, and sulphur isotopic data (e.g., Rye et al., 1992) have been utilized widely (e.g., Alpers and Brimhall, 1988) to distinguish between supergene and hypogene occurrences. No isotopic data are available herein, but uncontestedly hypogene alunite has not been observed at Cerro Colorado, and we consider the porcelaneous habit, textural relationships (veinlets cutting all hypogene veins), and particularly the geologic context and age as evidence for the supergene origin of the analyzed samples.

Sampling and analysis

Numerous alunite-group samples were collected from the open pit and drill core. After preliminary X-ray study, 20 were chosen to represent different alunite-group populations at different elevations. These include 11 samples from the Leached Cap, 6 from the Upper Sulphide Ore, 2 from the Upper Oxide Ore, and one from the Lower Sulphide Ore beneath the Lower Leached Zone. Open pit samples from the Main Zone were taken from the 2660 m to the 2450 m benches. Drill core permitted sampling down to 2300 m a.s.l., but only 3 samples could be separated from the core from between 2450 m and 2365 m in the West Zone. Samples were also collected from several sites on the 2580 m level of the Main Zone open pit, to establish the range of alunite-group minerals occurring at one elevation. Finally, CRCO 245, a pebble, was collected from the lower part of a gravel lens

separating the ignimbrite flow from the Main Zone (Fig. 3-4). This pebble is of a leached assemblage, and hosts an alunite veinlet. It is inferred to have been eroded from a higher elevation, and hence to represent an older association, than the supergene assemblages preserved *in situ*. Table 3-2 summarizes the locations and nature of the dated samples.

X-ray and electron microprobe analysis: All 20 samples were analyzed with an X-ray diffractometer and electron microprobe. Analytical techniques are summarized in Appendix 3. X-ray powder diffraction data (Table 3-2) confirmed the occurrence of alunite, natroalunite, jarosite, alunite mixed with minor natroalunite, natroalunite mixed with minor alunite, and jarosite mixed with alunite. All mixed samples appeared homogeneous in hand specimen and transmitted light, owing to the extremely fine-grained intergrowths. However, alunite and jarosite could be distinguished in mixed samples under high magnification (Fig. 3-21b). X-ray patterns show that all 006 and 009 reflections of the alunite yield peaks systematically lower in intensity than for Marysvale alunite (JCPDS file number 14-136). Whereas in the standard these reflections have relative intensities of 100 and 70, respectively, the Cerro Colorado samples show intensities of only 13 and 8. In a study of synthetic alunite, Parker (1962) recorded a similar relationship for sodium-bearing ($\text{Na}_2\text{O} = 1.64$ wt%) alunite and demonstrated that the *c* dimension of the unit cell shows a marked linear shrinkage with increasing Na content. A slight decrease in the unit cell dimension may also result from substitution of hydronium for Na^+ and K^+ (Parker, 1962; Stoffregen et al., 2000). Results of electron microprobe analyses (Table 3-3) show an almost complete range of composition between alunite and natroalunite, but with a small gap at $0.62 < \text{Na} < 0.8$ (Fig. 3-22), which may reflect the limited range of sampling. On the basis of unit-cell dimension variation in low-temperature alunite, Stoffregen and Alpers (1992) inferred that intermediate alunite-natroalunite compositions are not common. Stoffregen and Cygan (1990) compiled compositional data for naturally occurring, low-temperature alunite, revealing continuity between alunite and natroalunite, but suggested that

Table 3-2. Locations, mineralogical characteristics and $^{40}\text{Ar}/^{39}\text{Ar}$ ages of supergene alunite-group samples from Cerro Colorado

| Sample no. | U.T.M. coordinates | Elevation (m a.s.l.) | Location | Habit | Hypogene setting | Supergene setting | Mineralogy ¹ | K (wt.%) | Age $\pm 2\sigma$ (Ma) |
|-------------------------|----------------------------------|----------------------|--|---|---|---------------------------------|---------------------------|----------|------------------------|
| CRCO 245 | 473600E, 7783823N (not original) | 2580 (not original) | Gravel with clasts of leached facies deposited below ignimbrite flow, east wall, Main Zone | 4 mm-thick, yellowish-gray veinlet | Quartz-sericite-clay altered andesite clast | Hematitic Leached Cap | Alunite | 5.81 | 35.26 \pm 0.68 |
| CRCO 201 | 472950E, 7783616N | 2655 | Cerro Colorado, 10 m below top of the hill | 7 mm-thick, pale greenish-yellow, porcelaneous vein | Western quartz-sericite-pyrite and tourmaline-altered breccia | Jarositic-hematitic Leached Cap | Natroalunite | 3.30 | 17.14 \pm 0.42 |
| CRCO 328 | 473070E, 7783620N | 2640 | Cerro Colorado, east slopes | 3 mm-thick, pale greenish-yellow, porcelaneous veinlet | Western quartz-sericite-pyrite altered breccia | Jarositic-hematitic Leached Cap | Natroalunite (Quartz) | 3.51 | 17.62 \pm 0.67 |
| CRCO 331A ² | 473090E, 7783610N | 2620 | Cerro Colorado, east slopes | 1 cm-thick, dark yellowish, porcelaneous vein | Western quartz-sericite-pyrite and tourmaline-altered breccia | Jarositic-hematitic Leached Cap | Jarosite+Alunite (Quartz) | 5.38 | 24.17 \pm 0.69 |
| CRCO 331B | 473090E, 7783610N | 2620 | Cerro Colorado, east slopes | 1 cm-thick, white to yellowish-gray vein cutting dark-yellowish veins of sample # CRCO 331A | Western quartz-sericite-pyrite and tourmaline-altered breccia | Jarositic-hematitic Leached Cap | Natroalunite | 3.70 | 15.68 \pm 1.36 |
| CRCO 218 | 473685E, 7783780N | 2580 | Main Zone, east wall, north side | 8 cm-thick, pale yellowish-orange, porcelaneous vein | Eastern quartz-sericite-pyrite altered breccia | Hematitic Leached Cap | Alunite (Quartz) | 6.37 | 26.49 \pm 0.65 |
| CRCO 221 | 473700E, 7783750N | 2580 | Main Zone, east wall | 10 cm-thick, whitish vein | Eastern quartz-sericite-pyrite altered breccia | Hematitic Leached Cap | Natroalunite | 0.52 | 22.42 \pm 1.06 |
| CRCO 243 | 473720E, 7783721N | 2580 | Main Zone, east wall | 5 cm-thick, light greenish-gray vein | Eastern quartz-sericite-pyrite altered breccia | Hematitic Leached Cap | Natroalunite (Quartz) | 0.98 | 14.59 \pm 2.46 |
| CRCO 230 | 473810E, 7783400N | 2580 | Main Zone, east wall, south side | 1 cm-thick, pale reddish-brown vein | Eastern quartz-sericite-pyrite altered breccia | Hematitic Leached Cap | Alunite (Quartz) | 6.44 | 31.94 \pm 0.49 |
| CRCO 248 ⁽²⁾ | 473140E, 7783450N | 2580 | Main Zone, west wall, between the Main and West Zone | 2 cm-thick, dark yellowish-orange vein | Quartz-sericite-clay altered andesite | Hematitic Leached Cap | Jarosite+Alunite (Quartz) | 6.49 | 22.30 \pm 0.53 |

Table 3-2. (Cont.)

| | | | | | | | | | |
|-------------|----------------------|------|---------------------------------|---|--|---|-----------------------------------|------|-----------------------------|
| CRCO 290 | 473787E, 7783408N | 2560 | Main Zone, east wall | 7 mm-thick, yellowish vein | Eastern quartz-sericite- pyrite altered breccia | Locally jarositic Leached Cap | Jarosite (Quartz) | 3.49 | 24.81 ± 0.44 |
| CRCO 254 | 473694E, 7783709N | 2550 | Main Zone, east wall | 1.5 cm-thick, pale greenish- yellow, porcelaneous vein | Eastern quartz-sericite- pyrite altered breccia | Top of the Upper Sulphide Ore | Alunite (Natroalunite) | 6.37 | (13.00 ± 0.45) ³ |
| CRCO 127 | 473688E, 7783696N | 2540 | Main Zone, east wall | 1 cm-thick, light olive, porcelaneous vein | Eastern quartz-sericite- pyrite altered breccia | Top of the Upper Sulphide Ore | Natroalunite (Alunite) | 3.41 | (13.69 ± 0.63) |
| CRCO 199 | 473647E, 7783684N | 2530 | Main Zone, east wall | 2 cm-thick, pale greenish yellow, porcelaneous vein | Eastern quartz-sericite- pyrite altered breccia | Upper Sulphide Ore | Alunite (Natroalunite, Quartz) | 5.96 | (15.63 ± 0.62) |
| CRCO 271 | 473663E, 7783704N | 2520 | Main Zone, east wall | 3 cm-thick, moderate greenish-yellow, porcelaneous vein | Eastern quartz-sericite- pyrite altered breccia | Upper Sulphide Ore | Alunite (Natroalunite) | 4.90 | (12.40 ± 1.81) |
| CRCO 347 | 473654E, 7783420N | 2510 | Main zone, center of the pit | 0.5 cm-thick, light olive, porcelaneous vein | Eastern quartz-sericite- pyrite altered breccia | Upper Sulphide Ore | Alunite | 7.99 | 19.55 ± 1.62 |
| CRCO 322 | 473532E, 7783478N | 2450 | Main Zone, center of the pit | 1.5 cm-thick, yellowish gray, porcelaneous vein | Eastern quartz-sericite- pyrite altered porphyry intrusive | Upper Sulphide Ore | Alunite (Natroalunite, Quartz) | 7.24 | (20.47 ± 0.54) |
| CRCO 209-48 | 472528E, 7783236N | 2450 | West Zone, drill core | Up to 8mm-thick, moderate greenish-yellow, porcelaneous bodies in chrysocolla vein | Quartz-sericite-clay altered andesite | Upper Oxide Ore (partly leached) | Alunite | 7.92 | 21.49 ± 0.49 |
| CRCO 209-39 | 472528E, 7783236N | 2430 | West Zone, drill core | 3 mm-thick, yellowish gray veinlet | Quartz-sericite-clay altered andesite | Upper Oxide Ore | Natroalunite (Quartz) | 4.37 | 20.83 ± 0.72 |
| CRCO 205-28 | 472440E, 7783324N | 2365 | West Zone, drill core | 3-4 mm thick, light greenish yellow veinlets surrounding sulfide veins | Quartz-sericite-chlorite- clay altered andesite | Lower Sulphide Ore a few m below Lower Leached Zone | Natroalunite (Quartz) | 1.15 | 20.88 ± 0.98 |

¹ Minor phases are shown in brackets.² For samples CRCO 331A and CRCO 248, comprising fragments of jarosite in a matrix of alunite, average K content are given. Detailed analyses are in Table 3-3.³ Dates in brackets represent integrated ages for samples for which plateaus were not attained. See text for discussion.

Table 3-3. Composition of supergene alunite-group minerals at Cerro Colorado

| CRCO | alunite | | | | | | natroalunite | | | | | | jarosite | | | mixed alunite-natroalunite | | | | | | |
|--------------------------------|---------|-------|--------|--------|-------|--------|--------------|-------|--------|--------|-------|-------|----------|-------|-------|----------------------------|-------|--------|-------|-------|-------|--------|
| | 245 | 331A | 218 | 230 | 248 | matrix | 221 | 243 | 209-39 | 205-28 | 201 | 328 | 331B | 331A | 248 | 290 | 254 | 199 | 271 | 322 | 127 | |
| K ₂ O | 7.00 | 5.12 | 7.67 | 7.76 | 7.87 | 9.63 | 9.54 | 0.63 | 1.18 | 5.26 | 1.38 | 3.98 | 4.23 | 4.46 | 8.14 | 7.78 | 4.20 | 7.67 | 7.18 | 5.90 | 8.72 | 4.11 |
| Na ₂ O | 2.01 | 3.26 | 2.13 | 1.86 | 1.38 | 0.19 | 0.78 | 6.49 | 6.14 | 3.51 | 5.60 | 4.54 | 4.33 | 4.24 | 0.58 | 1.07 | 2.48 | 2.42 | 2.43 | 3.01 | 1.28 | 4.66 |
| CaO | 0.57 | 0.00 | 0.41 | 0.24 | 0.00 | 0.66 | 0.14 | 0.17 | 0.19 | 0.25 | 0.75 | 0.10 | 0.13 | 0.16 | 0.00 | 0.00 | 0.45 | 0.00 | 0.23 | 0.35 | 0.27 | 0.12 |
| MgO | 0.29 | 0.00 | 0.39 | 0.15 | 0.00 | 0.18 | 0.33 | 0.11 | 0.17 | 0.00 | 0.00 | 0.25 | 0.15 | 0.15 | 0.00 | 0.00 | 0.00 | 0.13 | 0.09 | 0.18 | 0.12 | 0.09 |
| Fe ₂ O ₃ | 1.12 | 3.59 | 2.16 | 1.95 | 6.73 | 4.14 | 1.66 | 0.73 | 1.08 | 3.72 | 7.35 | 1.42 | 2.10 | 1.69 | 44.06 | 42.65 | 38.61 | 1.41 | 1.82 | 2.29 | 0.60 | 1.40 |
| Al ₂ O ₃ | 36.33 | 34.79 | 37.34 | 38.12 | 33.33 | 32.87 | 36.95 | 37.30 | 38.18 | 34.94 | 31.47 | 35.99 | 36.64 | 36.44 | 1.29 | 4.08 | 4.42 | 37.45 | 37.42 | 36.81 | 36.71 | 38.25 |
| SO ₃ | 34.93 | 37.36 | 36.14 | 36.08 | 35.56 | 32.87 | 35.94 | 36.10 | 36.87 | 35.70 | 33.15 | 36.94 | 37.64 | 36.10 | 31.27 | 31.93 | 27.23 | 37.31 | 36.31 | 35.61 | 35.45 | 37.98 |
| P ₂ O ₅ | 1.32 | 0.33 | 0.67 | 0.94 | 0.48 | 1.74 | 0.00 | 0.86 | 0.62 | 0.66 | 1.98 | 0.29 | 0.48 | 0.16 | 0.23 | 0.39 | 1.70 | 0.37 | 0.93 | 1.57 | 0.48 | 0.24 |
| SiO ₂ | 1.84 | 0.18 | 0.39 | 0.00 | 0.29 | 0.24 | 0.00 | 1.11 | 1.10 | 0.00 | 0.87 | 0.19 | 0.00 | 1.39 | 0.00 | 0.00 | 0.00 | 0.36 | 0.00 | 0.00 | 0.00 | 0.00 |
| TiO ₂ | 0.11 | 0.00 | 0.00 | 0.29 | 0.25 | 0.09 | 0.10 | 0.00 | 0.10 | 0.00 | 0.12 | 0.00 | 0.00 | 0.00 | 0.28 | 0.00 | 0.27 | 0.00 | 0.20 | 0.00 | 0.00 | 0.00 |
| H ₂ O ¹ | 12.90 | 12.75 | 13.11 | 13.06 | 12.46 | 12.01 | 12.68 | 12.99 | 13.26 | 12.54 | 12.19 | 12.78 | 13.03 | 12.87 | 9.23 | 9.68 | 8.81 | 13.10 | 12.99 | 12.89 | 13.02 | 13.25 |
| Total (wt%) | 98.42 | 97.38 | 100.41 | 100.44 | 98.35 | 94.63 | 98.12 | 96.47 | 98.89 | 96.58 | 94.85 | 96.47 | 98.74 | 97.65 | 95.08 | 97.58 | 88.15 | 100.21 | 99.61 | 98.61 | 96.64 | 100.09 |
| K | 0.622 | 0.458 | 0.672 | 0.679 | 0.716 | 0.913 | 0.861 | 0.056 | 0.102 | 0.478 | 0.128 | 0.357 | 0.371 | 0.396 | 0.909 | 0.835 | 0.495 | 0.670 | 0.632 | 0.523 | 0.791 | 0.355 |
| Na | 0.272 | 0.443 | 0.283 | 0.247 | 0.191 | 0.028 | 0.107 | 0.871 | 0.806 | 0.484 | 0.790 | 0.617 | 0.577 | 0.572 | 0.098 | 0.175 | 0.443 | 0.321 | 0.325 | 0.405 | 0.176 | 0.611 |
| Ca | 0.042 | 0.000 | 0.030 | 0.018 | 0.000 | 0.053 | 0.011 | 0.012 | 0.014 | 0.019 | 0.058 | 0.007 | 0.010 | 0.012 | 0.000 | 0.000 | 0.044 | 0.000 | 0.017 | 0.026 | 0.021 | 0.009 |
| Mg | 0.030 | 0.000 | 0.040 | 0.015 | 0.000 | 0.020 | 0.034 | 0.011 | 0.018 | 0.000 | 0.000 | 0.027 | 0.015 | 0.016 | 0.000 | 0.000 | 0.000 | 0.013 | 0.009 | 0.019 | 0.013 | 0.009 |
| Fe | 0.059 | 0.189 | 0.124 | 0.101 | 0.361 | 0.232 | 0.088 | 0.038 | 0.055 | 0.199 | 0.402 | 0.075 | 0.109 | 0.088 | 2.904 | 2.701 | 2.683 | 0.073 | 0.095 | 0.120 | 0.032 | 0.071 |
| Al | 2.979 | 2.875 | 3.021 | 3.082 | 2.800 | 2.878 | 3.078 | 3.040 | 3.046 | 2.933 | 2.698 | 2.977 | 2.969 | 2.992 | 0.133 | 0.405 | 0.481 | 3.023 | 3.044 | 3.014 | 3.074 | 3.052 |
| S | 1.824 | 1.966 | 1.862 | 1.858 | 1.901 | 1.833 | 1.907 | 1.874 | 1.873 | 1.908 | 1.810 | 1.946 | 1.942 | 1.887 | 2.055 | 2.017 | 1.887 | 1.918 | 1.881 | 1.857 | 1.890 | 1.929 |
| P | 0.078 | 0.020 | 0.039 | 0.055 | 0.029 | 0.109 | 0.000 | 0.050 | 0.035 | 0.040 | 0.122 | 0.017 | 0.028 | 0.010 | 0.017 | 0.028 | 0.132 | 0.022 | 0.054 | 0.093 | 0.029 | 0.014 |
| Si | 0.128 | 0.012 | 0.027 | 0.000 | 0.021 | 0.018 | 0.000 | 0.076 | 0.075 | 0.000 | 0.063 | 0.013 | 0.000 | 0.097 | 0.000 | 0.000 | 0.000 | 0.025 | 0.000 | 0.000 | 0.000 | 0.000 |
| Ti | 0.006 | 0.000 | 0.000 | 0.015 | 0.014 | 0.005 | 0.005 | 0.000 | 0.005 | 0.000 | 0.007 | 0.000 | 0.000 | 0.000 | 0.019 | 0.000 | 0.019 | 0.000 | 0.010 | 0.000 | 0.000 | 0.000 |
| OH | 6.000 | 6.000 | 6.000 | 6.000 | 6.000 | 6.000 | 6.000 | 6.000 | 6.000 | 6.000 | 6.000 | 6.000 | 6.000 | 6.000 | 6.000 | 6.000 | 6.000 | 6.000 | 6.000 | 6.000 | 6.000 | 6.000 |

¹ H₂O content calculated on the basis of six OH in the mineral formula.

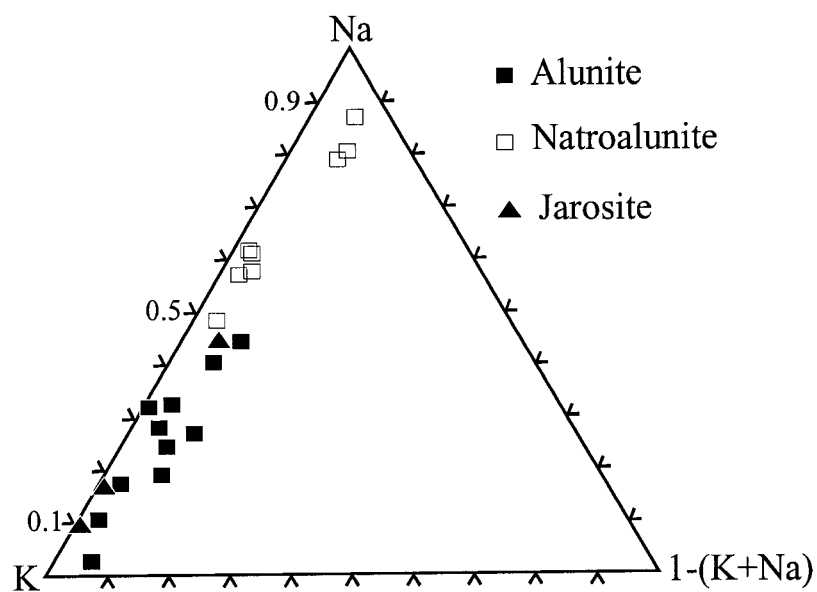


Fig. 3-22:

Ternary alkali-site diagram for supergene alunite-group minerals, Cerro Colorado. Solid solution between alunite and natroalunite is extensive, but with a possible compositional gap at $0.62 < \text{Na} < 0.8$. Mineral names are assigned on the basis of X-ray powder diffraction analysis.

“chemical equilibrium is not generally attained between alunite and aqueous solutions below 100° C” (p. 217). Ca and P contents are very low in the Cerro Colorado samples and no other component was observed in the EDS spectra. The slight deficiency in the total alkalis and the overall totals (Table 3-3) may be evidence for the presence of hydronium in the alkali site.

3.7. $^{40}\text{Ar}/^{39}\text{Ar}$ Geochronology of Alunite-Group Minerals

The reliability of the Ar-based dating of alunite has been discussed by Love et al. (1994, 1998), Itaya et al. (1996) and Vasconcelos (1999), and several studies document K-Ar (e.g., Alpers and Brimhall, 1988; Sillitoe and McKee, 1996) and $^{40}\text{Ar}/^{39}\text{Ar}$ (e.g., Vasconcelos et al., 1994; Mote et al., 2001a) dates for supergene alunite. Laser-induced incremental-heating $^{40}\text{Ar}/^{39}\text{Ar}$ techniques (Appendix 3) were applied herein to samples well documented in terms of field relationships, mineralogy and composition. The age spectra are illustrated in Figure 3-23 and analytical details are provided in Appendix 4. An apparent age plateau was defined as at least three consecutive concordant steps within 95 percent confidence level representing over 50 percent of the Ar released (Dalrymple and Lanphere, 1974). All plateau ages satisfy the Critical-Value test of McIntyre (1963). The locations of the samples and their plateau ages in the supergene profile are plotted on enlarged segments of the cross sections (Fig. 3-24). Some sample dates have been projected onto these sections, while the elevations of samples CRCO 347, 209-48 and 209-39 have been slightly adjusted to maintain their locations in specific ore facies.

$^{40}\text{Ar}/^{39}\text{Ar}$ age spectra for alunite-group minerals

Several studies, cited earlier, have demonstrated that supergene alunite is an appropriate candidate for $^{40}\text{Ar}/^{39}\text{Ar}$ dating, although in general the configurations of the apparent age spectra are more complex and/or disturbed than those for hypogene samples. The $^{40}\text{Ar}/^{39}\text{Ar}$ age spectra

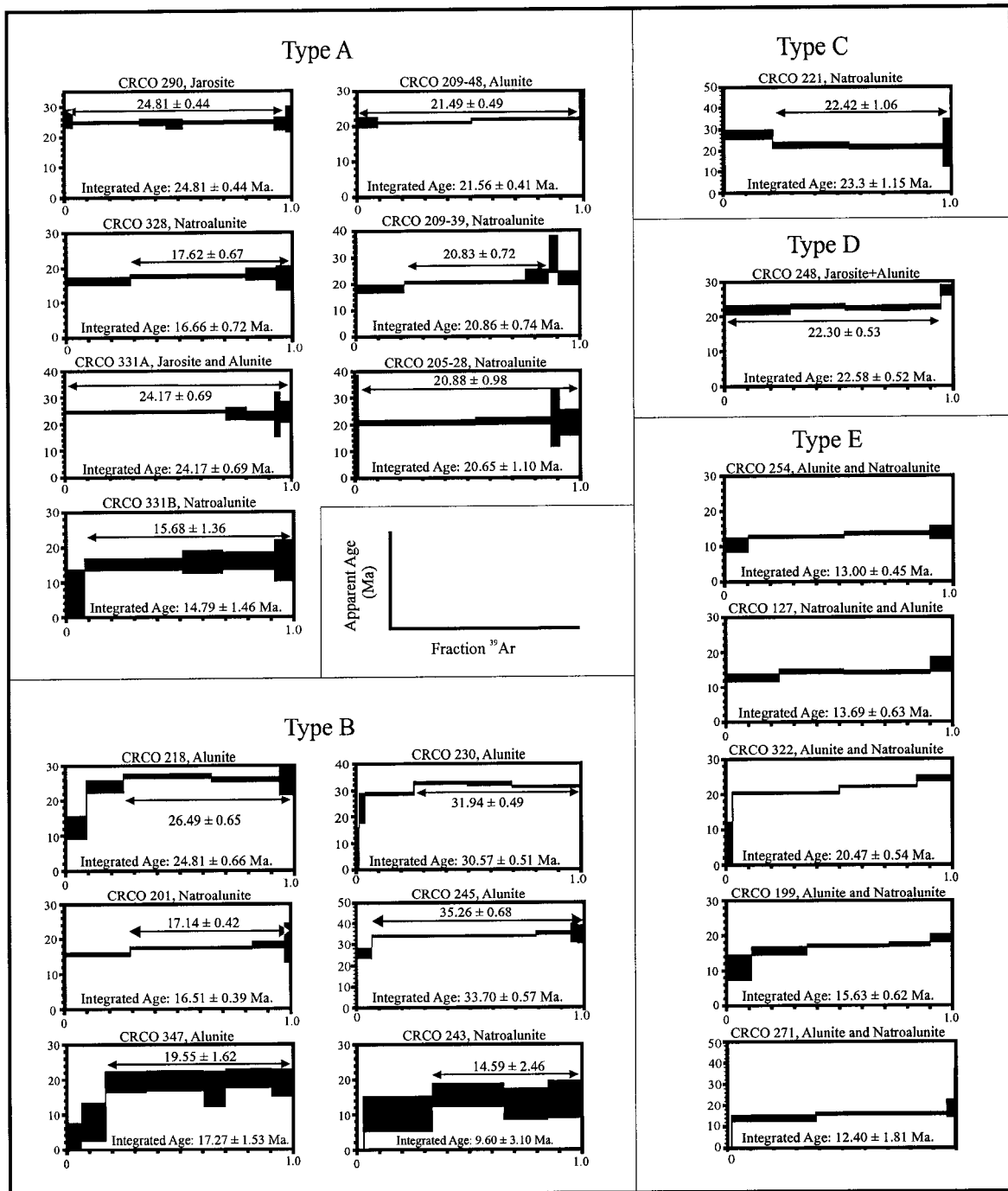


Fig. 3-23:

$^{40}\text{Ar}/^{39}\text{Ar}$ incremental-heating age spectra of supergene alunite-group minerals from Cerro Colorado, divided (see text) into Type A - samples with acceptable plateaus, Type B - samples with acceptable plateaus but also exhibiting evidence of radiogenic ^{40}Ar -loss, Type C - sample with ^{39}Ar loss through recoil, Type D - sample characterized by mixture of older (jarosite) and younger minerals (alunite), and Type E - mixed alunite-natroalunite samples which do not attain plateaus.

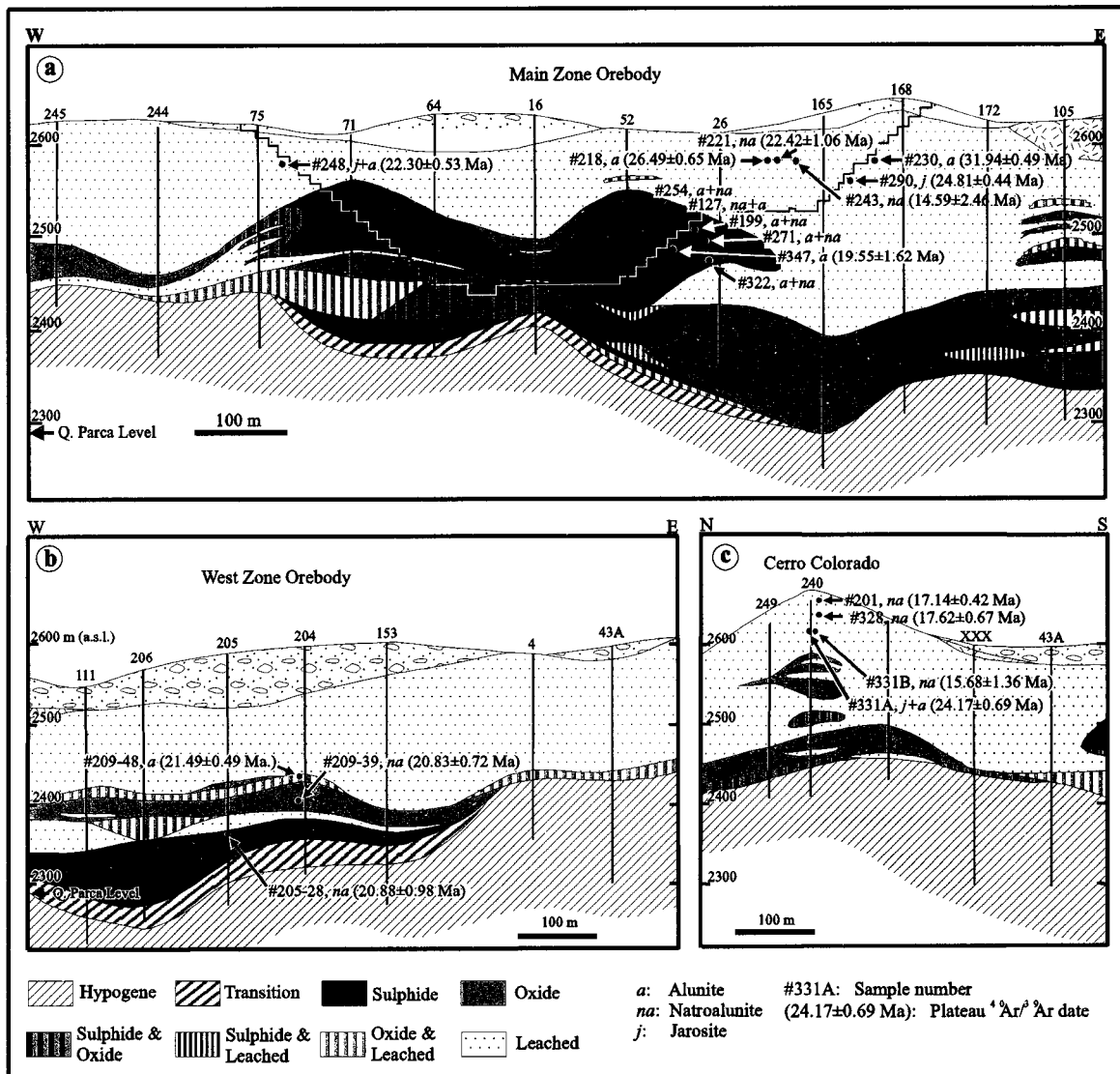


Fig. 3-24: Locations of the dated alunite-group samples on enlarged cross sections of the Main Zone (E-W) (a), West Zone (N-S) (b), and Cerro Colorado hill (N-S) (c). See Figs. 3-10, 3-11 and 3-13, respectively, for full cross sections. Sample 245, taken from red gravel below ignimbrite on the Main Zone (Fig. 3-4), is not shown because original elevation is not known.

for the Cerro Colorado alunite-group minerals are herein assigned to five types (Fig. 3-23) on the basis of their configuration and the mineral species.

Type A: In these samples, the spectra incorporate acceptable plateaus and Ar recoil is absent or negligible. Radiogenic ^{40}Ar was released during mineral breakdown at high experimental temperature and the samples did not host any contamination. The high errors in several of the initial heating stages are attributed to atmospheric ^{40}Ar adsorbed onto the grain surfaces. The amount of the released radiogenic gas increases at higher temperatures and the apparent age can be determined from this part of the spectrum. At very high temperatures (i.e., the last steps), much of the radiogenic Ar has already been released and the mineral undergoes phase transformation. This, combined with the gas released from inclusions in associated quartz, increases the uncertainties in the apparent age determinations in the final steps.

Type B: These spectra are similar to the above except that they reveal evidence of radiogenic ^{40}Ar -loss from less retentive, poorly-crystalline sites (Vasconcelos, 1999). The spectra include an interval, before reaching the plateau, in which the apparent age represents a mixture of atmospheric and radiogenic gases from sites that have undergone some radiogenic ^{40}Ar -loss. At higher temperatures, well-crystallized sites break down, releasing radiogenic ^{40}Ar , and the plateau age represented by these subsequent stages is the best estimate of the true age for the mineral.

Type C: In this type, represented only by CRCO 221, anomalously old ages in the early heating stages plausibly reflect ^{39}Ar loss through recoil to the atmosphere or excess ^{40}Ar . Progressively higher temperatures release radiogenic ^{40}Ar and ^{39}Ar from retentive sites and an acceptable age plateau is attained. Samples CRCO 245, 230 and 218, although classified as Type

B, show younger ages at lower temperatures, slightly older ages at intermediate temperatures, and finally slightly younger ages at the highest temperatures.

Type D: This category is represented only by CRCO 248, which, although exhibiting a plateau (22.30 ± 0.53 Ma, 94% of Ar released), records a distinctly older apparent age (27.39 ± 1.56 Ma) at high temperature. This configuration is inferred to represent a mixture of older and younger minerals, in this case jarosite and alunite, respectively. Electron-backscatter images of the specimen show that alunite cements fragmented jarosite (Fig. 3-21b). If the jarosite released radiogenic ^{40}Ar throughout the heating process, the plateau obtained would represent an average age for the old jarosite and the young alunite. However, in this sample, jarosite probably released more radiogenic ^{40}Ar at higher temperature, resulting in the older apparent age of the last step. By mineralogical analogy, CRCO 331A, identical to CRCO 248 but yielding a plateau spectrum, should be classified in this group. The only difference is that an old high temperature step is not present, probably because of a lower jarosite:alunite ratio, and hence the average plateau age (24.17 Ma) is closer to that of the younger phase.

Type E: This type comprises samples that have lost Ar and/or K throughout their history. The spectra are best described as “staircases”, in which all steps represent mixtures of gases derived from the sites that have lost Ar and/or K. These samples are mixtures of alunite and natroalunite and may have experienced Na-K exchange after precipitation. The spectra of these samples do not attain plateaus, and hence provide no information about the age of the sample, and are therefore excluded in this study (5 out of 20 samples). Conventional K-Ar dates for these samples would be misleading.

Age relationships

The acceptable age plateaus for supergene alunite, natroalunite and jarosite from Cerro Colorado range overall from 35.26 ± 0.68 to 14.59 ± 2.59 Ma, extending from the earliest-Oligocene to the mid – Miocene. The oldest, >30 Ma, ages corroborate the K-Ar dates presented by Sillitoe and McKee (1996), although the $^{40}\text{Ar}/^{39}\text{Ar}$ ages for alunites from their sample site (summit of Cerro Colorado) are considerably younger than the K-Ar dates. The new age spectra demonstrate that leaching and supergene sulphide enrichment were underway within 15 m.y. after hypogene mineralization. However, only 3 out of 15 plateau ages are older than 24 Ma, supporting the implications of the geological profile that a large portion of the earliest supergene horizon has been eroded. It is inferred that alunite and natroalunite formed throughout the supergene history, but plateau ages indicate that early veins are dominated by alunite and the later veins by natroalunite. There is no simple relationship between plateau age and elevation, but this reflects the complexity of the supergene environment and none of the dates conflicts with plausible genetic models for the evolution of the profile.

3.8. Evolution of the Supergene Profile

The anatomy and chronology of the supergene profile are evidence for a protracted and multi-stage supergene evolution at Cerro Colorado. The preserved supergene facies reflect much of the mid-Cenozoic tectonic history of the Pacific piedmont at this latitude prior to the profound climatic desiccation in the late-Middle Miocene. In this section, we summarize the development of the supergene profile, before addressing the relevance of this approach to other Chilean and Peruvian porphyry deposits.

The oldest alunite date obtained (CRCO 245: 35.26 ± 0.68 Ma) is from Leached Cap detritus deposited in a small valley below the ignimbrite overlying the Main Zone. The source of the clast is not known, but it was almost certainly derived from a leached horizon situated at a

higher elevation than is now preserved. The dated assemblage is, moreover, dominated by hematite, presumably after chalcocite-rich ore, indicating that a considerable thickness of the original cap has been eroded. In addition, the jarositic assemblages exposed prior to mining on the summit of Cerro Colorado may not represent the earliest enrichment processes, because this area of the deposit was dominated by porphyry bodies with very low copper grades and high pyrite contents, such as are unlikely to generate a hematitic cap. Sillitoe and McKee (1996) obtained a conventional K-Ar age of 34.3 ± 1.1 Ma for alunite from this zone, i.e., slightly younger than our date from the gravel. It is therefore evident that supergene processes had begun by the latest-Eocene, and plausibly at the onset of the Incaic orogeny. On this basis, the following stages for the development of the supergene blanket are proposed:

Precursor events: Middle to late Eocene ($< 51.8 \pm 0.5$ Ma to ca. 42 Ma). In this interval, the hypogene mineralization was partly unroofed. There is no indication of the previous existence of a major volcanic edifice over the deposit, and exposure of Cu-poor advanced argillic and phyllic assemblages of, respectively, the shallower-Main and Transitional hypogene stages may have begun shortly after original hydrothermal activity. There is, however, no record of significant enrichment during this stage, perhaps because of the equable, temperate global climatic conditions implied by the Eocene paleobotanical record and oxygen isotopic data for pelagic fauna (Raymo and Ruddiman, 1992; Gregory-Wodzicki, 2000). The Incaic orogeny is considered herein to mark the end of this stage and the initiation of major uplift, erosion and enrichment. There is no direct evidence of the age of the earliest Incaic deformation at this immediate latitude, but, as noted above, the thick clastic successions of the Salar de Atacama Basin (Mpodozis et al., 1999) and, on a more regional scale, the Potoco Formation (Horton et al., 2001) require major uplift in northernmost Chile in the late Eocene. Moreover, Huete et al. (1977) and Maksaeu (1979) record magmatic activity and development of a regional unconformity in the

interval 34 to 42 Ma between latitudes 21° and 22° S, while Hammerschmidt et al. (1992), in a study of the area adjacent to the Domeyko Fault at 22° S, record biotite $^{40}\text{Ar}/^{39}\text{Ar}$ ages of 38.50 ± 0.9 and 38.45 ± 0.60 Ma for two ash-fall tuffs separated by a distinct angular unconformity, thereby providing a precise datum for, presumably, a late event in the orogeny.

Stage I: Late Eocene to earliest-Oligocene (ca. 42 Ma to $> 35.26 \pm 0.68$ Ma). The first major cycle of supergene activity, involving oxidation of the hypogene ore, presumably with the development of a jarositic leached cap and a chalcocite blanket occurred during this stage. The jarositic cap is entirely eroded and the former existence of a sulphide enrichment zone is recorded only by the preserved Leached Cap. The morphology of the supergene profile (Fig. 3-10) indicates that the early chalcocite blanket formed at (present-day) elevations of at least 2650 m a.s.l., and that the supergene sulphide ore in the Main Zone developed beneath a paleo-hill, where the water table lay at a higher elevation. There is no evidence of the regional geomorphologic environment in which this early supergene activity took place.

Stage II: Early Oligocene to Early Miocene ($> 35.26 \pm 0.68$ Ma to $< 22.42 \pm 1.06$ Ma). Continued uplift and erosion now caused further leaching and thickening of the early chalcocite blanket, while the original cap and probably some of the newly-formed hematitic Leached Cap, including much of the paleo-hill, were eroded. As a result, the extant Upper Supergene Ore, dominated by chalcocite, formed in both the Main and West Zones, with upgrading of the supergene blanket. This protracted stage is recorded by alunite and natroalunite dates of 31.94 ± 0.49 , 26.49 ± 0.65 , 24.81 ± 0.44 and 22.42 ± 1.06 Ma (Figs. 3-24a and c). All of these samples represent hematitic Leached Cap, and thus chalcocite-pyrite protore, and hence the dates directly define the age of leaching of the early chalcocite blanket. It is not, however, clear whether this long interval involved essentially continuous deepening of the profile or a succession of discrete

uplift events. It is generally accepted (e.g., Sandeman et al., 1995) that the mid-Oligocene was a period of tectonic quiescence in the central Andes, separating the Incaic and Pehuenche (Aymará) orogenic pulses. However, the remnants of a thin leached zone within the Upper Sulphide Ore (Fig. 3-11) may be evidence of episodes of uplift at this time in northern Chile.

Figure 3-24a shows that samples CRCO 218, 221 and 230, from the same present-day elevation, have different $^{40}\text{Ar}/^{39}\text{Ar}$ ages. This may be, however, in part due to the irregular morphology of the earlier supergene blanket. A similar situation is seen today where there is a more than 100 m variation in the elevation of the Lower Sulphide Ore (cf. Figs. 3-10 and 3-12). Such irregularity may be attributed to variations in the depth of the water table and in permeability (e.g., Lichtner and Biino, 1992) or may have been caused by a temporary rise of the water table, causing alunite to form at the same or higher elevations than the older sulphate veins. Although this process could slow or even halt enrichment, a recent rise of the water table has inhibited oxidation of supergene sulphide blankets in other Chilean deposits, as in the wider Radomiro Tomic-Chuquicamata-MM district (M. Zentilli, pers. commun., 2000).

Stage III: Early Miocene ($>21.49 \pm 0.49$ Ma to 19.25 ± 0.43 Ma). It is proposed that rapid uplift at this time caused a drastic fall in the water table, and a renewal of intense leaching to form the Lower Leached Zone. The chalcocite blanket was thickened below the Lower Leached Zone and oxidized above it, forming the main brochantite-atacamite ore in the Main and West Zones, within both NW- and NE-trending fractures. No samples from the Lower Leached Zone *proper* have been dated, but natroalunite samples from immediately above and below it in the West Zone (Fig. 3-24b: CRCO 205-28 and 209-30) yielded sensibly identical ages of 20.83 ± 0.72 and 20.88 ± 0.98 Ma, respectively. An alunite from sulphide ore above the Lower Leached Zone in the Main Zone (Fig. 3-24a: CRCO 347) yielded an age of 19.55 ± 1.62 Ma, falling, within error, in the range of dates from the West Zone. Sample CRCO 209-48, representing partly

leached and oxidized Upper Oxide Ore in the West Zone (Fig. 3-24b), yielded an age of 21.49 ± 0.49 Ma, indicating that oxidation of the supergene sulphide ore above the Lower Leached Zone was penecontemporaneous with leaching. The extent of in situ oxidation above the Lower Leached Zone varied markedly throughout the Main and West Zones because of hypogene mineralogical differences. Thus, the Upper Sulphide Ore in the West Zone, dominated by hypogene sericite-chlorite-clay alteration with little remanent sulphide, was oxidized in situ above the Lower Leached Zone to form the Upper Oxide Ore, whereas in the pyrite-rich (i.e., phyllically altered) areas of the Main Zone portions of the Upper Sulphide Ore were preserved.

It is possible that continuous uplift and oxidation of a chalcocite blanket resulted in the oxidation of its upper part and a displacement of its floor to lower elevations. These changes could reflect involvement of areas with only minor remanent sulphide, especially pyrite, in the upper levels of the supergene blanket, compared to the hypogene-dominated protore at lower levels. However, the Lower Leached Zone at Cerro Colorado is well developed below the Upper Sulphide Ore in the Main Zone (Figs. 3-14 and 3-17), where abundant late pyrite veins have survived. This strongly implies a sudden drop of the water table to elevations below the Lower Leached Zone, with renewal of intense leaching above it, rather than a gradual uplift.

It is proposed that the earliest-Miocene Pehuenchean event was responsible for rapid uplift at ca. 20-22 Ma, developing the Choja Pediplain and the Lower Sulphide Ore, or at least a major part of it, in a relatively brief period (i.e., 1-2 m.y.), before the blanketing of the deposit by the ignimbrite flow. However, shortly after its development, the Choja Pediplain was disrupted into a horst and graben topography during Early Miocene extension (Hartley et al., 2000); west and southwest of Cerro Colorado (Fig. 3-2) remnants of the erosion surface are preserved as the flat summits of the Sierra de Tarapacá and Sierra Juan de Morales blocks (Galli, 1967 and 1968). It is also tentatively proposed that the uplift, as well as the abundance of both hypogene and supergene clay minerals in the higher elevations of the Main Zone, prompted the development of

a shallow valley, a precursor of the present embayment, resulting in deeper oxidation of the northern sector of the orebody (e.g., Figs. 3-14 and 3-15). The occurrence of weak sericite-chlorite-clay alteration and abundant hydrothermal biotite also may have intensified this deep oxidation.

Despite continuous leaching and downward thickening of the supergene blanket, the overall grade of the Upper Sulphide Ore, ca. 1 - 1.5 percent Cu, did not increase significantly. We infer that this was because there was little residual sulphide in the Upper Supergene Ore at this stage, so that renewed uplift caused only in situ oxidation of the ore. However, the Lower Leached Zone developed in horizons dominated by pyrite-rich hypogene assemblages, i.e., the transition zone between supergene sulphide and hypogene ore, thereby generating the ca. 1 percent Cu Lower Sulphide Ore (Figs. 3-12a and b). In areas where pyrite was abundant, within and adjacent to breccia pipes, strong leaching of the Upper Sulphide Ore resulted in local upgrading of its lower parts to over 2 percent Cu (Figs. 3-10 and 3-11: Main Zone).

Stage IV: Early to Middle Miocene (19.25 ± 0.43 Ma to $< 14.59 \pm 2.46$ Ma). At 19.25 ± 0.43 Ma, an ignimbrite flow, up to 95 m thick and partly welded, covered much of the deposit and surrounding area, temporarily interrupting supergene processes. Gravels underlying the ignimbrite host exotic mineralization 1.5 km NNE of the mine (Figs. 3-25a and b). The ignimbrite is extensively argillized in its lower 5 to 20 m, where it hosts thin chrysocolla veins. Thick and abundant chrysocolla veins formed along NW-trending fractures in the underlying deposit, especially in the north sector of the Main Zone (Figs. 3-15, 3-19, 3-26a), below the postulated evolving paleo-valley. A group of natroalunite veins, which cut older jarosite/alunite veins in the Leached Cap (Fig. 3-24a and c), formed during this stage, and yield ages of 17.62 ± 0.67 , 17.14 ± 0.42 , 15.68 ± 1.36 and 14.59 ± 2.46 Ma.

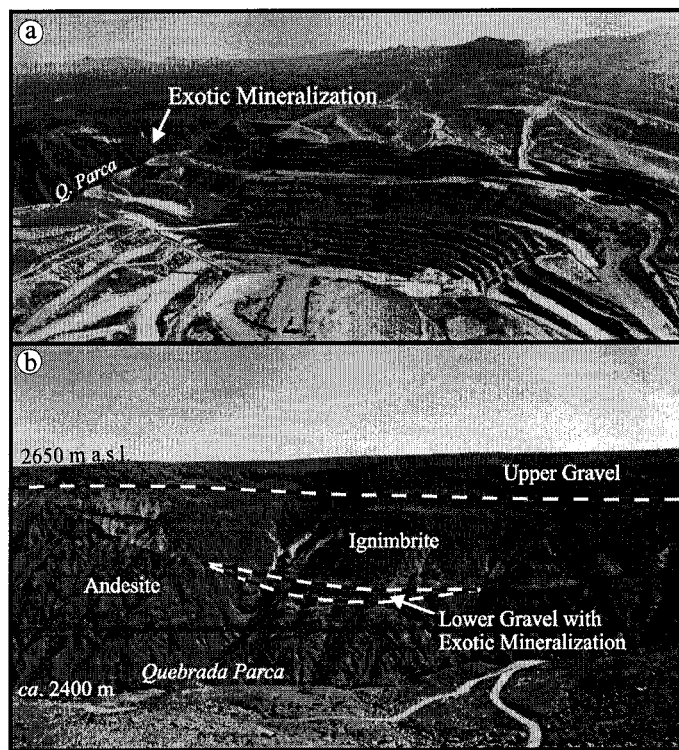


Fig. 3-25:

(a) Location of exotic mineralization NNE of the mine. Oblique aerial view (1995) looking northeast. (b) A closer view of the exotic mineralization on the north wall of Quebrada Parca. The Lower Gravel (containing red, hematitic clasts) and overlying ignimbrite filled a shallow N-trending valley. Looking north (1996).

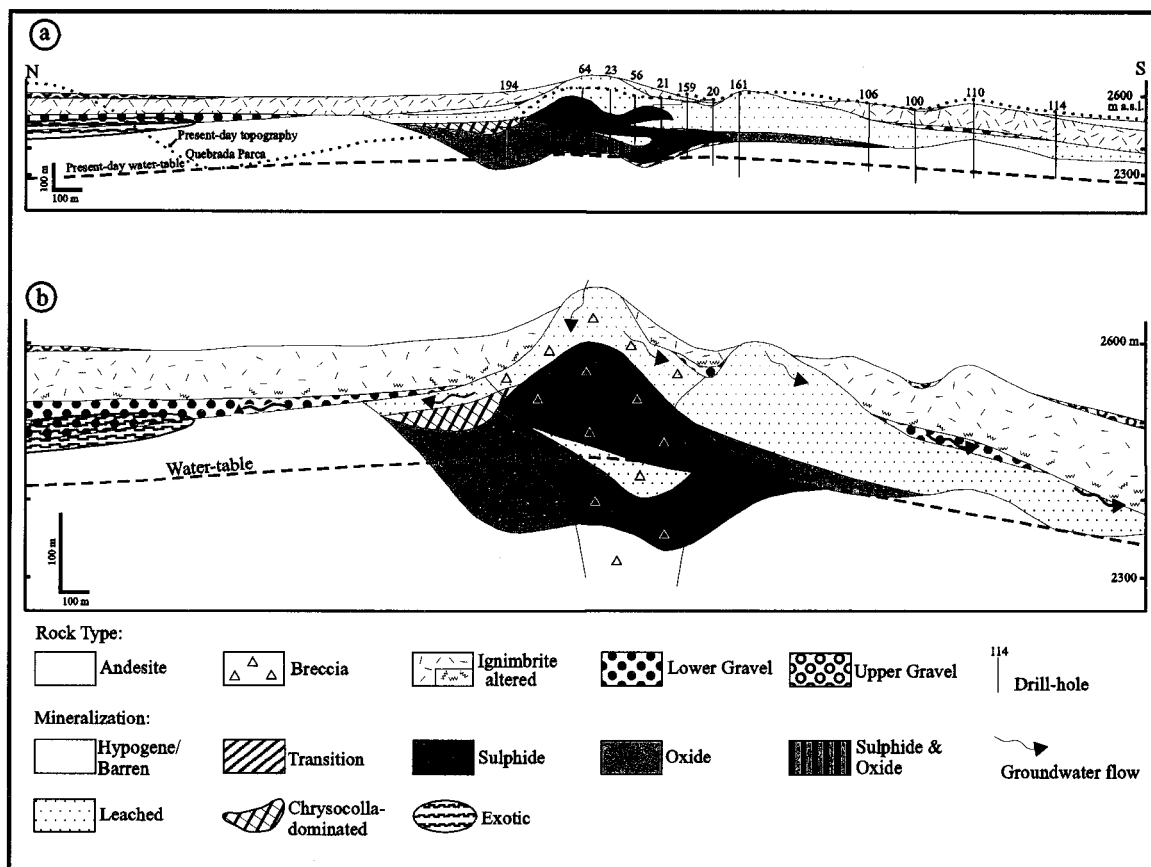


Fig. 3-26:

Context of chrysocolla mineralization. (a) N-S cross section (true-scale) through the Main Zone orebody at Cerro Colorado (see Fig. 3-14) and surrounding area, showing inferred relationships at ca. 19 Ma. Pre-ignimbrite topography dips to the north and south, and the Lower, locally red, Gravel, derived from the inferred paleo-hill extends to the north and south. The supergene blanket is oxidized to brochantite-atacamite in the north, but chrysocolla veins are dominant along NW-trending fractures in its upper part. Exotic mineralization occurs in the Lower Gravel and pre-Neogene bedrock north of Quebrada Parca. (b) Model for development of exotic mineralization and genetically linked chrysocolla veins generated by lateral groundwater flow through permeable zones of Lower Gravel and along the contact of ignimbrite and bedrock, after partial capping of the deposit by 19.25 Ma ignimbrite (see text). Model is drawn on the basis of above N-S cross section, but with vertical exaggeration of 3:1.

Under the prevailing topographic conditions, partial capping of the deposit by the ash-flow would be likely to have resulted in lateral groundwater flow along the permeable zone between ignimbrite and bedrock (Fig. 3-26b). Accumulation of both ignimbrite and gravel over the deposit under persisting semi-arid climatic conditions presumably resulted in the rise of the water table to ca. 2400 m a.s.l. Despite the locally great thickness of the ignimbrite, especially to the south and east of the deposit (see also Fig. 3-10), small hills over the Main Zone are inferred to have remained uncovered and to have served as “windows” for meteoric water penetration. Groundwater flow was focused through the lower 20 m of the ignimbrite, the Lower Gravel and the upper part of the underlying supergene profile, and was aided by dilating NW-trending fractures (see above). In areas where chalcocite was accompanied by abundant pyrite and the enriched blanket was closer to the pre-ignimbrite surface (e.g., Upper Sulphide Ore in the Main Zone located below the paleo-hill), oxidation was reactivated without downward thickening of the chalcocite blanket. Groundwater dissolved copper and, a short distance to the north, precipitated abundant chrysocolla within the fractures. It is proposed that these relationships record at least an incipient stage in the formation of exotic mineralization such as is preserved beneath the ignimbrite on the north slope of the Parca canyon at an elevation of ca. 2500 m a.s.l. (Figs. 3-3, 3-25 and 3-26a), where chrysocolla fills fractures in Cerro Empexa andesites and impregnates the matrix of a thin overlying gravel unit above it. It is not known whether a large volume of similar exotic mineralization has been eroded by the canyon, but the source of exotic mineralization is inferred to have been Cerro Colorado because the same gravel unit would extrapolate uphill across Quebrada Parca to the Main Zone, and because the porphyry stock at Cerro Quipisca, 2.5 km northwest of Cerro Colorado (Figs. 3-3 and 3-7), hosts only minor copper veins (Galli, 1968).

Stage V: Middle Miocene to present (< 14.59 Ma). By the late-Middle Miocene, a regional climatic desiccation (Alpers and Brimhall, 1988) terminated significant supergene processes and preserved the existing supergene orebody from continued lateral metal dispersal. The steep-walled Quebrada Parca canyon incised the Pampa del Tamarugál surface and deepened the transverse paleo-valley to expose the Main orebody. Development of the canyon lowered the water-level to elevations below the Lower Sulphide Ore, especially in the northern parts of the blanket, resulting in weak in situ oxidation of the ore.

In summary, the Cerro Colorado deposit displays evidence of a polystage supergene history (Bouzari and Clark, 2000) extending over at least 20 m.y., and resulting in a complex profile (Table 3-4). The supergene processes were significantly influenced by regional tectonic events. These included the late Eocene Incaic and the Early Miocene Pehuenchean uplifts. We infer that, of these, the immediately post-Incaic enrichment probably contributed more to the overall Cu upgrading. However, the extensive oxidation of the supergene ore which occurred as a result of the later event contributed significantly to the economic value of the deposit through conversion of clay-rich, sulphide assemblages (e.g., chalcocite) to relatively clay-free, and hence less refractory, oxidized ore (e.g., brochantite). Considerable copper may, however, have been lost from the Main Zone during the development of the paleo-valley. Indeed, partial blanketing of the deposit by the thick ignimbrite flow soon after the Pehuenchean uplift is considered to have interrupted fluvial erosion of the main part of the enriched blanket, as well as providing a suitable environment for the formation of exotic mineralization through imposing lateral groundwater flow.

Table 3-4. Summary of post-hypogene events at Cerro Colorado and in northern Chile and southern Peru

| Period | Events at Cerro Colorado | Regional Events |
|--------------------------------------|--|---|
| Early - to - late Eocene | <i>Precursor events (< 51.8 to ca. 42 Ma)</i> : Hypogene mineralization was partly unroofed. Supergene processes <i>may</i> have affected shallow Cu-poor advanced argillic and phyllic zones. | The convergence direction of the Farallón and American Plates changed from north or NNE to NE (Refs. 1, 2) ¹ . The magmatic arc shifted eastward between 55 and 48 Ma. (Refs. 3, 4). The Incaic orogeny (initiated at ca. 42 Ma) caused significant uplift and both initial soft-linked en echelon-dextral and sinistral-transpressive movement along Domeyko Fault System (Ref. 5). Porphyry Cu mineralization (e.g., Ataspaca and El Salvador) locally emplaced along this structure (Refs. 5, 6). |
| Late Eocene - to - early Oligocene | <i>Stage I (ca. 42 to > 35.26 Ma)</i> : The first major cycle of supergene activity resulted in development of a presumably jarositic cap and a chalcocite enrichment blanket. | Emplacement of porphyry Cu systems along the Domeyko Fault System continued throughout the early Oligocene (Refs. 5, 7). Uplifted Incaic terrain in northern Chile (Ref. 3, 8) provided source of the Potoco Formation clastics in Bolivia (Ref. 9) and plausibly acted as a rain-shadow on the Pacific slopes of the proto-Andes. This, along with a global cooling event at the beginning of Oligocene (Ref. 10), provided favorable climatic and landform conditions for supergene enrichment. |
| Early Oligocene - to - Early Miocene | <i>Stage II (> 35.26 to < 22.42 Ma)</i> : The chalcocite blanket was leached and deepened due to continued erosion. A hematitic leached cap formed over the chalcocite blanket and major parts of the early jarositic cap were eroded. | Much of the central Andes experienced tectonic quiescence (Refs. 11, 12), but displacement and porphyry emplacement continued along Domeyko Fault (Ref. 5). Alluvial sediments were deposited through the Oligocene in northern Chile (Refs. 13, 14) and southern Peru (Ref. 11). |
| Early Miocene | <i>Stage III (> 21.49 to 19.25 Ma)</i> : The Lower Leached Zone developed below the chalcocite blanket due to a drastic fall in the water-table. The chalcocite blanket was thickened below the Lower Leached Zone and oxidized above it. | The Pehuenchea (Aymará) tectonic event caused regional uplift and development of the Altos de Camilaca (southern Peru) (Refs. 15, 16), Choja (northernmost Chile) (Ref. 17), and Checo del Cobre (Copiapó area) (Refs. 18) pediplains. Major enrichment occurred in the upper Eocene - lower Oligocene Cu deposits (Ref. 19). Ignimbrite eruption began by 25 Ma in southern Peru and northernmost Chile (Ref. 16). Extension due to subduction-related tectonic erosion in the fore-arc zones (Ref. 20) during the Early Miocene resulted in development of asymmetric basins (e.g., Azapá Basin, Ref. 21) with horst and graben topography (e.g., Sierra Juan de Morales, Ref. 17). |
| Early - to - Middle Miocene | <i>Stage IV (19.25 to < 14.59 Ma)</i> : Supergene activity was temporarily interrupted by a thick ignimbrite flow, partially covering the deposit. Lateral groundwater flow reactivated oxidation, generating chrysocolla veins in the upper levels of the deposit, along dilating NW-trending fractures, and exotic mineralization below the ignimbrite flow as far as 1.5 km NNE of the mine. | E-W shortening caused W-verging thrusting along NW-trending structures in the Moquella-Confluencia (Refs. 21, 22, 23) and Mamiña (Ref. 17) areas, contributing to the uplift of the Altiplano (Refs. 21, 22, 23). The Domeyko Fault System experienced sinistral movement prior to the Middle Miocene (Refs. 5, 24). |
| Middle Miocene - to Present | <i>Stage V (< 14.59 Ma)</i> : All significant supergene processes terminated because of climatic desiccation. | Further E-W shortening resulted in the rise of the Altiplano (Ref. 25) and hyperaridity (Ref. 19, 26). |

References: (1): Pilger (1984); (2): Pardo-Casas and Molnar (1987); (3): Hammerschmidt et al., (1992); (4): Scheuber et al., (1994); (5): Tomlinson and Blanco (1997); (6): Clark et al., (1990b); (7) Richards et al., (2001); (8): Maksaeu (1979); (9): Horton et al., (2001); (10): Raymo and Ruddiman (1992); (11): Sandeman et al.(1995), (12): Jaillard et al., (2000); (13): Flint et al., (1993); (14): Coira et al., (1982); (15): Tosdal et al., (1984); (16): C. Quang, A.H. Clark, and J.K.W. Lee, unpublished report for Rio Tinto Mining and Exploration Ltd, Lima (2001); (17): Galli (1967); (18): Mortimer (1973); (19): Sillitoe and McKee (1996); (20): Hartley et al., (2000); (21): Muñoz and Charrier (1996); (22): Charrier et al., (1999); (23): Garcia et al., (1999); (24): Carrasco et al., (1999); (25): Allmendinger et al., (1997); (26): Alpers and Brimhall (1988).

3.9. Regional Correlations and Comparisons

The wide range of supergene profiles exhibited by the pre-Miocene central Andean porphyry deposits, summarized in Figure 3-27 and Table 3-5, undoubtedly records variations in hypogene ore mineralogy and alteration and post-hypogene geomorphologic conditions but, more importantly, also reflects the overall duration of their supergene activity. It is therefore germane to compare the documented supergene profiles of porphyry Cu deposits of different ages in the region. In Table 3-5, estimates are included of the enrichment rate, calculated on the basis of the total amount of transported copper (kg) generated per year in a 10,000 m² plan-area of deposit. The total amount of the transported copper is estimated for a block of enriched blanket, assuming an average thickness for combined supergene sulphide and oxide zones (Fig. 3-27), with fixed plan dimensions of 100 m by 100 m for all deposits. The difference between the supergene and hypogene grades were accepted as the net supergene upgrade. The longest period of enrichment established for a Paleocene to middle Eocene deposit (i.e., 24 m.y. at Spence, see below) is applied to all deposits in this belt. Similarly, the 7 m.y. history of enrichment at El Salvador (see below) was accepted as the duration of enrichment for all upper Eocene to lower Oligocene deposits, i.e., the ca. 36 Ma alunite and jarosite dates at El Salvador were excluded in this calculation. The calculated enrichment rate does not take into account the amount of copper lost to exotic mineralization, which is discussed separately.

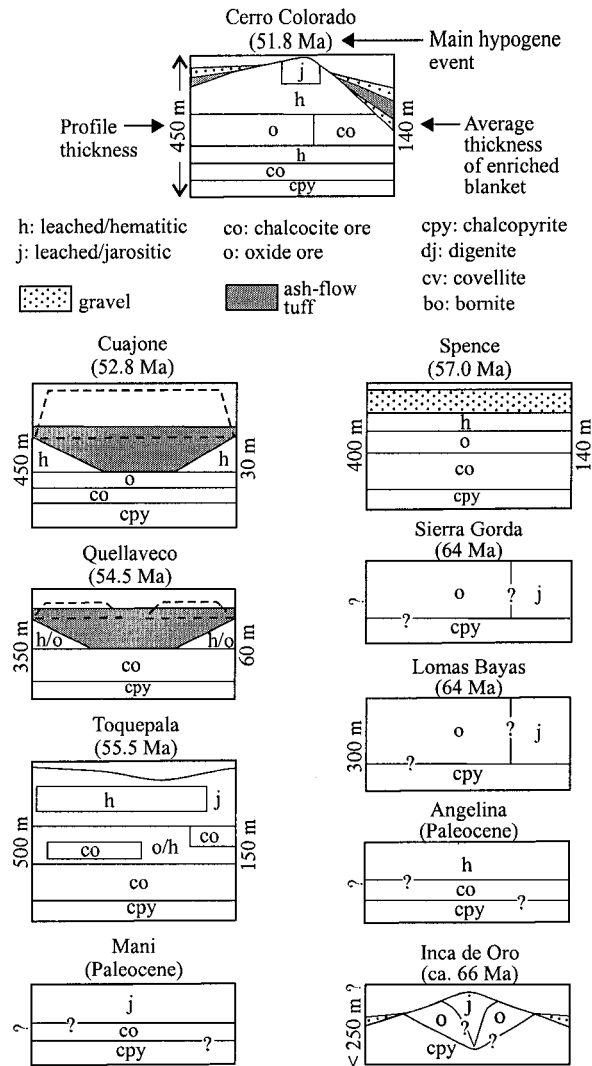
Paleocene to middle Eocene deposits

The main geochronologic database for the supergene profiles of other Paleocene to middle Eocene Cu deposits of northern Chile (Sillitoe and McKee, 1996) comprises single K-Ar dates for surface alunite samples (Figs. 3-1 and 3-27 and Table 3-5). Except at Angelina (31.0 Ma), enrichment in these deposits apparently significantly postdated the early

Fig. 3-27:

Simplified schematic cross sections showing the anatomies of the supergene profiles of selected central Andean Paleogene porphyry Cu deposits. Paleocene to middle Eocene deposits exhibit complex profiles with abundant oxidized supergene ore reflecting their polystage histories of leaching, oxidation and enrichment. Thick ignimbrite blanketing during the early stages of enrichment (dashed lines) and after the main stage of enrichment (gray-fill ornament) had a major effect on the intensity and preservation of the supergene blanket (see text and Table 3-5). In contrast, Upper Eocene to lower Oligocene deposits exhibit simpler profiles with thicker supergene sulphide blankets, except at Radomiro Tomic, which is deeply oxidized. All cross sections are drawn with the same vertical scale. Hypogene mineralization is represented by chalcopyrite, except at Chuqicamata where distinction between supergene and hypogene ore is uncertain. This Figure should be viewed in conjunction with Table 3-5. For references see Table 3-5.

a: Paleocene - middle Eocene deposits



b: Upper Eocene - lower Oligocene deposits

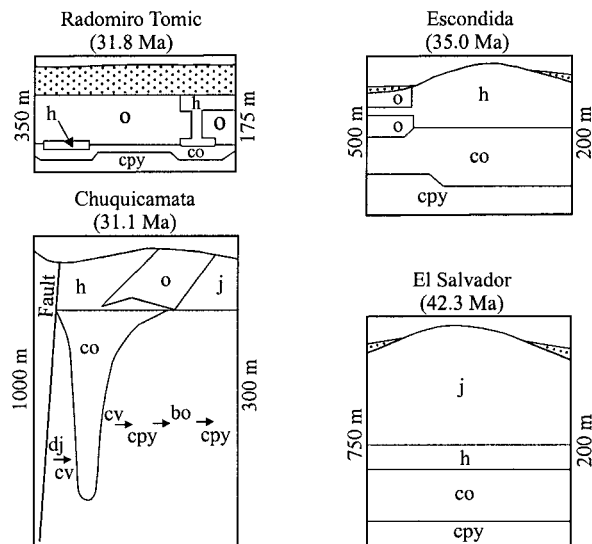


Table 3-5. Comparison of the evolution of supergene mineralization in central Andean Paleogene porphyry Cu deposits

| Deposit | Hypogene Tonnage (Mt) | Hypogene Cu Grade (%) | Supergene Tonnage (Mt) | Supergene Cu Grade (%) | Enrichment ¹ Rate (kg/y) | Supergene Geochronology (K-Ar dates, unless indicated otherwise) | Comments | References |
|----------------|-----------------------|-----------------------|------------------------|------------------------|-------------------------------------|--|--|--|
| Cuajone | 1550 | 0.65 | >75 | 1.0 | 0.11 | No radiometric dates for supergene blankets. Age of enrichment is constrained through correlation with the 24 Ma Altos de Camilaca Surface (the oldest preserved landform in this region) but enrichment possibly began as early as early Oligocene. Thus, an older (i.e., Incaic) landform may be represented by Toquepala Group/Moquegua Fm. Unconformity. | Polystage history of enrichment at Toquepala, with well-defined leached zones separating chalcocite horizons, is very similar to that at Cerro Colorado. In contrast, the Cuajone deposit exhibits a simpler and markedly thinner profile because of early blanketing by a thick ignimbrite flow (dashed lines in Fig. 27a). Eruption of the Middle Miocene ignimbrite (shown by gray fill in Fig. 27a) prevented further erosion of the deposit. At Quellaveco, ignimbrite blanketing through the Early and Middle Miocene was poly-cyclic but short-lived, and a more protracted supergene history resulted in a thicker enriched blanket. | Tosdal (1978) Tosdal et al., (1981) Anderson (1982) Clark et al., (1990a) Sandeman et al., (1995) Quang et al., unpubl., (2001) Southern Peru Copper Corp., unpubl., (2001) Minera Quellaveco S.A., unpubl., (2001) A.H. Clark, unpubl. data |
| Quellaveco | 900 ² | 0.5 | | >0.8 | 0.22 | | | |
| Toquepala | 300 | 0.83 | 558 | 1.03 | 0.31 | | | |
| Cerro Colorado | | 0.5 | 228 | 1.0 | 0.73 | 15 alunite group minerals yielded ⁴⁰ Ar/ ³⁹ Ar ages between 35.26 ± 0.68 and 14.59 ± 2.46 Ma. | Uplift during middle Eocene Incaic orogeny initiated enrichment, forming a chalcocite blanket. Leaching and enrichment continued until the Early Miocene Pehuenchean event which caused rapid uplift and generated the Lower Leached Zone, with attendant deepening of the chalcocite blanket. | This study |
| Mani | | | | | | Alunite from jarositic cap: 21.0 ± 2.6 Ma | | Sillitoe and McKee (1996) |
| Spence | 150 | 0.6 | 250 | 1.22 | 0.90 | 13 ⁴⁰ Ar/ ³⁹ Ar alunite/natroalunite dates from 44.44 ± 0.54 to 27.74 ± 5.42 Ma, a history extended to 20.9 ± 2.2 Ma by a K-Ar date. | Spence records both the oldest and most protracted supergene enrichment. High-sulfidation type mineralization occurred during the intermediate stages of enrichment. | Rowland, unpubl., (2001) Rowland and Clark (2001) A. Bertens, pers. commun., (2001) |
| Sierra Gorda | | | | | | Alunite from jarositic cap: 14.1 ± 1.2 Ma | | Sillitoe and McKee (1996) |
| Lomas Bayas | | | 90.9 | 0.37 | | Alunite from jarositic cap: 20.8 ± 1.6 Ma | Deeply oxidized ore includes antlerite and brochantite which replaced preexisting chalcocite mineralization. | Sillitoe and McKee (1996) www.falconbridge.com |
| Angelina | | | | | | Alunite from hematitic cap: 31.0 ± 2.0 Ma | | Sillitoe and McKee (1996) |
| Inca de Oro | | | | | | Alunite from jarositic cap: 14.2 ± 1.2 Ma | | Palacios et al., (1992) Sillitoe and McKee (1996) |
| Radomiro Tomic | 1300 | 0.53 | 1380 | 0.76 | 1.44 | No data, but proximity to Chuquicamata implies a similar chronology. | The in situ oxidation of the upper parts of an early chalcocite blanket formed the atacamite-rich oxide ore. This profile is comparable to the West Zone orebody at Cerro Colorado. | Cuadra and Rojas (2001) |
| Chuquicamata | 5400 | 0.48 | 3085 ³ | 1.32 | 9.00 | 7 Alunite samples from leached cap and top of enriched blanket: 19.0 ± 1.4 to 15.2 ± 1.0 Ma | Mineralization is strongly influenced by hypogene setting. The chalcocite orebody, with a vertical dimension at least 5-times its horizontal, does not resemble any known supergene profile. However, enrichment certainly upgraded upper 400-500 m of the deposit. | Taylor (1935) Jarrell (1944) Sillitoe and McKee (1996) Reynolds et al., (1998) Ballard et al., (2001) Ossandón et al., (2001) |
| Escondida | 1300 | 0.6 | 962 | 1.89 | 9.21 | Alunites from hematitic cap: (3130 m a.s.l.): 16.4 ± 1.4 Ma (3036 m a.s.l.): 17.7 ± 1.4 Ma (2936 m a.s.l.): 14.7 ± 1.2 Ma Alunite from enriched zone: (2851 m a.s.l.): 18.0 ± 1.4 Ma | Leaching of a preexisting supergene sulfide blanket formed exceptionally thick and high-grade chalcocite ore and a thick hematitic cap similar to the Stage II at Cerro Colorado. Oxide ore with a well developed middle leached zone formed in the biotitized andesite. | Alpers (1986) Alpers and Brimhall (1988) Richards et al., (1999) Padilla et al., (2001) A.H. Clark, unpubl. data |
| El Salvador | | 0.65 | >300 | 1.6 | 6.79 | Alunites: 36.0±5.0 & 36.1±1.2 Ma 5 Jarosites: 10-20 Ma ⁴⁰ Ar/ ³⁹ Ar dates: Jarosite from 3250 m a.s.l., coarse and fine fractions, respectively: 35.85 ± 3.18 and 43.9 ± 2.6 Ma 9 Alunites, 2690-2950 m a.s.l.: 12.89 ± 0.06 to 19.44 ± 0.6 Ma | Thick jarositic cap is preserved and only a small portion of the chalcocite blanket is leached to hematite. Uncertainty exists regarding the origin of ca. ≥ 36 Ma alunite and jarosite. | Gustafson and Hunt (1975) Gustafson et al., (2001) Mote et al., (2001) Watanabe and Hedenquist, (2001) |

¹ Enrichment Rate (kg/y): indicates the total amount of transported copper generated per year over a 10,000 m² plan-area of the deposit.² This tonnage is the sum of hypogene and supergene mineralization.³ This tonnage includes some hypogene ore.

enrichment stages at Cerro Colorado and the upper parts of these deposits may have been extensively eroded, but, as Sillitoe and McKee (1996) emphasize, the dates clearly demonstrate the importance of the Early Miocene supergene event throughout northern Chile. However, a considerably longer duration of supergene leaching and enrichment (from 44.4 Ma to after 20.9 Ma) is documented for the Spence porphyry copper deposit (Rowland and Clark, 2001; M.G. Rowland and A.H. Clark, unpublished report to Rio Algom Exploration Inc., Toronto, 2001). This deposit thus bears the closest similarities to the situation at Cerro Colorado and also provides evidence that significant enrichment may have also occurred there prior to ca. 42 Ma.

Comparative geochronologic data are lacking for the lower Eocene Toquepala, Quellaveco and Cuajone deposits of southern Peru (Figs. 3-1 and 3-27 and Table 3-5), where the age of supergene enrichment is constrained only through correlation with dated erosion surfaces (Tosdal, 1978; Clark et al., 1990a; C. Quang, A.H. Clark and J.K.W. Lee, unpublished report for Rio Tinto Mining and Exploration Ltd, Lima, 2001). The oldest preserved landform in this region is the 24 Ma Altos de Camilaca Surface, and at least some early enrichment in the three deposits clearly occurred below this regionally-developed pediplain. Uplift in this transect, however, had undoubtedly commenced prior to the latest-Oligocene, during the Incaic orogeny, yielding the thick succession of fine clastics making up the lower member of the Moquegua Formation which unconformably overlies the eroded Cretaceous to lower Eocene arc (Tosdal et al., 1981; Sandeman et al., 1995). Unroofing of the deposits may therefore have commenced by the early Oligocene, and the complex and polystage profile at Toquepala (Clark et al., 1990a) is in permissive agreement with a supergene history similar to that at Cerro Colorado.

Upper Eocene to lower Oligocene deposits

The giant deposits clustered at intervals along the Domeyko Fault System (Fig. 3-1) were emplaced 10 m.y. or more after Cerro Colorado, and might therefore be predicted to have

experienced shorter and less complex supergene histories. These deposits, however, range in age from at least 42.3 Ma (El Salvador: Gustafson et al., 2001) to 31.1 Ma (Chuquicamata II: Reynolds et al., 1998) at, respectively, the initiation and termination of Incaic (*sensu lato*) tectonic activity along the Domeyko Fault. The older deposits would be expected to bear the closest similarities to Cerro Colorado, and in this context, the geochronologic data available for supergene assemblages at El Salvador (e.g., Gustafson and Hunt, 1975; Gustafson et al., 2001; Mote et al., 2001a) are instructive. The thick supergene blanket which constitutes the main orebody in this deposit (Fig. 3-27 and Table 3-5) formed below a jarosite-dominated cap, with a thin intervening hematitic horizon (Gustafson and Hunt, 1975). Recent $^{40}\text{Ar}/^{39}\text{Ar}$ dating by Gustafson et al. (2001) of the coarse fraction of a jarosite sample from a high elevation in the system yielded an age of 35.85 ± 3.18 Ma, thereby supporting Gustafson and Hunt's (1975) K-Ar alunite dates for the initiation of supergene processes. However, Gustafson et al. (2001) also report an age of 43.9 ± 2.6 Ma for the fine fraction of the same jarosite sample. It is not clear if this older date records supergene or hypogene activity (see Watanabe and Hedenquist, 2001), but that the dating of mineral aggregates may be misleading is shown by the results for mixed alunite+natroalunite samples at Cerro Colorado (this study). Similarly, Gustafson et al. (2001) report anomalously young and disturbed hypogene alunite ages at El Salvador which were ascribed to the effects of supergene processes. Mote et al. (2001a) documented $^{40}\text{Ar}/^{39}\text{Ar}$ plateau dates for supergene alunite from the Quebrada Turquesa and Rioluta paleospring feeder systems, cutting the rhyolite cap of the deposit, which range from 19.44 ± 0.6 to 12.89 ± 0.06 Ma. These largely Middle Miocene dates are similar to the K-Ar ages for supergene jarosite recorded, but discounted, by Gustafson and Hunt (1975) because of their apparent incompatibility with local geomorphologic relationships. These ages would imply a supergene history with a duration approaching that which we document herein for the much older Cerro Colorado deposit but, if so, may indicate that enrichment was less intense between ca. 35 and ca. 19 Ma. The majority of the

alunite dates presented by Mote et al. (2001a), i.e., 19.44-12.89 Ma, broadly correspond to the inferred (Mortimer, 1973) period of relative tectonic stability separating the formations of the Checo del Cobre and Atacama pediplains, but overlapping with the earlier stages in the development of the latter erosional feature. Thus, Nishiizumi et al. (1998) record dates of 10.5-15.3 Ma for ignimbrites intercalated in the “Atacama Gravel”, extending the range (9.2-12.9 Ma) established by Clark et al. (1967b) for the upper half of the aggradation facies of the younger pediplain. It is therefore probable that strong leaching and enrichment at El Salvador were stimulated by both the incision of the presumably upper Oligocene or Lower Miocene Checo del Cobre pediplain and the initial episodes of subsequent Middle Miocene Atacama uplift and erosion. As is emphasized by Sillitoe et al. (1968) and Mortimer (1973), the semi-arid climatic conditions prevailing during development of the major Atacama pediplain would have been favorable for enrichment, but intense climatic desiccation shortly after ca. 9-9.5 Ma terminated both pedimentation and supergene activity at this latitude: thus, the youngest segments of the pediplain truncate supergene profiles.

Further north, the Escondida mine (Figs. 3-1 and 3-27 and Table 3-5) exploits an exceptionally rich supergene sulphide blanket, with a thickness of up to ca. 400 m and underlying a leached cap with a preserved thickness of 200 m (Padilla et al., 2001). Hypogene mineralization, hosted largely by the 37.9 ± 1.1 Ma Escondida porphyry cluster (Richards et al., 1999), was initiated at 34.99 ± 0.35 Ma ($^{40}\text{Ar}/^{39}\text{Ar}$ age plateau for hydrothermal biotite: A.H. Clark, unpublished report to Minera Escondida Ltda., 2001), and had largely terminated by 34.7 ± 1.7 Ma (Richards et al., op. cit.). The higher grades and thicker sections of the chalcocite blanket lie below a hematitic cap within the strongly quartz-sericite -altered stock (Figures 10 and 11 of Padilla et al., 2001). The thick leached cap at Escondida probably formed in several stages, with leached zones initially separated by chalcocite ore. Such zones would have been destroyed in the pyrite-rich stock because of extensive leaching, but mine records indicate that the western Cu

oxide orebody (320 Mt at 0.7 percent Cu: C. Alcayaga, pers. commun., 1998), hosted by pyrite-poor biotitized andesite, comprises an upper brochantite-antlerite zone separated from a lower brochantite-dominated zone by a well-defined leached horizon (Figure 3-27), evidence for episodic uplift, oxidation and leaching. K-Ar dating of alunites by Alpers (1986) and Alpers and Brimhall (1988) yielded ages no older than Early Miocene (Table 3-5). The younger alunites from the higher elevations of the leached cap are similar in age to those which formed at Cerro Colorado after the ignimbrite eruption event.

The slightly younger, 34.6-31.1 Ma (Reynolds et al., 1998; Ballard et al., 2001), Chuquicamata deposit (Figs. 3-1 and 3-27 and Table 3-5) displays a complex and zoned sulphide mineralization (Ossandón et al., 2001). Chalcocite extends to 900 m below the pre-mine surface in strongly fractured, quartz-sericite -altered rocks (Ossandón et al., 2001), but it is uncertain that it is exclusively supergene. However, a ca. 200 m-thick leached cap with an oxide zone overlies the sulphide ore (Taylor, 1935; Ossandón et al., 2001). Chalcocite was converted to oxide ore (Taylor, 1935; Jarrell, 1944; Ossandón et al., 2001) in the moderately pyritic protore (Ossandón et al., 2001) whereas, above the pyrite-rich zone farther west, the main chalcocite zone is converted to hematite. Detailed mapping by Taylor (1935) of the oxide facies of the orebody clearly delimited a leached zone below the oxide ore, merging westward with the hematitic cap (Fig. 3-27), a relationship comparable to that of the Lower Leached Zone and Leached Cap at Cerro Colorado (e.g., Fig. 3-9: hole 26). It is clear that both the mineralogy and grade distribution of the unusually rich supergene ore were strongly influenced by the hypogene characteristics of the deposit. From the supergene blanket anatomy, it may be inferred that its evolution was very similar to that at Escondida. Thus, Sillitoe and McKee (1996), on the basis of K-Ar dates for 7 alunite samples from the leached cap and the top of the sulphide blanket, documented an age range of 15.2 ± 1.0 to 19.0 ± 1.4 Ma for enrichment at Chuquicamata, an interval very similar to that outlined at Escondida (Alpers and Brimhall, 1988). The recently described supergene profile

at the nearby Radomiro Tomic deposit (Cuadra and Rojas, 2001) is similar to that at Chuquicamata, except that the simpler hypogene mineralogical relationships resulted in an anatomy comparable to that of the West Zone orebody at Cerro Colorado (Figs. 3-27 and 3-12a).

The above comparison confirms that both the duration of supergene processes and erosion rates have a fundamental effect on the anatomy of supergene profiles. Thus, Paleocene to middle Eocene deposits experienced greater erosion and developed complex profiles with multi-horizon hematitic leached zones and considerable proportions of oxidized ore. Gravel and ash-flow covers are widespread. Upper Eocene to lower Oligocene deposits experienced briefer episodes of supergene enrichment and, where originally pyrite-rich, developed simpler profiles with a leached cap overlying supergene sulphide ore. Where two or more leached horizons are present in these deposits, as at Escondida and Radomiro Tomic, the younger horizons are thin. Nonetheless, these deposits exhibit a wide range of profiles because of variations in the erosion rate. These variations are probably due to the evolution of the overlying landforms rather than the age of enrichment. Thus, jarosite caps are preserved in the least eroded deposits, e.g., El Salvador, whereas the development of hematitic caps and pockets of oxidized ore overlying the sulphide blanket reveals deeper erosion, as at Escondida and Chuquicamata. This erosion may remove the leached cap and oxidize much of the supergene sulphide blanket (e.g., Radomiro Tomic), thereby generating profiles similar to that at Cerro Colorado.

Exotic mineralization

The largest-known exotic deposits are clustered around upper Eocene to lower Oligocene porphyry deposits. The major Mina Sur exotic orebody (310 Mt at 1.17 % Cu; Ossandón et al., 2001) is centered 10 km south of Chuquicamata in the basal section of a gravel unit below an 8.4 Ma ash-flow (Mortimer et al., 1977; Munchmeyer, 1996). The Damiana deposit (1.8 Mt of copper; Mote et al., 2001b), located immediately west of the El Salvador deposit, is hosted

mainly in andesitic bedrock, with minor mineralization occurring in the overlying gravels (Munchmeyer, 1996; Mote et al., 2001a). Exotic deposits also formed in the gravels at Huinquintipa (Munchmeyer, 1996) in the Collahuasi district (Fig. 3-1), 5 km west of the only weakly enriched (Lee, 1994) Rosario deposit, and in the gravels overlying the Radomiro Tomic deposit (Munchmeyer, 1996; Cuadra and Rojas, 2001). In contrast, exotic ores are absent in most of the Paleocene to middle Eocene porphyry belt, except in the Cerro Colorado area (this study) and at Sagasca (Fig. 3-2), where, however, the parent deposit has not been discovered. This is paradoxical because a longer duration of supergene activity would be expected to result in increased lateral migration of copper. We suggest that exotic deposits may have formed but were destroyed by intense and polycyclic mid-Miocene pedimentation oceanward of the porphyry centers, especially north of 20° S. Thus, in the Toquepala-Quellaveco-Cuajone district (Fig. 3-1), the major 17.6 to 19.1 Ma Pampa Lagunas pediment (Tosdal et al., 1984; Clark et al., 1990a; C. Quang, A.H. Clark and J.K.W. Lee, unpublished report for Rio Tinto Mining and Exploration Ltd, Lima, 2001) may have eroded any exotic horizons generated through Early Miocene supergene activity. The lower enrichment rates (< 1 kg/y, Table 3-5) of these older deposits also suggest that considerable copper may have been lost. Among the upper Eocene to lower Oligocene porphyry deposits, Escondida, with the highest enrichment rate (9.21 kg/y), is not known to have associated exotic mineralization. In contrast, El Salvador, which has similar thickness of enriched blanket and hypogene grades to those at Escondida, generated exotic mineralization and the enrichment rate is 6.79 kg/y. In addition to the hypogene differences, e.g., more pyrite at Escondida, this may imply that copper dispersion was minimal at Escondida and that an inverse relationship exists between the enrichment rate and the development of exotic mineralization. The anomalously low enrichment rate (1.44 kg/y) in the deeply eroded and oxidized Radomiro Tomic, which has lost copper to the gravels, may thereby be explained. The copper loss cannot, however, explain the situation at Chuquicamata (enrichment rate of 9.00 kg/y)

where the largest-known exotic mineralization occurred. In addition to the unique hypogene mineralogy and structural setting, this high rate may be related to the exceptionally large size of the deposit which could accommodate copper loss without significant decrease in enrichment rate.

Documented relationships in northern Chile (Munchmeyer, 1996) suggest that exotic deposits normally form late in the evolution of the parental supergene profile, when a considerable thickness of chalcocite has already been generated and chalcopyrite survives only at deeper levels. If pyrite is still present at these advanced stages, the low pH attending its oxidation would ensure the release of Cu through destruction of chalcocite, while the sluggish reactivity of pyrite, relative to chalcopyrite, would permit the lateral escape of the dissolved Cu. Thus, Mote et al. (2001a), providing the first direct age data for an exotic deposit, demonstrated that Cu was developed at Damiana occurred from 25 to 11 Ma and peaked around 14 Ma. However, on the basis of an age spectrum for birnessite from a fracture in Eocene andesite, they argue that exotic mineralization was already underway at 35.35 ± 1.6 Ma, i.e., at the time indicated by the alunite and jarosite dates of Gustafson and Hunt (1975) and Gustafson et al. (2001) for early supergene enrichment at El Salvador. We consider, however, that the chronology of processes that gave rise to the Damiana exotic orebody remains problematic. Thus, the documented stratigraphic and geomorphologic relationships in this area render it improbable that the Atacama Gravels, the aggradational facies of the ≤ 15 Ma Atacama Pediplain, which host part of the Damiana orebody, are as old as the Eocene-Oligocene boundary. Even if the lower part of the clastic succession accumulated during erosion of the earlier, probably upper Oligocene to Lower Miocene Checo del Cobre surface, the birnessite date would still be at least 15 m.y. older than the overlying gravels. We therefore suggest that although the importance of Miocene enrichment is demonstrated for the El Salvador district, the contribution of late Eocene to early Oligocene supergene processes is uncertain, particularly with regard to the exotic mineralization.

3.10. Supergene Metallogeny in the Central Andes

Supergene processes are optimized when hypogene ore or protore is uplifted and exposed to oxidative weathering (e.g., Anderson, 1982) in a semi-arid climate (e.g., Mortimer, 1973; Alpers and Brimhall, 1988) and, commonly, under relatively stable and sub-planar landform conditions (e.g., Clark et al., 1967a; 1990a; Sillitoe et al., 1968). Therefore, the complexly interrelated climatic conditions, tectonically induced uplift/erosion events, and geomorphologic relationships are all fundamental to the metallogeny of supergene mineralization in an environment such as the central Andes.

Our research, and that of Sillitoe and McKee (1996) and Brimhall and Mote (1997), demonstrate that supergene processes were active through much of the mid-Cenozoic beneath the now desertic Pacific slopes of the Cordillera Occidental in northern Chile. $^{40}\text{Ar}/^{39}\text{Ar}$ and K-Ar dates for supergene alunite, including those of Rowland and Clark (2001), confirm that Paleocene to middle Eocene porphyry and allied Cu deposits experienced intense late Eocene to early Oligocene enrichment, whereas the main episode of enrichment in the upper Eocene to lower Oligocene deposits occurred during the latest- Oligocene to Early Miocene (Sillitoe and McKee, 1996; this work). There is a consensus that global climatic desiccation in the late-Middle Miocene was the main cause for termination of supergene enrichment processes in this region (Mortimer, 1973; Alpers and Brimhall, 1988; Sillitoe and McKee, 1996), but the influence of climate on the *initiation* of economically important supergene activity has been uncertain. We argue that the development, as at Cerro Colorado, of thick leaching – cum – sulphide enrichment profiles by the earliest-Oligocene indicates that at least semi-arid conditions prevailed on the Pacific slope at this time. In this context, it is significant that a marked global cooling, recorded by an abrupt increase in the $\delta^{18}\text{O}$ of the shells of marine organisms, occurred at ca. 36 Ma, an event plausibly resulting from major growth of the Antarctic ice-sheet (Raymo and Ruddiman, 1992; Miller et al., 1987).

The ensuing establishment of a cool “proto-Humboldt Current” would have been one factor favorable for mid-Cenozoic supergene activity. Incaic orogenic uplift may also have provided positive feedback at this time. The age of this tectonism is locally well constrained to the interval 41-45 Ma in the Cordillera Occidental of central Peru (Noble et al., 1979; McKee and Noble, 1989), whereas Farrar et al. (1988) documented intense deformation and uplift at 38-41 Ma in the Cordillera Oriental of southeast Peru and northwest Bolivia. Incaic tectonic processes are similarly apparent in northern Chile, Hammerschmidt et al. (1992) providing $^{40}\text{Ar}/^{39}\text{Ar}$ evidence for a major 38 Ma unconformity at ca. latitude 22° S and Horton et al. (2001) positing a westerly, Chilean source for the late Eocene to early Oligocene Potoco Formation clastic sediments on the present altiplano. It is therefore likely that porphyry centers in the Paleocene to middle Eocene belt would have been situated on the oceanward slope of an uplifting “Incaic” terrain, and would have been unroofed in a rain-shadow. Given suitable landforms, therefore, conditions would have been favorable for supergene upgrading.

Paradoxically, no convincing evidence has been recorded that the lower Eocene deposits in southern Peru experienced supergene activity prior to the latest-Oligocene. Thus, the oldest, uppermost, leached zones in the Toquepala deposit lie ca. 50-100 m below the 24 Ma Altos de Camilaca surface (Tosdal et al., 1984; Clark et al., 1990a; C. Quang, A.H. Clark and J.K.W. Lee, unpublished report for Rio Tinto Mining and Exploration Ltd, Lima, 2001). It remains possible, however, that pre-existing supergene zones were destroyed during the development of this regional pediplain, the end-product of protracted uplift commencing at 26-27 Ma, and the fine-grained nature of much of the clastic fill of the contiguous Moquegua Basin implies that the deposits were subject to slow erosion through the Oligocene. Unless Incaic contraction and uplift were diachronous in northern Chile, it is possible that El Salvador and other older deposits emplaced along the Domeyko Fault System to the south may have been exhumed and enriched

before ca. 38 Ma, as is suggested by some geochronologic data (Gustafson and Hunt, 1975; Gustafson et al., 2001).

The intensity of supergene processes remains poorly constrained for the period separating the Incaic from the Pehuenchean/Aymará tectonic events. The only evidence for supergene activity comprises the early Oligocene to Early Miocene $^{40}\text{Ar}/^{39}\text{Ar}$ alunite dates from Cerro Colorado (this study) and Spence (M.G. Rowland, unpublished report to Rio Algom Exploration Inc., Toronto, 2001; Rowland and Clark, 2001). We propose, however, that enrichment continued at Cerro Colorado and perhaps elsewhere in the Paleocene to middle Eocene porphyry deposits. Although there is no record of major tectonic deformation and uplift during this period (Sandeman et al., 1995), displacement and porphyry emplacement occurred along the Domeyko Fault at least until 31.1 Ma (Reynolds et al., 1998). Moreover, the likely persistence of a semi-arid climate in northern Chile would have favored slow pediplanation, preceding the formation of the Chaja Surface and its correlatives at the beginning of the Miocene. Both climatic and geomorphologic conditions would therefore have promoted supergene processes during the Oligocene, albeit less strongly than before or after that 12 m.y. interval.

The Early Miocene was marked by the major Pehuenchean (Aymará) uplift event, which clearly rejuvenated supergene activity in the upper Eocene to lower Oligocene porphyry deposits (Sillitoe and McKee, 1996), generating the major Lower Leached Zone at Cerro Colorado, and probably similar ore zones in other Paleocene to lower Eocene deposits. Clark et al. (1967a), Sillitoe et al. (1968), and Mortimer (1973) recognized the Checo del Cobre ("Intermediate") pediplain in the Copiapó area (Fig.3-1) which, although not precisely constrained in age, was almost certainly the landform controlling supergene enrichment in the upper Eocene to lower Oligocene Cu deposits of that region. As emphasized by those authors, the most widely preserved erosional feature in the area, the >15-9.5 Ma Atacama pediplain, developed immediately prior to the onset of hyperaridity; it therefore generated no significant enrichment, but deeply truncated

pre-existing supergene profiles, a relationship of great importance for the traditional *pequeña minería* industry prior to 1980 (Sillitoe, 1969).

Despite the lack of evidence for major tectonic activity through much of the Oligocene in northern Chile, and the scarcity of supergene alunite dates older than 21 Ma in the Domeyko Fault-associated porphyry Cu deposits, the new data for the Cerro Colorado orebody do not provide support for the existence of two distinct supergene metallogenic episodes coinciding, respectively, with Incaic and Pehuenchean /Aymará tectonism. It is, rather, implicit that once climatic and landform conditions favorable for supergene upgrading had been imposed in the late Eocene, leaching and enrichment persisted until the Miocene, at least in northern Chile. Thus, the surviving upper leached/enriched profile at Cerro Colorado developed during the extended period of relative tectonic quiescence *following* the Incaic orogeny. We therefore propose the occurrence of a single, protracted (~ 30 m.y.) supergene metallogenic epoch in northern Chile which terminated with the major upgrading in the Early Miocene, an event that had the greatest impact along the younger of the two porphyry copper belts.

3.11. Concluding Statement

A growing body of evidence indicates that whereas Paleocene to middle Eocene porphyry deposits were subject to supergene leaching and enrichment for a minimum of 20 m.y., at least in northern Chile, the upgrading of the upper Eocene to lower Oligocene deposits was accomplished in less than ca. 8 m.y. Higher-grade supergene blankets would therefore be expected in the older deposits. However, at Cerro Colorado and all other Paleocene to middle Eocene deposits the enrichment rate, over a 10,000 m² plan-area of deposit (Table 3-5), was less than 1 kg/y, whereas most similarly endowed upper Eocene to lower Oligocene deposits were enriched at a rate exceeding 1 kg/y (> 6 kg/y if the deeply oxidized Radomiro Tomic deposit is excluded). Time was clearly only one of several factors contributing to the magnitude of enrichment, and in this

region the total hypogene sulphide content was apparently more critical. Thus, the enormous volume of pyrite-rich phyllic alteration at Escondida provided acid solutions sufficient to increase the grade cumulatively over a brief period, whereas the sulphide-poor alteration which dominated hypogene assemblages at Cerro Colorado resulted in the oxidation of the early enriched blanket without further downward enrichment during the Early Miocene. This factor also contributed to the complexity of the supergene profiles in the Paleocene to middle Eocene deposits, which contrast strikingly with the fundamentally simple profiles developed in most of the upper Eocene to lower Oligocene deposits. Additionally, the lower apparent enrichment rate for the upper Eocene to lower Oligocene deposits may be attributed to the subsequent copper loss by laterally moving solutions.

The distribution, setting and age of the chrysocolla vein system at Cerro Colorado provide insight into the factors influencing the development of exotic mineralization. Deepening of the supergene blanket, i.e., Lower Sulphide Ore, at Cerro Colorado, was interrupted by the accumulation of a thick but discontinuous cover of gravels and ash-flows with an easterly provenance, at a time when the deposit was undergoing monoclinal uplift and tilting, thereby constraining lateral fluid flow along and adjacent to the permeable interface between bedrock and ignimbrite. Similar uplift, monoclinal tilting and erosion of upper Oligocene to lower Miocene, Pehuenchean, pediments took place throughout northern Chile and probably provided conditions favorable for exotic mineralization where earlier-formed supergene profiles were being exhumed. Documented relationships strongly suggest that exotic assemblages developed late in the supergene evolution of the deposits, and the evidence for early development of the Damiana orebody at El Salvador (Mote et al., 2001a) remains, in our opinion, problematic. Whereas it is probable that, if exotic mineralization had formed at Cerro Colorado during Incaic uplift, it would have been destroyed in the course of later tectonism, we propose that conditions may have been too pluvial prior to the late Oligocene for exotic precipitation of copper.

3.12. Acknowledgments

Research at Cerro Colorado, the basis for the senior author's doctoral thesis, was funded by Rio Algom Exploration Ltd., through the good offices of Kelly O'Connor and Tom Warren, and by grants to A.H.C. from the Natural Sciences and Engineering Research Council of Canada (NSERC). Fieldwork would not have been possible without the full cooperation and encouragement of Orlando Alvarez, chief mine geologist, Eduardo Fernández, mine geologist, and Riochilex exploration manager, Jack McClintock, and senior geologist, Angus Campbell. $^{40}\text{Ar}/^{39}\text{Ar}$ dating and microprobe analysis at Queen's University benefited greatly from the advice of Drs. Douglas Archibald and Peter Roeder, respectively. Jeremy Richards and Timothy Mote are thanked for their constructive and insightful reviews.

Permission to publish this study, a contribution to the Queen's University Central Andean Metallogenic Project, has been given by BHP Billiton Base Metals, who also contributed funding for the colour prints. We thank James Macdonald and Richard Pape for their cooperation.

CONCLUSIONS

The protore of the Cerro Colorado porphyry Cu (-Mo) deposit, northern Chile, was emplaced in the early-middle Eocene at a depth of ca. 3 km and subsequently uplifted, exhumed and weathered to form the supergene orebody. Both the hypogene protore and supergene orebody exhibit features that are not commonly recorded in porphyry copper deposits in the Andean context or worldwide. Interpretation of these features has led to the development of new concepts for the processes and environments of metal concentration in porphyry systems and on the supergene metallogenesis of the central Andes. These aspects are summarized below in approximate chronological sequence.

4.1. Birth of a geothermal system: barren potassic-sodic alteration

The earliest hypogene activity at Cerro Colorado generated an extensive blanket, ca. 8 km² in area, of pervasive, fine-grained potassic-sodic alteration. Despite significant addition of K, Na, Mg, Fe⁺², Cl and F, no sulphides were deposited. Further, the fluids of this Early Stage were not boiling and had moderate temperatures ($\leq 380^{\circ}\text{C}$) and low salinities (≤ 8 wt percent NaCl equiv.). These features differ significantly from those of mineralized potassic zones in documented, mineralized porphyry deposits, and are instead similar to those in geothermal fields, in which extensive biotite alteration takes place at $\geq 270^{\circ}\text{C}$ (e.g., Reyes, 1990). The initial stages of alteration at Cerro Colorado are therefore envisaged to have developed under conditions similar to those in geothermal systems during which rising hydrothermal fluids cool significantly before dispersing laterally in the shallow crust. Scattered observations from uneconomic zones of several major porphyry Cu deposits, e.g., El Salvador, Chile (Gustafson and Hunt, 1975) and

Sierrita-Esperanza, Arizona (Titley et al., 1986), indicate that such barren potassic zones may be common in porphyry systems, but have been only rarely and sparsely documented (Titley, 1993 and 1995b), perhaps because of their potential importance to exploration. The details of alteration mineralogy and fluid characteristics are different in each deposit, but the large size and barren or low-grade nature are universal. It is thus apparent that, although most explored geothermal fields have not evolved into the true porphyry environment, porphyry Cu systems may have had early geothermal-style histories. Experimental data and theoretical reasoning (e.g., Fournier, 1992; Norton and Knight, 1977) suggest that such geothermal “ground preparation” would be a natural consequence of the emplacement of plutons in the cool, water-laden, shallow crust before the forceful, focused release of fluids through stocks, dikes or structures.

4.2. Transition to the porphyry environment: prograde path

Following the Early Stage, a significant increase in the temperature and salinity of the hydrothermal system was associated with fluid boiling, major stockwork development and sulphide deposition, all features typical of major porphyry systems. Such prograde relationships are probably an inherent feature of the mature stages of magmatic-hydrothermal systems, although they may also have been stimulated by mafic melt incursion into the parental magma chamber. The generation of high-temperature fluids at Cerro Colorado was not a singular event, but occurred periodically during the entire duration of sulphide deposition, from the Main to the Late Stages. The late emplacement of unaltered dykes implies that magmatic activity persisted after hydrothermal activity and no major retrograde hydrothermal history is recorded.

4.3. Rise of the fluids: quasi-simultaneous development of intermediate- and advanced argillic alteration

Boiling of the high-temperature fluids in the shallow crust at the onset of Main Stage mineralization caused the development of an extensive stockwork along which fluids could easily rise, prompting further boiling in an example of positive feedback relationships. This led to the segregation of fluids of specific densities, the lower-density, vapour-rich, fractions accumulating predominantly at the shallowest levels. Further, the incursion of meteoric water probably contributed to fluid quenching at shallow depths. Thus, as the fluids rose, their temperature, salinity and pH all decreased, generating a zoned pattern of alteration, from intermediate- to advanced argillic facies. It is argued that such a quasi-simultaneous zoning is likely to occur in any hydrothermal system involving rising fluids in the near-surface environment: it has indeed been well documented in numerous geothermal fields, but only rarely in mineralized porphyry-epithermal centres, e.g., Far Southeast-Lepanto, Luzon (Hedenquist et al., 1998).

4.4. Protracted supergene history: complex supergene profile

The deposit is inferred to have been unroofed at the onset of the Incaic orogeny at ca. 42 Ma, initiating supergene oxidation of the protore and the development of the sulphide enrichment blanket, processes which continued until climatic desiccation in the Middle Miocene. This protracted supergene evolution resulted in an unusually complex supergene profile, incorporating several leached and oxidized horizons, a characteristic of the central Andean Paleocene – middle Eocene deposits but rare in the younger upper Eocene – lower Oligocene deposits, most of which experienced much briefer, ca. 7 m.y., supergene histories. The episodic uplift and erosion of the Pacific margin of the South American plate during the weathering history of the deposit had a major impact on the anatomy of the supergene profile. Thus, the Early Miocene Pehuenchean

(Aymar ) tectonic event caused regional uplift, a drastic fall of the water-table and the development of an erosional pediplain, the Choja surface, beneath which the upper portions of the Incaic chalcocite blanket were oxidized and its lower portions leached. The partial blanketing of the deposit by a thick ignimbrite flow soon after the Early Miocene uplift prevented further fluvial erosion of the supergene orebody and led to the rise of the water-table, imposing lateral groundwater flow which generated incipient exotic mineralization.

4.5. Climatic changes: controls on supergene metallogenesis

There is a consensus that global climatic desiccation in the later-Middle Miocene was the main cause for the termination of supergene enrichment processes in northern Chile, despite the existence of favourable, stable landforms (e.g., Mortimer, 1973; Alpers and Brimhall, 1988). It is reasonable to argue that the Paleogene initiation of supergene processes similarly reflected a major climatic change, probably in the late Eocene. Thus, the marked global cooling at ca. 36 Ma, an event plausibly resulting from major growth of the Antarctic ice-sheet (Raymo and Ruddiman, 1992), may have stimulated the establishment of a cool “proto-Humboldt Current” which led to the imposition of semi-arid conditions along the Pacific slope of the Andes. Further, the Incaic orogeny, which was responsible for the accumulation of thick clastic successions in the present-day Altiplano (Horton et al., 2001), provided positive climatic and physiographic feedback for the supergene enrichment of porphyry centres undergoing exhumation in the oceanward rain-shadow of an uplifting terrain. That climatic conditions remained favourable for supergene enrichment during the entire late Eocene – Early Miocene interval is supported by supergene alunite dates from Cerro Colorado, evidence for a single Cenozoic supergene metallogenetic epoch in northern Chile, ca. 20, or even 30, m.y. in duration.

REFERENCES

- Ague, J.J., 1994, Mass transfer during Barrovian metamorphism of pelites, south-central Connecticut; I, Evidence for changes in composition and volume: *American Journal of Science*, v. 294, p. 989-1057.
- Ague, J.J., and, van Haren, J.L.M., 1996, Assessing metasomatic mass and volume changes using the bootstrap, with application to deep crustal hydrothermal alteration of marble: *Economic Geology*, v. 91, p. 1169-1182.
- Ahmad, S.N, and Rose, A., W., 1980, Fluid inclusions in porphyry and skarn ore at Santa Rita, New Mexico: *Economic Geology*, v. 75, p. 229-250.
- Aitchison, J., 1986, *The statistical analysis of compositional data*: London, Chapman and Hall, 416p.
- 1989, Measure of location of compositional data sets: *Mathematical Geology*, v. 21, p. 787-790.
- Aja, S.U, Rosenberg, P.E., and Kittrick, J.A., 1991a, Illite equilibria in solutions; I, Phase relationships in the system $K_2O-Al_2O_3-SiO_2-H_2O$ between 25 and 250°C: *Geochimica et Cosmochimica Acta*, v. 55, p. 1353-1364.
- Aja, S.U, Rosenberg, P.E., and Kittrick, J.A., 1991b, Illite equilibria in solutions; II, Phase relationships in the system $K_2O-MgO-Al_2O_3-SiO_2-H_2O$: *Geochimica et Cosmochimica Acta*, v. 55, p. 1365-1374.
- Allmendinger, R.W., Jordan, T.E., Kay, S.M., and Isacks, B.L., 1997, The evolution of the Altiplano-Puna plateau of the Central Andes: *Annual Review of Earth and Planetary Sciences*, v. 25, p. 139-174.

- Alpers, C.N., 1986, Geochemical and geomorphological dynamics of supergene copper sulfide ore formation and preservation at La Escondida, Antofagasta, Chile: Unpublished Ph.D. thesis, University of California, Berkeley, 184 p.
- Alpers, C.N., and Brimhall, G.H., 1988, Middle Miocene climatic change in the Atacama Desert, northern Chile: Evidence from supergene mineralization at La Escondida: Geological Society of America Bulletin, v. 100, p.1640-1656.
- 1989, Paleohydrologic evolution and geochemical dynamics of cumulative supergene metal enrichment at La Escondida, Atacama Desert, northern Chile: Economic Geology, v. 84, p. 229-255.
- Alt, J.C, and Jiang, W., 1991, Hydrothermally precipitated mixed-layer illite-smectite in Recent massive sulfide deposits from the sea floor: Geology, v. 19, p. 570-573.
- Anderson, A.T., Jr., Newman, S., Williams, S.N., Druitt, T.H., Skirius, C., and Stolper, E.H, 1989, H₂O, CO₂, Cl, and gas in Plinian and ash-flow Bishop rhyolite: Geology, v. 17, p. 221-225.
- Anderson, C.A., 1950, Alteration and mineralization in the Bagdad porphyry copper deposit, Arizona: Economic Geology, v. 45, p. 609-628.
- 1955, Oxidation of copper sulfides and secondary sulfide enrichment: Economic Geology 50th Anniversary Volume, part 1, p. 324-340.
- Anderson, J.A., 1982, Characteristics of leached capping and techniques of appraisal, *in* Titley, S.R., ed., Advances in geology of the porphyry copper deposits, southwestern North America: Tucson, The University of Arizona Press, p. 275-295.
- Arancibia, O.N., and Clark, A.H., 1996, Early magnetite-amphibole-plagioclase alteration-mineralization in the Island copper porphyry copper-gold-molybdenum deposit, British Columbia: Economic Geology, v. 91, p. 402-438.

- Arévalo, C., Rivera, O., Iriarte, S., and Mpodozis, C., 1994, Cuencas extensionales y campos de calderas del Cretácico Superior-Terciario inferior en la Precordillera de Copiapó (27° to 28° S), Chile, *in* Campos, E., Cecioni, A., eds.: VII Congreso Geológico Chileno, v. 2, p. 1288-1292.
- Atkinson, W.W., Jr., Souviron, A., Vehrs, T.L., and Faunes, G.A., 1996, Geology and mineral zoning of the Los Pelambres porphyry copper deposit, Chile, *in* Camus, F., Sillitoe, R.H., and Petersen, R., eds., Andean copper deposits: new discoveries, mineralization, style and metallogeny: Society of Economic Geologists Special Publication 5, p. 131-156.
- Ballard, J.R., Palin, J.M., Williams, I.S., Campbell, I.H., and Faunes, A., 2001, Two ages of porphyry intrusion resolved for the super-giant Chuquibambilla copper deposit of northern Chile by ELA-ICP-MS and SHRIMP: *Geology*, v. 29, p. 383-386.
- Beane, R.E., and Titley, S.R., 1981, Porphyry copper deposits. Part II. Hydrothermal alteration and mineralization, *in* Skinner, B.J., ed.: Economic Geology 75th Anniversary Volume, p. 235-269.
- Beeson, J.J., 1917, The disseminated copper ores of Bingham Canyon, Utah: *Transactions of the American Institute of Mining, Metallurgical and Petroleum Engineers*, v. 54, p. 356-401.
- Bodnar, R.J., 1994, Synthetic fluid inclusions: XII. The system H₂O-NaCl. Experimental determination of the halite liquidus and isochores for a 40 wt% NaCl solution: *Geochimica et Cosmochimica Acta*, v. 58, p. 1053-1063.
- Bodnar, R.J., and Vityk, M.O., 1994, Interpretation of microthermometric data for H₂O-NaCl fluid inclusions, *in* De Vivo, B., and Frezzotti, M.L., eds., *Fluid Inclusions in Minerals: Methods and Applications: Short Course of the Working Group (IMA) "Inclusions in Minerals"*, p.117-130.

- Bodnar, R.J., Burnham, C.W., and Sterner, S.M., 1985, Synthetic fluid inclusions in natural quartz. III. Determination of phase equilibrium properties in the system H₂O-NaCl to 1000°C and 1500 bars: *Geochimica et Cosmochimica Acta*, v. 49, p. 1861-1873.
- Bodnar, R.J., Binns, P.R., and Hall, D.L., 1989, Synthetic fluid inclusions; VI, Quantitative evaluation of the decrepitation behaviour of fluid inclusions in quartz at one atmosphere confining pressure: *Journal of Metamorphic Geology*, v. 7, p. 229-242.
- Boutwell, J.M., 1905, Ore deposits of Bingham, Utah: U. S. Geological Survey Bulletin, 260, p. 236-241.
- Bouzari, F., and Clark, A.H., 2000, Definition of a protracted history of supergene alteration in the Cerro Colorado porphyry copper deposit, Chile, through Ar-Ar dating of alunite-group minerals [abs.]: *Geological Society of America, Abstracts with Programs*, v. 32, p. A-110.
- Bouzari, F., and Clark, A.H., 2002, Anatomy, evolution, and metallogenic significance of the supergene orebody of the Cerro Colorado porphyry copper deposit; I Region, northern Chile: *Economic Geology*, v. 97, p. 1701-1740.
- Bowman, J.R., Parry, W.T., Kropp, W.P., and Kruer, S.A., 1987, Chemical and isotopic evolution of hydrothermal solutions at Bingham, Utah: *Economic Geology*, v. 82, p. 395-428.
- Brathwaite, R.L., Simpson, M.P., Faure, K., and Skinner, D.N.B., 2001, Telescoped porphyry Cu-Mo-Au mineralisation, advanced argillic alteration and quartz-sulphide-gold-anhydrite veins in the Thames District, New Zealand: *Mineralium Deposita*, v. 36, p. 623-640.
- Brimhall, G.H., 2000, Supergene enrichment of ore deposits at active continental margins [abs.]: *Geological Society of America, Abstracts with Programs*, v. 32, p. A-4.
- Brimhall, G.H., and Dietrich, William E., 1987, Constitutive mass balance relations between chemical composition, volume, density, porosity, and strain in metasomatic hydrochemical systems; results on weathering and pedogenesis: *Geochimica et Cosmochimica Acta*, v. 51, p. 567-587.

- Brimhall, G.H., and Mote, T.I., 1997, Optimal secondary mineralization in the Andes: Vadose response to global Cenozoic cooling events, glaciation, eustacy and desiccation [abs.]: Geological Society of America, Abstract with Programs, v. 29, p. 17.
- Burnham, C.W., 1967, Hydrothermal fluid at the magmatic stage, *in* Barnes, H.L. ed., Geochemistry of hydrothermal ore deposits: Holt, Reinhart and Winston, Inc., New York, p. 34-76.
- 1979, Magmas and hydrothermal fluids, *in* Barnes, H.L., ed., Geochemistry of hydrothermal ore deposits, second edition: Holt, Reinhart and Winston, Inc., New York, p. 71-136.
- 1981, Physicochemical constraints on porphyry mineralization, *in* Dickinson, W.R. and Payne, W.D., eds., Relations of tectonics to ore deposits in the southern Cordillera: Arizona Geological Society Digest 14, p. 71-77.
- Burnham, C.W., and Ohmoto, H., 1980, Late-stage processes of felsic magmatism, *in* Ishihara, S., and Takenouchi, S., eds., Granitic magmatism and related mineralization: Mining Geology Special Issue 8, p. 1-11.
- Candela, P.A., 1989a, Magmatic ore-forming fluids; thermodynamic and mass transfer calculations of metal concentrations, *in* Whitney, J.A., and Naldrett, A.J. eds., Ore deposition associated with magmas: Reviews in Economic Geology, v. 4, p. 203-221.
- Candela, P.A., 1989b, Felsic magmas, volatiles, and metallogenesis, *in* Whitney, J.A., and Naldrett, A.J. eds., Ore deposition associated with magmas: Reviews in Economic Geology, v. 4, p. 223-233.
- Candela, P.A., and Holland, H.D., 1984, The partitioning of copper and molybdenum between silicate melts and aqueous fluids: *Geochimica et Cosmochimica Acta*, v. 48, p. 373-380.

- Candela, P.A., and Holland, H.D., 1986, A mass transfer model for copper and molybdenum in magmatic hydrothermal systems; the origin of porphyry-type ore deposits: *Economic Geology*, v. 81, p. 1-19.
- Carrasco, P., Wilke, H., and Schneider, H., 1999, Post Eocene deformational events in the north segment of the Precordilleran fault system, Copaquiri (21° S): 4th International Symposium on Andean Geodynamics, Göttingen, Germany, Institut de Recherche pour le Développement, Paris, p. 249-252.
- Carten, R.B., 1986, Sodium-calcium metasomatism; chemical, temporal, and spatial relationships at the Yerington, Nevada, porphyry copper deposit: *Economic Geology*, v. 81, p. 1495-1519.
- Charrier, R., Hérail, G., Flynn, J., Riquelme, R., García, M., Croft, D., and Wyss, A., 1999, Opposite thrust-vergencies in the Pre-Cordillera and western Cordillera of northern Chile, and structurally linked Cenozoic paleo-environmental evolution: 4th International Symposium on Andean Geodynamics, Göttingen, Germany, Institut de Recherche pour le Développement, Paris, p. 253-256.
- Chávez, W.X., 2000, Supergene oxidation of copper deposits: Zoning and distribution of copper oxide minerals: *Society of Economic Geologists Newsletter*, no. 41, p. 1, 10-21.
- Clark, A.H., 1993, Are outsize porphyry copper deposits either anatomically or environmentally distinctive?, *in* Whiting, B.H., Hodgson, C.J., and Mason, R., eds., *Giant ore deposits: Society of Economic Geologists Special Publication 2*, p. 213-283.
- Clark, A.H., 2003, The Paleocene – middle Eocene Porphyry copper-molybdenum provinces of southern Peru: hypogene and supergene ore-genesis and metallogenesis: Field course notes, ProExplo, Lima, April, 2003, 115p.

- Clark, A.H., Cooke, R.U., Mortimer, C., and Sillitoe, R.H., 1967a, Relationships between supergene mineral alteration and geomorphology, southern Atacama desert, Chile; an interim report: Institution of Mining and Metallurgy, Transactions, Section B: Applied Earth Science, v. 76, p. B89-B96.
- Clark, A.H., Mayer, A.E.S., Mortimer, C., Sillitoe, R.H., Cooke, R.U., and Snelling N.J., 1967b, Implications of the isotopic ages of ignimbrite flows, southern Atacama desert, Chile: *Nature*, v. 215, p. 723-724.
- Clark, A.H., Farrar, E., Caelles, J.C., Haynes, S.J., Lortie, R.B., McBride, S.L., Quirt, G.S., Robertson, R.C.R., and Zentilli, M., 1976, Longitudinal variations in the metallogenetic evolution of the central Andes; a progress report, *in* Strong, D.F., ed., *Metallogeny and plate tectonics*, Geological Association of Canada, Special Paper 14, p. 23-58.
- Clark, A.H., Tosdal, R.M., Farrar, E., and Plazolles, A., 1990a, Geomorphologic environment and age of supergene enrichment of the Cuajone, Quellaveco and Toquepala porphyry copper deposits, southern Peru: *Economic Geology*, v. 85, p. 1604-1628.
- Clark, A.H., Farrar, E., Kontak, D.J., Langridge, R.J., Arenas F.M.J, France, L.J., McBride, S.L., Woodman, P.L., Wasteneys, H.A., Sandeman, H.A., and Archibald, D.A., 1990b, Geologic and geochronologic constraints on the metallogenetic evolution of the Andes of southeastern Peru: *Economic Geology*, v. 85, p. 1520-1583.
- Clark, G.H., 1990, Panguna copper-gold deposit, *in* Hughes, F.E., ed., *Geology of the mineral deposits of Australia and Papua New Guinea: Monograph series*, Australasian Institute of Mining and Metallurgy, Melbourne, p. 1807-1816.
- Cline, J.S., 1995, Genesis of porphyry copper deposits; the behavior of water, chloride, and copper in crystallizing melts, *in* Pierce, F.W., and Bolm, J.G. eds., *Porphyry copper deposits of the American Cordillera: Arizona Geological Society Digest*, v. 20, p. 69-82.

- Cline, J.S., and Bodnar, R.J., 1991, Can economic porphyry copper mineralization be generated by a typical calc-alkaline melt?: *Journal of Geophysical Research*, v. 96, p. 8113-8126.
- Cline, J.S., and Bodnar, R.J., 1994, Direct evolution of brine from a crystallizing silicic melt at the Questa, New Mexico, Molybdenum Deposit: *Economic Geology*, v. 89, p. 1780-1802.
- Coira, B., Davidson, J., Mpodozis, C., and Ramos, V., 1982, Tectonic and magmatic evolution of the Andes of northern Argentina and Chile: *Earth Science Reviews*: v. 18, p. 303-332.
- Cox, D.P., 1985, Geology of the Tanama and Helecho porphyry copper deposits and vicinity, Puerto Rico: U. S. Geological Survey Professional Paper, P 1327, 59p.
- Creasey, S.C., 1965, Geology of the San Manuel area, Pinal County, Arizona: U. S. Geological Survey Professional Paper, 471, 64 p.
- Cuadra C. P., and Rojas S. G., 2001, Oxide mineralization at the Radomiro Tomic porphyry copper deposit, northern Chile: *Economic Geology*, v. 96, p. 387-400.
- Czamanske, G.K., Force, E.R., and Moore, W.J., 1981, Some geologic and potential resource aspects of rutile in porphyry copper deposits: *Economic Geology*, v. 76, p. 2240-2246.
- Dalrymple, G.B., and Lanphere, M.A., 1974, $^{40}\text{Ar}/^{39}\text{Ar}$ age spectra of some undisturbed terrestrial samples: *Geochimica et Cosmochimica Acta*, v. 38, p. 715-738.
- Dalrymple, G.B., Alexander, E.C., Jr., Lanphere, M.A., and Kraker, G.P., 1981, Irradiation of samples for $^{40}\text{Ar}/^{39}\text{Ar}$ dating using the Geological Survey TRIGA reactor: U.S. Geological Survey Professional Paper 1176, 55 p.
- Darke, K.E., Boyce, A.J., Clapperton, C.M., Fallick, A.E., Redwood, S.D., and Rice, C.M., 1997, Supergene mineralization at the Kori Kollo gold mine, Bolivia: *Exploration and Mining Geology*, v. 6, p. 209-221.
- Diamond, L.W., 2001, Review of the systematics of $\text{CO}_2\text{-H}_2\text{O}$ fluid inclusions: *Lithos*, v. 55, p. 69-99.

- Dilles, J.H., and Einaudi, M.T., 1992, Wall-rock alteration and hydrothermal flow paths about the Ann-Mason porphyry copper deposit, Nevada; a 6-km vertical reconstruction: *Economic Geology*, v. 87, p. 1963-2001.
- Dilles, J.H., Einaudi, M.T., Proffett, J.M., and Barton, M.D., 2000, Overview of the Yerington porphyry copper district; magmatic to nonmagmatic sources of hydrothermal fluids; their flow paths and alteration effects on rocks and Cu-Mo-Fe-Au ores, *in* Dilles, J.H., Barton, M.D., Johnson, D.A., Proffett, J.M., and Einaudi, M.T., eds., Part I, Contrasting styles of intrusion-associated hydrothermal systems: Society of Economic Geologists, Guidebook Series, v. 32, p. 55-66.
- Efron, B., 1979, Bootstrap methods: Another look at the jackknife: *Annual Statistics*, v. 7, p. 1-26.
- Embley, R.W., Jonasson, I.R., Perfit, M.R., Franklin, J.M., Tivey, M.A., Malahoff, A., Smith, M.F., and Francis, T.J.G., 1988, Submersible investigation of an extinct hydrothermal system on the Galapagos Ridge: Sulfide mounds, stockwork zone, and differentiated lavas: *Canadian Mineralogists*, v. 26, p. 517-539.
- Emmons, S.F., 1901, The secondary enrichment of ore deposits: *Transactions of the Society of Mining Engineers, American Institute of Mining, Metallurgical and Petroleum Engineers, Incorporated (AIME)*, v. 30, p. 177-217.
- Emmons, W.H., 1913, The enrichment of sulphide ores: *U. S. Geological Survey Bulletin* 529, 260 p.
- 1917, The enrichment of ore deposits: *U.S. Geological Survey Bulletin* 625, 530 p.
- 1927, Relations of the disseminated copper ores in porphyry to igneous intrusives: *Transactions of the American Institute of Mining, Metallurgical and Petroleum Engineers*, v. 75, p. 797-815.

- Essene, E.J., and Peacor, D.R., 1995, Clay mineral thermometry; a critical perspective: *Clays and Clay Minerals*, v. 43, p. 540-553.
- Farrar, E., Clark, A.H., Kontak, D.J., and Archibald, D.A., 1988, Zongo-San Gabán Zone: Eocene foreland boundary of the central Andean orogen, northwest Bolivia and southern Peru: *Geology*, v. 16, p. 55-58.
- Flint, S., Turner, P., Jolley, E.J., and Hartley, A.J., 1993, Extensional tectonics in convergent margin basins: An example from the Salar de Atacama, Chilean Andes: *Geological Society of America Bulletin*, v. 105, p. 603-617.
- Force, E.R., Czamanske, G.K., and Moore, W.J., 1980, Recovering rutile from porphyry copper deposits: *U. S. Geological Survey Professional Paper*, P 1175, p. 7-8.
- Fournier, R.O., 1999, Hydrothermal processes related to movement of fluid from plastic into brittle rock in the magmatic-epithermal environment: *Economic Geology*, v. 94, p. 1193-1211.
- Frank, M.R., Candela, P.A., and Piccoli, P.M., 1998, Estimated copper concentrations in magmatic vapor and brine, in a sulfur-bearing brine-vapor-haplogranitic melt-intermediate solid solution-pyrrhotite system at 800°C and 100 Mpa [abs.]: *Geological Society of America, Programs with Abstracts*, v. 30, p. 371.
- Fulginiti, P., Malfitano, G., and Sbrana, A., 1997, The Pantelleria caldera geothermal system; data from the hydrothermal minerals: *Journal of Volcanology and Geothermal Research*, v. 75, p. 251-270.
- Galli O., C., 1967, Pediplain in northern Chile and the Andean uplift: *Science*, v. 158, p. 653-655.
- 1968, *Carta Geológica de Chile: Cuadrángulo Juan de Morales, Provincia de Tarapacá*, Escala 1:50,000: Instituto de Investigaciones Geológicas de Chile, Carta no. 18, 53 p.
- García, M., Hérail, G., and Gardeweg, M., 1999, Oligo-Miocene ignimbritic volcanism of northern Chile (Arica region): *Stratigraphy and geomorphology: 4th International*

- Symposium on Andean Geodynamics, Göttingen, Germany, Institut de Recherche pour le Développement, Paris, p. 253-256.
- Gendall, I.R., Quevedo, L.A., Sillitoe, R.H., Spencer, R.M., Puente, C.O., Leon, J.P., and Povedo, R.R., 2000, Discovery of a Jurassic porphyry copper belt, Panguí area, southern Ecuador: Society of Economic Geologists Newsletter: v. 43, p. 1, 8-15.
- Gerth, H., 1955, Der geologische Bau der südamerikanischen Kordillere (Geologie von Südamerika 2. Bd.): Gebrüder Bornträger, Berlin, 264p.
- Gilmour, P., Andrew, R.L., Bernstein, M., Maxwell, I., and Morrissey, C.J., 1995, Porphyry copper deposits: history, recent developments, exploration, economics, *in* Pierce, F.W., Bolm, J.G., eds., Porphyry copper deposits of the American Cordillera: Arizona Geological Society Digest, 20, p. 128-155.
- Grant, J.N., Halls, C., Sheppard, S.M.F., and Avila, W., Evolution of the porphyry tin deposits of Bolivia, *in* Ishihara, S., and Takenouchi, S., eds., Granitic magmatism and related mineralization: Mining Geology Special Issue, no 8, p. 151-173.
- Graton, L.C., 1913, Investigation of copper enrichment: Engineering and Mining Journal, v. 96, p. 885-887.
- Gregory-Wodzicki, K.M., 2000, Uplift history of the central and northern Andes: A review: Geological Society of America Bulletin, v. 112, p. 1091-1105.
- Gustafson, L.B., 1979, Porphyry copper deposits and calc-alkaline volcanism, *in* McElhinny, M.W., eds., The Earth; its origin, structure and evolution: Academic Press, London, p. 427-464.
- Gustafson, L.B., and Hunt, J.P., 1975, The porphyry copper deposit at El Salvador, Chile: Economic Geology, v. 70, p. 857-912.
- Gustafson, L.B., and Quiroga, G.J., 1995, Patterns of mineralization and alteration below the porphyry copper orebody at El Salvador, Chile: Economic Geology, v. 90, p. 2-16.

- Gustafson, L.B., Orquera, W., McWilliams, M., Castro, M., Olivares, O., Rojas, G., Maluenda, J., and Mendez, M., 2001, Multiple centers of mineralization in the Indio Muerto district, El Salvador, Chile: *Economic Geology*, v. 96, p. 325-350.
- Haas, J.L., Jr., 1971, The effect of salinity on the maximum thermal gradient of a hydrothermal system at hydrostatic pressure: *Economic Geology*, v. 66, p. 940-946.
- 1976, Physical properties of the coexisting phases and thermodynamic properties of the H₂O component in boiling NaCl solutions: *U.S. Geological Survey Bulletin*, 1421-A, 73p.
- Hammerschmidt, K., Döbel, R., and Friedrichsen, H., 1992, Implication of ⁴⁰Ar/³⁹Ar dating of Early Tertiary volcanic rocks from the north-Chilean Precordillera: *Tectonophysics*, v. 202, p. 55-81.
- Harrison, T.M., Duncan, I., and McDougall, I., 1985, Diffusion of ⁴⁰Ar in biotite: Temperature, pressure and compositional effects. *Geochimica and Cosmochimica Acta*, v. 49, p. 2461-2468.
- Hartley, A.J., May, G., Chong, G., Turner, P., Kape, S.J., and Jolley, E.J., 2000, Development of a continental forearc: A Cenozoic example from the Central Andes, northern Chile: *Geology*, v. 28, p. 331-334.
- Hedenquist, J.W., 1990, The thermal and geochemical structure of the Broadlands-Ohaaki geothermal system, New Zealand: *Geothermics*, v. 19, p. 151-185.
- Hedenquist, J.W., and Henley, R.W., 1985, The importance of CO₂ on freezing point measurements of fluid inclusions: Evidence from active geothermal systems and implications for epithermal ore deposition: *Economic Geology*, v. 80, p. 1379-1406.
- Hedenquist, J.W., and Lowenstern, J.B., 1994, The role of magmas in the formation of hydrothermal ore deposits: *Nature*, v. 370, p. 519-527.

- Hedenquist, J.W., Arribas, A., Jr., and Reynolds, T.J., 1998, Evolution of an intrusion-centered hydrothermal system: Far Southeast-Lepanto porphyry and epithermal Cu-Au deposits, Philippines: *Economic Geology*, v. 93, p. 373-404.
- Heinrich, C.A., Guenther, D., Audetat, A., Ulrich, T., and Frischknecht, R., 1999, Metal fractionation between magmatic brine and vapor, determined by microanalysis of fluid inclusions: *Geology*, v. 27, p. 755-758.
- Hemley, J.J., and Hunt, J.P., 1992, Hydrothermal ore-forming processes in the light of studies in rock-buffered systems; II, Some general geologic applications: *Economic Geology*, v. 87, p. 23-43.
- Hemley, J.J., Hostetler, P.B., Gude, A.J., and Mountjoy, W.T., 1969, Some stability relations of alunite: *Economic Geology*, v. 64, p. 599-612.
- Hodgson, J., 1995, The case for derivation of metals from crustal sources, with implications for the search of giants, *in* Clark, A.H., ed., Giant ore deposits – II, Controls on the scale of orogenic magmatic-hydrothermal mineralization: Proceedings of the second giant ore deposits workshop: Department of Geological Sciences, Queen's University, Kingston, Ontario, p. 481-513.
- Holland, H.D., 1972, Granites, solutions, and base metal deposits: *Economic Geology*, v. 67, p. 281-301.
- Horton, B.K., Hampton, B.A., and Waanders, G.L., 2001, Paleogene synorogenic sedimentation in the Altiplano plateau and implication for initial mountain building in the central Andes: *Geological Society of America, Bulletin*, v. 113, p. 1387-1400.
- Hower, J., and Altaner, S.P., 1983, The petrologic significance of illite/smectite: *Clay Minerals Society, 20th annual meeting*; Buffalo, New York, Program and Abstracts. 40p.
- Huete, C., Makshev, V., Moscoso, R., Ulriksen, C., and Vergara, H., 1977, Antecedentes geocronológicos de rocas intrusivas y volcánicas en la Cordillera de los Andes comprendida

- entre la Sierra Moreno y El Río Loa, y los 21° y 22° lat. sur, II Región, Chile: *Revista Geológica de Chile*, no 4, p. 35-41.
- Hunt, J.P., 1957, Rock alteration, mica and clay minerals in certain areas of the United States and Lark mines, Bingham, Utah: unpublished Ph.D. thesis, University of California, Berkeley, 321 p.
- Isacks, B.L., 1988, Uplift of the central Andean plateau and bending of the Bolivian orocline: *Journal of Geophysical Research*, v. 93, p. 3211-3231.
- Itaya, T., Arribas, A., Jr., and Okada, T., 1996, Argon release systematics of hypogene and supergene alunite based on progressive heating experiments from 100 to 1000°C: *Geochimica et Cosmochimica Acta*, v. 60, p. 4525-4535.
- Jacobs, D.C., and Parry, W.T., 1979, Geochemistry of biotite in the Santa Rita porphyry copper deposit, New Mexico: *Economic Geology*, v. 74, p. 860-887.
- Jaillard, E., Hérail, G., Monfret, T., Díaz-Martínez, E., Baby, P., Lavenu, A., and Dumont, J.F., 2000, Tectonic evolution of the Andes of Ecuador, Peru, Bolivia and northernmost Chile, *in* Cordani, U.G., Milani, E.J., Thomaz Filho, A., and Campos, D.A., eds., *Tectonic evolution of South America: 31st International Geological Congress*, Rio de Janeiro, Brazil, p. 481-559.
- Jambor, J.L., 1999, Nomenclature of the alunite supergroup: *Canadian Mineralogist*, v. 37, p. 1323-1341.
- Jarrell, O.W., 1944, Oxidation at Chuquicamata, Chile: *Economic Geology*, v. 39, p. 251-286.
- Kemp, J.F., 1905, Secondary enrichment in ore-deposits of copper: *Economic Geology*, v. 1, p. 11-25.
- Kerr, P.F., Kulp, J.L., Patterson, C.M., and Wright, R.J., 1950, Hydrothermal alteration at Santa Rita, New Mexico: *Geological Society of America Bulletin*, v. 61, p. 275-347.
- Kilinc, I.A., and Burnham, C.W., 1972, Partitioning of chloride between a silicate melt and coexisting aqueous phase from 2 to 8 Kilobars: *Economic Geology*, v. 67, p. 231-235.

- Kontak, D.J., and Clark, A.H., 2002, Genesis of the giant, bonanza San Rafael lode tin deposit, Peru: *Economic Geology*, v. 97, p. 1741-1778.
- Lambert, S.J., and Epstein, S., 1980, Stable isotope investigations of an active geothermal system in Valles Caldera, Jemez Mountains, New Mexico: *Journal of Volcanology and Geothermal Research*, v. 8, p. 111-129.
- Lee, A.W., 1994, Evolution of the Rosario copper-molybdenum porphyry deposit and associated copper-silver vein system, Collahuasi district, I Región, northern Chile: Unpublished M.Sc. thesis, Queen's University, Kingston, Ontario, Canada, 75 p.
- Lichtner, P.C., and Biino, G.G., 1992, A first approach to supergene enrichment of a porphyry copper protore: I. Cu-Fe-S subsystem: *Geochimica et Cosmochimica Acta*, v. 56, p. 3987-4013.
- Lindgren, W., 1933, *Mineral deposits*, 4th edition: McGraw-Hill Book Co., New York and London, 930p.
- Long, K., 1995, Production and reserves of Cordilleran (Alaska to Chile) porphyry copper deposits, in Pierce, F.W., Bolm, J.G., eds, *Porphyry copper deposits of the American Cordillera*: Arizona Geological Society Digest, 20, p. 35-68
- Love, D.A., Clark, A.H., Hodgson, C.J., Farrar, E., and Archibald, D.A., 1994, $^{40}\text{Ar}/^{39}\text{Ar}$ dating of alunitic and adularia-sericite alteration-mineralization facies, Mt. Skukum epithermal Au deposit, Yukon [abs.]: *Geological Society of America, Abstracts with Programs*, 26 (7), p. 142.
- Love, D.A., Clark, A.H., Hodgson, C.J., Mortensen, J.K., Archibald, D.A., and Farrar, E., 1998, The timing of adularia-sericite-type mineralization and alunite-kaolinite-type alteration, Mount Skukum epithermal gold deposit, Yukon Territory, Canada: ^{40}Ar - ^{39}Ar and U-Pb geochronology: *Economic Geology*, v. 93, p. 437-462.

- Lowell, J.D., Guilbert, J.M., 1970, Lateral and vertical alteration-mineralization zoning in porphyry ore deposits: *Economic Geology*, v. 65, p. 373-408.
- Lowenstern, J.B., 1994, Chlorine, fluid immiscibility, and degassing in peralkaline magmas from Pantelleria, Italy: *American Mineralogist*, v. 79, p. 353-369.
- Maksaev, J.V., 1979, Las fases tectónicas Incaica y Quechua en la Cordillera de los Andes del Norte Grande de Chile: *Actas II Congreso Geológico Chileno (2, Tomo 1)*, p. B63-B77.
- Marsh, T.M., Einaudi, M.T., and McWilliams, M., 1997, $^{40}\text{Ar}/^{39}\text{Ar}$ geochronology of Cu-Au and Au-Ag mineralization in the Potrerillos District, Chile: *Economic Geology*, v. 92, p. 784-806.
- Manske, S.L., and Paul, A.H., 2002, Geology of a major new porphyry copper center in the Superior (Pioneer) District, Arizona: *Economic Geology*, v. 97, p. 197-220.
- McBride, S.L., 1972, A potassium-argon age investigation of igneous and metamorphic rocks from Catamarca and La Rioja provinces, Argentina: Unpublished M.Sc. thesis, Queen's University, Kingston, Ontario, 101 p.
- 1977, A K-Ar study of the Cordillera Real, Bolivia, and its regional setting: Unpublished Ph.D. thesis, Queen's University, Kingston, Ontario, 231 p.
- McIntyre, D.B., 1963, Precision and resolution in geochronometry, *in* Albritton, C.C., ed., *The fabric of geology*: Freeman, Cooper, and Company, Stanford, California, p. 112-134.
- McKee, E.H., and Noble, D.C., 1989, Cenozoic tectonic events, magmatic pulses, and base- and precious-metal mineralization in the central Andes, *in* Ericksen, G.E., Cañas Pinochet, M.T., and Reinemund, J.A., eds., *Geology of the Andes and its relation to hydrocarbon and mineral resources*: Houston, Texas, Circum-Pacific Council for Energy and Mineral Resources, Earth Science Series, v. 11, p. 189-194.
- McKibben, M.A., and Hardie, L.A., 1997, Ore-forming brines in active continental rifts, *in* Barnes, H.L., ed., *Geochemistry of hydrothermal ore deposits*, 3 edition: John Wiley and Sons, Inc., p. 877-935.

- Meldrum, S.J., Aquino, R.S., Gonzales, R.I., Burke, R.J., Suyadi, A., Irianto, B., and Clarke, D.S., 1994, The Batu Hijau porphyry copper-gold deposit, Sumbawa Island, Indonesia: *Journal of Geochemical Exploration*, v. 50, p. 203-220.
- Meyer, C., and Hemley, J.J., 1967, Wall rock alteration, *in* Barnes, H.L., ed., *Geochemistry of hydrothermal ore deposits*: Holt, Reinhart and Winston, Inc., New York, p. 166-235.
- Meyer, C., Shea, E.P., and Goddard, C.C., Jr., 1968, Ore deposits at Butte, Montana, *in* Ridge, J.D., ed., *Ore deposits of the United States, 1933-1967*, v. 2, p. 1373-1416.
- Miller, K.G., Fairbanks, R.G., and Mountain, G.S., 1987, Tertiary oxygen isotope synthesis, sea level history, and continental margin erosion: *Paleoceanography*, v. 2, p. 1-19.
- Moore, J.N., Powell, T.S., Heizler, M.T., and Norman, D.I., 2000, Mineralization and hydrothermal history of the Tiwi geothermal system, Philippines: *Economic Geology*, v. 95, p. 1001-1023.
- Mortimer, C., 1973, The Cenozoic history of the southern Atacama Desert, Chile: *Journal of the Geological Society of London*, v. 129, p. 505-526.
- Mortimer, C., and Sarič, N., 1975, Cenozoic studies in northernmost Chile: *Geologische Rundschau*, v. 64, p. 395-420.
- Mortimer, C., Farrar, E., and Sarič, N., 1974, K-Ar ages from Tertiary lavas of the northernmost Chilean Andes: *Geologische Rundschau*, v. 63, p. 484-490.
- Mortimer, C., Munchmeyer, C., and Urqueta, I., 1977, Emplacement of the Exótica orebody, Chile: *Institution of Mining and Metallurgy, Transactions, Section B, Applied Earth Science*, v. 86, p. B121-B127.
- Mote, T.I., Becker, T.A., Renne, P., and Brimhall, G.H., 2001a, Chronology of exotic mineralization at El Salvador, Chile, by $^{40}\text{Ar}/^{39}\text{Ar}$ dating of copper wad and supergene alunite: *Economic Geology*, v. 96, p. 351-366.
- Mote, T.I., Brimhall, G.H., Tidy-Finch, E., Muller, G., and Carrasco, P., 2001b, Application of mass-balance modeling of source, pathways, and sinks of supergene enrichment to

- exploration and discovery of the Quebrada Turquesa exotic copper orebody, El Salvador district, Chile: *Economic Geology*, v. 96, p. 367-386.
- Mpodozis, C., Marinovic, N., Smoje, I., 1993, Eocene left lateral strike slip faulting and clockwise block rotations in the Cordillera de Domeyko, west of Salar de Atacama, northern Chile: 2nd International Symposium on Andean Geodynamics, Oxford, United Kingdom, Institut de Recherche pour le Développement, Paris, p. 225-228.
- Mpodozis, C., Arriagda, C., and Roperch, P., 1999, Cretaceous to Paleogene geology of the Salar de Atacama Basin, northern Chile: a reappraisal of the Purilactis Group stratigraphy: 4th International Symposium on Andean Geodynamics, Göttingen, Germany, Institut de Recherche pour le Développement, Paris, p. 523-526.
- Münchmeyer, C., 1996, Exotic deposits – products of lateral migration of supergene solutions from porphyry copper deposits, *in* Camus, F., Sillitoe, R.H., and Petersen, R., eds., *Andean copper deposits: new discoveries, mineralization, style and metallogeny*: Society of Economic Geologists Special Publication 5, p. 43-58.
- Muñoz, N., and Charrier, R., 1996, Uplift of the western border of the Altiplano on a west-vergent thrust system, northern Chile: *Journal of South American Earth Sciences*, v. 9, p. 171-181.
- Muñoz, N., and Sepulveda, P., 1992, Estructuras compresivas con vergencia al Oeste en el borde oriental de la Depresión Central (19° 15' lat. Sur): *Revista Geológica de Chile* v. 19, p. 241-247.
- Nash, J.T., 1976, Fluid inclusion petrology-data from porphyry copper deposits and applications to exploration: U. S. Geological Survey Professional Paper 907-D, 16 p.
- Nishiizumi, K., Finkel, R.C., Brimhall, G.H., Mote, T., Mueller, G., and Tidy, E., 1998, Ancient exposure ages of alluvial fan surfaces compared with incised stream beds and bedrock in the Atacama Desert of north Chile [abs.]: Geological Society of America, Abstracts with Programs, 30 (7), p. 298.

- Noble, D.C., McKee, E.H., and Mégard, F., 1979, Early Tertiary “Incaic” tectonism, uplift, and volcanic activity, Andes of central Peru: *Geological Society of America Bulletin*, v. 90, p. 903-907.
- Norton, D.L., 1982, Fluid and heat transport phenomena typical of copper-bearing pluton environments; southeastern Arizona, *in* Titley, S.R., ed., *Advances in geology of porphyry copper deposits; southwestern North America*: University of Arizona Press, Tucson, p. 59-72.
- Norton, D.L., and Knapp, R., 1977, Transport phenomena in hydrothermal systems; the nature of porosity: *American Journal of Science*, v. 277, p. 913-936.
- Norton, D.L., and Knight, J.E., 1977, Transport phenomena in hydrothermal systems; cooling plutons: *American Journal of Science*, v. 277, p. 937-981.
- Okada, K., Hirabayashi, J., and Ossaka, J., 1982, Crystal structure of natroalunite and crystal chemistry of the alunite group: *Neues Jahrbuch für Mineralogie, Monatshefte* (12), p. 534-540.
- Osatenko, M.J., and Jones, M.B., 1976, Valley Copper, *in* Sutherland Brown, A., ed., *Porphyry deposits of the Canadian Cordillera*: Canadian Institute of Mining and Metallurgy, Special Volume 15, p. 130-143.
- Ossandón C., G., Fréaut C., R., Gustafson, L.B., Lindsay, D.D., and Zentilli, M., 2001, Geology of the Chuquicamata mine: A progress report: *Economic Geology*, v. 96, p. 249-270.
- Padilla G., R.A., Titley, S.R., and Pimental B., F., 2001, Geology of the Escondida porphyry copper deposit, Antofagasta Region, Chile: *Economic Geology*, v. 96, p. 307-324.
- Page, R., and Wenk, H.R., 1979, Phyllosilicate alteration of plagioclase studied by transmission electron microscopy: *Geology*, v. 7, p. 393-397.

- Palacios, C.M, Lahsen, A.A., and Sylvester, H., 1992, Low-sulfur epithermal gold mineralization at Inca de Oro, northern Chile: Mineralogy and fluid inclusions: *Journal of South American Earth Sciences*, v. 6, p. 183-189.
- Pardo-Casas, F., and Molnar, P., 1987, Relative motion of the Nazca (Farallón) and South America plates since late Cretaceous times: *Tectonics*, v. 6, p. 233-284.
- Parker, R.L., 1962, Isomorphous substitution in natural and synthetic alunite: *American Mineralogist*, v. 47, p. 127-136.
- Parry, W.T., Jasumback, M., and Wilson, P.N., 2002, Clay mineralogy of phyllic and intermediate argillic alteration at Bingham, Utah: *Economic Geology*, v. 97, p. 221-239.
- Parsons, A.B, 1933, *The porphyry coppers: The American Institute of Mining and Metallurgical Engineers*, New York, 581 p.
- Perry, E., and Hower, J., 1970, Burial diagenesis in Gulf Coast pelitic sediments: *Clays and Clay Minerals*, v. 18, p. 165-177.
- Pilger, R.H., Jr., 1984, Cenozoic plate kinematics, subduction and magmatism: *Journal of the Geological Society of London*, v. 141, p. 793-802.
- Porter, T.M., 1998, An overview of the world's porphyry and other hydrothermal copper and gold deposits and their distribution, *in* Porter, T.M., ed., *Porphyry and hydrothermal copper and gold deposits: a global perspective: Australian Mineral Foundation*, p. 3-17.
- Potter, R.W., II, 1977, Pressure correction for fluid-inclusion homogenization temperature based on the volumetric properties of the system NaCl-H₂O: *Journal of Research of the U.S. Geological Survey*, v. 5, p. 603-607.
- Preece, R.K., and Beane, R.E., 1986, Contrasting evolutions of hydrothermal alteration in quartz monzonite and quartz diorite wall rocks at the Sierrita porphyry copper deposit, Arizona: *Economic Geology*, v. 77, p. 1621-1641.

- Rae, A.J., Cooke, D.R., Phillips, D., Yeats, C., Ryan, C., and Hermoso, D., 2003, Spatial and temporal relationships between hydrothermal alteration assemblages at the Palinpinon geothermal field, Philippines [abs.]: implications for porphyry and epithermal ore deposits: Geological Association of Canada-Mineralogical Association of Canada annual meeting, Vancouver.
- Ranta, D.E., Ward, A.D., and Ganster, M.W., 1984, Ore zoning applied to geologic reserve estimation of molybdenum deposits, *in* Erickson, A.J., Jr., ed., Applied mining geology: Society of Mining Engineers of the American Institute of Mining, Metallurgical, and Petroleum Engineers, Inc., New York, p. 85-114.
- Raymo, M.E., and Ruddiman, W.F., 1992, Tectonic forcing of late Cenozoic climate: *Nature*, v. 359, p. 117-122.
- Reyes, A.G., 1990, Petrology of Philippine geothermal systems and the application of alteration mineralogy to their assessment: *Journal of Volcanology and Geothermal Research*, v. 43, p. 279-309.
- Reynolds, P., Ravenhurst, C., Zentilli, M., and Lindsay, D., 1998, High-precision $^{40}\text{Ar}/^{39}\text{Ar}$ dating of two consecutive hydrothermal events in the Chuquicamata porphyry copper system, Chile: *Chemical Geology*, v. 148, p. 45-60.
- Richards, J.P., Noble, S.R., and Pringle, M.S., 1999, A revised late Eocene age for porphyry Cu magmatism in the Escondida area, northern Chile: *Economic Geology*, v. 94, p. 1231-1247.
- Richards, J.P., Boyce, A.J., and Pringle, M.S., 2001, Geologic evolution of the Escondida area, northern Chile: A model for spatial and temporal localization of porphyry Cu mineralization: *Economic Geology*, v. 96, p. 271-305.
- Roedder, E., 1984, Fluid inclusions: Mineralogical Society of America, *Reviews in Mineralogy* v.12, 646 p.

- 1992, Optical microscopy identification of the phases in fluid inclusions in minerals: *The Microscope*, v. 40, p. 59-79.
- Roedder, E., and Bodnar, R.J., 1980, Geologic pressure determinations from fluid inclusion studies: *Annual Review of Earth and Planetary Sciences*, v. 8, p. 371-406.
- Rowins, S.M., and Williams-Jones, A. (convenors), 2003, Ore-forming processes in the porphyry copper (gold) and epithermal gold environments; what do we really know?: Special Session of the Geological Association of Canada-Mineralogical Association of Canada annual meeting, Vancouver.
- Rowland, M.G., 1998, The role of magmatic processes in the development of hypogene mineralisation at Quebrada Blanca, northern Chile: Unpublished Ph.D. thesis, University of London, 240p.
- Rowland, M.G., and Clark, A.H., 2001, Temporal overlap of supergene alteration and high-sulfidation mineralization in the Spence porphyry copper deposit, II Region, Chile [abs.]: *Geological Society of America, Abstracts with Programs*, v. 33, p. A-358.
- Rye, R.O., Bethke, P.M., and Wasserman, M.D., 1992, The stable isotope geochemistry of acid sulfate alteration: *Economic Geology*, v. 87, p. 225-262.
- Sales, R.H., and Meyer, C., 1948, Wall rock alteration at Butte, Montana: *Transactions of the American Institute of Mining and Metallurgical Engineers*, v. 178, p. 9-35.
- Sandeman, H.A., Clark, A.H., and Farrar, E., 1995, An integrated tectono-magmatic model for the evolution of the southern Peruvian Andes (13-20° S) since 55 Ma: *International Geology Review*, v. 37, p. 1039-1073.
- Sandeman, H.A., Archibald, D.A., Grant, J.W., Villeneuve, M.E., and Ford, F.D., 1999, Characterization of the chemical composition and ^{40}Ar - ^{39}Ar systematics of intralaboratory standard MAC-83 biotite: *Radiogenic Age and Isotopic Studies, Reports 12*, Geological Survey of Canada, Current Research 1999-F, p. 13-26

- Sasso, A.M., and Clark, A.H., 1998, The Farallón Negro Group, northwest Argentina: Magmatic, hydrothermal and tectonic evolution and implications for Cu-Au metallogeny in the Andean back-arc: Society of Economic Geologists Newsletter, no. 34. p. 1, 8-18.
- Semat, H., 1966, Fundamental of Physics, Fourth Edition: Holt, Rinehart and Winston Inc., 753 p.
- Servicio Nacional de Geología y Minería Chile, 1982, Mapa geológico de Chile, escala 1:1000,000, Hoja no 1 de 6, 17° 30' - 24° 00' Lat. S.
- Seyfried, W.E., Jr., and Bischoff, J.L., 1981, Experimental seawater-basalt interaction at 300°C, 500 bars, chemical exchange, secondary mineral formation and implications for the transport of heavy metals: *Geochimica et Cosmochimica Acta*, v. 45, p. 135-147.
- Seyfried, W.E., Jr, and Mottl, M.J., 1982, Hydrothermal alteration of basalt by seawater under seawater-dominated conditions: *Geochimica et Cosmochimica Acta*, v. 46, p. 985-1002.
- Scheuber, E., Bogdanic, T., Jensen, A., and Reutter, K.J., 1994, Tectonic development of the northern Chilean Andes in relation to plate convergence and magmatism since the Jurassic, *in* Reutter, K.J., Scheuber, E., and Wigger, P.J., eds., *Tectonics of the southern central Andes*: Springer-Verlag, Berlin, p. 121-139.
- Shepherd, T.J., Rankin, A.H., and Alderton, D.H.M., 1985, A practical guide to fluid inclusion studies: Blackie and Son Limited, Bishopbriggs, Glasgow, 239 p.
- Shinohara, H., and Hedenquist, J.W., 1997, Constraints on magma degassing beneath the Far Southeast porphyry Cu-Au deposit, Philippines: *Journal of Petrology*, v. 38, p. 1741-1752.
- Shinohara, H., Iiyama, J.T., and Matsuo, S., 1989, Partition of chlorine compounds between silicate melt and hydrothermal solutions; I, Partition of NaCl-KCl: *Geochimica et Cosmochimica Acta*, v. 53, p. 2617-2630.
- Sourirajan, S., and Kennedy, G.C., 1962, The system H₂O-NaCl at elevated temperatures and pressures: *American Journal of Science*, v. 260, p. 115-141.

- Sillitoe, R.H., 1969, Studies of the controls and mineralogy of the supergene alteration of copper deposits, northern Chile: Unpublished Ph.D. thesis, University of London, 498 p.
- 1972, A plate tectonic model for the origin of porphyry copper deposits: *Economic Geology*, v. 67, p. 184-197.
- 1983, Enargite-bearing massive sulfide deposits high in porphyry copper systems: *Economic Geology*, v. 78, p. 348-352.
- 1986, Space-time distribution, crustal setting and Cu/Mo ratios of central Andean porphyry copper deposits; metallogenic implications, *in* Friedrich, G.H., Genkin, A.D., Naldrett, Anthony J., Ridge, J.D., Sillitoe, R.H., and Vokes, F.M., eds., *Geology and metallogeny of copper deposits: Proceedings of the Copper Symposium; 27th international geological congress, Special Publication of the Society for Geology Applied to Mineral Deposits*, 4, p. 235-250.
- 1988, Epochs of intrusion-related copper mineralization in the Andes: *Journal of South American Earth Sciences*, v. 1, p. 89-108.
- 1997, Characteristics and controls of the largest porphyry copper-gold and epithermal gold deposits in the circum-Pacific region: *Australian Journal of Earth Sciences*, v. 44, p. 373-388.
- 2000, Exploration and discovery of base- and precious-metal deposits in the circum-Pacific region - a late 1990s update: *Resource Geology Special issue* 21, 65p.
- Sillitoe, R.H., and Clark, A.H., 1969, Copper and copper-iron sulfides as the initial products of supergene oxidation, Copiapó mining district, northern Chile: *American Mineralogist*, v. 54, p. 1684-1710.
- Sillitoe, R.H., and Gappe, I.M., Jr., 1984, Philippine porphyry copper deposits; geologic setting and characteristics: *Committee for Co-Ordination of Joint Prospecting for Mineral Resources in Asian Offshore Areas*, 89p.

- Sillitoe, R.H., and McKee, E.H., 1996, Age of supergene oxidation and enrichment in the Chilean porphyry copper province: *Economic Geology*, v. 91, p. 164-179.
- Sillitoe, R.H., Mortimer, C., and Clark, A.H., 1968, A chronology of landform evolution and supergene mineral alteration, southern Atacama Desert, Chile: *Institution of Mining and Metallurgy, Transactions, Section B*, v. 77, p. B166-B169.
- Simmons, S.F., and Browne, P.R.L., 2000, Hydrothermal minerals and precious metals in the Broadlands-Ohaaki geothermal system; implications for understanding low-sulfidation epithermal environments: *Economic Geology*, v. 95, p. 971-999.
- Steiger, R.H., and Jäger, E., 1977, Subcommittee on geochronology, convention on the use of decay constants in geo- and cosmochemistry: *Earth and Planetary Science Letters*, v. 36, p. 359-362.
- Steinmann, G., 1929, *Geologie von Peru*: Heidelberg, Carl Winters Universitäts, Buchhandlung, 448p.
- Stoffregen, R.E., and Alpers, C.N., 1987, Woodhouseite and svanbergite in hydrothermal ore deposits: products of apatite destruction during advanced argillic alteration: *Canadian Mineralogist*, v. 25, p. 201-211.
-
- 1992, Observations on the unit cell parameters, water contents and δD of natural and synthetic alunite: *American Mineralogist*, v. 77, p. 1092-1098.
- Stoffregen, R.E., and Cygan, G.L., 1990, An experimental study of Na-K exchange between alunite and aqueous sulfate solutions: *American Mineralogist*, v. 75, p. 209-220.
- Stoffregen, R.E., Alpers, C.N., and Jambor, J.L., 2000, Alunite-jarosite crystallography, thermodynamics, and geochronology, *in* Alpers, C.N., Jambor, J.L., and Nordstrom, D.K., eds., *Sulfate minerals, crystallography, geochemistry, and environmental significance: Reviews in Mineralogy and Geochemistry*, v. 40, Mineralogical Society of America, p. 453-479.

- Swayne, W.H., and Trask, F., 1960, Geology of El Salvador: Mining Engineering, v. 12, p. 344-348.
- Taylor, A.V., Jr., 1935, Ore deposits of Chuquicamata, Chile: 16th International Geological Congress, Washington D.C., Proceedings, v. 2, p. 473-484.
- Thomas N., A., 1967, Carta geológica de Chile: Cuadrángulo Mamiña, Provincia de Tarapacá, Escala 1:50,000: Instituto de Investigaciones Geológicas de Chile, Carta no. 17, 49 p.
- Titley, S.R., 1978, Geologic history, hypogene features and processes of secondary sulfide enrichment at the Plesyumi copper prospect, New Britain, Papua New Guinea: Economic Geology, v. 73, p.768-784.
- 1993, Characteristics of porphyry copper occurrence in the American Southwest, *in* Kirkham, R.V., Sinclair, W.D., Thorpe, R.I., and Duke, J.M., eds., Mineral deposit modeling: Geological Association of Canada Special Paper 40, p. 433-464.
- 1995a, Process and products of supergene copper enrichment, *in* Pierce, F.W. and Bolm, J.G. eds., Porphyry copper deposits of the American Cordillera: Arizona Geological Society Digest 20, p.156-168.
- 1995b, Size aspects of porphyry copper systems, southwestern North America, *in* Clark, A.H., ed., Giant ore deposits – II, Controls on the scale of orogenic magmatic-hydrothermal mineralization: Proceedings of the second giant ore deposits workshop: Department of Geological Sciences, Queen's University, Kingston, Ontario, p. 374-401.
- Titley, S.R., and Beane, R.E., 1981, Porphyry copper deposits; Part I, Geologic settings, petrology, and tectogenesis, *in* Skinner, B.J. eds., Economic Geology 75th Anniversary Volume, p. 214-235.
- Titley, S.R., Thompson, R.C., Haynes, F.M., Manske, S.L., Robison, L.C., and White, J.L., 1986, Evolution of fractures and alteration in the Sierrita-Esperanza hydrothermal system, Pima County, Arizona: Economic Geology, v. 81, p. 343-370.

- Tomasson, J., and Kristmannsdottir, H., 1972, high temperature alteration minerals and thermal brines, Reykjanes, Iceland: *Contributions to Mineralogy and Petrology*, v. 36, p. 123-134.
- Tomlinson, A., and Blanco, N., 1997, Structural evolution and displacement history of the West Fault system, Precordillera, Chile: Part 1. Premineral history, Part 2. Synmineral history: *VIII Congreso Geológico Chileno, Antofagasta*, v. III, p. 1873-1882.
- Torrible, 2002, *Copper: The Mining Journal Annual Review 2002*.
- Tosdal, R.M., 1978, The timing of the geomorphic and tectonic evolution of the southwesternmost Peruvian Andes: Unpublished M.Sc. thesis, Queen's University, Kingston, Ontario, 136p.
- Tosdal, R.M., and Richards, J.P., 2001, Magmatic and structural controls on the development of porphyry Cu \pm Mo \pm Au deposits: *Economic Geology Reviews*, v.14, p. 157-181.
- Tosdal, R.M., Farrar, E., Clark, A.H., 1981, K-Ar geochronology of the late Cenozoic volcanic rocks of the Cordillera Occidental, southernmost Peru: *Journal of Volcanology and Geothermal Research*, v. 10, p. 157-173.
- Tosdal, R.M., Clark, A.H., and Farrar, E., 1984, Cenozoic polyphase landscape and tectonic evolution of the Cordillera Occidental, southernmost Peru: *Geological Society of America Bulletin*, v. 95, p. 1318-1332.
- Ulrich, T., Guenther, D., and Heinrich, C.A., 2001, The evolution of a porphyry Cu-Au deposit, based on LA-ICP-MS analysis of fluid inclusions; Bajo de la Alumbrera, Argentina: *Economic*, v. 96, p. 1743-1774.
- Urusova, M.A., 1975, Volume properties of aqueous solutions of sodium chloride at elevated temperatures and pressures: *Russian Journal of Inorganic Chemistry*, v. 20, p. 1717-1721.
- Vasconcelos, P.M., 1999, K-Ar and $^{40}\text{Ar}/^{39}\text{Ar}$ geochronology of weathering processes: *Annual Review of Earth Planetary Sciences*, v. 27, p. 183-229.

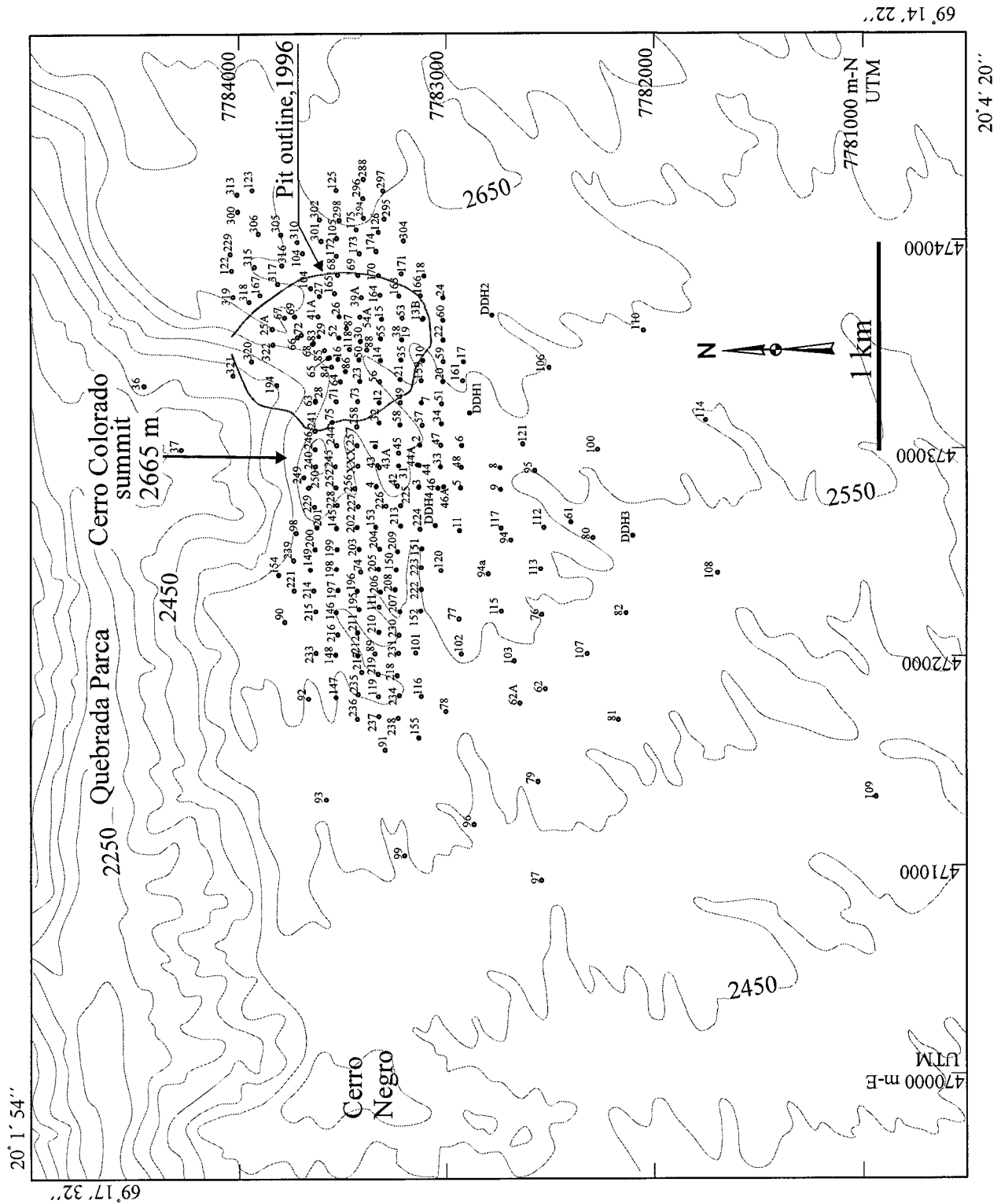
- Vasconcelos, P.M., Brimhall, G.H., Becker, T.A., and Renne, P.R., 1994, $^{40}\text{Ar}/^{39}\text{Ar}$ analysis of supergene jarosite and alunite: Implications to the paleoweathering history of the western USA and West Africa: *Geochimica et Cosmochimica Acta*, v. 58, p. 401-420.
- Velde, B., 1992, The stability of clays, *in* Price, G.D., and Ross, N.L., eds., *The stability of minerals*: Chapman and Hall, p. 329-351.
- Vergara, M., Marangunic, C., Bellón, H., and Brousse, R., 1986, Edades K-Ar de las ignimbritas de las quebradas Juan de Morales y Sagasca, norte de Chile: *Comunicaciones, Universidad de Chile*, Santiago, no. 36, p. 1-7.
- Watanabe, Y., and Hedenquist, J.W., 2001, Mineralogic and stable isotope zonation at the surface over the El Salvador porphyry copper deposit, Chile: *Economic Geology*, v. 96, p.1755-1797.
- Webster, J.D., 1992a, Fluid-melt interactions involving Cl-rich granites; experimental study from 2 to 8 kbar: *Geochimica et Cosmochimica Acta*, v. 56, p. 659-678.
- 1992b, Water solubility and chlorine partitioning in Cl-rich granitic systems; effects of melt composition at 2 kbar and 800°C: *Geochimica et Cosmochimica Acta*, v. 56, p. 679-687.
- 1997, Exsolution of magmatic volatile phases from Cl-enriched mineralizing granitic magmas and implications for ore metal transport: *Geochimica et Cosmochimica Acta*, v. 61, p. 1017-1029.
- Weissberg, B.G., Browne, P.R.L., and Seward, T.M., 1979, Ore metals in active geothermal systems, *in* Barnes, H.L., *Geochemistry of hydrothermal ore deposits*, 2 edition: John Wiley and Sons, p. 738-780.
- Wertime, T.A., 1964, Man's first encounters with metallurgy: *Science*, v. 146, p. 1257-1267.
- White, D.E., 1981, Active geothermal systems and hydrothermal ore deposits, *in* Skinner, B.J. eds., *Economic Geology 75th Anniversary Volume*, p. 392-423.

- Whitney, J.A., 1975a, The effects of pressure, temperature, and XH_2O on phase assemblage in four synthetic rock compositions: *Journal of Geology*, v. 83, p. 1-31.
- 1975b, Vapor generation in a quartz monzonite magma; a synthetic model with application to porphyry copper deposits: *Economic Geology*, v. 70, p. 346-358.
- 1989, Origin and evolution of silicic magmas: *in* Whitney, J.A. and Naldrett, A.J., eds., *Ore deposition associated with magmas: Reviews in Economic Geology*, v. 4, p. 183-201.
- Williams, A.E., and McKibben, Michael A., 1989, A brine interface in the Salton Sea geothermal system, California; fluid geochemical and isotopic characteristics: *Geochimica et Cosmochimica Acta*, v. 53, p. 1905-1920.
- Williams, S.A., and Cesbron, F.P., 1977, Rutile and apatite; useful prospecting guides for porphyry copper deposits: *Mineralogical Magazine*, v. 41, p. 288-292.
- Williams, T.J., Candela, P.A., and Piccoli, P.M., 1991, An experimental determination of copper partitioning between a water saturated high-silica rhyolite and a chloride-bearing two-phase aqueous mixture at 800°C and 1 kilobar [abs.]: *Geological Society of America, Programs with Abstracts*, v. 23, p. A291.
- Williams, T.J., Candela, P.A., and Piccoli, P.M., 1992, The partitioning of copper between a high-silica rhyolite and a chloride-bearing, two-phase aqueous mixture; comparison of experimental results at 1 kilobar, 800°C, and ½ kilobar, 850°C [abs.]: *EOS*, v. 73, p. 606.
- Williams, T.J., Candela, P.A., and Piccoli, P.M., 1995, The partitioning of copper between silicate melts and two-phase aqueous fluids; an experimental investigation at 1 kbar, 800°C and 0.5 kbar, 850°C: *Contributions to Mineralogy and Petrology*, v. 121, p. 388-399.
- Xiao, Z., Gammons, C.H., and Williams-Jones, A.E., 1998, Experimental study of copper chloride complexing in hydrothermal solutions at 40 to 300°C and saturated water vapor pressure: *Geochimica et Cosmochimica Acta*, v. 62, p. 2949-2964.

Yau, Y., Peacor, D.R., Beane, R.E., Essene, E.J., and McDowell, S.D., 1988, Microstructures, formation mechanisms, and depth-zoning of phyllosilicates in geothermally altered shales, Salton Sea, California: *Clays and Clay Minerals*, v. 36, p. 1-10

APPENDIX 1

Drill-hole map, Cerro Colorado



APPENDIX 2

Composition of Hydrothermal Phyllosilicate Minerals, Cerro Colorado

| Sample number | Biotite (magnetic? BQPP) | | | | Biotite (from biotite-albite-magnetite alteration) | | | | | | | | | | | |
|--------------------------------|--------------------------|-------|-------|-------|--|--------|--------|--------|--------|--------|--------|--------|--------|--------|--------|--------|
| | 83-18 | 83-18 | 83-18 | 83-18 | 83-54 | 83-54 | 83-54 | 83-58 | 83-58 | 83-58 | 83-58 | 83-58 | 83-58 | 83-58 | 83-58 | 83-58 |
| Elevation (m a.s.l.) | 2136 | 2136 | 2136 | 2136 | 2221.8 | 2221.8 | 2221.8 | 2231.3 | 2231.3 | 2231.3 | 2231.3 | 2231.3 | 2231.3 | 2231.3 | 2231.3 | 2231.3 |
| Analyzed point | a1 | a2 | b1 | b2 | a | b | a1 | a2 | b | c1 | c2 | a1 | a2 | a1 | a2 | b |
| SiO ₂ | 37.29 | 37.47 | 37.75 | 38.44 | 38.23 | 38.02 | 37.74 | 38.19 | 39.97 | 39.26 | 38.95 | 37.26 | 37.33 | 39.14 | 204-21 | 204-21 |
| TiO ₂ | 3.88 | 4.03 | 3.14 | 3.2 | 3.15 | 2.96 | 3.5 | 3.8 | 2.53 | 3.13 | 3.07 | 3.12 | 3.4 | 2.77 | 3.19 | 3.19 |
| Al ₂ O ₃ | 15.2 | 15.21 | 15.82 | 15.9 | 16.74 | 16.56 | 15.61 | 15.55 | 14.65 | 14.65 | 14.95 | 16.49 | 16.32 | 16.04 | 16.4 | 16.4 |
| FeO | 13.26 | 13.55 | 12.41 | 13.01 | 12.25 | 14.36 | 14.87 | 14.67 | 14.06 | 12.92 | 12.75 | 15.43 | 15.48 | 12.26 | 13.05 | 13.05 |
| MnO | 0.24 | 0.11 | — | — | — | — | — | — | — | — | — | — | 0.17 | — | 0.13 | 0.13 |
| MgO | 14.57 | 14.32 | 14.72 | 14.93 | 15.57 | 14.06 | 13.98 | 13.87 | 15.67 | 16.69 | 16.37 | 13.93 | 14.04 | 16.24 | 15.31 | 15.31 |
| CaO | 0.07 | — | — | — | — | 0.05 | 0.09 | 0.11 | 0.14 | 0.09 | 0.1 | — | 0.07 | 0.15 | — | — |
| Na ₂ O | 0.11 | — | — | — | 0.19 | 0.12 | 0.13 | 0.13 | 0 | 0.18 | 0.16 | — | — | — | — | — |
| K ₂ O | 9.41 | 9.18 | 9.75 | 9.6 | 9.6 | 9.52 | 9.39 | 9.19 | 8.95 | 8.66 | 8.77 | 9.73 | 9.74 | 9.9 | 10 | 10 |
| Cl | 0.15 | 0.16 | 0.18 | 0.13 | 0.17 | 0.21 | 0.13 | 0.23 | 0.18 | 0.19 | 0.16 | 0.25 | 0.26 | 0.17 | 0.23 | 0.23 |
| F | 0.72 | 0.79 | 0.76 | 0.68 | NA | 0.71 | NA | NA | NA | NA | NA | 0.27 | 0.44 | 0.80 | 0.85 | 0.85 |
| H ₂ O ¹ | 3.63 | 3.60 | 3.61 | 3.72 | 4.07 | 3.69 | 4.00 | 4.00 | 4.07 | 4.06 | 4.05 | 3.86 | 3.80 | 3.73 | 3.64 | 3.64 |
| Total | 98.53 | 98.42 | 98.14 | 99.61 | 99.97 | 100.26 | 99.44 | 99.74 | 100.22 | 99.83 | 99.33 | 100.34 | 101.05 | 101.20 | 100.56 | 100.56 |
| Si | 5.60 | 5.62 | 5.66 | 5.67 | 5.59 | 5.61 | 5.62 | 5.65 | 5.84 | 5.73 | 5.72 | 5.53 | 5.51 | 5.67 | 5.55 | 5.55 |
| Al | 2.40 | 2.38 | 2.34 | 2.33 | 2.41 | 2.39 | 2.38 | 2.35 | 2.16 | 2.27 | 2.28 | 2.47 | 2.49 | 2.33 | 2.45 | 2.45 |
| Al | 0.29 | 0.32 | 0.45 | 0.44 | 0.47 | 0.49 | 0.35 | 0.36 | 0.36 | 0.26 | 0.30 | 0.41 | 0.35 | 0.41 | 0.40 | 0.40 |
| Ti | 0.44 | 0.46 | 0.35 | 0.36 | 0.35 | 0.33 | 0.39 | 0.42 | 0.28 | 0.34 | 0.34 | 0.35 | 0.38 | 0.30 | 0.35 | 0.35 |
| Fe | 1.67 | 1.70 | 1.56 | 1.61 | 1.50 | 1.77 | 1.85 | 1.82 | 1.72 | 1.58 | 1.57 | 1.92 | 1.91 | 1.49 | 1.61 | 1.61 |
| Mn | 0.03 | 0.01 | 0.00 | 0.00 | 0.00 | 0.00 | 0.00 | 0.00 | 0.00 | 0.00 | 0.00 | 0.00 | 0.02 | 0.00 | 0.02 | 0.02 |
| Mg | 3.26 | 3.20 | 3.29 | 3.28 | 3.39 | 3.09 | 3.10 | 3.06 | 3.41 | 3.63 | 3.58 | 3.08 | 3.09 | 3.51 | 3.36 | 3.36 |
| Ca | 0.01 | 0.00 | 0.00 | 0.00 | 0.00 | 0.01 | 0.01 | 0.02 | 0.02 | 0.01 | 0.02 | 0.00 | 0.01 | 0.02 | 0.00 | 0.00 |
| Na | 0.03 | 0.00 | 0.00 | 0.00 | 0.05 | 0.03 | 0.04 | 0.04 | 0.00 | 0.05 | 0.05 | 0.00 | 0.00 | 0.00 | 0.00 | 0.00 |
| K | 1.80 | 1.76 | 1.86 | 1.81 | 1.79 | 1.79 | 1.78 | 1.74 | 1.67 | 1.61 | 1.64 | 1.84 | 1.84 | 1.83 | 1.88 | 1.88 |
| Cl | 0.04 | 0.04 | 0.05 | 0.03 | 0.04 | 0.05 | 0.03 | 0.06 | 0.05 | 0.05 | 0.04 | 0.06 | 0.07 | 0.04 | 0.06 | 0.06 |
| F | 0.34 | 0.38 | 0.36 | 0.32 | 0.00 | 0.33 | 0.00 | 0.00 | 0.00 | 0.00 | 0.00 | 0.13 | 0.21 | 0.37 | 0.40 | 0.40 |
| OH | 3.64 | 3.60 | 3.61 | 3.66 | 3.96 | 3.63 | 3.97 | 3.95 | 3.96 | 3.96 | 3.97 | 3.82 | 3.74 | 3.61 | 3.57 | 3.57 |

| Biotite (biotite-albite-magnetite alteration) | | | | | | Chlorite (from sericite-chlorite-caly alteration) | | | | | | | | | | | | | |
|---|--------|-------|-------|-------|-------|---|--------|--------|--------|--------|--------|--------|--------|--------|--------|---------|---------|--------|--|
| Sample number | 25-9 | 25-9 | 25-9 | 25-9 | 25-9 | 83-54 | 83-54 | 83-54 | 83-54 | 83-58 | 83-58 | 83-58 | 83-58 | 210-10 | 210-10 | 153-13 | 153-13 | 206-22 | |
| Elevation (m a.s.l.) | 2422 | 2422 | 2422 | 2422 | 2422 | 2221.8 | 2221.8 | 2221.8 | 2221.8 | 2231.3 | 2231.3 | 2231.3 | 2231.3 | 2252.5 | 2252.5 | 2289.07 | 2289.07 | 2299.5 | |
| Analyzed point | al | a2 | b1 | b2 | b2 | c1 | c2 | d | d1 | d2 | e | a1 | a2 | a1 | a2 | a1 | a2 | al | |
| SiO ₂ | 37.07 | 37.47 | 37.42 | 37.61 | 37.61 | 27.13 | 27.15 | 27.39 | 27.25 | 27.36 | 27.2 | 27.43 | 27.28 | 27.5 | 27.33 | 27.5 | 27.33 | 27.5 | |
| TiO ₂ | 2.89 | 3.03 | 3.43 | 3.48 | 3.48 | — | 0.09 | 0.1 | 0.08 | 0.15 | 0.17 | 0.1 | 0.07 | 0.09 | 0.11 | — | — | — | |
| Al ₂ O ₃ | 16.44 | 16.77 | 16.16 | 15.53 | 15.53 | 22.39 | 21.79 | 20.6 | 20.63 | 20.35 | 21.01 | 22.06 | 22.46 | 22.74 | 22.95 | 23.49 | 22.95 | 23.49 | |
| FeO | 15.19 | 14.7 | 14.5 | 14.29 | 14.29 | 15.47 | 15.31 | 18.41 | 17.28 | 17.88 | 17.78 | 11.76 | 12.64 | 10.37 | 10.27 | 9.74 | 10.27 | 9.74 | |
| MnO | — | 0.12 | 0.11 | — | — | 0.12 | 0.21 | 0.28 | 0.29 | 0.25 | 0.12 | 0.08 | 0.08 | — | — | 0.07 | — | 0.07 | |
| MgO | 14.53 | 13.77 | 14.13 | 14.37 | 14.37 | 22.13 | 21.87 | 20.72 | 20.55 | 20.61 | 20.04 | 24.31 | 24.29 | 25.66 | 24.82 | 25.32 | 24.82 | 25.32 | |
| CaO | 0.06 | — | 0.15 | 0.48 | 0.48 | 0.08 | 0.08 | 0.14 | — | 0.06 | 0.08 | 0.16 | — | 0.14 | 0.07 | 0.06 | 0.07 | 0.06 | |
| Na ₂ O | 0.26 | — | 0.12 | 0.11 | 0.11 | — | — | — | — | — | — | — | — | — | — | — | — | — | |
| K ₂ O | 9.45 | 9.39 | 9.29 | 9.39 | 9.39 | 0.07 | — | — | 0.04 | — | 0.04 | — | 0.09 | — | 0.06 | — | 0.06 | — | |
| Cl | 0.23 | 0.26 | 0.23 | 0.2 | 0.2 | 0.02 | — | — | 0.05 | 0.03 | — | 0.06 | — | 0.02 | — | — | — | — | |
| F | NA | NA | NA | NA | NA | NA | NA | NA | NA | NA | NA | NA | NA | NA | NA | NA | NA | NA | |
| H ₂ O | 3.99 | 3.98 | 3.99 | 3.99 | 3.99 | 11.99 | 11.88 | 11.82 | 11.68 | 11.72 | 11.72 | 12.01 | 12.10 | 12.20 | 12.09 | 12.21 | 12.09 | 12.21 | |
| Total | 100.11 | 99.49 | 99.53 | 99.45 | 99.45 | 99.40 | 98.38 | 99.46 | 97.85 | 98.41 | 98.16 | 97.97 | 99.01 | 98.72 | 97.70 | 98.39 | 97.70 | 98.39 | |
| Si | 5.50 | 5.57 | 5.56 | 5.59 | 5.59 | 5.43 | 5.48 | 5.56 | 5.59 | 5.60 | 5.57 | 5.47 | 5.41 | 5.41 | 5.42 | 5.40 | 5.42 | 5.40 | |
| Al | 2.50 | 2.43 | 2.44 | 2.41 | 2.41 | 2.57 | 2.52 | 2.44 | 2.41 | 2.40 | 2.43 | 2.53 | 2.59 | 2.59 | 2.58 | 2.60 | 2.58 | 2.60 | |
| Al | 0.38 | 0.50 | 0.39 | 0.32 | 0.32 | 2.70 | 2.67 | 2.48 | 2.58 | 2.50 | 2.64 | 2.66 | 2.65 | 2.68 | 2.79 | 2.84 | 2.79 | 2.84 | |
| Ti | 0.32 | 0.34 | 0.38 | 0.39 | 0.39 | 0.00 | 0.01 | 0.02 | 0.01 | 0.02 | 0.03 | 0.02 | 0.01 | 0.01 | 0.02 | 0.00 | 0.02 | 0.00 | |
| Fe | 1.89 | 1.83 | 1.80 | 1.78 | 1.78 | 2.59 | 2.59 | 3.12 | 2.97 | 3.06 | 3.05 | 1.96 | 2.10 | 1.71 | 1.70 | 1.60 | 1.70 | 1.60 | |
| Mn | 0.00 | 0.02 | 0.01 | 0.00 | 0.00 | 0.02 | 0.04 | 0.05 | 0.05 | 0.04 | 0.02 | 0.01 | 0.01 | 0.00 | 0.00 | 0.01 | 0.00 | 0.01 | |
| Mg | 3.21 | 3.05 | 3.13 | 3.19 | 3.19 | 6.60 | 6.59 | 6.27 | 6.29 | 6.28 | 6.12 | 7.23 | 7.18 | 7.52 | 7.34 | 7.41 | 7.34 | 7.41 | |
| Ca | 0.01 | 0.00 | 0.02 | 0.08 | 0.08 | 0.02 | 0.02 | 0.03 | 0.00 | 0.01 | 0.02 | 0.03 | 0.00 | 0.03 | 0.02 | 0.01 | 0.02 | 0.01 | |
| Na | 0.08 | 0.00 | 0.04 | 0.03 | 0.03 | 0.00 | 0.00 | 0.00 | 0.00 | 0.00 | 0.00 | 0.00 | 0.00 | 0.00 | 0.00 | 0.00 | 0.00 | 0.00 | |
| K | 1.79 | 1.78 | 1.76 | 1.78 | 1.78 | 0.02 | 0.00 | 0.00 | 0.01 | 0.00 | 0.01 | 0.00 | 0.02 | 0.00 | 0.02 | 0.00 | 0.02 | 0.00 | |
| Cl | 0.06 | 0.07 | 0.06 | 0.05 | 0.05 | 0.01 | 0.00 | 0.00 | 0.02 | 0.01 | 0.00 | 0.02 | 0.00 | 0.01 | 0.00 | 0.00 | 0.00 | 0.00 | |
| F | 0.00 | 0.00 | 0.00 | 0.00 | 0.00 | 0.00 | 0.00 | 0.00 | 0.00 | 0.00 | 0.00 | 0.00 | 0.00 | 0.00 | 0.00 | 0.00 | 0.00 | 0.00 | |
| OH | 3.95 | 3.94 | 3.95 | 3.96 | 3.96 | 16.00 | 16.00 | 16.00 | 15.99 | 15.99 | 16.00 | 15.99 | 16.00 | 16.00 | 16.00 | 16.00 | 16.00 | 16.00 | |

| Sample number | Chlorite (from SCC alteration) | | | | | Muscovite (from sericite-chlorite-clay alteration) | | | | | | | | | | | |
|--------------------------------|--------------------------------|--------|--------|--------|--------|--|--------|--------|--------|--------|--------|--------|--------|--------|--------|--------|--------|
| | 206-22 | 206-10 | 206-10 | 206-10 | 206-10 | 83-54 | 83-54 | 206-10 | 206-10 | 206-10 | 210-10 | 210-10 | 206-22 | 206-22 | 204-11 | 204-11 | 204-21 |
| Elevation (m a.s.l.) | 2299.5 | 2299.5 | 2299.5 | 2299.5 | 2299.5 | 2221.8 | 2221.8 | 2249.9 | 2249.9 | 2249.9 | 2252.5 | 2252.5 | 2281.5 | 2281.5 | 2318 | 2318 | 2347.6 |
| Analyzed point | a2 | a1 | a2 | a2 | a2 | e1 | e2 | b1 | b2 | b2 | b1 | b2 | b1 | b2 | a1 | a2 | c1 |
| SiO ₂ | 28 | 28.5 | 28.76 | 28.76 | 28.76 | 45.23 | 44.08 | 46.18 | 45.97 | 45.97 | 45.52 | 45.41 | 45.25 | 45.21 | 46.5 | 45.51 | 43.21 |
| TiO ₂ | — | — | 0.1 | 0.1 | 0.1 | 0.1 | 0.08 | 0.23 | 0.21 | 0.21 | 0.53 | 0.54 | 0.42 | 0.35 | 0.43 | 0.8 | 0.52 |
| Al ₂ O ₃ | 22.83 | 20.95 | 20.23 | 20.23 | 20.23 | 29.12 | 29.44 | 32.68 | 33.17 | 33.17 | 31.98 | 33.32 | 32.01 | 32.05 | 31.11 | 32.8 | 30.2 |
| FeO | 6.41 | 9.68 | 9.38 | 9.38 | 9.38 | 3.96 | 4.24 | 0.84 | 0.85 | 0.85 | 2.91 | 2.62 | 1.89 | 1.87 | 1.59 | 1.96 | 1.99 |
| MnO | 0.14 | 0.42 | 0.31 | 0.31 | 0.31 | 0.1 | — | — | — | — | — | — | — | — | — | — | — |
| MgO | 27.8 | 26.64 | 26.7 | 26.7 | 26.7 | 5.61 | 6.49 | 3.29 | 3.09 | 3.09 | 2.27 | 1.71 | 3.53 | 3.69 | 4.38 | 2.1 | 3.38 |
| CaO | 0.08 | — | — | — | — | 0.09 | 0.06 | 0.15 | 0.13 | 0.13 | — | — | — | — | 0.05 | 0 | 0.09 |
| Na ₂ O | — | — | — | — | — | 0.13 | 0.18 | 0.2 | 0.28 | 0.28 | 0.4 | 0.42 | 0.3 | 0.36 | 0.28 | 0.33 | 0.18 |
| K ₂ O | — | — | — | — | — | 10.8 | 10.67 | 10.35 | 10.65 | 10.65 | 10.44 | 10.47 | 10.46 | 10.59 | 10.79 | 10.66 | 10.32 |
| Cl | 0.05 | — | — | — | — | 0.05 | 0.09 | — | — | — | — | — | 0.05 | — | — | 0.03 | — |
| F | NA | NA | NA | NA | NA | 0.46 | 0.4 | 0.35 | 0.34 | 0.34 | NA | NA | NA | NA | NA | NA | 0.13 |
| H ₂ O | 12.28 | 12.18 | 12.11 | 12.11 | 12.11 | 4.17 | 4.18 | 4.29 | 4.30 | 4.30 | 4.40 | 4.43 | 4.39 | 4.41 | 4.46 | 4.41 | 4.14 |
| Total | 97.59 | 98.37 | 97.59 | 97.59 | 97.59 | 99.82 | 99.91 | 98.56 | 98.99 | 98.99 | 98.45 | 98.92 | 98.30 | 98.53 | 99.59 | 98.60 | 94.16 |
| Si | 5.47 | 5.61 | 5.70 | 5.70 | 5.70 | 6.18 | 6.04 | 6.23 | 6.19 | 6.19 | 6.21 | 6.15 | 6.16 | 6.15 | 6.25 | 6.18 | 6.17 |
| Al | 2.53 | 2.39 | 2.30 | 2.30 | 2.30 | 1.82 | 1.96 | 1.77 | 1.81 | 1.81 | 1.79 | 1.85 | 1.84 | 1.85 | 1.75 | 1.82 | 1.83 |
| Al | 2.72 | 2.47 | 2.42 | 2.42 | 2.42 | 2.87 | 2.79 | 3.43 | 3.45 | 3.45 | 3.35 | 3.47 | 3.30 | 3.29 | 3.18 | 3.42 | 3.25 |
| Ti | 0.00 | 0.00 | 0.02 | 0.02 | 0.02 | 0.01 | 0.01 | 0.02 | 0.02 | 0.02 | 0.05 | 0.06 | 0.04 | 0.04 | 0.04 | 0.08 | 0.06 |
| Fe | 1.05 | 1.59 | 1.55 | 1.55 | 1.55 | 0.45 | 0.49 | 0.10 | 0.10 | 0.10 | 0.33 | 0.30 | 0.22 | 0.21 | 0.18 | 0.22 | 0.24 |
| Mn | 0.02 | 0.07 | 0.05 | 0.05 | 0.05 | 0.01 | 0.00 | 0.00 | 0.00 | 0.00 | 0.00 | 0.00 | 0.00 | 0.00 | 0.00 | 0.00 | 0.00 |
| Mg | 8.09 | 7.82 | 7.88 | 7.88 | 7.88 | 1.14 | 1.33 | 0.66 | 0.62 | 0.62 | 0.46 | 0.35 | 0.72 | 0.75 | 0.88 | 0.43 | 0.72 |
| Ca | 0.02 | 0.00 | 0.00 | 0.00 | 0.00 | 0.01 | 0.01 | 0.02 | 0.02 | 0.02 | 0.00 | 0.00 | 0.00 | 0.00 | 0.01 | 0.00 | 0.01 |
| Na | 0.00 | 0.00 | 0.00 | 0.00 | 0.00 | 0.03 | 0.05 | 0.05 | 0.07 | 0.07 | 0.11 | 0.11 | 0.08 | 0.10 | 0.07 | 0.09 | 0.05 |
| K | 0.00 | 0.00 | 0.00 | 0.00 | 0.00 | 1.88 | 1.86 | 1.78 | 1.83 | 1.83 | 1.82 | 1.81 | 1.82 | 1.84 | 1.85 | 1.85 | 1.88 |
| Cl | 0.02 | 0.00 | 0.00 | 0.00 | 0.00 | 0.01 | 0.02 | 0.00 | 0.00 | 0.00 | 0.00 | 0.00 | 0.01 | 0.00 | 0.00 | 0.01 | 0.00 |
| F | 0.00 | 0.00 | 0.00 | 0.00 | 0.00 | 0.20 | 0.17 | 0.15 | 0.15 | 0.15 | 0.00 | 0.00 | 0.00 | 0.00 | 0.00 | 0.00 | 0.06 |
| OH | 15.99 | 16.00 | 16.00 | 16.00 | 16.00 | 3.80 | 3.82 | 3.86 | 3.86 | 3.86 | 4.00 | 4.00 | 3.99 | 4.00 | 4.00 | 3.99 | 3.94 |

| Sample number | Muscovite (SCC) | | | Muscovite (from quartz-sericite-clay) | | | | | | Muscovite (from advanced argillite alteration) | | | | | | | | | | | |
|--------------------------------|-----------------|--------|--------|---------------------------------------|--------|--------|--------|--------|--------|--|--------|-------|-------|-------|-------|-------|-------|-------|-------|-------|-------|
| | 204-21 | 204-21 | 204-21 | 206-39 | 206-39 | 206-39 | 204-24 | 204-24 | 204-24 | 199-9 | 199-9 | 199-9 | 199-9 | 199-9 | 199-9 | 199-9 | 199-9 | 199-9 | 199-9 | 199-9 | 199-9 |
| Elevation (m a.s.l.) | 2347.6 | 2347.6 | 2347.6 | 2350.4 | 2350.4 | 2350.4 | 2357.4 | 2357.4 | 2357.4 | 2285 | 2285 | 2285 | 2285 | 2285 | 2285 | 2285 | 2285 | 2285 | 2285 | 2285 | 2285 |
| Analyzed point | c2 | c3 | | a1 | a2 | a1 | a2 | a1 | a2 | c1 | c2 | d1 | d2 | a1 | a2 | a1 | a2 | a1 | a2 | a1 | a2 |
| SiO ₂ | 45.78 | 45.46 | | 45.29 | 45.72 | 46.48 | 46.6 | | | 45.7 | 46.08 | 45.71 | 46.61 | 44.37 | 45.6 | 46.15 | 46.93 | 48.25 | 48.9 | | |
| TiO ₂ | 0.48 | 0.45 | | 0.75 | 0.44 | 0.57 | 0.51 | | | 0.73 | 0.72 | 0.58 | 0.51 | 0.4 | 0.47 | 0.07 | 0.27 | — | — | | |
| Al ₂ O ₃ | 32.64 | 32.61 | | 33.06 | 34.06 | 34.76 | 34.86 | | | 34.71 | 34.71 | 36.15 | 34.89 | 31.48 | 31.78 | 35.48 | 34.87 | 34.93 | 34.99 | | |
| FeO | 2.47 | 2.46 | | 3.54 | 2.69 | 1.74 | 1.52 | | | 2.17 | 2.52 | 1.55 | 1.01 | 4.23 | 3.56 | 1 | 0.6 | 1.03 | 0.72 | | |
| MnO | — | — | | 0.09 | — | — | — | | | — | — | — | — | — | 0.08 | — | — | — | 0.1 | | |
| MgO | 2.83 | 2.59 | | 1.48 | 1.12 | 0.69 | 0.79 | | | 0.69 | 0.78 | 0.25 | 0.93 | 3.33 | 2.75 | 1.15 | 0.89 | 0.43 | 0.41 | | |
| CaO | — | — | | — | 0.1 | 0 | 0.09 | | | — | — | 0.06 | — | 0.09 | 0.07 | — | — | 0.18 | 0.25 | | |
| Na ₂ O | 0.36 | 0.37 | | 0.53 | 0.37 | 0.6 | 0.51 | | | 0.48 | 0.55 | 0.5 | 0.53 | 0.32 | 0.39 | 0.35 | 0.4 | 0.14 | 0.21 | | |
| K ₂ O | 10.54 | 10.53 | | 10.6 | 10.28 | 10.28 | 10.27 | | | 10.17 | 10.16 | 10.6 | 9.78 | 10.8 | 10.5 | 10.57 | 9.98 | 9.72 | 9.55 | | |
| Cl | 0.05 | — | | — | 0.05 | 0.03 | — | | | 0.03 | 0.03 | — | 0.07 | 0.14 | 0.05 | 0.04 | 0.05 | — | 0.04 | | |
| F | 0.23 | 0.1 | | NA | NA | NA | NA | | | NA | NA | NA | NA | NA | NA | NA | NA | NA | NA | | |
| H ₂ O | 4.34 | 4.38 | | 4.43 | 4.44 | 4.49 | 4.50 | | | 4.46 | 4.49 | 4.50 | 4.47 | 4.35 | 4.42 | 4.48 | 4.47 | 4.53 | 4.56 | | |
| Total | 99.72 | 98.95 | | 99.77 | 99.27 | 99.64 | 99.65 | | | 99.14 | 100.04 | 99.90 | 98.80 | 99.51 | 99.67 | 99.29 | 98.46 | 99.21 | 99.73 | | |
| Si | 6.17 | 6.16 | | 6.13 | 6.16 | 6.20 | 6.21 | | | 6.14 | 6.15 | 6.09 | 6.23 | 6.07 | 6.18 | 6.16 | 6.28 | 6.38 | 6.42 | | |
| Al | 1.84 | 1.84 | | 1.88 | 1.84 | 1.80 | 1.79 | | | 1.86 | 1.85 | 1.91 | 1.77 | 1.93 | 1.82 | 1.84 | 1.72 | 1.62 | 1.58 | | |
| Al | 3.35 | 3.38 | | 3.40 | 3.57 | 3.67 | 3.68 | | | 3.64 | 3.61 | 3.76 | 3.72 | 3.15 | 3.25 | 3.75 | 3.77 | 3.83 | 3.84 | | |
| Ti | 0.05 | 0.05 | | 0.08 | 0.05 | 0.06 | 0.05 | | | 0.07 | 0.07 | 0.06 | 0.05 | 0.04 | 0.05 | 0.01 | 0.03 | 0.00 | 0.00 | | |
| Fe | 0.28 | 0.28 | | 0.40 | 0.30 | 0.19 | 0.17 | | | 0.24 | 0.28 | 0.17 | 0.11 | 0.48 | 0.40 | 0.11 | 0.07 | 0.11 | 0.08 | | |
| Mn | 0.00 | 0.00 | | 0.01 | 0.00 | 0.00 | 0.00 | | | 0.00 | 0.00 | 0.00 | 0.00 | 0.00 | 0.01 | 0.00 | 0.00 | 0.00 | 0.01 | | |
| Mg | 0.57 | 0.52 | | 0.30 | 0.23 | 0.14 | 0.16 | | | 0.14 | 0.16 | 0.05 | 0.19 | 0.68 | 0.56 | 0.23 | 0.18 | 0.09 | 0.08 | | |
| Ca | 0.00 | 0.00 | | 0.00 | 0.01 | 0.00 | 0.01 | | | 0.00 | 0.00 | 0.01 | 0.00 | 0.01 | 0.01 | 0.00 | 0.00 | 0.03 | 0.04 | | |
| Na | 0.09 | 0.10 | | 0.14 | 0.10 | 0.16 | 0.13 | | | 0.13 | 0.14 | 0.13 | 0.14 | 0.09 | 0.10 | 0.09 | 0.10 | 0.04 | 0.05 | | |
| K | 1.81 | 1.82 | | 1.83 | 1.77 | 1.75 | 1.75 | | | 1.74 | 1.73 | 1.80 | 1.67 | 1.89 | 1.82 | 1.80 | 1.70 | 1.64 | 1.60 | | |
| Cl | 0.01 | 0.00 | | 0.00 | 0.01 | 0.01 | 0.00 | | | 0.01 | 0.01 | 0.00 | 0.02 | 0.03 | 0.01 | 0.01 | 0.01 | 0.00 | 0.01 | | |
| F | 0.10 | 0.04 | | 0.00 | 0.00 | 0.00 | 0.00 | | | 0.00 | 0.00 | 0.00 | 0.00 | 0.00 | 0.00 | 0.00 | 0.00 | 0.00 | 0.00 | | |
| OH | 3.90 | 3.96 | | 4.00 | 3.99 | 3.99 | 4.00 | | | 3.99 | 3.99 | 4.00 | 3.99 | 3.97 | 3.99 | 3.99 | 3.99 | 4.00 | 3.99 | | |

| Sample number | Muscovite (advanced argillic) | | | Muscovite (from phyllic alteration) | | | | | | | |
|--------------------------------|-------------------------------|--------|--------|-------------------------------------|--------|--------|--------|--------|--------|------|------|
| | 204-46 | 204-46 | 204-46 | 119-10 | 119-10 | 119-10 | 119-10 | 119-10 | 119-10 | 198 | 198 |
| Elevation (m a.s.l.) | 2439 | 2439 | 2439 | 2289 | 2289 | 2289 | 2289 | 2289 | 2530 | 2530 | 2530 |
| Analyzed point | b1 | b1 | b2 | b1 | b2 | c1 | c2 | a1 | a2 | | |
| SiO ₂ | 46.81 | 45.77 | 45.77 | 45.46 | 45.56 | 46.24 | 47.15 | 45.99 | 44.51 | | |
| TiO ₂ | 0.37 | 0.48 | 0.48 | 0.58 | 0.58 | 0.16 | 0.07 | 0.24 | 0.28 | | |
| Al ₂ O ₃ | 34.49 | 36.7 | 36.7 | 31.37 | 33.01 | 33.01 | 32.99 | 34.52 | 34.12 | | |
| FeO | 0.37 | 0.46 | 0.46 | 3.17 | 2.66 | 2.72 | 2.61 | 0.25 | 0.19 | | |
| MnO | — | — | — | — | 0.15 | — | — | — | — | | |
| MgO | 1.36 | 0.33 | 0.33 | 2.44 | 1.15 | 0.66 | 0.8 | 0.84 | 0.58 | | |
| CaO | — | 0.06 | 0.06 | — | — | — | 0.06 | 0.08 | 0 | | |
| Na ₂ O | 0.56 | 0.54 | 0.54 | 0.7 | 0.58 | 0.39 | 0.31 | 0.31 | 0.33 | | |
| K ₂ O | 10.45 | 10.33 | 10.33 | 10.19 | 10.18 | 10 | 9.79 | 10.01 | 9.71 | | |
| Cl | — | 0.04 | 0.04 | — | 0.03 | — | 0.04 | 0.03 | — | | |
| F | NA | NA | NA | 0.27 | 0.27 | 0.25 | 0.38 | NA | NA | | |
| H ₂ O | 4.49 | 4.50 | 4.50 | 4.26 | 4.27 | 4.28 | 4.26 | 4.40 | 4.29 | | |
| Total | 98.90 | 99.21 | 99.21 | 98.44 | 98.44 | 97.71 | 98.46 | 96.67 | 94.01 | | |
| Si | 6.25 | 6.10 | 6.10 | 6.22 | 6.21 | 6.31 | 6.37 | 6.26 | 6.23 | | |
| Al | 1.75 | 1.91 | 1.91 | 1.78 | 1.79 | 1.69 | 1.63 | 1.74 | 1.78 | | |
| Al | 3.68 | 3.86 | 3.86 | 3.28 | 3.51 | 3.63 | 3.63 | 3.80 | 3.85 | | |
| Ti | 0.04 | 0.05 | 0.05 | 0.06 | 0.06 | 0.02 | 0.01 | 0.03 | 0.03 | | |
| Fe | 0.04 | 0.05 | 0.05 | 0.36 | 0.30 | 0.31 | 0.30 | 0.03 | 0.02 | | |
| Mn | 0.00 | 0.00 | 0.00 | 0.00 | 0.02 | 0.00 | 0.00 | 0.00 | 0.00 | | |
| Mg | 0.27 | 0.07 | 0.07 | 0.50 | 0.23 | 0.13 | 0.16 | 0.17 | 0.12 | | |
| Ca | 0.00 | 0.01 | 0.01 | 0.00 | 0.00 | 0.00 | 0.01 | 0.01 | 0.00 | | |
| Na | 0.15 | 0.14 | 0.14 | 0.19 | 0.15 | 0.10 | 0.08 | 0.08 | 0.09 | | |
| K | 1.78 | 1.76 | 1.76 | 1.78 | 1.77 | 1.74 | 1.69 | 1.74 | 1.73 | | |
| Cl | 0.00 | 0.01 | 0.01 | 0.00 | 0.01 | 0.00 | 0.01 | 0.01 | 0.00 | | |
| F | 0.00 | 0.00 | 0.00 | 0.12 | 0.12 | 0.11 | 0.16 | 0.00 | 0.00 | | |
| OH | 4.00 | 3.99 | 3.99 | 3.89 | 3.88 | 3.90 | 3.84 | 3.99 | 4.00 | | |

H₂O computed by difference. Number of ions calculated on the basis of 24 O, F and Cl for biotite and muscovite and 36 for chlorite. The low total value of sample 198 is due to the very fine-grained nature of the muscovite and possibly contamination by clay minerals. — : undetected. NA: not analyzed.

APPENDIX 3

Analytical Techniques

X-ray diffraction and electron microprobe techniques

All alunite group samples were examined with an X-ray diffractometer set to traverse at 0.1° 2θ per six seconds. Copper radiation ($\lambda=1.54184$) was used exclusively. Diffraction patterns were collected from 10 to $75^{\circ} 2\theta$.

All samples were analyzed at Queen's University with an ARL-SEMQ electron microprobe equipped with an energy dispersive spectrometer. An accelerating voltage of 15 kV and a beam current of 40 na were used. Spectra were collected for an accumulated time of 120 secs. (six spots at 20 secs.) and a rastered beam ($9\mu\text{m}$ by $9\mu\text{m}$ in diameter) was used to analyse all alunite samples and standards to minimize problems with the displacement of sodium and potassium. Marysvale alunite (Stoffregen and Alpers, 1987) was used as a primary standard. A sodium-bearing andesitic glass was employed as a standard for sodium and iron and a calcium phosphate standard for phosphorus.

$^{40}\text{Ar}/^{39}\text{Ar}$ techniques

Biotite samples were handpicked and inspected for purity under a polarizing microscope. Small chips of alunite group minerals were separated from larger veins and hence no analytical preparation was necessary (Vasconcelos et al., 1994). Mineral separates and monitors were wrapped in Al-foil and the resulting disks stacked into an Al-container. $^{40}\text{Ar}/^{39}\text{Ar}$ flux monitors, MAC-83 biotite with a published age of 24.36 ± 0.17 (2σ) (Sandeman et al., 1999), were inserted at ca. 0.5 cm intervals along the irradiation containers. Mineral separates and monitors were irradiated with fast neutrons in the McMaster University Nuclear Reactor, Hamilton, Ontario, for 8 hours. Samples were dated at the Geochronology Laboratory of the Department of Geological

Sciences and Geological Engineering at Queen's University using an 8W Lexel 3500 continuous argon-ion laser and a MAP 216 mass spectrometer. Heating periods were ca. 3 minutes at increasing power-settings (0.5 to 4.0 W). Dates and errors are calculated using formulae provided by Dalrymple et al. (1981) and the constants recommended by Steiger and Jäger (1977). An apparent plateau age was defined as at least three consecutive concordant steps representing over 50 percent of the Ar-released for which no difference in age can be detected between any two fraction at the 95 percent level of confidence (Dalrymple and Lanphere, 1974). The latter requirement was tested using the Critical-Value test of McIntyre (1963). In sample CRCO 209-39, a two-step quasi-plateau was inferred.

APPENDIX 4

$^{40}\text{Ar}/^{39}\text{Ar}$ Analytical Data, Cerro Colorado

| Step no. | Laser Power (W) | ^{40}Ar | ^{39}Ar | ^{38}Ar | ^{37}Ar | ^{36}Ar | Ca/K | Cl/K | % ^{40}Ar atm | f ^{39}Ar | $^{40}\text{Ar}/^{39}\text{ArK}$ | Age (Ma) | 2 σ error |
|---|-----------------|---------------------|--------------------|-------------------|-------------------|-------------------|-------|-------|------------------------|--------------------|----------------------------------|-------------------|------------------|
| CRCO 83-60 Hydrothermal Biotite: | | | | | | | | | | | | | |
| J = 0.003619 \pm 0.000034, Volume ^{39}ArK = 53.96 \times 1E-10, Integrated Age = 50.18 \pm 1.97, Plateau Age = 50.41 \pm 1.72 (99.4 % of ^{39}ArK) | | | | | | | | | | | | | |
| 1 | 0.75 | 0.712 \pm 0.011 | 0.039 \pm 0.003 | 0.010 \pm 0.003 | 0.017 \pm 0.002 | 0.008 \pm 0.002 | 0.000 | 0.033 | 71.75 | 0.51 | 6.651 \pm 19.873 | 42.9 \pm 126.7 | |
| 2 | 1.25 | 1.866 \pm 0.021 | 0.166 \pm 0.004 | 0.033 \pm 0.003 | 0.017 \pm 0.002 | 0.008 \pm 0.002 | 0.000 | 0.038 | 33.39 | 2.86 | 7.773 \pm 3.305 | 50.1 \pm 21.0 | |
| 3 | 1.75 | 8.397 \pm 0.046 | 0.924 \pm 0.009 | 0.176 \pm 0.007 | 0.019 \pm 0.002 | 0.010 \pm 0.002 | 0.003 | 0.040 | 13.56 | 16.92 | 7.862 \pm 0.575 | 50.6 \pm 3.7 | |
| 4 | 2.25 | 5.567 \pm 0.033 | 0.659 \pm 0.009 | 0.127 \pm 0.007 | 0.018 \pm 0.002 | 0.008 \pm 0.002 | 0.000 | 0.040 | 7.94 | 12 | 7.801 \pm 0.812 | 50.2 \pm 5.2 | |
| 5 | 2.75 | 4.009 \pm 0.025 | 0.472 \pm 0.006 | 0.090 \pm 0.005 | 0.017 \pm 0.002 | 0.007 \pm 0.002 | 0.000 | 0.039 | 9.71 | 8.55 | 7.703 \pm 1.115 | 49.6 \pm 7.1 | |
| 6 | 3.25 | 3.408 \pm 0.021 | 0.410 \pm 0.007 | 0.081 \pm 0.005 | 0.017 \pm 0.002 | 0.007 \pm 0.002 | 0.000 | 0.041 | 4.27 | 7.38 | 8.018 \pm 1.298 | 51.6 \pm 8.2 | |
| 7 | 4 | 4.116 \pm 0.022 | 0.498 \pm 0.006 | 0.095 \pm 0.006 | 0.017 \pm 0.002 | 0.007 \pm 0.002 | 0.000 | 0.039 | 5.59 | 9.03 | 7.833 \pm 1.041 | 50.4 \pm 6.6 | |
| 8 | 8 | 18.837 \pm 0.094 | 2.314 \pm 0.017 | 0.439 \pm 0.01 | 0.018 \pm 0.002 | 0.008 \pm 0.002 | 0.001 | 0.040 | 3.66 | 42.7 | 7.821 \pm 0.256 | 50.4 \pm 1.6 | |
| CRCO 206-14 Hydrothermal Muscovite: | | | | | | | | | | | | | |
| J = 0.003631 \pm 0.000028, Volume ^{39}ArK = 25.09 \times 1E-10, Integrated Age = 51.69 \pm 0.60, Plateau Age = 51.76 \pm 0.58 (99.7% of ^{39}ArK) | | | | | | | | | | | | | |
| 1 | 0.25 | 0.445 \pm 0.009 | 0.011 \pm 0.002 | 0.004 \pm 0.002 | 0.012 \pm 0.002 | 0.005 \pm 0.001 | 0.198 | 0.052 | 115.78 | 0.04 | -6.60 \pm 49.52 | -43.8 \pm 332.4 | |
| 2 | 0.75 | 2.705 \pm 0.028 | 0.070 \pm 0.003 | 0.009 \pm 0.002 | 0.013 \pm 0.002 | 0.011 \pm 0.002 | 0.062 | 0.018 | 84.7 | 0.27 | 5.87 \pm 7.39 | 38.1 \pm 47.4 | |
| 3 | 1.25 | 4.306 \pm 0.034 | 0.226 \pm 0.005 | 0.009 \pm 0.002 | 0.013 \pm 0.002 | 0.012 \pm 0.002 | 0.027 | 0.002 | 56.81 | 0.89 | 8.13 \pm 2.26 | 52.5 \pm 14.4 | |
| 4 | 1.75 | 10.306 \pm 0.046 | 0.972 \pm 0.011 | 0.019 \pm 0.003 | 0.012 \pm 0.002 | 0.011 \pm 0.002 | 0.002 | 0.000 | 22.07 | 3.87 | 8.19 \pm 0.56 | 52.9 \pm 3.6 | |
| 5 | 2.25 | 22.080 \pm 0.100 | 2.323 \pm 0.017 | 0.039 \pm 0.003 | 0.013 \pm 0.002 | 0.014 \pm 0.002 | 0.002 | 0.000 | 14.83 | 9.26 | 8.04 \pm 0.24 | 51.9 \pm 1.6 | |
| 6 | 2.75 | 21.912 \pm 0.094 | 2.421 \pm 0.017 | 0.039 \pm 0.004 | 0.012 \pm 0.002 | 0.011 \pm 0.002 | 0.001 | 0.000 | 10.6 | 9.64 | 8.04 \pm 0.22 | 51.9 \pm 1.4 | |
| 7 | 3.25 | 39.228 \pm 0.102 | 4.680 \pm 0.031 | 0.072 \pm 0.005 | 0.012 \pm 0.002 | 0.008 \pm 0.002 | 0.001 | 0.000 | 3.86 | 18.66 | 8.01 \pm 0.12 | 51.7 \pm 0.8 | |
| 8 | 4 | 36.348 \pm 0.101 | 4.325 \pm 0.025 | 0.066 \pm 0.005 | 0.013 \pm 0.002 | 0.008 \pm 0.002 | 0.001 | 0.000 | 3.86 | 17.24 | 8.03 \pm 0.14 | 51.9 \pm 0.9 | |
| 9 | 5 | 36.569 \pm 0.138 | 4.424 \pm 0.029 | 0.066 \pm 0.005 | 0.013 \pm 0.002 | 0.007 \pm 0.002 | 0.001 | 0.000 | 2.8 | 17.63 | 7.99 \pm 0.14 | 51.6 \pm 0.9 | |
| 10 | 6 | 46.055 \pm 0.157 | 5.646 \pm 0.032 | 0.086 \pm 0.006 | 0.029 \pm 0.003 | 0.006 \pm 0.002 | 0.009 | 0.000 | 1.7 | 22.51 | 7.97 \pm 0.12 | 51.5 \pm 0.8 | |
| 83-53 Hydrothermal Muscovite + Chlorite: | | | | | | | | | | | | | |
| J = 0.003627 \pm 0.000030, Volume ^{39}ArK = 82.69 \times 1E-10, Integrated Age = 51.92 \pm 0.48, Plateau Age = 51.82 \pm 0.50 (74.3 % of ^{39}ArK) | | | | | | | | | | | | | |
| 1 | 0.25 | 11.647 \pm 0.039 | 0.206 \pm 0.004 | 0.020 \pm 0.003 | 0.013 \pm 0.002 | 0.041 \pm 0.002 | 0.024 | 0.009 | 96.92 | 0.25 | 1.71 \pm 2.87 | 11.2 \pm 18.6 | |
| 2 | 0.75 | 25.805 \pm 0.064 | 1.769 \pm 0.015 | 0.081 \pm 0.005 | 0.037 \pm 0.002 | 0.052 \pm 0.002 | 0.041 | 0.006 | 55.91 | 2.14 | 6.39 \pm 0.37 | 41.3 \pm 2.4 | |
| 3 | 1.25 | 43.480 \pm 0.075 | 4.674 \pm 0.029 | 0.141 \pm 0.006 | 0.067 \pm 0.003 | 0.027 \pm 0.002 | 0.033 | 0.003 | 16.48 | 5.65 | 7.73 \pm 0.13 | 49.9 \pm 0.8 | |
| 4 | 1.75 | 74.823 \pm 0.133 | 7.915 \pm 0.047 | 0.152 \pm 0.009 | 0.040 \pm 0.003 | 0.021 \pm 0.003 | 0.010 | 0.001 | 7.22 | 9.57 | 8.73 \pm 0.11 | 56.3 \pm 0.7 | |
| 5 | 2.25 | 60.162 \pm 0.137 | 6.686 \pm 0.039 | 0.140 \pm 0.006 | 0.028 \pm 0.003 | 0.020 \pm 0.002 | 0.007 | 0.001 | 8.11 | 8.09 | 8.23 \pm 0.10 | 53.1 \pm 0.6 | |
| 6 | 2.75 | 51.892 \pm 0.096 | 6.059 \pm 0.038 | 0.132 \pm 0.008 | 0.023 \pm 0.003 | 0.013 \pm 0.002 | 0.005 | 0.002 | 5.78 | 7.33 | 8.03 \pm 0.12 | 51.8 \pm 0.7 | |
| 7 | 3.25 | 71.477 \pm 0.125 | 8.482 \pm 0.051 | 0.200 \pm 0.012 | 0.023 \pm 0.003 | 0.014 \pm 0.002 | 0.004 | 0.002 | 4.64 | 10.26 | 8.00 \pm 0.09 | 51.6 \pm 0.6 | |
| 8 | 4 | 99.001 \pm 0.181 | 11.723 \pm 0.068 | 0.297 \pm 0.018 | 0.023 \pm 0.003 | 0.019 \pm 0.003 | 0.003 | 0.003 | 4.8 | 14.18 | 8.00 \pm 0.09 | 51.6 \pm 0.6 | |
| 9 | 5 | 164.957 \pm 0.228 | 19.537 \pm 0.112 | 0.503 \pm 0.026 | 0.030 \pm 0.005 | 0.028 \pm 0.004 | 0.003 | 0.003 | 4.36 | 23.63 | 8.04 \pm 0.08 | 51.9 \pm 0.5 | |
| 10 | 6 | 73.264 \pm 0.110 | 8.603 \pm 0.049 | 0.210 \pm 0.010 | 0.023 \pm 0.003 | 0.015 \pm 0.002 | 0.004 | 0.002 | 4.88 | 10.4 | 8.06 \pm 0.10 | 52.0 \pm 0.6 | |
| 11 | 8 | 59.952 \pm 0.122 | 7.029 \pm 0.045 | 0.164 \pm 0.008 | 0.021 \pm 0.003 | 0.012 \pm 0.002 | 0.004 | 0.002 | 4.59 | 8.5 | 8.10 \pm 0.11 | 52.2 \pm 0.7 | |
| CRCO 339 Biotite (Ignimbrite): | | | | | | | | | | | | | |
| J = 0.003675 \pm 0.000028, Volume ^{39}ArK = 244.47 \times 1E-10, Integrated Age = 19.16 \pm 0.51, Plateau Age = 19.25 \pm 0.43 (98.42% of ^{39}ArK) | | | | | | | | | | | | | |
| 1 | 0.25 | 0.927 \pm 0.012 | 0.016 \pm 0.002 | 0.004 \pm 0.002 | 0.013 \pm 0.002 | 0.007 \pm 0.002 | 0.288 | 0.020 | 97.88 | 0.06 | 1.240 \pm 33.320 | 8.20 \pm 219.91 | |
| 2 | 0.75 | 2.498 \pm 0.027 | 0.075 \pm 0.003 | 0.008 \pm 0.002 | 0.036 \pm 0.002 | 0.012 \pm 0.002 | 0.926 | 0.011 | 99.62 | 0.30 | 0.097 \pm 7.663 | 0.64 \pm 50.79 | |
| 3 | 1.25 | 1.815 \pm 0.023 | 0.113 \pm 0.003 | 0.010 \pm 0.003 | 0.043 \pm 0.002 | 0.009 \pm 0.002 | 0.764 | 0.011 | 83.90 | 0.45 | 2.493 \pm 5.016 | 16.45 \pm 32.96 | |
| 4 | 1.75 | 1.766 \pm 0.021 | 0.190 \pm 0.004 | 0.015 \pm 0.003 | 0.037 \pm 0.002 | 0.007 \pm 0.002 | 0.362 | 0.012 | 70.62 | 0.77 | 2.614 \pm 2.786 | 17.25 \pm 18.30 | |
| 5 | 2.25 | 2.877 \pm 0.021 | 0.371 \pm 0.005 | 0.029 \pm 0.003 | 0.019 \pm 0.002 | 0.009 \pm 0.002 | 0.059 | 0.013 | 61.54 | 1.51 | 2.892 \pm 1.341 | 19.07 \pm 8.80 | |
| 6 | 2.75 | 1.886 \pm 0.023 | 0.336 \pm 0.006 | 0.028 \pm 0.004 | 0.016 \pm 0.002 | 0.006 \pm 0.002 | 0.037 | 0.015 | 42.74 | 1.37 | 3.069 \pm 1.366 | 20.23 \pm 8.96 | |
| 7 | 3.25 | 3.306 \pm 0.026 | 0.659 \pm 0.008 | 0.052 \pm 0.005 | 0.019 \pm 0.002 | 0.008 \pm 0.002 | 0.031 | 0.014 | 42.91 | 2.69 | 2.775 \pm 0.758 | 18.31 \pm 4.97 | |
| 8 | 4.00 | 4.602 \pm 0.029 | 1.016 \pm 0.010 | 0.081 \pm 0.005 | 0.021 \pm 0.002 | 0.009 \pm 0.002 | 0.026 | 0.015 | 34.66 | 4.15 | 2.885 \pm 0.537 | 19.03 \pm 3.53 | |

| Step no. | Laser Power (W) | ⁴⁰ Ar | ³⁹ Ar | ³⁸ Ar | ³⁷ Ar | ³⁶ Ar | Ca/K | Cl/K | % ⁴⁰ Ar atm | ¹ ³⁹ Ar | ⁴⁰ Ar*/ ³⁹ ArK | Age (Ma) 2σ error |
|----------|-----------------|------------------|------------------|------------------|------------------|------------------|-------|-------|------------------------|-------------------------------|--------------------------------------|-------------------|
| 9 ○ | 6.00 | 83.767 ± 0.202 | 21.681 ± 0.104 | 1.601 ± 0.032 | 0.072 ± 0.005 | 0.070 ± 0.004 | 0.008 | 0.014 | 23.48 | 88.71 | 2.923 ± 0.051 | 19.28 ± 0.34 |

CRCO 313-21 Biotite (Ignimbrite):

| | | | | | | | | | | | | |
|---|------|----------------|----------------|---------------|---------------|---------------|-------|-------|-------|-------|----------------|----------------|
| J = 0.003674 ± 0.000028, Volume ³⁹ ArK = 192.78 × 1E-10, Integrated Age = 19.13 ± 0.68, Plateau Age = 19.12 ± 0.61 (97.85% of ³⁹ ArK) | | | | | | | | | | | | |
| 1 | 0.25 | 1.745 ± 0.018 | 0.033 ± 0.002 | 0.004 ± 0.002 | 0.012 ± 0.002 | 0.009 ± 0.002 | 0.102 | 0.010 | 94.53 | 0.16 | 2.896 ± 17.664 | 19.10 ± 115.85 |
| 2 | 0.75 | 2.088 ± 0.030 | 0.136 ± 0.004 | 0.011 ± 0.002 | 0.014 ± 0.002 | 0.009 ± 0.002 | 0.054 | 0.012 | 81.71 | 0.70 | 2.708 ± 4.155 | 17.86 ± 27.27 |
| 3 | 1.25 | 1.988 ± 0.018 | 0.251 ± 0.005 | 0.020 ± 0.003 | 0.013 ± 0.002 | 0.007 ± 0.002 | 0.022 | 0.013 | 59.00 | 1.29 | 3.126 ± 2.161 | 20.60 ± 14.16 |
| 4 ○ | 1.75 | 2.526 ± 0.019 | 0.442 ± 0.006 | 0.034 ± 0.004 | 0.013 ± 0.002 | 0.007 ± 0.002 | 0.013 | 0.014 | 48.35 | 2.28 | 2.849 ± 1.080 | 18.78 ± 7.09 |
| 5 ○ | 2.25 | 4.090 ± 0.027 | 0.792 ± 0.010 | 0.066 ± 0.005 | 0.013 ± 0.002 | 0.009 ± 0.002 | 0.007 | 0.015 | 40.24 | 4.10 | 3.007 ± 0.616 | 19.82 ± 4.04 |
| 6 ○ | 2.75 | 3.442 ± 0.023 | 0.688 ± 0.008 | 0.057 ± 0.005 | 0.013 ± 0.002 | 0.008 ± 0.002 | 0.009 | 0.015 | 38.65 | 3.56 | 2.977 ± 0.779 | 19.63 ± 5.11 |
| 7 ○ | 3.25 | 7.689 ± 0.040 | 1.463 ± 0.013 | 0.115 ± 0.004 | 0.015 ± 0.002 | 0.015 ± 0.002 | 0.008 | 0.014 | 44.32 | 7.58 | 2.871 ± 0.357 | 18.93 ± 2.34 |
| 8 ○ | 6.00 | 76.950 ± 0.277 | 15.484 ± 0.097 | 1.162 ± 0.029 | 0.035 ± 0.004 | 0.110 ± 0.004 | 0.004 | 0.014 | 41.05 | 80.34 | 2.896 ± 0.089 | 19.09 ± 0.58 |

CRCO 297 Biotite (Ignimbrite):

| | | | | | | | | | | | | |
|---|------|-----------------|---------------|---------------|---------------|---------------|-------|-------|--------|-------|-----------------|----------------|
| J = 0.003675 ± 0.000030, Volume ³⁹ ArK = 220.4 × 1E-10, Integrated Age = 1.31 ± 7.04 | | | | | | | | | | | | |
| | 0.25 | 72.795 ± 0.159 | 0.216 ± 0.006 | 0.071 ± 0.007 | 0.026 ± 0.004 | 0.259 ± 0.006 | 0.156 | 0.020 | 103.57 | 0.97 | -12.210 ± 8.807 | -82.83 ± 61.14 |
| 1 | 0.75 | 889.738 ± 1.616 | 3.807 ± 0.085 | 1.011 ± 0.067 | 0.137 ± 0.034 | 3.106 ± 0.071 | 0.085 | 0.023 | 103.10 | 17.26 | -7.275 ± 5.581 | -48.89 ± 38.02 |
| 2 | 1.25 | 323.169 ± 0.590 | 4.351 ± 0.059 | 0.758 ± 0.041 | 0.154 ± 0.014 | 1.089 ± 0.024 | 0.084 | 0.026 | 99.24 | 19.73 | 0.536 ± 1.680 | 3.55 ± 11.12 |
| 3 | 1.75 | 138.635 ± 0.310 | 4.055 ± 0.037 | 0.598 ± 0.028 | 0.114 ± 0.008 | 0.447 ± 0.011 | 0.065 | 0.026 | 94.39 | 18.39 | 1.887 ± 0.828 | 12.47 ± 5.45 |
| 4 | 2.25 | 56.530 ± 0.120 | 2.935 ± 0.023 | 0.401 ± 0.013 | 0.081 ± 0.004 | 0.170 ± 0.004 | 0.060 | 0.026 | 86.61 | 13.31 | 2.545 ± 0.449 | 16.79 ± 2.95 |
| 5 | 2.75 | 68.299 ± 0.119 | 1.192 ± 0.012 | 0.195 ± 0.008 | 0.046 ± 0.004 | 0.229 ± 0.006 | 0.071 | 0.026 | 97.44 | 5.40 | 1.439 ± 1.420 | 9.52 ± 9.36 |
| 6 | 3.25 | 35.847 ± 0.074 | 1.252 ± 0.012 | 0.186 ± 0.009 | 0.050 ± 0.003 | 0.115 ± 0.003 | 0.075 | 0.027 | 91.44 | 5.67 | 2.414 ± 0.764 | 15.94 ± 5.02 |
| 7 | 4.00 | 39.220 ± 0.085 | 1.413 ± 0.013 | 0.202 ± 0.010 | 0.051 ± 0.003 | 0.124 ± 0.004 | 0.070 | 0.026 | 90.33 | 6.40 | 2.649 ± 0.753 | 17.48 ± 4.95 |
| 8 | 5.00 | 36.318 ± 0.082 | 1.234 ± 0.013 | 0.177 ± 0.009 | 0.045 ± 0.003 | 0.115 ± 0.003 | 0.066 | 0.026 | 90.35 | 5.59 | 2.805 ± 0.815 | 18.50 ± 5.35 |
| 9 | 6.45 | 32.818 ± 0.084 | 1.610 ± 0.014 | 0.219 ± 0.007 | 0.048 ± 0.003 | 0.097 ± 0.003 | 0.056 | 0.025 | 83.80 | 7.29 | 3.264 ± 0.527 | 21.51 ± 3.45 |

CRCO 313-28 Biotite (Ignimbrite):

| | | | | | | | | | | | | |
|--|------|-----------------|---------------|---------------|---------------|---------------|-------|-------|--------|-------|------------------|------------------|
| J = 0.003673 ± 0.000028, Volume ³⁹ ArK = 251.74 × 1E-10, Integrated Age = 7.14 ± 3.75 | | | | | | | | | | | | |
| 1 | 0.25 | 329.392 ± 0.500 | 0.436 ± 0.024 | 0.328 ± 0.026 | 0.028 ± 0.011 | 1.164 ± 0.026 | 0.104 | 0.055 | 104.19 | 1.73 | -31.770 ± 18.267 | -223.85 ± 137.03 |
| 2 | 0.75 | 484.717 ± 0.823 | 3.571 ± 0.065 | 0.845 ± 0.040 | 0.111 ± 0.015 | 1.683 ± 0.035 | 0.076 | 0.031 | 102.52 | 14.18 | -3.447 ± 2.957 | -22.99 ± 19.84 |
| 3 | 1.25 | 145.333 ± 0.275 | 4.514 ± 0.042 | 0.617 ± 0.026 | 0.131 ± 0.006 | 0.473 ± 0.011 | 0.072 | 0.024 | 95.72 | 17.93 | 1.346 ± 0.709 | 8.90 ± 4.67 |
| 4 | 1.75 | 61.430 ± 0.122 | 2.924 ± 0.024 | 0.345 ± 0.010 | 0.089 ± 0.004 | 0.188 ± 0.005 | 0.072 | 0.021 | 89.19 | 11.61 | 2.239 ± 0.472 | 14.78 ± 3.10 |
| 5 | 2.25 | 40.227 ± 0.085 | 1.862 ± 0.016 | 0.215 ± 0.009 | 0.062 ± 0.003 | 0.125 ± 0.003 | 0.074 | 0.020 | 89.48 | 7.39 | 2.240 ± 0.528 | 14.78 ± 3.47 |
| 6 | 2.75 | 56.658 ± 0.103 | 3.420 ± 0.026 | 0.380 ± 0.016 | 0.106 ± 0.004 | 0.161 ± 0.004 | 0.075 | 0.020 | 82.22 | 13.58 | 2.913 ± 0.366 | 19.20 ± 2.40 |
| 7 | 3.25 | 51.826 ± 0.107 | 3.242 ± 0.026 | 0.355 ± 0.011 | 0.097 ± 0.004 | 0.144 ± 0.004 | 0.072 | 0.020 | 80.54 | 12.88 | 3.077 ± 0.364 | 20.28 ± 2.39 |
| 8 | 4.00 | 36.552 ± 0.074 | 2.293 ± 0.021 | 0.245 ± 0.010 | 0.077 ± 0.003 | 0.102 ± 0.003 | 0.078 | 0.019 | 80.02 | 9.10 | 3.151 ± 0.379 | 20.76 ± 2.48 |
| 9 | 6.00 | 48.634 ± 0.075 | 2.920 ± 0.021 | 0.322 ± 0.012 | 0.167 ± 0.005 | 0.136 ± 0.004 | 0.145 | 0.020 | 80.59 | 11.60 | 3.200 ± 0.368 | 21.08 ± 2.41 |

CRCO 245 Alunite:

| | | | | | | | | | | | | |
|---|------|-----------------|----------------|---------------|---------------|---------------|-------|-------|--------|-------|----------------|---------------|
| J = 0.003635 ± 0.000028, Volume ³⁹ ArK = 260.30 × 1E-10, Integrated Age = 33.70 ± 0.57, Plateau Age = 35.26 ± 0.68 (92.92% of ³⁹ ArK) | | | | | | | | | | | | |
| 1 | 0.50 | 9.729 ± 0.057 | 0.119 ± 0.004 | 0.017 ± 0.003 | 0.016 ± 0.002 | 0.039 ± 0.002 | 0.006 | 0.012 | 100.68 | 0.42 | -0.629 ± 6.087 | -4.13 ± 40.01 |
| 2 | 0.75 | 18.621 ± 0.080 | 1.740 ± 0.014 | 0.078 ± 0.005 | 0.026 ± 0.002 | 0.045 ± 0.002 | 0.021 | 0.006 | 62.24 | 6.65 | 4.020 ± 0.373 | 26.17 ± 2.41 |
| 3 ○ | 1.25 | 112.812 ± 0.485 | 18.687 ± 0.111 | 0.595 ± 0.021 | 0.113 ± 0.005 | 0.053 ± 0.005 | 0.018 | 0.004 | 12.47 | 71.79 | 5.252 ± 0.082 | 34.12 ± 0.53 |
| 4 ○ | 1.75 | 24.212 ± 0.101 | 3.958 ± 0.026 | 0.138 ± 0.007 | 0.041 ± 0.003 | 0.014 ± 0.002 | 0.022 | 0.004 | 10.21 | 15.18 | 5.461 ± 0.146 | 35.46 ± 0.94 |
| 5 ○ | 2.25 | 4.905 ± 0.034 | 0.759 ± 0.009 | 0.030 ± 0.004 | 0.020 ± 0.002 | 0.008 ± 0.002 | 0.020 | 0.005 | 14.61 | 2.88 | 5.495 ± 0.704 | 35.68 ± 4.52 |
| 6 ○ | 3.50 | 5.167 ± 0.031 | 0.808 ± 0.010 | 0.032 ± 0.003 | 0.020 ± 0.002 | 0.008 ± 0.002 | 0.021 | 0.005 | 15.61 | 3.07 | 5.377 ± 0.683 | 34.92 ± 4.39 |

CRCO 201 Natroalunite:

| | | | | | | | | | | | | |
|---|------|---------------|---------------|---------------|---------------|---------------|-------|-------|-------|------|---------------|--------------|
| J = 0.003638 ± 0.000028, Volume ³⁹ ArK = 242.05 × 1E-10, Integrated Age = 16.51 ± 0.39, Plateau Age = 17.14 ± 0.42 (70.77% of ³⁹ ArK) | | | | | | | | | | | | |
| 1 | 0.50 | 4.056 ± 0.030 | 0.170 ± 0.005 | 0.046 ± 0.004 | 0.016 ± 0.002 | 0.019 ± 0.002 | 0.003 | 0.053 | 95.97 | 0.66 | 0.975 ± 3.486 | 6.39 ± 22.80 |

| Step no. | Laser Power (W) | ^{40}Ar | ^{39}Ar | ^{38}Ar | ^{37}Ar | ^{36}Ar | Ca/K | Cl/K | % ^{40}Ar atm | $f^{39}\text{Ar}$ | $^{40}\text{Ar}^*/^{39}\text{ArK}$ | Age (Ma) 2σ error |
|----------|-----------------|------------------|------------------|------------------|------------------|------------------|-------|-------|------------------------|-------------------|------------------------------------|--------------------------|
| 2 | 0.75 | 26.464 ± 0.153 | 6.920 ± 0.042 | 1.733 ± 0.029 | 0.024 ± 0.003 | 0.040 ± 0.002 | 0.004 | 0.054 | 38.45 | 28.56 | 2.321 ± 0.099 | 15.17 ± 0.64 |
| 3 ○ | 1.25 | 42.385 ± 0.170 | 12.985 ± 0.074 | 6.980 ± 0.072 | 0.029 ± 0.002 | 0.034 ± 0.002 | 0.003 | 0.120 | 19.51 | 53.63 | 2.595 ± 0.051 | 16.95 ± 0.33 |
| 4 ○ | 1.75 | 14.685 ± 0.062 | 3.484 ± 0.023 | 2.241 ± 0.032 | 0.020 ± 0.002 | 0.024 ± 0.002 | 0.004 | 0.145 | 35.18 | 14.36 | 2.699 ± 0.163 | 17.63 ± 1.06 |
| 5 ○ | 3.50 | 4.161 ± 0.037 | 0.681 ± 0.009 | 0.430 ± 0.012 | 0.017 ± 0.002 | 0.013 ± 0.002 | 0.003 | 0.142 | 53.54 | 2.78 | 2.814 ± 0.880 | 18.38 ± 5.71 |

CRCO 328 Natroalunite:

| | | | | | | | | | | | | |
|--|------|----------------|---------------|---------------|---------------|---------------|-------|-------|--------|-------|----------------|----------------|
| J = 0.003642 ± 0.000028, Volume ^{39}ArK = 140.85 × 1E-10, Integrated Age = 16.66 ± 0.72, Plateau Age = 17.62 ± 0.67 (71.59% of ^{39}ArK) | | | | | | | | | | | | |
| 1 | 0.50 | 25.288 ± 0.123 | 0.105 ± 0.004 | 0.106 ± 0.005 | 0.018 ± 0.002 | 0.095 ± 0.003 | 0.049 | 0.202 | 103.75 | 0.68 | -9.980 ± 9.117 | -66.79 ± 62.16 |
| 2 | 0.75 | 27.890 ± 0.110 | 3.914 ± 0.026 | 2.256 ± 0.037 | 0.025 ± 0.002 | 0.067 ± 0.002 | 0.007 | 0.129 | 64.85 | 27.73 | 2.475 ± 0.187 | 16.19 ± 1.22 |
| 3 ○ | 1.25 | 27.180 ± 0.119 | 7.153 ± 0.040 | 4.247 ± 0.049 | 0.029 ± 0.002 | 0.033 ± 0.002 | 0.006 | 0.133 | 28.47 | 50.74 | 2.685 ± 0.089 | 17.56 ± 0.58 |
| 4 ○ | 1.75 | 6.903 ± 0.036 | 1.865 ± 0.015 | 1.134 ± 0.018 | 0.019 ± 0.002 | 0.012 ± 0.002 | 0.004 | 0.137 | 23.77 | 13.17 | 2.786 ± 0.279 | 18.21 ± 1.81 |
| 5 ○ | 3.50 | 7.381 ± 0.038 | 1.091 ± 0.012 | 0.667 ± 0.016 | 0.018 ± 0.002 | 0.021 ± 0.002 | 0.005 | 0.137 | 61.31 | 7.68 | 2.593 ± 0.561 | 16.96 ± 3.65 |

CRCO 331A Jarosite & Alunite:

| | | | | | | | | | | | | |
|---|------|----------------|----------------|---------------|---------------|---------------|-------|-------|-------|-------|---------------|--------------|
| J = 0.003648 ± 0.000028, Volume ^{39}ArK = 191.22 × 1E-10, Integrated Age = 24.17 ± 0.69, Plateau Age = 24.17 ± 0.69 (100.00% of ^{39}ArK) | | | | | | | | | | | | |
| 1 ○ | 0.50 | 96.720 ± 0.291 | 13.587 ± 0.076 | 0.730 ± 0.020 | 0.023 ± 0.004 | 0.160 ± 0.005 | 0.002 | 0.009 | 46.97 | 71.04 | 3.744 ± 0.109 | 24.48 ± 0.70 |
| 2 ○ | 0.75 | 17.454 ± 0.069 | 1.762 ± 0.014 | 0.155 ± 0.007 | 0.029 ± 0.003 | 0.043 ± 0.002 | 0.025 | 0.016 | 62.97 | 9.16 | 3.648 ± 0.370 | 23.85 ± 2.40 |
| 3 ○ | 1.25 | 19.577 ± 0.066 | 2.373 ± 0.020 | 0.198 ± 0.009 | 0.030 ± 0.003 | 0.044 ± 0.002 | 0.020 | 0.015 | 57.44 | 12.36 | 3.485 ± 0.280 | 22.79 ± 1.82 |
| 4 ○ | 1.75 | 6.700 ± 0.035 | 0.485 ± 0.008 | 0.058 ± 0.005 | 0.018 ± 0.002 | 0.023 ± 0.002 | 0.012 | 0.021 | 74.32 | 2.48 | 3.568 ± 1.291 | 23.33 ± 8.39 |
| 5 ○ | 3.50 | 9.647 ± 0.045 | 0.957 ± 0.011 | 0.081 ± 0.005 | 0.019 ± 0.002 | 0.027 ± 0.002 | 0.008 | 0.014 | 63.04 | 4.95 | 3.715 ± 0.626 | 24.28 ± 4.06 |

CRCO 331B Natroalunite:

| | | | | | | | | | | | | |
|---|------|----------------|---------------|---------------|---------------|---------------|-------|-------|-------|-------|---------------|--------------|
| J = 0.003651 ± 0.000030, Volume ^{39}ArK = 69.68 × 1E-10, Integrated Age = 14.79 ± 1.46, Plateau Age = 15.68 ± 1.36 (91.82% of ^{39}ArK) | | | | | | | | | | | | |
| 1 | 0.75 | 25.341 ± 0.067 | 0.579 ± 0.008 | 0.182 ± 0.006 | 0.017 ± 0.002 | 0.089 ± 0.003 | 0.003 | 0.062 | 98.27 | 8.18 | 0.734 ± 1.379 | 4.83 ± 9.06 |
| 2 ○ | 1.25 | 33.286 ± 0.071 | 2.993 ± 0.022 | 1.057 ± 0.021 | 0.020 ± 0.002 | 0.094 ± 0.003 | 0.005 | 0.077 | 78.84 | 42.85 | 2.314 ± 0.266 | 15.18 ± 1.73 |
| 3 ○ | 1.75 | 14.389 ± 0.058 | 1.228 ± 0.013 | 0.471 ± 0.013 | 0.018 ± 0.002 | 0.044 ± 0.002 | 0.006 | 0.084 | 78.82 | 17.50 | 2.433 ± 0.504 | 15.96 ± 3.29 |
| 4 ○ | 3.00 | 16.415 ± 0.058 | 1.588 ± 0.015 | 0.643 ± 0.015 | 0.021 ± 0.002 | 0.047 ± 0.002 | 0.012 | 0.089 | 75.65 | 22.67 | 2.468 ± 0.406 | 16.18 ± 2.65 |
| 5 ○ | 4.00 | 6.175 ± 0.025 | 0.621 ± 0.008 | 0.242 ± 0.011 | 0.017 ± 0.002 | 0.021 ± 0.002 | 0.007 | 0.085 | 74.25 | 8.80 | 2.479 ± 0.911 | 16.26 ± 5.94 |

CRCO 218 Alunite:

| | | | | | | | | | | | | |
|--|------|----------------|---------------|---------------|---------------|---------------|-------|-------|-------|-------|---------------|--------------|
| J = 0.003653 ± 0.000030, Volume ^{39}ArK = 126.06 × 1E-10, Integrated Age = 24.81 ± 0.66, Plateau Age = 26.49 ± 0.65 (74.88% of ^{39}ArK) | | | | | | | | | | | | |
| 1 | 0.50 | 6.817 ± 0.140 | 1.156 ± 0.071 | 0.066 ± 0.012 | 0.049 ± 0.003 | 0.020 ± 0.002 | 0.116 | 0.009 | 66.88 | 9.11 | 1.877 ± 0.503 | 12.33 ± 3.29 |
| 2 | 0.75 | 9.972 ± 0.060 | 2.032 ± 0.018 | 0.073 ± 0.005 | 0.053 ± 0.003 | 0.014 ± 0.002 | 0.070 | 0.004 | 23.52 | 16.01 | 3.670 ± 0.272 | 24.02 ± 1.77 |
| 3 ○ | 1.25 | 22.197 ± 0.063 | 4.856 ± 0.028 | 0.147 ± 0.006 | 0.087 ± 0.003 | 0.012 ± 0.002 | 0.056 | 0.003 | 8.15 | 38.45 | 4.137 ± 0.110 | 27.06 ± 0.72 |
| 4 ○ | 1.75 | 16.660 ± 0.049 | 3.728 ± 0.026 | 0.097 ± 0.005 | 0.073 ± 0.003 | 0.011 ± 0.002 | 0.059 | 0.002 | 9.52 | 29.51 | 3.972 ± 0.130 | 25.99 ± 0.84 |
| 5 ○ | 3.50 | 4.270 ± 0.027 | 0.881 ± 0.010 | 0.027 ± 0.003 | 0.030 ± 0.002 | 0.008 ± 0.002 | 0.059 | 0.003 | 15.78 | 6.92 | 3.897 ± 0.617 | 25.50 ± 4.01 |

CRCO 221 Natroalunite:

| | | | | | | | | | | | | |
|---|------|----------------|---------------|---------------|---------------|---------------|-------|-------|-------|-------|----------------|---------------|
| J = 0.003656 ± 0.000030, Volume ^{39}ArK = 71.74 × 1E-10, Integrated Age = 23.38 ± 1.15, Plateau Age = 22.42 ± 1.06 (78.20% of ^{39}ArK) | | | | | | | | | | | | |
| 1 | 0.50 | 1.219 ± 0.015 | 0.035 ± 0.002 | 0.011 ± 0.003 | 0.018 ± 0.002 | 0.009 ± 0.002 | 0.190 | 0.056 | 99.92 | 0.37 | 0.001 ± 17.632 | 0.01 ± 116.29 |
| 2 | 0.75 | 1.498 ± 0.019 | 0.059 ± 0.003 | 0.017 ± 0.004 | 0.020 ± 0.002 | 0.010 ± 0.002 | 0.284 | 0.054 | 91.19 | 0.71 | 2.209 ± 9.988 | 14.51 ± 65.35 |
| 3 | 1.25 | 10.204 ± 0.047 | 1.494 ± 0.015 | 0.171 ± 0.006 | 0.130 ± 0.004 | 0.018 ± 0.002 | 0.299 | 0.022 | 36.63 | 20.71 | 4.235 ± 0.344 | 27.72 ± 2.23 |
| 4 ○ | 1.75 | 11.711 ± 0.057 | 2.372 ± 0.017 | 0.239 ± 0.009 | 0.216 ± 0.005 | 0.017 ± 0.002 | 0.331 | 0.020 | 28.03 | 32.96 | 3.472 ± 0.219 | 22.76 ± 1.42 |
| 5 ○ | 3.50 | 14.720 ± 0.127 | 2.952 ± 0.027 | 0.291 ± 0.010 | 0.275 ± 0.006 | 0.021 ± 0.002 | 0.345 | 0.019 | 31.27 | 41.06 | 3.357 ± 0.175 | 22.01 ± 1.14 |
| 6 ○ | 4.00 | 3.124 ± 0.019 | 0.308 ± 0.007 | 0.033 ± 0.004 | 0.040 ± 0.002 | 0.012 ± 0.002 | 0.320 | 0.018 | 62.37 | 4.18 | 3.634 ± 1.741 | 23.81 ± 11.33 |

CRCO 243 Natroalunite:

| | | | | | | | | | | | | |
|--|------|----------------|---------------|---------------|---------------|---------------|-------|-------|--------|-------|------------------|-----------------|
| J = 0.003658 ± 0.000032, Volume ^{39}ArK = 40.79 × 1E-10, Integrated Age = 9.60 ± 3.10, Plateau Age = 14.59 ± 2.46 (66.64% of ^{39}ArK) | | | | | | | | | | | | |
| 1 | 0.50 | 47.907 ± 0.112 | 0.125 ± 0.005 | 0.041 ± 0.005 | 0.016 ± 0.003 | 0.174 ± 0.004 | 0.029 | 0.007 | 104.25 | 2.89 | -17.297 ± 10.869 | -117.92 ± 76.57 |
| 2 | 0.75 | 36.969 ± 0.117 | 1.250 ± 0.014 | 0.107 ± 0.006 | 0.033 ± 0.003 | 0.123 ± 0.003 | 0.055 | 0.012 | 94.61 | 30.47 | 1.569 ± 0.776 | 10.33 ± 5.09 |

| Step no. | Laser Power (W) | ⁴⁰ Ar | ³⁹ Ar | ³⁸ Ar | ³⁷ Ar | ³⁶ Ar | Ca/K | Cl/K | % ⁴⁰ Ar atm | f ³⁹ Ar | ⁴⁰ Ar*/ ³⁹ ArK | Age (Ma) |
|----------|-----------------|------------------|------------------|------------------|------------------|------------------|-------|-------|------------------------|--------------------|--------------------------------------|--------------|
| | | | | | | | | | | | | 2σ error |
| 3 o | 1.25 | 19.464 ± 0.081 | 1.292 ± 0.012 | 0.095 ± 0.007 | 0.034 ± 0.003 | 0.060 ± 0.002 | 0.055 | 0.011 | 84.02 | 31.49 | 2.382 ± 0.528 | 15.65 ± 3.45 |
| 4 o | 1.75 | 8.290 ± 0.044 | 0.799 ± 0.010 | 0.064 ± 0.006 | 0.027 ± 0.003 | 0.028 ± 0.002 | 0.059 | 0.013 | 80.57 | 19.39 | 1.987 ± 0.687 | 13.06 ± 4.50 |
| 5 o | 3.50 | 5.924 ± 0.138 | 0.651 ± 0.009 | 0.054 ± 0.005 | 0.027 ± 0.003 | 0.020 ± 0.002 | 0.071 | 0.014 | 75.66 | 15.77 | 2.182 ± 0.823 | 14.34 ± 5.39 |

CRCO 230 Alunite:

| | | | | | | | | | | | | |
|---|------|----------------|---------------|---------------|---------------|---------------|-------|-------|-------|-------|---------------|---------------|
| J = 0.003665 ± 0.000034, Volume ³⁹ ArK = 202.45 × 1E-10, Integrated Age = 30.57 ± 0.51, Plateau Age = 31.94 ± 0.49 (73.86% of ³⁹ ArK) | | | | | | | | | | | | |
| 1 | 0.50 | 1.179 ± 0.013 | 0.292 ± 0.006 | 0.016 ± 0.003 | 0.015 ± 0.002 | 0.008 ± 0.002 | 0.009 | 0.007 | 78.31 | 1.41 | 0.714 ± 1.680 | 4.72 ± 11.08 |
| 2 | 0.75 | 2.756 ± 0.021 | 0.554 ± 0.007 | 0.020 ± 0.004 | 0.016 ± 0.002 | 0.007 ± 0.002 | 0.006 | 0.004 | 23.50 | 2.70 | 3.540 ± 0.883 | 23.26 ± 5.76 |
| 3 | 1.25 | 20.558 ± 0.046 | 4.389 ± 0.025 | 0.150 ± 0.007 | 0.025 ± 0.002 | 0.009 ± 0.002 | 0.009 | 0.004 | 5.59 | 21.65 | 4.353 ± 0.122 | 28.55 ± 0.79 |
| 4 o | 1.75 | 24.851 ± 0.071 | 4.770 ± 0.030 | 0.157 ± 0.007 | 0.036 ± 0.003 | 0.008 ± 0.002 | 0.017 | 0.004 | 3.13 | 23.53 | 4.981 ± 0.109 | 32.63 ± 0.71 |
| 5 o | 2.50 | 20.580 ± 0.041 | 3.962 ± 0.024 | 0.126 ± 0.008 | 0.030 ± 0.002 | 0.008 ± 0.002 | 0.015 | 0.004 | 3.51 | 19.54 | 4.939 ± 0.131 | 32.36 ± 0.85 |
| 6 o | 3.50 | 31.314 ± 0.069 | 6.237 ± 0.035 | 0.213 ± 0.009 | 0.037 ± 0.002 | 0.010 ± 0.002 | 0.014 | 0.004 | 4.26 | 30.78 | 4.749 ± 0.084 | 31.13 ± 0.54 |
| 7 | 4.00 | 0.996 ± 0.013 | 0.084 ± 0.004 | 0.006 ± 0.002 | 0.015 ± 0.002 | 0.007 ± 0.002 | 0.000 | 0.004 | 58.72 | 0.38 | 4.274 ± 6.253 | 28.04 ± 40.71 |

CRCO 248 Jarosite & Alunite:

| | | | | | | | | | | | | |
|---|------|-----------------|----------------|---------------|---------------|---------------|-------|-------|-------|-------|---------------|--------------|
| J = 0.003667 ± 0.000034, Volume ³⁹ ArK = 401.84 × 1E-10, Integrated Age = 22.58 ± 0.52, Plateau Age = 22.30 ± 0.53 (94.49% of ³⁹ ArK) | | | | | | | | | | | | |
| 1 o | 0.50 | 123.977 ± 0.400 | 11.688 ± 0.075 | 0.227 ± 0.014 | 0.019 ± 0.004 | 0.292 ± 0.008 | 0.001 | 0.000 | 68.40 | 29.08 | 3.320 ± 0.205 | 21.83 ± 1.34 |
| 2 o | 0.75 | 55.174 ± 0.149 | 9.506 ± 0.053 | 0.154 ± 0.009 | 0.018 ± 0.003 | 0.079 ± 0.003 | 0.001 | 0.000 | 39.64 | 23.65 | 3.470 ± 0.103 | 22.81 ± 0.67 |
| 3 o | 1.25 | 33.737 ± 0.140 | 6.379 ± 0.037 | 0.104 ± 0.005 | 0.018 ± 0.003 | 0.046 ± 0.002 | 0.002 | 0.000 | 35.25 | 15.86 | 3.391 ± 0.104 | 22.29 ± 0.68 |
| 4 o | 1.75 | 23.940 ± 0.079 | 4.844 ± 0.026 | 0.079 ± 0.005 | 0.018 ± 0.003 | 0.030 ± 0.002 | 0.002 | 0.000 | 30.83 | 12.04 | 3.383 ± 0.129 | 22.24 ± 0.85 |
| 5 o | 3.50 | 27.134 ± 0.080 | 5.570 ± 0.036 | 0.104 ± 0.005 | 0.019 ± 0.002 | 0.032 ± 0.002 | 0.003 | 0.001 | 29.18 | 13.85 | 3.415 ± 0.118 | 22.45 ± 0.77 |
| 6 | 4.00 | 11.189 ± 0.052 | 2.221 ± 0.022 | 0.075 ± 0.005 | 0.025 ± 0.003 | 0.012 ± 0.002 | 0.018 | 0.004 | 16.33 | 5.51 | 4.173 ± 0.240 | 27.39 ± 1.56 |

CRCO 290 Jarosite:

| | | | | | | | | | | | | |
|--|------|----------------|---------------|---------------|---------------|---------------|-------|--------|-------|-------|---------------|--------------|
| J = 0.003668 ± 0.000034, Volume ³⁹ ArK = 285.98 × 1E-10, Integrated Age = 24.81 ± 0.44, Plateau Age = 24.81 ± 0.44 (100.00% of ³⁹ ArK) | | | | | | | | | | | | |
| 1 o | 0.25 | 8.184 ± 0.029 | 1.086 ± 0.011 | 0.024 ± 0.003 | 0.022 ± 0.002 | 0.018 ± 0.002 | 0.026 | 0.001 | 46.53 | 3.77 | 3.971 ± 0.474 | 26.09 ± 3.09 |
| 2 o | 0.50 | 47.240 ± 0.105 | 8.366 ± 0.046 | 0.121 ± 0.007 | 0.073 ± 0.003 | 0.057 ± 0.002 | 0.027 | -0.000 | 32.37 | 29.24 | 3.781 ± 0.088 | 24.85 ± 0.58 |
| 3 o | 0.75 | 17.595 ± 0.046 | 3.298 ± 0.023 | 0.050 ± 0.005 | 0.032 ± 0.002 | 0.022 ± 0.002 | 0.020 | -0.000 | 28.16 | 11.51 | 3.786 ± 0.187 | 24.88 ± 1.22 |
| 4 o | 1.25 | 12.089 ± 0.036 | 2.116 ± 0.016 | 0.036 ± 0.003 | 0.026 ± 0.002 | 0.019 ± 0.002 | 0.022 | 0.000 | 34.17 | 7.38 | 3.708 ± 0.263 | 24.37 ± 1.72 |
| 5 o | 1.75 | 27.133 ± 0.070 | 5.218 ± 0.031 | 0.078 ± 0.004 | 0.046 ± 0.002 | 0.030 ± 0.002 | 0.023 | -0.000 | 26.99 | 18.23 | 3.755 ± 0.107 | 24.68 ± 0.70 |
| 6 o | 2.25 | 30.477 ± 0.066 | 6.231 ± 0.038 | 0.108 ± 0.007 | 0.067 ± 0.003 | 0.028 ± 0.002 | 0.033 | 0.000 | 21.95 | 21.77 | 3.776 ± 0.097 | 24.82 ± 0.64 |
| 7 o | 2.75 | 10.546 ± 0.037 | 1.564 ± 0.014 | 0.041 ± 0.004 | 0.037 ± 0.002 | 0.021 ± 0.002 | 0.057 | 0.002 | 44.74 | 5.44 | 3.675 ± 0.344 | 24.16 ± 2.24 |
| 8 o | 3.75 | 7.026 ± 0.038 | 0.769 ± 0.010 | 0.017 ± 0.003 | 0.018 ± 0.002 | 0.019 ± 0.002 | 0.018 | 0.000 | 56.70 | 2.66 | 3.903 ± 0.663 | 25.65 ± 4.32 |

CRCO 254 Alunite & Natroalunite:

| | | | | | | | | | | | | |
|---|------|----------------|---------------|---------------|---------------|---------------|-------|-------|--------|-------|----------------|---------------|
| J = 0.003670 ± 0.000034, Volume ³⁹ ArK = 187.17 × 1E-10, Integrated Age = 13.00 ± 0.45 | | | | | | | | | | | | |
| 1 | 0.50 | 4.376 ± 0.024 | 0.094 ± 0.004 | 0.008 ± 0.002 | 0.015 ± 0.002 | 0.020 ± 0.002 | 0.024 | 0.003 | 102.90 | 0.46 | -1.425 ± 5.785 | -9.46 ± 38.50 |
| 2 | 0.75 | 10.264 ± 0.062 | 1.871 ± 0.016 | 0.042 ± 0.004 | 0.020 ± 0.002 | 0.029 ± 0.002 | 0.010 | 0.001 | 69.64 | 9.96 | 1.601 ± 0.330 | 10.57 ± 2.17 |
| 3 | 1.25 | 22.036 ± 0.079 | 7.851 ± 0.043 | 0.146 ± 0.007 | 0.037 ± 0.002 | 0.027 ± 0.002 | 0.010 | 0.001 | 28.52 | 41.92 | 1.954 ± 0.072 | 12.89 ± 0.47 |
| 4 | 1.75 | 16.850 ± 0.065 | 7.028 ± 0.040 | 0.126 ± 0.006 | 0.033 ± 0.002 | 0.012 ± 0.002 | 0.009 | 0.001 | 10.43 | 37.52 | 2.087 ± 0.071 | 13.76 ± 0.47 |
| 5 | 3.50 | 5.038 ± 0.036 | 1.906 ± 0.016 | 0.035 ± 0.004 | 0.021 ± 0.002 | 0.008 ± 0.002 | 0.013 | 0.001 | 14.70 | 10.14 | 2.121 ± 0.286 | 13.99 ± 1.88 |

CRCO 127 Natroalunite & Alunite:

| | | | | | | | | | | | | |
|---|------|----------------|---------------|---------------|---------------|---------------|-------|--------|--------|-------|------------------|------------------|
| J = 0.003671 ± 0.000034, Volume ³⁹ ArK = 180.56 × 1E-10, Integrated Age = 13.69 ± 0.63 | | | | | | | | | | | | |
| 1 | 0.50 | 24.145 ± 0.063 | 0.042 ± 0.003 | 0.020 ± 0.003 | 0.016 ± 0.002 | 0.089 ± 0.003 | 0.000 | -0.004 | 102.77 | 0.19 | -19.877 ± 26.181 | -136.69 ± 187.04 |
| 2 | 0.75 | 3.991 ± 0.023 | 0.033 ± 0.003 | 0.007 ± 0.002 | 0.015 ± 0.003 | 0.019 ± 0.002 | 0.000 | 0.003 | 101.78 | 0.14 | -2.839 ± 22.894 | -18.90 ± 153.22 |
| 3 | 1.25 | 21.785 ± 0.059 | 4.263 ± 0.030 | 0.124 ± 0.006 | 0.029 ± 0.003 | 0.051 ± 0.002 | 0.011 | 0.003 | 61.70 | 23.57 | 1.921 ± 0.166 | 12.68 ± 1.09 |
| 4 | 1.75 | 22.870 ± 0.045 | 5.110 ± 0.029 | 0.166 ± 0.007 | 0.040 ± 0.003 | 0.045 ± 0.002 | 0.018 | 0.004 | 50.91 | 28.27 | 2.160 ± 0.129 | 14.25 ± 0.85 |
| 5 | 2.25 | 24.549 ± 0.046 | 6.884 ± 0.040 | 0.231 ± 0.008 | 0.048 ± 0.003 | 0.038 ± 0.002 | 0.017 | 0.004 | 39.21 | 38.09 | 2.130 ± 0.098 | 14.05 ± 0.64 |
| 6 | 3.50 | 9.185 ± 0.038 | 1.767 ± 0.015 | 0.108 ± 0.006 | 0.033 ± 0.003 | 0.022 ± 0.002 | 0.035 | 0.010 | 51.44 | 9.74 | 2.477 ± 0.332 | 16.33 ± 2.18 |

| Step no. | Laser Power (W) | ⁴⁰ Ar | ³⁹ Ar | ³⁸ Ar | ³⁷ Ar | ³⁶ Ar | Ca/K | Cl/K | % ⁴⁰ Ar atm | f ³⁹ Ar | ⁴⁰ Ar*/ ³⁹ ArK | Age (Ma) | 2σ error |
|---|-----------------|------------------|------------------|------------------|------------------|------------------|-------|--------|------------------------|--------------------|--------------------------------------|------------------|----------|
| CRCO 199: Alunite & Natroalunite | | | | | | | | | | | | | |
| J = 0.003674 ± 0.000034, Volume ³⁹ ArK = 310.90 × 1E-10, Integrated Age = 15.63 ± 0.62 | | | | | | | | | | | | | |
| 1 | 0.50 | 29.746 ± 0.061 | 0.059 ± 0.003 | 0.024 ± 0.003 | 0.016 ± 0.002 | 0.110 ± 0.003 | 0.032 | -0.001 | 104.27 | 0.16 | -24.825 ± 17.147 | -172.54 ± 125.06 | |
| 2 | 0.75 | 83.543 ± 0.134 | 3.491 ± 0.028 | 0.126 ± 0.009 | 0.036 ± 0.004 | 0.268 ± 0.006 | 0.022 | 0.002 | 93.16 | 11.21 | 1.608 ± 0.552 | 10.62 ± 3.64 | |
| 3 | 1.25 | 65.921 ± 0.119 | 7.602 ± 0.047 | 0.190 ± 0.008 | 0.066 ± 0.003 | 0.168 ± 0.005 | 0.025 | 0.001 | 73.03 | 24.44 | 2.308 ± 0.182 | 15.23 ± 1.19 | |
| 4 | 1.75 | 46.970 ± 0.106 | 11.261 ± 0.056 | 0.251 ± 0.010 | 0.087 ± 0.004 | 0.067 ± 0.003 | 0.023 | 0.002 | 38.76 | 36.21 | 2.520 ± 0.070 | 16.63 ± 0.46 | |
| 5 | 2.25 | 22.406 ± 0.063 | 5.712 ± 0.034 | 0.129 ± 0.006 | 0.059 ± 0.003 | 0.030 ± 0.002 | 0.028 | 0.002 | 33.06 | 18.36 | 2.588 ± 0.107 | 17.07 ± 0.70 | |
| 6 | 3.50 | 13.745 ± 0.052 | 2.870 ± 0.019 | 0.074 ± 0.005 | 0.041 ± 0.003 | 0.024 ± 0.002 | 0.033 | 0.002 | 39.71 | 9.21 | 2.847 ± 0.180 | 18.77 ± 1.18 | |
| 7 | 4.00 | 4.567 ± 0.023 | 0.135 ± 0.004 | 0.009 ± 0.003 | 0.017 ± 0.002 | 0.019 ± 0.002 | 0.063 | 0.002 | 89.32 | 0.41 | 3.721 ± 4.018 | 24.49 ± 26.27 | |
| CRCO 271 Alunite & Natroalunite: | | | | | | | | | | | | | |
| J = 0.003675 ± 0.000034, Volume ³⁹ ArK = 286.01 × 1E-10, Integrated Age = 12.40 ± 1.81 | | | | | | | | | | | | | |
| 1 | 0.50 | 256.998 ± 0.505 | 0.171 ± 0.015 | 0.179 ± 0.023 | 0.016 ± 0.010 | 0.898 ± 0.022 | 0.046 | 0.008 | 102.80 | 0.57 | -43.927 ± 40.021 | -317.62 ± 316.42 | |
| 2 | 0.75 | 83.478 ± 0.212 | 0.437 ± 0.013 | 0.066 ± 0.007 | 0.020 ± 0.004 | 0.298 ± 0.007 | 0.047 | 0.001 | 103.70 | 1.50 | -7.213 ± 4.807 | -48.47 ± 32.74 | |
| 3 | 1.25 | 131.120 ± 0.287 | 10.520 ± 0.066 | 0.312 ± 0.020 | 0.169 ± 0.008 | 0.374 ± 0.009 | 0.056 | 0.002 | 83.23 | 36.77 | 2.059 ± 0.266 | 13.60 ± 1.75 | |
| 4 | 1.75 | 108.413 ± 0.187 | 16.378 ± 0.090 | 0.556 ± 0.024 | 0.455 ± 0.011 | 0.238 ± 0.007 | 0.103 | 0.004 | 63.31 | 57.26 | 2.396 ± 0.122 | 15.82 ± 0.80 | |
| 5 | 2.25 | 12.758 ± 0.038 | 0.940 ± 0.010 | 0.045 ± 0.004 | 0.054 ± 0.003 | 0.039 ± 0.002 | 0.161 | 0.006 | 79.41 | 3.26 | 2.763 ± 0.647 | 18.23 ± 4.25 | |
| 6 | 3.50 | 5.983 ± 0.033 | 0.188 ± 0.005 | 0.013 ± 0.003 | 0.021 ± 0.002 | 0.024 ± 0.002 | 0.131 | 0.004 | 91.67 | 0.63 | 2.690 ± 2.984 | 17.74 ± 19.59 | |
| CRCO 347 Alunite: | | | | | | | | | | | | | |
| J = 0.003676 ± 0.000034, Volume ³⁹ ArK = 177.55 × 1E-10, Integrated Age = 17.27 ± 1.53, Plateau Age = 19.55 ± 1.62 (83.00% of ³⁹ ArK) | | | | | | | | | | | | | |
| 1 | 0.50 | 235.988 ± 0.600 | 11.367 ± 0.137 | 0.568 ± 0.052 | 0.245 ± 0.026 | 0.836 ± 0.026 | 0.032 | 0.005 | 97.62 | 6.36 | 0.457 ± 0.694 | 3.03 ± 4.59 | |
| 2 | 0.75 | 692.143 ± 1.235 | 18.962 ± 0.187 | 0.910 ± 0.070 | 0.286 ± 0.034 | 2.317 ± 0.054 | 0.028 | 0.002 | 96.62 | 10.64 | 1.199 ± 0.857 | 7.93 ± 5.66 | |
| 3 | 1.25 | 670.862 ± 1.501 | 32.096 ± 0.324 | 1.038 ± 0.074 | 0.339 ± 0.036 | 2.004 ± 0.051 | 0.023 | 0.001 | 85.69 | 18.04 | 2.948 ± 0.480 | 19.44 ± 3.15 | |
| 4 | 1.75 | 908.061 ± 1.603 | 44.565 ± 0.382 | 1.459 ± 0.114 | 0.516 ± 0.049 | 2.671 ± 0.070 | 0.032 | 0.002 | 85.05 | 25.07 | 3.005 ± 0.468 | 19.82 ± 3.07 | |
| 5 | 2.25 | 567.173 ± 1.041 | 17.093 ± 0.159 | 0.703 ± 0.068 | 0.309 ± 0.032 | 1.821 ± 0.046 | 0.036 | 0.001 | 91.98 | 9.59 | 2.622 ± 0.801 | 17.30 ± 5.26 | |
| 6 | 3.50 | 702.488 ± 1.797 | 35.941 ± 0.276 | 1.145 ± 0.087 | 0.401 ± 0.040 | 2.049 ± 0.052 | 0.027 | 0.002 | 83.84 | 20.21 | 3.114 ± 0.439 | 20.53 ± 2.88 | |
| 7 | 4.00 | 462.724 ± 0.971 | 18.010 ± 0.157 | 0.669 ± 0.053 | 0.271 ± 0.030 | 1.442 ± 0.037 | 0.026 | 0.002 | 88.49 | 10.10 | 2.910 ± 0.620 | 19.20 ± 4.07 | |
| CRCO 322 Alunite & Natroalunite: | | | | | | | | | | | | | |
| J = 0.003676 ± 0.000032, Volume ³⁹ ArK = 242.20 × 1E-10, Integrated Age = 20.47 ± 0.54 | | | | | | | | | | | | | |
| 1 | 0.50 | 38.718 ± 0.063 | 0.104 ± 0.004 | 0.033 ± 0.004 | 0.016 ± 0.002 | 0.143 ± 0.004 | 0.065 | 0.006 | 105.44 | 0.40 | -21.820 ± 11.225 | -150.84 ± 80.93 | |
| 2 | 0.75 | 44.892 ± 0.086 | 0.567 ± 0.010 | 0.046 ± 0.004 | 0.019 ± 0.002 | 0.158 ± 0.004 | 0.026 | 0.003 | 100.28 | 2.31 | -0.255 ± 2.062 | -1.69 ± 13.69 | |
| 3 | 1.25 | 51.190 ± 0.081 | 11.410 ± 0.059 | 0.221 ± 0.011 | 0.056 ± 0.003 | 0.058 ± 0.002 | 0.013 | 0.001 | 30.46 | 47.10 | 3.085 ± 0.061 | 20.35 ± 0.40 | |
| 4 | 1.75 | 32.025 ± 0.055 | 8.398 ± 0.042 | 0.154 ± 0.009 | 0.051 ± 0.003 | 0.017 ± 0.002 | 0.016 | 0.001 | 10.79 | 34.66 | 3.365 ± 0.058 | 22.18 ± 0.38 | |
| 5 | 3.50 | 15.348 ± 0.038 | 3.769 ± 0.024 | 0.069 ± 0.005 | 0.028 ± 0.002 | 0.010 ± 0.002 | 0.012 | 0.001 | 7.69 | 15.53 | 3.716 ± 0.136 | 24.48 ± 0.89 | |
| CRCO 209-48 Alunite: | | | | | | | | | | | | | |
| J = 0.003676 ± 0.000032, Volume ³⁹ ArK = 232.28 × 1E-10, Integrated Age = 21.56 ± 0.41, Plateau Age = 21.49 ± 0.35 (98.18% of ³⁹ ArK) | | | | | | | | | | | | | |
| 1 | 0.50 | 10.537 ± 0.072 | 2.248 ± 0.020 | 0.042 ± 0.003 | 0.028 ± 0.003 | 0.016 ± 0.002 | 0.022 | 0.001 | 30.66 | 9.65 | 3.209 ± 0.232 | 21.16 ± 1.52 | |
| 2 | 0.75 | 36.016 ± 0.119 | 9.560 ± 0.052 | 0.158 ± 0.007 | 0.050 ± 0.003 | 0.023 ± 0.002 | 0.013 | 0.000 | 14.59 | 41.15 | 3.183 ± 0.065 | 20.99 ± 0.42 | |
| 3 | 1.25 | 40.716 ± 0.127 | 11.008 ± 0.063 | 0.172 ± 0.007 | 0.038 ± 0.003 | 0.018 ± 0.002 | 0.008 | 0.000 | 8.84 | 47.38 | 3.337 ± 0.057 | 22.00 ± 0.37 | |
| 4 | 1.75 | 1.900 ± 0.018 | 0.379 ± 0.006 | 0.009 ± 0.002 | 0.015 ± 0.002 | 0.007 ± 0.002 | 0.006 | 0.000 | 21.94 | 1.60 | 3.831 ± 1.448 | 25.23 ± 9.47 | |
| 5 | 3.50 | 1.318 ± 0.013 | 0.058 ± 0.003 | 0.006 ± 0.002 | 0.015 ± 0.002 | 0.009 ± 0.002 | 0.018 | 0.003 | 83.68 | 0.22 | 3.992 ± 10.759 | 26.28 ± 70.32 | |
| CRCO 209-39 Natroalunite: | | | | | | | | | | | | | |
| J = 0.003676 ± 0.000030, Volume ³⁹ ArK = 139.90 × 1E-10, Integrated Age = 20.86 ± 0.74, Plateau Age = 20.83 ± 0.72 (63.21% of ³⁹ ArK) | | | | | | | | | | | | | |
| 1 | 0.50 | 30.461 ± 0.055 | 3.022 ± 0.018 | 0.193 ± 0.008 | 0.043 ± 0.003 | 0.079 ± 0.002 | 0.035 | 0.010 | 72.21 | 21.56 | 2.767 ± 0.241 | 18.26 ± 1.59 | |
| 2 | 0.75 | 38.469 ± 0.069 | 7.421 ± 0.044 | 0.295 ± 0.011 | 0.070 ± 0.003 | 0.056 ± 0.002 | 0.028 | 0.006 | 39.39 | 53.01 | 3.105 ± 0.098 | 20.48 ± 0.64 | |
| 3 | 1.25 | 9.051 ± 0.038 | 1.432 ± 0.014 | 0.057 ± 0.004 | 0.028 ± 0.003 | 0.019 ± 0.002 | 0.034 | 0.005 | 44.67 | 10.19 | 3.443 ± 0.414 | 22.69 ± 2.71 | |

| Step no. | Laser Power (W) | ⁴⁰ Ar | ³⁹ Ar | ³⁸ Ar | ³⁷ Ar | ³⁶ Ar | Ca/K | Cl/K | % ⁴⁰ Ar atm | f ³⁹ Ar | ⁴⁰ Ar*/ ³⁹ ArK | Age (Ma) 2σ error |
|----------|-----------------|------------------|------------------|------------------|------------------|------------------|-------|-------|------------------------|--------------------|--------------------------------------|-------------------|
| 4 | 1.75 | 4.589 ± 0.024 | 0.545 ± 0.008 | 0.025 ± 0.003 | 0.066 ± 0.003 | 0.012 ± 0.002 | 0.351 | 0.006 | 43.43 | 3.85 | 4.689 ± 1.071 | 30.83 ± 6.98 |
| 5 | 3.50 | 9.268 ± 0.038 | 1.499 ± 0.015 | 0.062 ± 0.005 | 0.289 ± 0.006 | 0.019 ± 0.002 | 0.686 | 0.005 | 45.03 | 10.67 | 3.348 ± 0.384 | 22.07 ± 2.52 |
| 6 | 4.00 | 1.411 ± 0.010 | 0.108 ± 0.004 | 0.008 ± 0.003 | 0.016 ± 0.002 | 0.008 ± 0.002 | 0.026 | 0.006 | 65.66 | 0.72 | 4.443 ± 4.949 | 29.23 ± 32.29 |

CRCO 205-28 Natroalunite:

| | | | | | | | | | | | | |
|--|------|----------------|---------------|---------------|---------------|---------------|-------|-------|-------|-------|---------------|---------------|
| J = 0.003676 ± 0.000030, Volume ³⁹ ArK = 81.39 × 1E-10, Integrated Age = 20.65 ± 1.10, Plateau Age = 20.88 ± 0.98 (98.34% of ³⁹ ArK) | | | | | | | | | | | | |
| 1 | 0.50 | 7.745 ± 0.049 | 0.143 ± 0.005 | 0.019 ± 0.003 | 0.028 ± 0.003 | 0.030 ± 0.002 | 0.355 | 0.015 | 98.03 | 1.66 | 1.083 ± 4.801 | 7.17 ± 31.72 |
| 2 o | 0.75 | 26.070 ± 0.052 | 4.224 ± 0.027 | 0.318 ± 0.011 | 0.417 ± 0.007 | 0.048 ± 0.002 | 0.355 | 0.013 | 48.61 | 51.82 | 3.134 ± 0.157 | 20.67 ± 1.03 |
| 3 o | 1.25 | 15.867 ± 0.047 | 2.715 ± 0.018 | 0.225 ± 0.009 | 0.272 ± 0.006 | 0.029 ± 0.002 | 0.354 | 0.015 | 44.26 | 33.28 | 3.215 ± 0.217 | 21.19 ± 1.42 |
| 4 o | 1.75 | 2.914 ± 0.020 | 0.331 ± 0.006 | 0.031 ± 0.003 | 0.046 ± 0.003 | 0.011 ± 0.002 | 0.350 | 0.015 | 61.32 | 3.97 | 3.338 ± 1.620 | 22.00 ± 10.61 |
| 5 o | 3.50 | 5.838 ± 0.026 | 0.763 ± 0.009 | 0.066 ± 0.004 | 0.089 ± 0.003 | 0.017 ± 0.002 | 0.362 | 0.015 | 58.76 | 9.27 | 3.104 ± 0.758 | 20.47 ± 4.97 |

Measured volumes are × 1E-10 cm³

All ages are Ma and errors are 2σ standard error

% ⁴⁰Ar atm: percentage of atmospheric ⁴⁰Ar

f³⁹Ar: fraction of ³⁹Ar

⁴⁰Ar*: Radiogenic ⁴⁰Ar

³⁹ArK: ³⁹Ar from K

o: Steps used to determine plateau age

Isotope Production Ratios:

(⁴⁰Ar/³⁹Ar) K = 0.0302

(³⁷Ar/³⁹Ar) Ca = 1416.4306

(³⁶Ar/³⁹Ar) Ca = 0.3952

Ca/K = 1.83 × (³⁷ArCa/³⁹ArK)

APPENDIX 5

Fluid Inclusion Data, Cerro Colorado

| Sample no. | Alteration Assemblages | Elevation (m a.s.l.) | Inclusion Type (see Table 2-4) | Te (-) | Tm Ice (-) | Tm NaCl | Salinity (wt.% NaCl equiv.) | Th (L-V) |
|------------|--------------------------|-------------------------|-----------------------------------|--------|------------|---------|--------------------------------|----------|
| 83-40 | biotite-albite-magnetite | 2193 | 3 | | 1.9 | | 3.2 | 236 |
| 83-40 | biotite-albite-magnetite | 2193 | 3 | | 2.1 | | 3.5 | 227 |
| 83-40 | biotite-albite-magnetite | 2193 | 3 | | 3.5 | | 5.7 | 225 |
| 83-40 | biotite-albite-magnetite | 2193 | 3 | | | | | 196 |
| 83-40 | biotite-albite-magnetite | 2193 | 3 | | | | | 199 |
| 83-40 | biotite-albite-magnetite | 2193 | 3 | | 2.6 | | 4.3 | 217 |
| 83-40 | biotite-albite-magnetite | 2193 | 3 | | 2.1 | | 3.5 | 199 |
| 83-40 | biotite-albite-magnetite | 2193 | 3 | | 2.5 | | 4.2 | 215 |
| 83-40 | biotite-albite-magnetite | 2193 | 3 | | 2.3 | | 3.9 | 223 |
| 83-40 | biotite-albite-magnetite | 2193 | 3 | | 2.0 | | 3.4 | 194 |
| 83-40 | biotite-albite-magnetite | 2193 | 3 | | | | | 198 |
| 83-40 | biotite-albite-magnetite | 2193 | 3 | | | | | 212 |
| 83-40 | biotite-albite-magnetite | 2193 | 3 | | 4.5 | | 7.2 | 250 |
| 83-40 | biotite-albite-magnetite | 2193 | 3 | | 2.5 | | 4.2 | 249 |
| 83-40 | biotite-albite-magnetite | 2193 | 3 | | | | | 186 |
| 83-40 | biotite-albite-magnetite | 2193 | 3 | | 4.2 | | 6.7 | 220 |
| 83-40 | biotite-albite-magnetite | 2193 | 3 | | 4.1 | | 6.6 | 233 |
| 83-40 | biotite-albite-magnetite | 2193 | 3 | | 4.0 | | 6.4 | 222 |
| 83-40 | biotite-albite-magnetite | 2193 | 3 | | 2.5 | | 4.2 | 242 |
| 83-40 | biotite-albite-magnetite | 2193 | 3 | | 1.3 | | 2.2 | 246 |
| 83-40 | biotite-albite-magnetite | 2193 | 3 | | 1.4 | | 2.4 | 249 |
| 83-40 | biotite-albite-magnetite | 2193 | 3 | | 1.1 | | 1.9 | 245 |
| 83-40 | biotite-albite-magnetite | 2193 | 3 | | 3.2 | | 5.3 | 229 |
| 83-40 | biotite-albite-magnetite | 2193 | 3 | | 2.4 | | 4.0 | 219 |
| 83-40 | biotite-albite-magnetite | 2193 | 3 | | 4.2 | | 6.7 | 247 |
| 83-50 | biotite-albite-magnetite | 2210 | 3 | | 1.9 | | 3.2 | 206 |
| 83-50 | biotite-albite-magnetite | 2210 | 3 | | | | | 210 |
| 83-50 | biotite-albite-magnetite | 2210 | 3 | | | | | 220 |
| 83-50 | biotite-albite-magnetite | 2210 | 3 | | | | | 230 |
| 83-50 | biotite-albite-magnetite | 2210 | 3 | | | | | 196 |
| 83-50 | biotite-albite-magnetite | 2210 | 3 | | | | | 217 |
| 83-50 | biotite-albite-magnetite | 2210 | 3 | | | | | 225 |
| 83-50 | biotite-albite-magnetite | 2210 | 3 | | | | | 247 |
| 83-50 | biotite-albite-magnetite | 2210 | 3 | | | | | 234 |
| 83-50 | biotite-albite-magnetite | 2210 | 3 | | | | | 241 |
| 83-58 | biotite-albite-magnetite | 2230 | 3 | | 0.1 | | 0.2 | 270 |
| 83-58 | biotite-albite-magnetite | 2230 | 3 | | 3.6 | | 5.9 | 240 |
| 83-58 | biotite-albite-magnetite | 2230 | 3 | | 0.5 | | 0.9 | 222 |
| 83-58 | biotite-albite-magnetite | 2230 | 3 | | 1.0 | | 1.7 | 230 |
| 83-58 | biotite-albite-magnetite | 2230 | 3 | | 2.1 | | 3.5 | 237 |
| 83-58 | biotite-albite-magnetite | 2230 | 3 | | 4.2 | | 6.7 | 266 |
| 83-58 | biotite-albite-magnetite | 2230 | 3 | | 4.5 | | 7.2 | 212 |
| 83-58 | biotite-albite-magnetite | 2230 | 3 | | 3.9 | | 6.3 | 242 |
| 83-58 | biotite-albite-magnetite | 2230 | 3 | | 2.0 | | 3.4 | 240 |
| 83-58 | biotite-albite-magnetite | 2230 | 3 | | 0.1 | | 0.2 | 311 |
| 83-58 | biotite-albite-magnetite | 2230 | 3 | | 3.5 | | 5.7 | 199 |

| Sample no. | Alteration Assemblages | Elevation | Inclusion Type | Te (-) | Tm Ice (-) | Tm NaCl | Salinity | Th (L-V) |
|------------|--------------------------|-----------|----------------|--------|------------|---------|----------|----------|
| 83-58 | biotite-albite-magnetite | 2230 | 3 | | 3.5 | | 5.7 | 216 |
| 83-58 | biotite-albite-magnetite | 2230 | 3 | | 2.0 | | 3.4 | 271 |
| 83-58 | biotite-albite-magnetite | 2230 | 3 | | 3.0 | | 5.0 | 245 |
| 83-58 | biotite-albite-magnetite | 2230 | 3 | | 2.0 | | 3.4 | 261 |
| 83-58 | biotite-albite-magnetite | 2230 | 3 | | 2.4 | | 4.0 | 236 |
| 83-58 | biotite-albite-magnetite | 2230 | 3 | | | | | 251 |
| 83-58 | biotite-albite-magnetite | 2230 | 3 | | 1.9 | | 3.2 | 258 |
| 83-58 | biotite-albite-magnetite | 2230 | 3 | | 3.0 | | 5.0 | 243 |
| 83-58 | biotite-albite-magnetite | 2230 | 3 | | | | | 225 |
| 83-58 | biotite-albite-magnetite | 2230 | 3 | | | | | 225 |
| 83-58 | biotite-albite-magnetite | 2230 | 3 | | | | | 225 |
| 83-58 | biotite-albite-magnetite | 2230 | 3 | | 2.0 | | 3.4 | 210 |
| 83-58 | biotite-albite-magnetite | 2230 | 3 | | 5.0 | | 7.9 | 208 |
| 83-58 | biotite-albite-magnetite | 2230 | 3 | | 4.0 | | 6.4 | 191 |
| 83-58 | biotite-albite-magnetite | 2230 | 3 | | 4.0 | | 6.4 | 214 |
| 83-58 | biotite-albite-magnetite | 2230 | 3 | | 0.7 | | 1.2 | 236 |
| 83-58 | biotite-albite-magnetite | 2230 | 3 | | | | | 225 |
| 83-58 | biotite-albite-magnetite | 2230 | 3 | | | | | 245 |
| 83-58 | biotite-albite-magnetite | 2230 | 3 | | 2.0 | | 3.4 | 205 |
| 83-58 | biotite-albite-magnetite | 2230 | 3 | | | | | 206 |
| 83-58 | biotite-albite-magnetite | 2230 | 3 | | | | | 208 |
| 83-58 | biotite-albite-magnetite | 2230 | 3 | | | | | 227 |
| 83-58 | biotite-albite-magnetite | 2230 | 3 | | | | | 235 |
| 83-58 | biotite-albite-magnetite | 2230 | 3 | | | | | 236 |
| 83-58 | biotite-albite-magnetite | 2230 | 3 | | 3.0 | | 5.0 | 213 |
| 83-58 | biotite-albite-magnetite | 2230 | 3 | | 3.0 | | 5.0 | 241 |
| 83-58 | biotite-albite-magnetite | 2230 | 3 | | 3.0 | | 5.0 | 257 |
| 83-58 | biotite-albite-magnetite | 2230 | 3 | | 5.0 | | 7.9 | 230 |
| 83-58 | biotite-albite-magnetite | 2230 | 3 | | 4.1 | | 6.6 | 228 |
| 83-58 | biotite-albite-magnetite | 2230 | 3 | | 4.0 | | 6.4 | 236 |
| 83-58 | biotite-albite-magnetite | 2230 | 3 | | 1.5 | | 2.6 | 189 |
| 83-58 | biotite-albite-magnetite | 2230 | 3 | | | | | 198 |
| 83-58 | biotite-albite-magnetite | 2230 | 3 | | | | | 209 |
| 83-58 | biotite-albite-magnetite | 2230 | 3 | | | | | 208 |
| 83-58 | biotite-albite-magnetite | 2230 | 3 | | | | | 250 |
| 83-58 | biotite-albite-magnetite | 2230 | 3 | | | | | 240 |
| 83-58 | biotite-albite-magnetite | 2230 | 3 | | | | | 224 |
| 83-58 | biotite-albite-magnetite | 2230 | 3 | | | | | 233 |
| 83-58 | biotite-albite-magnetite | 2230 | 3 | | | | | 246 |
| 83-58 | biotite-albite-magnetite | 2230 | 3 | | | | | 226 |
| 83-58 | biotite-albite-magnetite | 2230 | 3 | | | | | 220 |
| 83-58 | biotite-albite-magnetite | 2230 | 3 | | 2.1 | | 3.5 | 268 |
| 83-58 | biotite-albite-magnetite | 2230 | 3 | | 2.0 | | 3.4 | 266 |
| 83-58 | biotite-albite-magnetite | 2230 | 3 | | | | | 242 |
| 83-58 | biotite-albite-magnetite | 2230 | 3 | | | | | 239 |
| 83-58 | biotite-albite-magnetite | 2230 | 3 | | 2.1 | | 3.5 | 244 |
| 83-58 | biotite-albite-magnetite | 2230 | 3 | | 4.8 | | 7.6 | 246 |
| 83-58 | biotite-albite-magnetite | 2230 | 3 | | 1.5 | | 2.6 | 273 |
| 83-58 | biotite-albite-magnetite | 2230 | 3 | | | | | 242 |

| Sample no. | Alteration Assemblages | Elevation | Inclusion Type | Te (-) | Tm Ice (-) | Tm NaCl | Salinity | Th (L-V) |
|------------|--------------------------|-----------|----------------|--------|------------|---------|----------|----------|
| 83-58 | biotite-albite-magnetite | 2230 | 3 | | | | | 241 |
| 83-58 | biotite-albite-magnetite | 2230 | 3 | | | | | 240 |
| 83-58 | biotite-albite-magnetite | 2230 | 3 | | | | | 242 |
| 83-58 | biotite-albite-magnetite | 2230 | 3 | | 1.0 | | 1.7 | 281 |
| 83-58 | biotite-albite-magnetite | 2230 | 3 | | 0.8 | | 1.4 | 228 |
| 83-58 | biotite-albite-magnetite | 2230 | 3 | | 0.9 | | 1.6 | 235 |
| 83-58 | biotite-albite-magnetite | 2230 | 3 | | 2.6 | | 4.3 | 251 |
| 83-58 | biotite-albite-magnetite | 2230 | 3 | | 2.0 | | 3.4 | 235 |
| 83-58 | biotite-albite-magnetite | 2230 | 3 | | 1.5 | | 2.6 | 242 |
| 83-58 | biotite-albite-magnetite | 2230 | 3 | | | | | 228 |
| 83-58 | biotite-albite-magnetite | 2230 | 3 | | | | | 215 |
| 83-58 | biotite-albite-magnetite | 2230 | 3 | | | | | 249 |
| 83-58 | biotite-albite-magnetite | 2230 | 3 | | | | | 221 |
| 83-58 | biotite-albite-magnetite | 2230 | 3 | | | | | 234 |
| 83-58 | biotite-albite-magnetite | 2230 | 3 | | | | | 248 |
| 83-58 | biotite-albite-magnetite | 2230 | 3 | | 2.2 | | 3.7 | 241 |
| 83-58 | biotite-albite-magnetite | 2230 | 3 | | 1.8 | | 3.1 | 236 |
| 83-58 | biotite-albite-magnetite | 2230 | 3 | | 2.6 | | 4.3 | 244 |
| 83-58 | biotite-albite-magnetite | 2230 | 3 | | 2.9 | | 4.8 | 247 |
| 83-58 | biotite-albite-magnetite | 2230 | 3 | | 4.1 | | 6.6 | 220 |
| 83-58 | biotite-albite-magnetite | 2230 | 3 | | | | | 234 |
| 83-58 | biotite-albite-magnetite | 2230 | 3 | | | | | 242 |
| 83-58 | biotite-albite-magnetite | 2230 | 3 | | 3.1 | | 5.1 | 229 |
| 83-58 | biotite-albite-magnetite | 2230 | 3 | | | | | 204 |
| 83-58 | biotite-albite-magnetite | 2230 | 3 | | | | | 243 |
| 83-58 | biotite-albite-magnetite | 2230 | 3 | | | | | 246 |
| 83-58 | biotite-albite-magnetite | 2230 | 3 | | | | | 230 |
| 83-58 | biotite-albite-magnetite | 2230 | 3 | | 1.7 | | 2.9 | 237 |
| 83-58 | biotite-albite-magnetite | 2230 | 3 | | | | | 231 |
| 83-58 | biotite-albite-magnetite | 2230 | 3 | | | | | 221 |
| 83-58 | biotite-albite-magnetite | 2230 | 3 | | 3.8 | | 6.2 | 227 |
| 83-44 | quartz-albite | 2199 | 1a | | | 330 | 40.6 | 345 |
| 83-44 | quartz-albite | 2199 | 1a | | | 333 | 40.9 | 544 |
| 83-44 | quartz-albite | 2199 | 1a | <55 | | 335 | 41.0 | 413 |
| 83-44 | quartz-albite | 2199 | 1a | | | 307 | 38.7 | 333 |
| 83-44 | quartz-albite | 2199 | 1b | | | 355 | 42.9 | 273 |
| 83-44 | quartz-albite | 2199 | 1b | | | 301 | 38.2 | 197 |
| 83-44 | quartz-albite | 2199 | 1b | | | 327 | 40.3 | 318 |
| 83-44 | quartz-albite | 2199 | 1b | | | 342 | 41.7 | 269 |
| 83-44 | quartz-albite | 2199 | 1b | | | 312 | 39.1 | 258 |
| 83-44 | quartz-albite | 2199 | 2b | | | 406 | 48.1 | 305 |
| 83-46 | quartz-albite | 2202 | 1a | | | 311 | 39.0 | 360 |
| 83-46 | quartz-albite | 2202 | 1a | <51 | | 348 | 42.2 | 370 |
| 83-46 | quartz-albite | 2202 | 4 | | | | | 369 |
| 83-58 | quartz-albite | 2232 | 1a | | | 347 | 42.1 | 502 |
| 83-58 | quartz-albite | 2232 | 1b | | | 355 | 42.9 | 235 |
| 83-58 | quartz-albite | 2232 | 2a | | | 322 | 40.0 | 397 |
| 83-58 | quartz-albite | 2232 | 2a | | | 349 | 42.3 | 370 |
| 83-58 | quartz-albite | 2232 | 2b | | | 324 | 40.1 | 316 |

| Sample no. | Alteration Assemblages | Elevation | Inclusion Type | Te (-) | Tm Ice (-) | Tm NaCl | Salinity | Th (L-V) |
|------------|------------------------|-----------|----------------|----------|------------|---------|----------|----------|
| 83-58 | quartz-albite | 2232 | 4 | | | | | 353 |
| 83-59 | quartz-albite | 2233 | 1a | 60 to 52 | | 292 | 37.6 | 450 |
| 83-59 | quartz-albite | 2233 | 1a | | | 321 | 39.9 | 339 |
| 83-59 | quartz-albite | 2233 | 1a | <49 | | 303 | 38.4 | 372 |
| 83-59 | quartz-albite | 2233 | 1a | | | 315 | 39.3 | 340 |
| 83-59 | quartz-albite | 2233 | 1a | | | 326 | 40.3 | 390 |
| 83-59 | quartz-albite | 2233 | 2a | <46.9 | | 318 | 39.6 | 373 |
| 83-59 | quartz-albite | 2233 | 2a | | | 338 | 41.3 | 351 |
| 83-59 | quartz-albite | 2233 | 2b | <32 | | 335 | 41.0 | 252 |
| 83-63 | quartz-albite | 2241 | 1b | | | 323 | 40.0 | 298 |
| 83-63 | quartz-albite | 2241 | 2b | | | 338 | 41.3 | 310 |
| 83-63 | quartz-albite | 2241 | 2b | | | 433 | 51.6 | 320 |
| 83-63 | quartz-albite | 2241 | 2b | <44.6 | | 350 | 42.4 | 336 |
| 83-63 | quartz-albite | 2241 | 4 | | | | | 390 |
| 83-63 | quartz-albite | 2241 | 4 | | | | | 376 |
| 83-79 | quartz-albite | 2283 | 1a | | | 303 | 38.4 | 327 |
| 83-79 | quartz-albite | 2283 | 1a | | | 327 | 40.4 | 348 |
| 83-79 | quartz-albite | 2283 | 1b | | | 322 | 39.9 | 275 |
| 83-79 | quartz-albite | 2283 | 1b | | | 235 | 33.8 | 174 |
| 83-79 | quartz-albite | 2283 | 1b | | | 281 | 36.7 | 257 |
| 83-79 | quartz-albite | 2283 | 1b | | | 245 | 34.4 | 237 |
| 83-79 | quartz-albite | 2283 | 1b | | | 333 | 40.9 | 224 |
| 83-79 | quartz-albite | 2283 | 1b | | | 313 | 39.2 | 258 |
| 83-79 | quartz-albite | 2283 | 2a | <58 | | 322 | 39.9 | 402 |
| 146-16 | quartz-albite | 2199 | 1b | | | 328 | 40.4 | 323 |
| 146-16 | quartz-albite | 2199 | 2a | | | 328 | 40.4 | 436 |
| 146-16 | quartz-albite | 2199 | 2b | | | 344 | 41.8 | 344 |
| 146-16 | quartz-albite | 2199 | 2b | 56 | | 330 | 40.6 | 324 |
| 146-16 | quartz-albite | 2199 | 2b | | | 307 | 38.7 | 241 |
| 146-16 | quartz-albite | 2199 | 4 | | | | | 426 |
| 83-72 | sericite-chlorite-clay | 2269 | 1b | | | 358 | 43.1 | 352 |
| 83-72 | sericite-chlorite-clay | 2269 | 2b | | | 364 | 43.7 | 281 |
| 83-72 | sericite-chlorite-clay | 2269 | 2b | | | 330 | 40.6 | 260 |
| 83-72 | sericite-chlorite-clay | 2269 | 4 | | | | | |
| 83-72 | sericite-chlorite-clay | 2269 | 4 | 65-55 | | | | |
| 83-72 | sericite-chlorite-clay | 2269 | 4 | | | | | |
| 83-79 | sericite-chlorite-clay | 2281 | 1a | | | 318 | 39.6 | 339 |
| 83-79 | sericite-chlorite-clay | 2281 | 1a | | | 246 | 34.4 | 444 |
| 83-79 | sericite-chlorite-clay | 2281 | 2a | | | 318 | 39.6 | 332 |
| 83-79 | sericite-chlorite-clay | 2281 | 2b | | | 341 | 41.5 | 323 |
| 83-79 | sericite-chlorite-clay | 2281 | 3 | | 3.7 | | 6.0 | 315 |
| 83-79 | sericite-chlorite-clay | 2281 | 3 | | 3.1 | | 5.1 | |
| 83-79 | sericite-chlorite-clay | 2281 | 3 | | 5.2 | | 8.1 | |
| 148-10 | sericite-chlorite-clay | 2326 | 1a | | | 122 | 28.7 | 380 |
| 148-10 | sericite-chlorite-clay | 2326 | 1b | | | 299 | 38.1 | 212 |
| 148-10 | sericite-chlorite-clay | 2326 | 3 | | 4.3 | | 6.9 | 236 |
| 148-10 | sericite-chlorite-clay | 2326 | 3 | | 7.0 | | 10.5 | 311 |
| 148-10 | sericite-chlorite-clay | 2326 | 3 | | 4.3 | | 6.9 | 256 |
| 148-10 | sericite-chlorite-clay | 2326 | 3 | | 6.0 | | 9.2 | 251 |

| Sample no. | Alteration Assemblages | Elevation | Inclusion Type | Te (-) | Tm Ice (-) | Tm NaCl | Salinity | Th (L-V) |
|------------|------------------------|-----------|----------------|--------|------------|---------|----------|----------|
| 148-10 | sericite-chlorite-clay | 2326 | 3 | | | | | 238 |
| 148-10 | sericite-chlorite-clay | 2326 | 3 | | | | | 252 |
| 148-10 | sericite-chlorite-clay | 2326 | 3 | | 7.0 | | 10.5 | 330 |
| 148-10 | sericite-chlorite-clay | 2326 | 3 | | 4.4 | | 7.0 | 247 |
| 148-10 | sericite-chlorite-clay | 2326 | 3 | | 4.3 | | 6.9 | 236 |
| 148-10 | sericite-chlorite-clay | 2326 | 3 | | 4.7 | | 7.4 | 272 |
| 148-10 | sericite-chlorite-clay | 2326 | 3 | | | | | 328 |
| 148-10 | sericite-chlorite-clay | 2326 | 3 | | | | | 263 |
| 148-10 | sericite-chlorite-clay | 2326 | 3 | | | | | 272 |
| 148-10 | sericite-chlorite-clay | 2326 | 3 | | | | | 239 |
| 148-10 | sericite-chlorite-clay | 2326 | 3 | | | | | 240 |
| 148-10 | sericite-chlorite-clay | 2326 | 3 | | 8.0 | | 11.7 | |
| 148-13 | sericite-chlorite-clay | 2336 | 1a | 61-50 | | 276 | 36.4 | 290 |
| 148-13 | sericite-chlorite-clay | 2336 | 1a | <40 | | 292 | 37.6 | 302 |
| 148-13 | sericite-chlorite-clay | 2336 | 1a | 57-31 | | 256 | 35.1 | 329 |
| 148-13 | sericite-chlorite-clay | 2336 | 1a | 76-43 | | 272 | 36.1 | 314 |
| 148-13 | sericite-chlorite-clay | 2336 | 1a | | | 277 | 36.5 | 312 |
| 148-13 | sericite-chlorite-clay | 2336 | 1a | | | 281 | 36.8 | 333 |
| 148-13 | sericite-chlorite-clay | 2336 | 1a | | | 267 | 35.8 | 336 |
| 148-13 | sericite-chlorite-clay | 2336 | 1b | 74-50 | | 264 | 35.6 | 205 |
| 148-13 | sericite-chlorite-clay | 2336 | 1b | | | 228 | 33.4 | 186 |
| 148-13 | sericite-chlorite-clay | 2336 | 1b | | | 216 | 32.7 | 197 |
| 148-13 | sericite-chlorite-clay | 2336 | 1b | | | 260 | 35.3 | 197 |
| 148-13 | sericite-chlorite-clay | 2336 | 1b | | | 278 | 36.5 | 248 |
| 148-13 | sericite-chlorite-clay | 2336 | 3 | 57-42 | | | | 235 |
| 210-10 | sericite-chlorite-clay | 2252 | 1a | | | 285 | 37.0 | 315 |
| 210-10 | sericite-chlorite-clay | 2252 | 1a | | | 287 | 37.2 | 315 |
| 210-10 | sericite-chlorite-clay | 2252 | 1b | | | 267 | 35.8 | 206 |
| 210-14 | sericite-chlorite-clay | 2265 | 1a | | | 289 | 37.3 | 307 |
| 210-14 | sericite-chlorite-clay | 2265 | 1a | | | 282 | 36.8 | 335 |
| 210-14 | sericite-chlorite-clay | 2265 | 1a | 56 | | 280 | 36.7 | 302 |
| 210-14 | sericite-chlorite-clay | 2265 | 1a | | | 164 | 30.2 | 298 |
| 210-14 | sericite-chlorite-clay | 2265 | 1a | | | 319 | 39.6 | 330 |
| 210-14 | sericite-chlorite-clay | 2265 | 1a | | | 278 | 36.6 | 338 |
| 210-14 | sericite-chlorite-clay | 2265 | 1a | | | 277 | 36.4 | 294 |
| 210-14 | sericite-chlorite-clay | 2265 | 1a | | | 277 | 36.5 | 312 |
| 210-14 | sericite-chlorite-clay | 2265 | 1a | | | 317 | 39.5 | 335 |
| 210-14 | sericite-chlorite-clay | 2265 | 1a | | | 306 | 38.6 | 312 |
| 210-14 | sericite-chlorite-clay | 2265 | 1a | | | 273 | 36.2 | 339 |
| 210-14 | sericite-chlorite-clay | 2265 | 1a | | | 380 | 45.3 | 402 |
| 210-14 | sericite-chlorite-clay | 2265 | 1a | | | 315 | 39.3 | 324 |
| 210-14 | sericite-chlorite-clay | 2265 | 1a | | | 298 | 38.0 | 333 |
| 210-14 | sericite-chlorite-clay | 2265 | 1a | | | 314 | 39.3 | 354 |
| 210-14 | sericite-chlorite-clay | 2265 | 1a | | | 242 | 34.2 | 378 |
| 210-14 | sericite-chlorite-clay | 2265 | 1a | <60 | | 311 | 39.0 | 319 |
| 210-14 | sericite-chlorite-clay | 2265 | 1a | | | 275 | 36.3 | 305 |
| 210-14 | sericite-chlorite-clay | 2265 | 1a | | | 259 | 35.3 | 319 |
| 210-14 | sericite-chlorite-clay | 2265 | 1a | | | 250 | 34.7 | 367 |
| 210-14 | sericite-chlorite-clay | 2265 | 1a | | | 279 | 36.6 | 326 |
| 210-14 | sericite-chlorite-clay | 2265 | 1a | | | 298 | 38.0 | 330 |

| Sample no. | Alteration Assemblages | Elevation | Inclusion Type | Te (-) | Tm Ice (-) | Tm NaCl | Salinity | Th (L-V) |
|------------|------------------------|-----------|----------------|--------|------------|---------|----------|----------|
| 210-14 | sericite-chlorite-clay | 2265 | 1a | | | 300 | 38.2 | 313 |
| 210-14 | sericite-chlorite-clay | 2265 | 1b | | | 314 | 39.3 | 304 |
| 210-14 | sericite-chlorite-clay | 2265 | 1b | | | 385 | 45.8 | 309 |
| 210-14 | sericite-chlorite-clay | 2265 | 1b | | | 408 | 48.2 | 313 |
| 210-14 | sericite-chlorite-clay | 2265 | 1b | 52-61 | | 307 | 38.7 | 292 |
| 210-14 | sericite-chlorite-clay | 2265 | 1b | | | 323 | 40.0 | 279 |
| 210-14 | sericite-chlorite-clay | 2265 | 1b | | | 297 | 37.9 | 289 |
| 210-14 | sericite-chlorite-clay | 2265 | 1b | | | 326 | 40.2 | 309 |
| 210-14 | sericite-chlorite-clay | 2265 | 1b | | | 319 | 39.6 | 308 |
| 210-14 | sericite-chlorite-clay | 2265 | 1b | | | 326 | 40.3 | 290 |
| 210-14 | sericite-chlorite-clay | 2265 | 1b | | | 323 | 40.0 | 237 |
| 210-14 | sericite-chlorite-clay | 2265 | 1b | | | 287 | 37.2 | 220 |
| 210-14 | sericite-chlorite-clay | 2265 | 2a | | | 323 | 40.0 | 344 |
| 210-14 | sericite-chlorite-clay | 2265 | 2b | | | 355 | 42.9 | 312 |
| 210-14 | sericite-chlorite-clay | 2265 | 2b | | | 309 | 38.9 | 269 |
| 210-14 | sericite-chlorite-clay | 2265 | 2b | | | 325 | 40.2 | 307 |
| 210-14 | sericite-chlorite-clay | 2265 | 4 | | | | | 340 |
| 210-14 | sericite-chlorite-clay | 2265 | 3 | | | | | 367 |
| 210-14 | sericite-chlorite-clay | 2265 | 3 | | | | | 389 |
| 210-14 | sericite-chlorite-clay | 2265 | 3 | | | | | 350 |
| 206-42 | quartz-sericite-clay | 2347 | 1a | | | 245 | 34.4 | 245 |
| 206-42 | quartz-sericite-clay | 2347 | 1a | | | 256 | 35.1 | 260 |
| 206-42 | quartz-sericite-clay | 2347 | 1a | | | 250 | 34.7 | 250 |
| 206-42 | quartz-sericite-clay | 2347 | 1a | | | 244 | 34.3 | 258 |
| 206-42 | quartz-sericite-clay | 2347 | 1a | | | 261 | 35.4 | 265 |
| 206-42 | quartz-sericite-clay | 2347 | 1a | | | 279 | 36.6 | 283 |
| 206-42 | quartz-sericite-clay | 2347 | 1a | | | 268 | 35.8 | 270 |
| 206-42 | quartz-sericite-clay | 2347 | 1b | | | 277 | 36.5 | 259 |
| 206-42 | quartz-sericite-clay | 2347 | 1b | | | 226 | 33.3 | 201 |
| 206-42 | quartz-sericite-clay | 2347 | 1b | | | 259 | 35.3 | 239 |
| 206-42 | quartz-sericite-clay | 2347 | 4 | | | | | |
| 206-42 | quartz-sericite-clay | 2347 | 3 | | 2.5 | | 4.2 | 231 |
| 206-42 | quartz-sericite-clay | 2347 | 3 | | 3.1 | | 5.1 | 239 |
| 206-42 | quartz-sericite-clay | 2347 | 3 | | 3.6 | | 5.9 | 243 |
| 210-81 | quartz-sericite-clay | 2384 | 1a | 60-50 | | 260 | 35.3 | 262 |
| 210-81 | quartz-sericite-clay | 2384 | 1a | | | 255 | 35.0 | 255 |
| 210-81 | quartz-sericite-clay | 2384 | 1a | | | 242 | 34.2 | 259 |
| 210-81 | quartz-sericite-clay | 2384 | 1a | | | 266 | 35.7 | 269 |
| 210-81 | quartz-sericite-clay | 2384 | 1a | | | 285 | 37.0 | 288 |
| 210-81 | quartz-sericite-clay | 2384 | 1b | | | 279 | 36.6 | 263 |
| 210-81 | quartz-sericite-clay | 2384 | 2a | | | 248 | 34.6 | 249 |
| 210-81 | quartz-sericite-clay | 2384 | 4 | | | | | |
| 210-81 | quartz-sericite-clay | 2384 | 3 | | 3.2 | | 5.3 | 232 |
| 210-81 | quartz-sericite-clay | 2384 | 3 | | 3.0 | | 5.0 | 223 |
| 210-81 | quartz-sericite-clay | 2384 | 3 | | 3.7 | | 6.0 | 237 |
| 210-98 | quartz-sericite-clay | 2431 | 1a | | | 283 | 36.9 | 298 |
| 210-98 | quartz-sericite-clay | 2431 | 1a | | | 251 | 34.7 | 263 |
| 210-98 | quartz-sericite-clay | 2431 | 1a | <65 | | 264 | 35.6 | 270 |
| 210-98 | quartz-sericite-clay | 2431 | 1a | | | 258 | 35.2 | 263 |

| Sample no. | Alteration Assemblages | Elevation | Inclusion Type | Te (-) | Tm Ice (-) | Tm NaCl | Salinity | Th (L-V) |
|------------|---------------------------|-----------|----------------|--------|------------|---------|----------|----------|
| 210-98 | quartz-sericite-clay | 2431 | 1a | | | 240 | 34.1 | 258 |
| 210-98 | quartz-sericite-clay | 2431 | 1a | | | 258 | 35.2 | 258 |
| 210-98 | quartz-sericite-clay | 2431 | 1a | | | 253 | 34.9 | 283 |
| 210-98 | quartz-sericite-clay | 2431 | 1a | | | 247 | 34.5 | 247 |
| 210-98 | quartz-sericite-clay | 2431 | 1b | | | 274 | 36.3 | 240 |
| 210-98 | quartz-sericite-clay | 2431 | 1b | | | 282 | 36.8 | 263 |
| 210-98 | quartz-sericite-clay | 2431 | 1b | | | 257 | 35.1 | 193 |
| 210-98 | quartz-sericite-clay | 2431 | 1b | | | 276 | 36.4 | 238 |
| 210-98 | quartz-sericite-clay | 2431 | 2a | | | 243 | 34.2 | 244 |
| 210-98 | quartz-sericite-clay | 2431 | 2a | | | 259 | 35.3 | 270 |
| 210-98 | quartz-sericite-clay | 2431 | 2a | | | 254 | 34.9 | 297 |
| 210-98 | quartz-sericite-clay | 2431 | 2a | | | 268 | 35.8 | 268 |
| 210-98 | quartz-sericite-clay | 2431 | 2a | <50 | | 205 | 32.1 | 295 |
| 210-98 | quartz-sericite-clay | 2431 | 2b | | | 280 | 36.7 | 260 |
| 210-98 | quartz-sericite-clay | 2431 | 3 | | 4.5 | | 7.2 | 221 |
| 210-98 | quartz-sericite-clay | 2431 | 3 | | 5.2 | | 8.1 | 260 |
| 210-98 | quartz-sericite-clay | 2431 | 3 | | 6.6 | | 10.0 | 249 |
| 206-48 | andalusite-diaspore | 2372 | 1b | | | 270 | 36.0 | 232 |
| 321 | deep phyllic (breccia) | 2440 | 1a | | | 255 | 35.0 | 314 |
| 321 | deep phyllic (breccia) | 2440 | 1a | | | 280 | 36.7 | 449 |
| 321 | deep phyllic (breccia) | 2440 | 1a | 65-55 | | 363 | 43.6 | 416 |
| 321 | deep phyllic (breccia) | 2440 | 1a | | | 290 | 37.4 | 486 |
| 321 | deep phyllic (breccia) | 2440 | 1a | | | 258 | 35.2 | 423 |
| 321 | deep phyllic (breccia) | 2440 | 1a | | | 312 | 39.1 | 351 |
| 321 | deep phyllic (breccia) | 2440 | 1a | | | 302 | 38.3 | 332 |
| 321 | deep phyllic (breccia) | 2440 | 1a | | | 296 | 37.9 | 309 |
| 321 | deep phyllic (breccia) | 2440 | 1b | | | 304 | 38.5 | 247 |
| 321 | deep phyllic (breccia) | 2440 | 1b | | | 294 | 37.7 | 247 |
| 321 | deep phyllic (breccia) | 2440 | 1b | | | 280 | 36.7 | 258 |
| 321 | deep phyllic (breccia) | 2440 | 1b | | | 283 | 36.9 | 261 |
| 321 | deep phyllic (breccia) | 2440 | 1b | | | 292 | 37.6 | 286 |
| 321 | deep phyllic (breccia) | 2440 | 1b | | | 290 | 37.4 | 273 |
| 321 | deep phyllic (breccia) | 2440 | 1b | <45 | | 290 | 37.4 | 277 |
| 321 | deep phyllic (breccia) | 2440 | 1b | | | 327 | 40.3 | 299 |
| 321 | deep phyllic (breccia) | 2440 | 1b | | | 362 | 43.5 | 254 |
| 321 | deep phyllic (breccia) | 2440 | 2b | | | 318 | 39.6 | 279 |
| 321 | deep phyllic (breccia) | 2440 | 2b | | | 396 | 47.0 | 240 |
| 200 | shallow phyllic (breccia) | 2530 | 3 | | 0.1 | | 0.2 | 175 |
| 200 | shallow phyllic (breccia) | 2530 | 3 | | 4.0 | | 6.4 | 180 |
| 200 | shallow phyllic (breccia) | 2530 | 3 | | 3.9 | | 6.3 | 179 |
| 200 | shallow phyllic (breccia) | 2530 | 3 | | | | | 90 |
| 200 | shallow phyllic (breccia) | 2530 | 3 | | 3.0 | | 5.0 | 259 |
| 200 | shallow phyllic (breccia) | 2530 | 3 | | | | | 109 |
| 200 | shallow phyllic (breccia) | 2530 | 3 | | 4.8 | | 7.6 | 334 |
| 200 | shallow phyllic (breccia) | 2530 | 3 | | | | | 158 |
| 251 | shallow phyllic (breccia) | 2550 | 3 | | 4.0 | | 6.4 | 233 |
| 251 | shallow phyllic (breccia) | 2550 | 3 | | 1.5 | | 2.6 | 226 |

| Sample no. | Alteration Assemblages | Elevation | Inclusion Type | Te (-) | Tm Ice (-) | Tm NaCl | Salinity | Th (L-V) |
|------------|---------------------------|-----------|----------------|--------|------------|---------|----------|----------|
| 251 | shallow phyllic (breccia) | 2550 | 3 | | | | | 191 |
| 251 | shallow phyllic (breccia) | 2550 | 3 | | | | | 285 |
| 251 | shallow phyllic (breccia) | 2550 | 3 | | 3.6 | | 5.9 | 246 |
| 251 | shallow phyllic (breccia) | 2550 | 3 | | 1.8 | | 3.1 | 139 |
| 251 | shallow phyllic (breccia) | 2550 | 3 | | | | | 155 |
| 251 | shallow phyllic (breccia) | 2550 | 3 | | | | | 172 |
| 251 | shallow phyllic (breccia) | 2550 | 3 | | | | | 262 |
| 251 | shallow phyllic (breccia) | 2550 | 3 | | 3.1 | | 5.1 | 268 |
| 251 | shallow phyllic (breccia) | 2550 | 3 | | 2.9 | | 4.8 | 227 |
| 251 | shallow phyllic (breccia) | 2550 | 3 | | | | | 207 |
| 251 | shallow phyllic (breccia) | 2550 | 3 | | | | | 213 |
| 251 | shallow phyllic (breccia) | 2550 | 3 | | | | | 226 |
| 251 | shallow phyllic (breccia) | 2550 | 3 | | 3.7 | | 6.0 | 294 |
| 251 | shallow phyllic (breccia) | 2550 | 3 | | | | | 205 |
| 253 | shallow phyllic (breccia) | 2550 | 3 | | 2.5 | | 4.2 | 235 |
| 253 | shallow phyllic (breccia) | 2550 | 3 | | 3.2 | | 5.3 | 214 |
| 253 | shallow phyllic (breccia) | 2550 | 3 | | 3.5 | | | 245 |
| 253 | shallow phyllic (breccia) | 2550 | 3 | | | | | 184 |
| 253 | shallow phyllic (breccia) | 2550 | 3 | | 3.2 | | 5.7 | 231 |
| 253 | shallow phyllic (breccia) | 2550 | 3 | | | | | 237 |
| 253 | shallow phyllic (breccia) | 2550 | 3 | | | | | 185 |
| 119-16 | phyllic (BQPP) | 2304 | 1a | | | 296 | 37.9 | 305 |
| 119-16 | phyllic (BQPP) | 2304 | 1a | | | 266 | 35.7 | 328 |
| 119-16 | phyllic (BQPP) | 2304 | 1a | | | 300 | 38.2 | 321 |
| 119-16 | phyllic (BQPP) | 2304 | 1a | | | 296 | 37.9 | 306 |
| 119-16 | phyllic (BQPP) | 2304 | 1a | | | 233 | 33.7 | 510 |
| 119-16 | phyllic (BQPP) | 2304 | 1a | | | 233 | 33.7 | 337 |
| 119-16 | phyllic (BQPP) | 2304 | 1a | | | 310 | 38.9 | 328 |
| 119-16 | phyllic (BQPP) | 2304 | 1a | | | 263 | 35.5 | 322 |
| 119-16 | phyllic (BQPP) | 2304 | 1a | | | 230 | 33.5 | 360 |
| 119-16 | phyllic (BQPP) | 2304 | 1a | | | 256 | 35.1 | 288 |
| 119-16 | phyllic (BQPP) | 2304 | 1a | | | 297 | 37.9 | 317 |
| 119-16 | phyllic (BQPP) | 2304 | 1a | | | 303 | 38.4 | 331 |
| 119-16 | phyllic (BQPP) | 2304 | 1a | | | 273 | 36.2 | 274 |
| 119-16 | phyllic (BQPP) | 2304 | 1a | | | 310 | 38.9 | 333 |
| 119-16 | phyllic (BQPP) | 2304 | 1a | | | 318 | 39.6 | 337 |
| 119-16 | phyllic (BQPP) | 2304 | 1a | | | 264 | 35.6 | 412 |
| 119-16 | phyllic (BQPP) | 2304 | 1a | | | 306 | 38.6 | 422 |
| 119-16 | phyllic (BQPP) | 2304 | 1b | | | 293 | 37.6 | 287 |
| 119-16 | phyllic (BQPP) | 2304 | 1b | | | 303 | 38.4 | 281 |
| 119-16 | phyllic (BQPP) | 2304 | 1b | | | 297 | 37.9 | 281 |
| 119-16 | phyllic (BQPP) | 2304 | 1b | | | 281 | 36.7 | 277 |
| 119-16 | phyllic (BQPP) | 2304 | 1b | | | 288 | 37.3 | 289 |
| 119-16 | phyllic (BQPP) | 2304 | 2a | | | 298 | 38.0 | 330 |
| 119-16 | phyllic (BQPP) | 2304 | 2a | | | 266 | 35.7 | 297 |
| 119-16 | phyllic (BQPP) | 2304 | 2a | | | 225 | 33.2 | 324 |
| 119-16 | phyllic (BQPP) | 2304 | 2a | | | 287 | 37.2 | 347 |
| 119-16 | phyllic (BQPP) | 2304 | 2a | | | 291 | 37.5 | 320 |
| 119-16 | phyllic (BQPP) | 2304 | 2a | | | 304 | 38.5 | 366 |

| Sample no. | Alteration Assemblages | Elevation | Inclusion Type | Te (-) | Tm Ice (-) | Tm NaCl | Salinity | Th (L-V) |
|------------|------------------------|-----------|----------------|--------|------------|---------|----------|----------|
| 119-16 | phyllic (BQPP) | 2304 | 2a | | | 278 | 36.5 | 443 |
| 119-16 | phyllic (BQPP) | 2304 | 2b | | | 275 | 36.3 | 267 |
| 119-16 | phyllic (BQPP) | 2304 | 4 | | | | | 337 |
| 119-16 | phyllic (BQPP) | 2304 | 4 | | | | | 371 |
| 119-16 | phyllic (BQPP) | 2304 | 4 | | | | | 245 |
| 119-46 | phyllic (BQPP) | 2384 | 1a | | | 246 | 34.4 | 320 |
| 119-46 | phyllic (BQPP) | 2384 | 1b | | | 328 | 40.4 | 325 |
| 119-46 | phyllic (BQPP) | 2384 | 2a | | | 274 | 36.2 | 321 |
| 119-46 | phyllic (BQPP) | 2384 | 2a | | | 253 | 34.9 | 320 |
| 119-46 | phyllic (BQPP) | 2384 | 2a | | | 279 | 36.6 | 294 |
| 198 | pyrite vein | 2530 | 3 | | | | | 302 |
| 198 | pyrite vein | 2530 | 3 | | 3.2 | | 5.3 | 350 |
| 198 | pyrite vein | 2530 | 3 | | 3.7 | | 6.0 | 357 |
| 198 | pyrite vein | 2530 | 3 | | | | | 308 |
| 198 | pyrite vein | 2530 | 3 | | 2.5 | | 4.2 | 352 |
| 198 | pyrite vein | 2530 | 3 | | | | | 341 |
| 198 | pyrite vein | 2530 | 3 | | | | | 318 |
| 198 | pyrite vein | 2530 | 3 | | | | | 318 |
| 198 | pyrite vein | 2530 | 3 | | | | | 321 |
| 198 | pyrite vein | 2530 | 3 | | | | | 325 |
| 198 | pyrite vein | 2530 | 3 | | | | | 368 |
| 198 | pyrite vein | 2530 | 3 | | | | | 328 |
| 198 | pyrite vein | 2530 | 3 | | | | | 364 |
| 198 | pyrite vein | 2530 | 3 | | 5.0 | | 7.9 | 361 |
| 198 | pyrite vein | 2530 | 3 | | 3.7 | | 6.0 | 340 |
| 198 | pyrite vein | 2530 | 3 | | | | | 340 |
| 198 | pyrite vein | 2530 | 3 | | | | | 292 |
| 198 | pyrite vein | 2530 | 3 | | 0.8 | | 1.4 | 314 |
| 198 | pyrite vein | 2530 | 3 | | 0.9 | | 1.6 | 313 |
| 198 | pyrite vein | 2530 | 3 | | | | | 315 |
| 198 | pyrite vein | 2530 | 3 | | | | | 316 |
| 200 | pyrite vein | 2530 | 3 | | | | | 309 |
| 200 | pyrite vein | 2530 | 3 | | 2.5 | | 4.2 | 310 |
| 200 | pyrite vein | 2530 | 3 | | | | | 315 |
| 200 | pyrite vein | 2530 | 3 | | | | | 316 |
| 200 | pyrite vein | 2530 | 3 | | | | | 316 |
| 200 | pyrite vein | 2530 | 3 | | | | | 313 |
| 200 | pyrite vein | 2530 | 3 | | 2.8 | | 4.6 | 303 |
| 200 | pyrite vein | 2530 | 3 | | | | | 323 |
| 200 | pyrite vein | 2530 | 3 | | | | | 316 |
| 200 | pyrite vein | 2530 | 3 | | | | | 315 |
| 200 | pyrite vein | 2530 | 3 | | | | | 303 |
| 200 | pyrite vein | 2530 | 3 | | | | | 310 |
| 200 | pyrite vein | 2530 | 3 | | 4.0 | | 6.4 | 334 |
| 200 | pyrite vein | 2530 | 3 | | 3.8 | | 6.2 | 327 |
| 200 | pyrite vein | 2530 | 3 | | 4.2 | | 6.7 | 297 |
| 200 | pyrite vein | 2530 | 3 | | | | | 305 |
| 200 | pyrite vein | 2530 | 3 | | 4.4 | | 7.0 | 287 |
| 200 | pyrite vein | 2530 | 3 | | 0.8 | | 1.4 | 336 |

| Sample no. | Alteration Assemblages | Elevation | Inclusion Type | Te (-) | Tm Ice (-) | Tm NaCl | Salinity | Th (L-V) |
|------------|------------------------|-----------|----------------|--------|------------|---------|----------|----------|
| 200 | pyrite vein | 2530 | 3 | | 3.0 | | 5.0 | 301 |
| 200 | pyrite vein | 2530 | 3 | | | | | 343 |
| 200 | pyrite vein | 2530 | 3 | | | | | 344 |
| 200 | pyrite vein | 2530 | 3 | | | | | 350 |
| 200 | pyrite vein | 2530 | 3 | | 2.0 | | 3.4 | 285 |
| 200 | pyrite vein | 2530 | 3 | | 4.5 | | 7.2 | 336 |
| 200 | pyrite vein | 2530 | 3 | | | | | 340 |
| 200 | pyrite vein | 2530 | 3 | | | | | 339 |
| 200 | pyrite vein | 2530 | 3 | | | | | 340 |
| 200 | pyrite vein | 2530 | 3 | | | | | 341 |
| 200 | pyrite vein | 2530 | 3 | | 3.5 | | 5.7 | 377 |
| 200 | pyrite vein | 2530 | 3 | | 3.6 | | 5.9 | 319 |
| 200 | pyrite vein | 2530 | 3 | | 3.5 | | 5.7 | 230 |
| 200 | pyrite vein | 2530 | 3 | | 1.4 | | 2.4 | 218 |
| 200 | pyrite vein | 2530 | 3 | | 1.4 | | 2.4 | 334 |
| 200 | pyrite vein | 2530 | 3 | | 0.7 | | 1.2 | 319 |
| 200 | pyrite vein | 2530 | 3 | | 0.7 | | 1.2 | 324 |
| 200 | pyrite vein | 2530 | 3 | | 0.8 | | 1.4 | 315 |
| 200 | pyrite vein | 2530 | 3 | | 0.7 | | 1.2 | 320 |
| 200 | pyrite vein | 2530 | 3 | | 0.7 | | 1.2 | 316 |
| 200 | pyrite vein | 2530 | 3 | | 3.2 | | 5.3 | 365 |
| 200 | pyrite vein | 2530 | 3 | | 1.3 | | 2.2 | 342 |
| 200 | pyrite vein | 2530 | 3 | | | | | 235 |
| 200 | pyrite vein | 2530 | 3 | | | | | 325 |
| 200 | pyrite vein | 2530 | 3 | | | | | 326 |
| 200 | pyrite vein | 2530 | 3 | | 1.1 | | 1.9 | 347 |

Te: Temperature of eutectic, i.e., first melting on warming a completely frozen inclusion.

Tm NaCl: Temperature of melting of salt (NaCl).

Th (L-V): Temperature of homogenization of the liquid and vapour phases.

VITA

Name: Farhad Bouzari
Date of birth: December 12, 1965
Birthplace: Tehran, Iran

University Education

1996-2003: Ph.D. candidate, Queen's University
1993-1995: M.Sc. in Mineral Exploration, Queen's University
1985-1990: B.Sc. in geology, Ferdowsi University of Mashhad, Iran

Professional Experience

1990-1993: Exploration geologist, Geological Survey of Iran

Awards

1993: Ministry of Science Research and Technology of Iran
1996: Reinhart Fellowship, Queen's University
1997: Rio Algom Exploration, Toronto

Publications

- Bouzari, F., and Clark, A.H., 2003, Prograde evolution of a major porphyry copper system: The Cerro Colorado protore, I Región, Chile: Abstract, Geological Association of Canada/Mineralogical Association of Canada, 2003 meeting, Vancouver, British Columbia, Canada.
- Bouzari, F., and Clark, A.H., 2002, Anatomy, evolution and metallogenic significance of the supergene orebody at the Cerro Colorado porphyry copper deposit, I Región, Chile: *Economic Geology*, v. 97, p 1701-1740.
- Bouzari, F., and Clark, A.H., 2000, Definition of a protracted history of supergene alteration in the Cerro Colorado porphyry copper deposit, Chile, through Ar-Ar dating of alunite-group minerals: *Geological Society of America, Abstracts with Programs*, v. 32, p. A-110.